Aus dem Institut für Prophylaxe und Epidemiologie der Kreislaufkrankheiten

Klinikum der Ludwig-Maximilians-Universität München

Direktor: Univ.-Prof. Dr. med. Christian Weber

Elucidating atherosclerosis B cell immunity in hyperlipidemic mice by next-generation sequencing

Dissertation

zum Erwerb des Doktorgrades der Naturwissenschaften

an der Medizinischen Fakultät der

Ludwig-Maximilians-Universität München

vorgelegt von

Xi Zhang

aus

Shanxi, China

Jahr

2023

Mit Genehmigung der Medizinischen Fakultät

der Ludwig-Maximilians-Universität München

Betreuerin:	Univ.-Prof. Dr. rer. nat. Sabine Steffens
Zweitgutachter:	PD Dr. rer. nat. Reinhard Obst
Dekan:	Prof. Dr. med. Thomas Gudermann
Tag der mündichen Prüfung:	09. Juli 2024

Table of Contents

Zusammenfassung (Deutsch)

Atherosklerose verursacht Erkrankungen wie Herzinfarkt und Schlaganfall. Die Erkrankung stellt die Haupttodesursache weltweit dar. Es gibt Hinweise darauf, dass Atherosklerose eine chronische und unheilbare entzündliche Erkrankung ist. Sowohl angeborene als auch adaptive Immunreaktionen werden als wesentliche pathogene Prinzipien mit der Entwicklung der Atherosklerose in Verbindung gebracht. Eine ungeklärte Frage ist: Welche Rolle spielen B Zellen während der klinisch relevanten Spätstadien der Erkrankung? Insbesondere bleibt ungeklärt, ob autoimmunreaktive B-2 Zellen während der verschiedenen Stadien der Atherosklerose gebildet werden, wo diese generiert werden und ob autoreaktive B-2 Zellen gegen Autoantigene der erkrankten Arterienwand gerichtet sind. Bisher wurde davon ausgegangen, dass B Zell-Immunreaktionen in sekundären Lymphorganen wie Lymphknoten und Milz stattfinden. Unsere Arbeitsgruppe hat eine alternative Hypothese verfolgt, nachdem sie tertiäre Lymphorgane, die sie als *artery tertiary lymphoid organs* (ATLOs) bezeichnet hat, in der Arterienwand in Mausmodellen und humanen Arterien beobachtet hatte. Frühere Studien der Arbeitsgruppe zeigten, dass ATLOs Germinalzentren und Plasmazellen enthalten. Folgend diesen Ergebnissen, wurde hier die Hypothese untersucht, ob B-2 Immunreaktionen in ATLOs organisiert werden. Mit Hilfe von *next-generation-sequencing* (NGS) wurde das B Zell Rezeptor (B cell receptor; BCR) Repertoire in verschiedenen Geweben in gealterten Wildtyp-Mäusen (WT) und Apolipoprotein-E-defizienten Mäusen (*Apoe*-/-) analysiert. Die Ergebnisse dieser Studie entschlüsselten das BCR-Repertoire bei Mäusen, die an fortgeschrittener Atherosklerose erkrankt waren. Sie stützen die Hypothese, dass Atherosklerose als echte B Zell-assoziierte Autoimmunerkrankung gelten kann. Diese Studie bietet daher eine Blaupause für die Suche und Identifizierung potenzieller Atherosklerose-spezifischer Autoantigene. Die Daten eröffnen ein neues Verständnis der Grundursachen der Atherosklerose.

Abstract (English)

Atherosclerosis causes multiple diseases such as heart attack and stroke. It constitutes the major cause of death worldwide. Increasing evidence indicates that atherosclerosis is a chronic unresolvable inflammatory disease. Both innate and adaptive immune responses are major pathogenic principles associated with the development of atherosclerosis. A fundamentally unanswered question is: what role do B cells play during the clinically relevant late stages of the disease? In particular, it remains unclear whether autoimmune reactive B-2 cells are formed during the different stages of atherosclerosis, where they are generated, and whether autoreactive B-2 cells are directed against autoantigens of the diseased artery wall. It was generally assumed that the B cell immune response of atherosclerosis occurs in secondary lymphoid organs (SLOs) including the spleen and lymph nodes (LNs). Our group has previously pursued an alternative hypothesis after describing artery tertiary lymphoid organs (ATLOs) in the diseased arterial wall in mouse models and humans. Previous work by our group has reported that the advanced stages of ATLOs contain activated germinal centres (GCs) and plasma cells (PCs). Following these results, this work investigated the hypothesis whether B-2 immune responses are organized in ATLOs. With the help of next-generation sequencing (NGS), the B cell receptor (BCR) repertoire was analyzed across different tissues in aged wild-type (WT) and Apolipoprotein E-deficient (*Apoe*$^{-/-}$) mice. The findings of this study systematically deciphered the BCR repertoire in mice burdened with advanced atherosclerosis, supporting the hypothesis that atherosclerosis may qualify as a *bona fide* B cell-associated autoimmune disease. This study therefore provides a blueprint to search for and identify potential atherosclerosis-specific autoantigens. Furthermore, the data on B-2 cell immunity in ATLOs appear to open multiple possibilities for understanding the root causes of atherosclerosis.

List of Figures

List of Figures

List of Tables

List of Abbreviations

APC	Antigen-presenting cell
Apoe$^{-/-}$	Apolipoprotein E-deficient
ATLO	Artery tertiary lymphoid organ
BCR	B cell receptor
BM	Bone marrow
BP	Biological process
cDC	Conventional dendritic cell
CDR3aa	CDR3 amino acid
CDR	Complementary-determining region
CSR	Class-switch recombination
CVD	Cardiovascular disease
D20	Total percentage of top 20 BCR clones
DC	Dendritic cell
DEG	Differentially expressed gene
DPBS	Dulbecco's phosphate-buffered saline
DZ	Dark zone
FACS	Fluorescence-activated cell sorting
FDC	Follicular dendritic cell
FDR	False discovery rate
FR	Framework region
GC	Germinal centre
GO	Gene Ontology
GSEA	Gene set enrichment analysis
HEV	High endothelial venule
IFN	Interferon
Ig	Immunoglobulin
IGH	Heavy chain
IGHD	Heavy chain diversity region
IGHJ	Heavy chain joining region
IGHV	Heavy chain variable region
IGK	Light chain, κ
IGL	Light chain, λ
IL	Interleukin
KEGG	Kyoto Encyclopedia of Genes and Genomes

LDL	Low-density lipoprotein
LN	Lymph node
LZ	Light zone
MACS	Magnetic-activated cell sorting
MHC	Major histocompatibility complex
NGS	Next-generation sequencing
ox-LDL	Oxidised low-density lipoprotein
OXPHOS	Oxidative phosphorylation
PCA	Principal component analysis
PCR	Polymerase chain reaction
PCs	Plasma cells
PerC	peritoneal cavities
PRR	Pattern recognition receptor
Rep-seq	Repertoire sequencing
RLN	Renal lymph node
RT	Room temperature
scBCR-seq	Single-cell BCR sequencing
scRNA-seq	Single-cell RNA sequencing
SHM	Somatic hypermutation
SLE	Systemic lupus erythematosus
SLO	Secondary lymphoid organ
SMC	Smooth muscle cell
TCR	T cell receptor
T_{fh} cell	Follicular T helper cell
T_h cell	T helper cell
TNF	Tumour necrosis factor
Top-Vseg	Top 10 IGHV segments (ranked by mean percentage)
T_{reg} cell	Regulatory T cell
UMAP	Uniform manifold approximation and projection
UMI	Unique molecular identifier
WT	Wild type

1 Introduction

1.1 Immune response

The human body is exposed to a vast array of pathogenic microorganisms and other injurious agents from the environment that may threaten normal tissue homeostasis and organ function. In some instances, these conditions can cause diseases. However, the overwhelming majority of pathogens are eliminated by the immune system to protect the body by mounting various types of immune responses (Parkin and Cohen, 2001). The defence mechanisms can be divided into two primary and general categories: innate immune responses and adaptive immune responses (Chaplin, 2003, Romagnani, 2006).

1.1.1 Innate immune response

Innate immune responses constitute the acute mechanisms of the immune system to remove injurious agents (Hoffmann and Akira, 2013). Innate immune responses involve both natural barriers and innate immune cells. Skin and mucus contribute to the first line of defence with both anatomically and chemically defined barriers. Pathogens capable of breaching such physical barriers will meet strong cellular defence roadblocks that are carried out by a series of distinct innate immune cells which are equipped with a series of effective mechanisms to eliminate the foreign invaders (Turvey and Broide, 2010). Innate immune cells include macrophages, several types of granulocytes, mast cells, and natural killer cells. These cells express pattern recognition receptors (PRRs) which allow recognising molecular patterns shared by many microbes and other injurious agents. The interactions of innate immune cells with pathogens trigger the production of mediators by immune cells which either directly destroy pathogens or regulate other cells that are involved in innate immunity (Kumar et al., 2011). For example, macrophages ingest microbes and produce chemical mediators to eliminate pathogens (Twigg, 2004). The powerful innate immune responses act rapidly within seconds to hours but with low specificity (Fearon and Locksley, 1996).

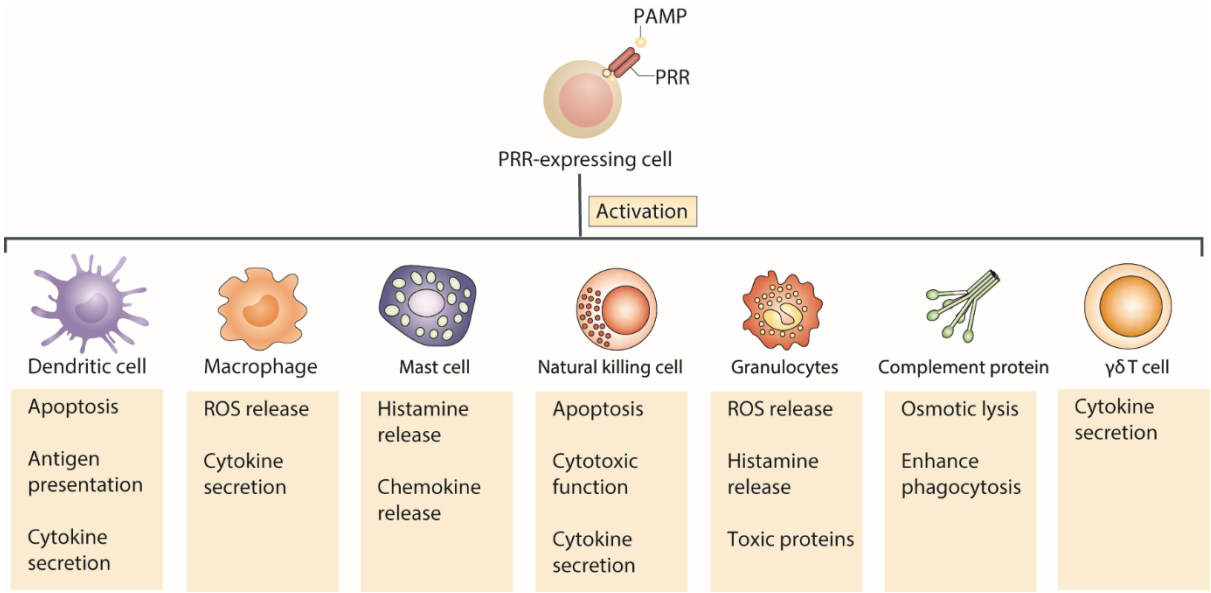

Figure 1.1 The innate immune system
Pathogens express on their surface or release pathogen-associated molecular patterns (PAMPs) into the extracellular space, where they activate PRRs expressed by innate immune cells. The activation leads to direct destruction of pathogens or the secretion of toxic mediators. ROS: reactive oxygen species; γδ T cell: gamma delta T cell (Modified from Dranoff, 2004, Kurts et al., 2013).

1.1.2 Adaptive immune response

Adaptive immune responses are organised by T lymphocytes (cellular immunity) or by B lymphocytes (humoral immunity). B cells and T cells share common lymphoid progenitors which differentiate from hematopoietic stem cells in the bone marrow (BM). Maturation of the respective progeny occurs separately with B cells developing in the BM and T cells developing in the thymus. Pro-B cells are precursors of B cell development. Pre-B cells first differentiate into immature B cells. The immature B cells immigrate to the spleen or mucosa-associated lymphoid tissues (MALTs) and subsequently undergo maturation. In T cell development, progenitors seed the thymus via the bloodstream and form pro-T cells which are CD4/CD8 double-negative. Similar to B cells, pro-T cells proceed to pre-T cells, followed by positive selection of CD4/CD8 double-positive T cells. Finally, CD4 (helper T cells) or CD8 (cytotoxic T cells) single-positive T cells are termed mature naïve T cells. These cells leave the thymus to populate peripheral lymphoid organs and other peripheral tissues (Siebenlist et al., 2005, Nemazee, 2006). Apart from conventional B-2 B cells, there is also a B cell population termed B-1 B cells, which predominantly develops in foetal livers and reside in body cavities. B-1 B cells can be separated into B-1a and B-1b subpopulations and these can be distinguished by the expression of CD5 (Baumgarth, 2016).

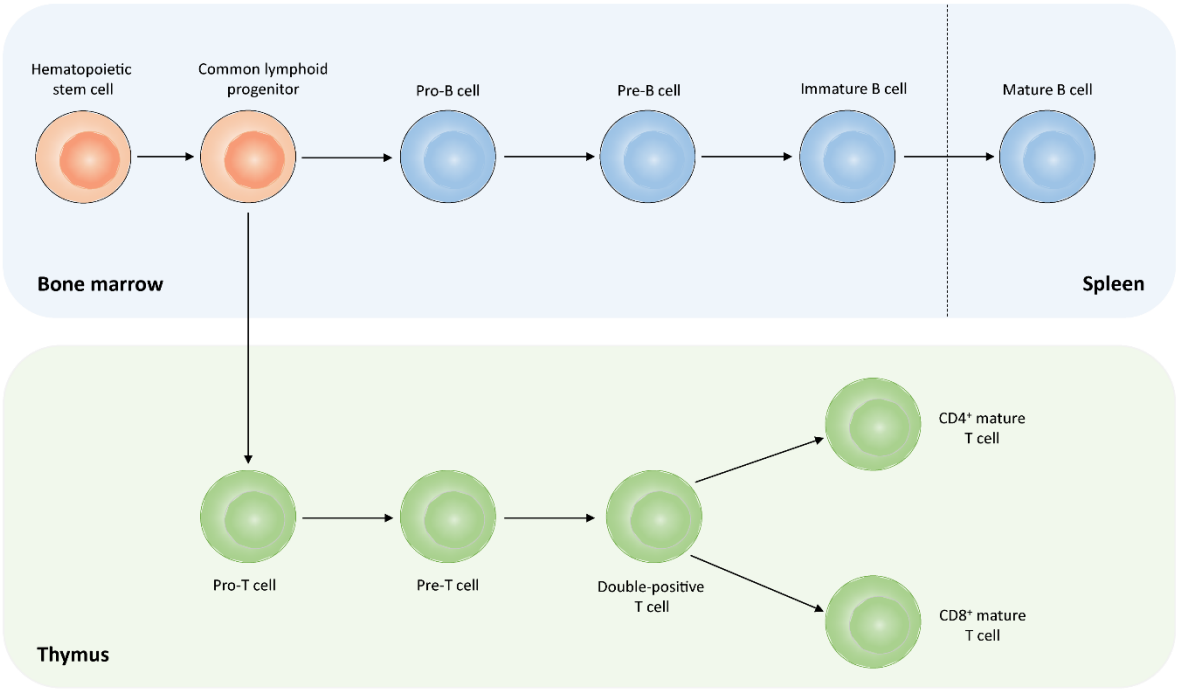

Figure 1.2 B cell and T cell development
Developmental stages are presented as labelled circles, with the name attached. Conventional B cells and T cells share common lymphoid progenitors which differentiate from hematopoietic stem cells in the BM. The subsequent development of B cells and T cells occurs in the BM and thymus, respectively. In the BM, the development progresses through the pro-B cell, pre-B cell and immature B cell stages. Immature B cells migrate to the spleen or mucosa-associated lymphoid tissues and finally differentiate into mature B cells. T cell development similarly progresses through the pro-T cell and pre-T cell stage, followed by a double-positive T cell stage. Mature T cells differentiate in the thymus.

Mature T cells and B cells which have not yet encountered antigen are defined as naïve cells (Edelman, 1991, Garcia et al., 1999). Cellular immunity by T cells provide protection against infected or aberrant cells. Naïve T cells are activated after recognizing antigens presented by virtue of antigen-presenting cells (APCs) such as macrophages, dendritic cells (DCs) and B cells (Sprent, 1995, Gaudino and Kumar, 2019). APCs express a set of proteins called major histocompatibility complex (MHC) molecules on their surface. Antigenic peptides are loaded onto MHC molecules and bind to distinct antigen-specific receptors expressed on the surface of T cells. Two families of MHC molecules are involved in antigen presentation. MHC class I molecules mediate activation of $CD8^+$ naïve T cells, and MHC class II interacts with $CD4^+$ naïve T cells (Neefjes et al., 2011). Activated T cells secrete cytokines such as interleukin 12 (IL-12) and interferons (IFNs**)** to stimulate proliferation and differentiation, resulting in the generation of effector T cells. Effector $CD4^+$ cells assist in the regulation of immune responses by releasing cytokines and mainly can be divided into T helper 1 (T_h1), T_h2, T_h17 or follicular

T helper cells (T_{fh}). Effector $CD8^+$ T cells kill target cells by inducing apoptosis or other means. The progeny of T cells may develop into memory T cells, which are functionally inactive but respond to the same antigen subsequent to repeated exposures (Germain, 1994). Unlike innate defence, adaptive immune responses are capable of exquisite *epitope specificity* on its target pathogens (Chaplin, 2010). The adaptive immune system is also responsible for immunological memory. Memory cells generated during primary exposure and react with prominently stronger and quicker responses when they meet the antigens a second time (Dempsey et al., 2003).

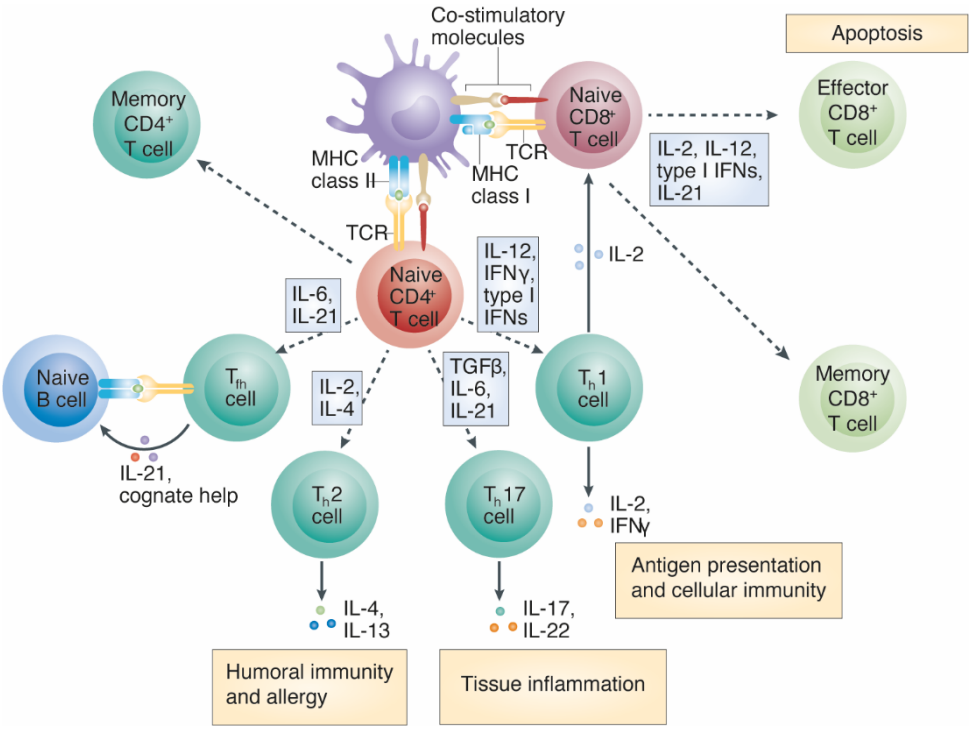

Figure 1.3 The T cell immune response
Antigens are presented by MHC I or MHC II molecules on the APC surface. They bind to the TCR of cognate naïve T cells for activation. Depending on the type of released cytokines, activated $CD4^+$ T cells differentiate into memory $CD4^+$ T cells and a variety of T_h cell subsets, resulting in distinct immunoregulatory functions. Activated $CD8^+$ T cells differentiate into effector and memory $CD8^+$ T cells, triggering programmed cell death. TGF: Transforming growth factor; TCR: T cell receptor (Modified from Desmet and Ishii, 2012, Medzhitov et al., 2011).

Humoral immunity is mediated by B cell-bound or secreted antibodies. Although small soluble antigens can activate naïve B cells through diffusion, generally naïve B cells encounter antigens after being attracted by APCs via their B cell receptors (BCRs) while concomitantly receiving help from T_H cells (Parker, 1993, Batista and Harwood, 2009, Harwood and Batista, 2010). All three cell types form aggregates termed the *immunological synapse* (IS) (Dustin, 2014).

Activated B cells migrate towards germinal centres (GCs) and undergo multiple rounds of somatic hypermutations (SHM) which refer to point mutations on BCR heavy chains during B cell differentiation (Teng and Papavasiliou, 2007). With the further encounter of antigens presented on the surface of follicular DCs (FDCs) accompanied by T_{fh} cells, B cells with the highest affinity to antigens receive survival signals for extended periods of time (hours) and begin to proliferate while those B cells that have a too low affinity to antigen to survive undergo apoptosis (Peperzak et al., 2012). This crucial process of B cell activation and maturation is called *affinity maturation* leading to clonal selection of ever-increasing affinity of the antigen for the BCRs (Chan and Brink, 2012). After multiple rounds of hypermutation and clonal selection, high-affinity B cells are generated that exit the GCs and either become plasma cells (PCs) or memory B cells (Kurosaki et al., 2015). Before the initiation of GCs, some activated B cells can migrate to extrafollicular sites, proliferate and differentiate into extrafollicular PCs that secrete low-affinity antibodies (MacLennan et al., 2003). The long-lived PCs are capable for homing to the BM to organize long-lasting humoral immunity.

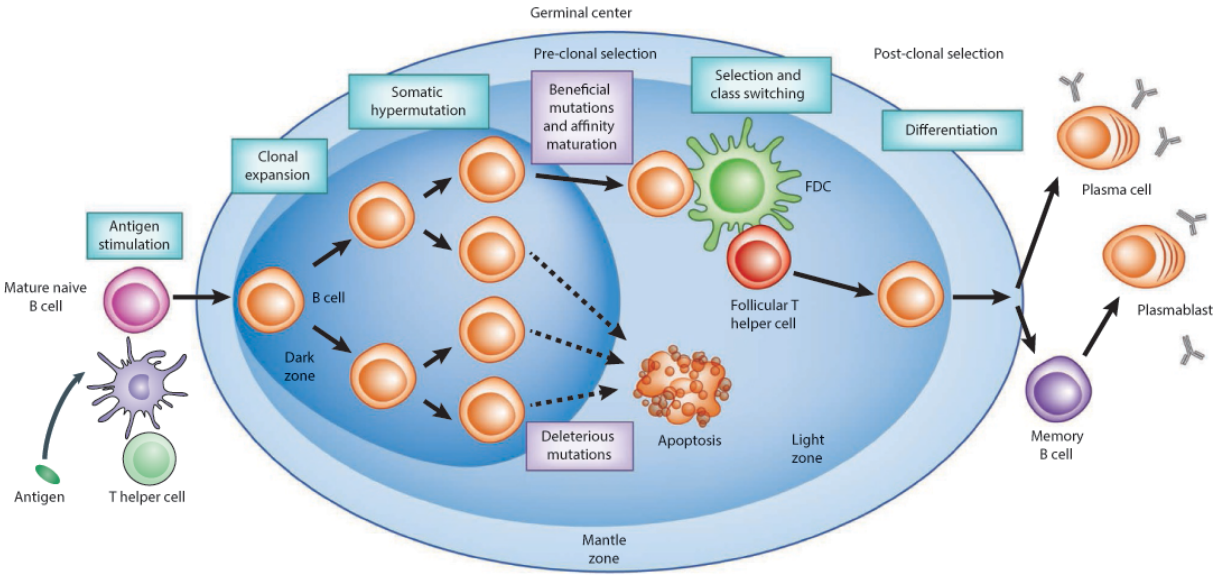

Figure 1.4 The IS and affinity maturation of B-2 cells in GCs
With the help of T_h cells, DCs present antigens to naïve mature B cells. Activated B-2 cells enter GCs for rapid proliferation, resulting in clonal expansion and SHM. They then encounter antigens which presented by FDCs to test antibody affinity. Only B cells bearing antibodies with high affinity can survive and differentiate into either PCs or memory B cells. When leaving GCs, memory B cells localize to the blood, spleen or lymph nodes (LNs), whereas PCs home to the peripheral lymphoid organs or home back to BM (Modified from Siegrist and Aspinall, 2009, Georgiou et al., 2014).

1.2 B cell diversity

1.2.1 Immunoglobulin (Ig) structure

BCRs are transmembrane receptors expressed on the surface of B cells. BCRs recognize antigens via short antigen sequences termed *epitopes*. BCRs are composed of two parts: membrane-bound Ig molecules and heterogeneous Igα/Igβ signal transduction proteins (Seda and Mraz, 2015). The majority of Igs are present in serum after secretion by PCs. The basic structure of immunoglobulin is a "Y"-shape monomer consisting of two heavy polypeptide chains and two light polypeptide chains bridged by disulfide bonds. In mammals, heavy chains contain 450-550 amino acid residues. They are clustered into five isotypes differing in size and composition, i.e. α, δ, ε, γ, and μ making up five classes of Igs together with light chains as IgA, IgD, IgE, IgG and IgM (Schroeder and Cavacini, 2010). Light chains with 211-217 amino acid residues are observed in two isotypes: κ and λ (Schroeder and Cavacini, 2010). Amino acid residues at the N'-end of light and heavy chains are very diverse and are therefore termed the variable regions. They account for ¼ of heavy chains and ½ of light chains, respectively. Three hypervariable fragments associated with Ig diversity in the variable regions are defined as complementary-determining regions (CDRs), with CDR3 yielding the most extensive variability (Shirai et al., 1999). Four fragments between CDRs are called framework regions (FRs), which are responsible for antigen binding and structure maintenance (Sela-Culang et al., 2013). The relatively constant C'-end is referred to as the constant region with the ability to determine the isotype of Ig chains. A total of six CDRs in paired heavy and light chains collectively contact antigens, contributing to antibody specificity determination and antigen recognition. The arm of the Y is organized by one variable domain and one constant domain, determining antigen specificity and referred to as the Fab (Fragment, antigen-binding) region (Wingren et al., 1996). The base of the Y termed Fc (Fragment, crystallizable) region only consists of heavy chains and plays a role in the class determination of Igs and interaction with complement proteins or Fc receptors (FcRs) (Woof and Burton, 2004).

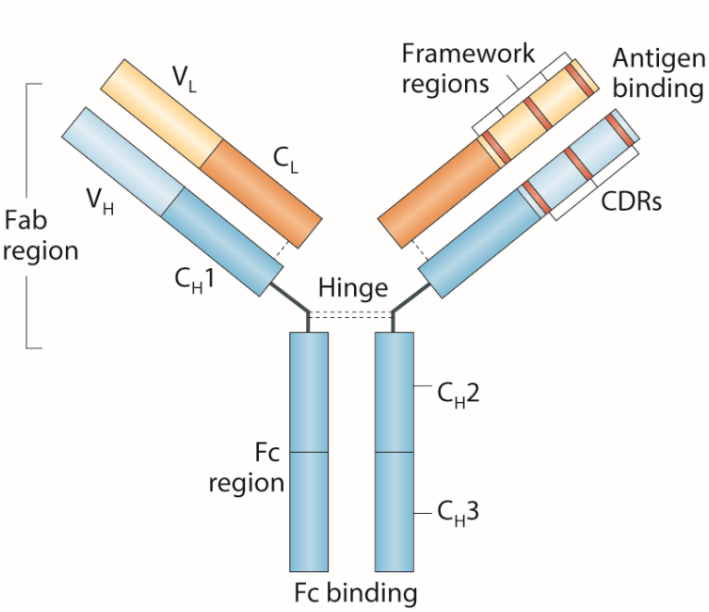

Figure 1.5 The structure of Ig monomers
The basic structure consists of two heavy (H) chains and two light (L) chains, held together in Y-shape by disulphide bridges. Heavy chains have four domains, whereas the light chains have two. The sequence of the first domain in both heavy and light chains is most variable, which is termed the variable (V) region to determine antigen-binding specificity. The variable region is composed of three CDRs and four supportive framework regions. The other domains form the constant I region to determine the subclass of Igs. The arm of Y is termed Fab region for antigen binding, and the base of Y is the Fc region for complement or Fc receptor binding (Taken from Hansel et al., 2010).

1.2.2 Ig gene rearrangement

Effective adaptive immune responses are critically dependent on the diversity of antigen receptors. However, the number of genes available to encode the receptors is limited by the size of the genome. Gene rearrangements allow B cells to generate an immense number of unique variable regions from a relatively small number of antibody genes (Market and Papavasiliou, 2003). There are multiple copies of four types of gene segments tandemly arranged in the genomes of mammals, namely the variable gene segment (V), the diversity gene segment (D), the joining gene segment (J) and the constant gene segment (C). Each copy is slightly different from the other copies. For example, the human genome harbours 61 V, 26 D, 6 J and 9 C segments for the heavy chain (Dunn-Walters, 2016). To construct a translatable RNA for mature BCRs, V(D)J recombination is carried out in the BM to assemble variable regions via recombinase activity. The heavy chains select one segment of V, D, J, respectively, and paste them to the C segments. The light chains are similarly rearranged as either the κ or the λ chain but exclude D segments. Furthermore, nucleotide addition or deletion, which has occurred in

each gene joint site contributes to the diversity of the BCR repertoire (Schatz and Ji, 2011). Once the variable region is generated successfully, it will silence the expression of any other variable region, known as allelic exclusion, ensuring monoallelic expression and preventing autoimmunity (Bergman and Cedar, 2004). The C segments have fewer copies but dominate the classes of Igs. All naïve mature B cells assemble μ and δ segments of constant region genes, producing both IgM and IgD. Nevertheless, after being activated by antigens, B cells develop the capacity to switch to express different C segments, resulting in the formation of IgA, IgG or IgE antibodies. This mechanism is termed class-switch recombination (CSR), providing diverse isotypes to govern distinct antigen clearance pathways after the antigen-antibody interaction, such as through complement activation, virus neutralization, cellular cytotoxicity or the release of chemokines and cytokines (Lu et al., 2018, van Erp et al., 2019). For example, IgM isotypes have an enhanced ability to activate complement, driving clearance of early infections, whereas IgG isotypes strongly induce functions like antibody-dependent cellular cytotoxicity and phagocytosis to eliminate invaders (Czajkowsky and Shao, 2009, de Taeye et al., 2019). Apart from recombination in the BM, activated B cells in the periphery also undergo SHM to experience antigen-triggered point mutations, expanding diversity even further (Odegard and Schatz, 2006).

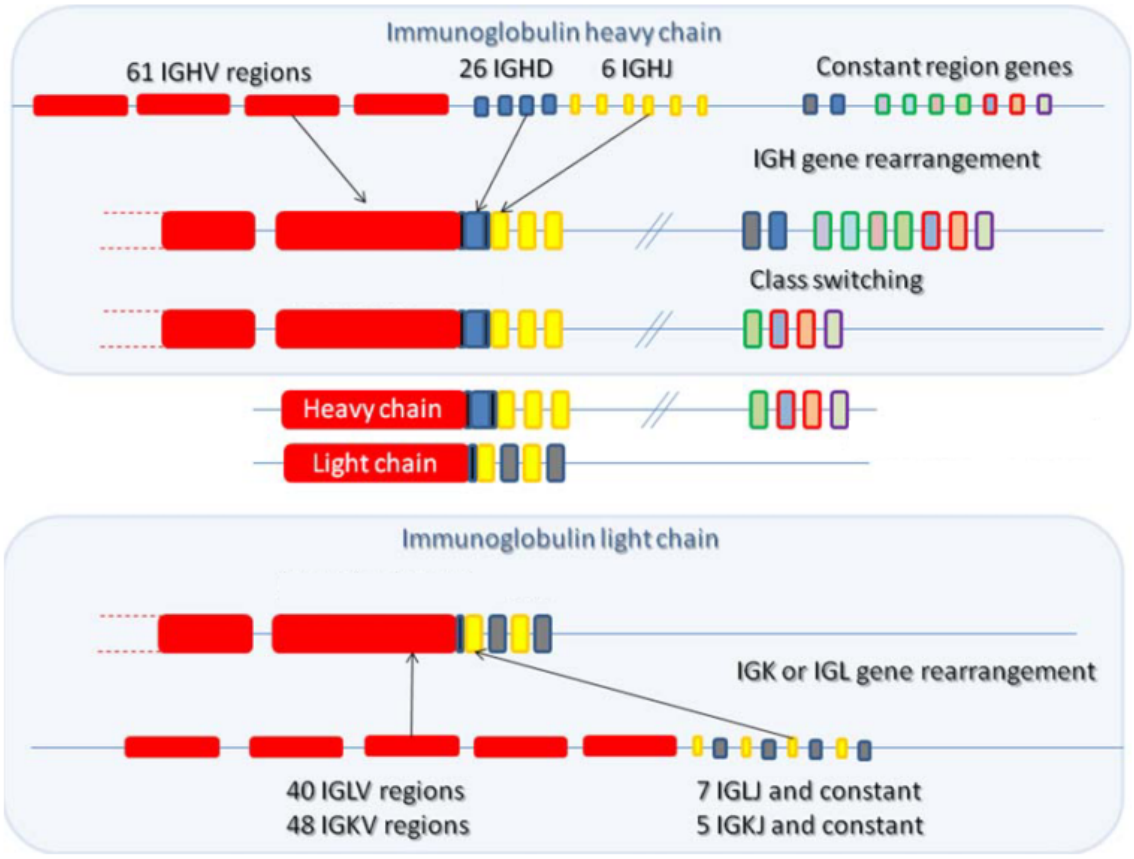

Figure 1.6 B cell gene rearrangement
A number of different genes are grouped in three loci in the genome, i.e., the heavy chain (IGH), the κ light chain (IGK) and the λ light chain (IGL). Heavy chains take one fragment from the variable (IGHV), diversity (IGHD) and joining (IGHJ) regions, respectively, and combines them. Light chain genes are rearranged similarly but without diversity regions. Successfully recombined Igs undergo class-switching to express a different fragment of constant region genes during activation by antigens (Taken from Dunn-Walters, 2016).

1.2.3 BCR repertoire and repertoire sequencing (Rep-seq)

The combinatorial mechanisms of B cells generate approximately 10^{10}-10^{11} functional BCR clonotypes by *reshuffling* the genetic code (Yaari and Kleinstein, 2015). This collection of total BCRs is referred to as the BCR repertoire (Calis and Rosenberg, 2014). While the primary repertoire is generated by V(D)J recombination, the secondary repertoire is generated after antigen recognition processes in the GC. Therefore, the quality of the repertoire alters depending on the stages of ongoing immune responses such as ageing, disease exposure and even treatment (Dunn-Walters, 2016). For example, narrowing of the CD8 T cell repertoire occurs during ageing (Blackman and Woodland, 2011). Therefore, dissecting the repertoire of Igs sheds light on understanding how the adaptive immune responses are organized. Recently, the rapid development of various sequencing technologies has stimulated sequencing of BCR or TCR repertoires from a single mammal (Robins, 2013). With the power of next-generation sequencing (NGS), the immunological repertoire had first been determined in small organisms like Zebrafish and has led to an improved understanding of the adaptive immune system in general (Weinstein et al., 2009). Despite the fact that the whole repertoire of humans is presently inaccessible due to its extremely large size, sequencing obtained by Rep-seq has the power of creating a temporal snapshot of the BCR repertoire and verify biomarkers for disease diagnosis or vaccine development (Jiang et al., 2013). Substantial antibody specificity comes from the IGH CDR3 region that is highly polymorphic owing to gene recombination and somatic hypermutation, leading it as the most common immune system compartment for Rep-seq to estimate the repertoire (Han et al., 2016).

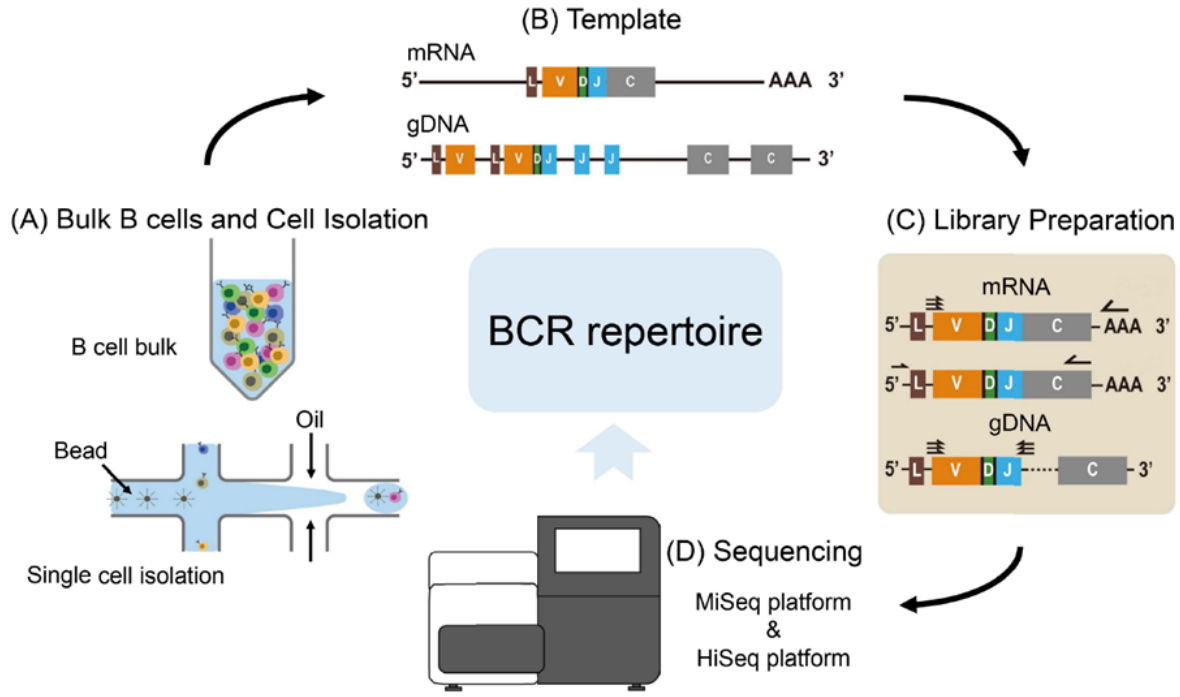

Figure 1.7 Overview of Rep-seq workflow
B cells are enriched for bulk sequencing or single-cell sequencing to be followed by library preparation. Both messenger RNA (mRNA) and genomic DNA (gDNA) can be used as a template depending on the purpose. Polymerase chain reaction (PCR) is introduced to construct a library based on the specific target primers. The library is passed to sequence at the NGS platforms such as Illumina MiSeq or Illumina HiSeq depending on sequencing length and depth (Modified from Kim and Park, 2019).

1.3 Autoimmunity

1.3.1 Immune tolerance

Gene rearrangement leads to a remarkably broad repertoire of distinct B cells and T cells with random specificity, of which a considerable portion of cells are capable to recognise self-antigens (Wardemann et al., 2003a). However, under physiological conditions, there is no immune response against self. The unresponsiveness preventing autoimmunity is due to the phenomenon called self-tolerance, allowing the immune system to discriminate non-self from self (van Driel, 2007). There are two layers of immune tolerance, i.e., central tolerance and peripheral tolerance. Central tolerance emerges in the BM or thymus at the immature B cell or T cell stages, respectively (Romagnani, 2006). Four mechanisms are involved in central tolerance. First, clonal deletion triggers suicidal deletion of autoreactive cells by apoptosis leading to elimination of autoreactive clones (Pelanda and Torres, 2012). This approach is largely regulated by the expression of B cell lymphoma 2 (BCL-2) interacting mediator of cell

death (BIM), which is a pro-apoptotic protein that belongs to BCL-2 family (Tsubata, 2017). Second, autoreactive cells have the ability to change their receptors away from self-reactivity, referred to as receptor editing. Light chains in BCRs or α chains in TCRs are rearranged further to alternatively form new non-autoreactive receptors (Nemazee, 2006). The receptor editing in immature B cells is facilitated by enforced expression of BCL-2 (Nemazee, 2017). Third, anergy is the functional inactivation of self-reactive cells, resulting in specific unresponsiveness to antigen stimulation. This mechanism is reversible as the anergic cells are capable of rescuing their responsiveness with time if the antigen is removed (Xing and Hogquist, 2012). Cells are required to recognize some microorganisms that carry epitopes similar to self-antigens, however, giving room to cross-reactivity that may trigger autoimmune responses (Klinman, 1996). Forth, regulatory T (T_{reg}) cells can imprint autoreactive clones with suppressive or regulatory functions. The suppressers execute their roles by producing anti-inflammatory cytokines, modulating the activation state and function of APCs or by direct cell-cell contact and multiple other means (Sakaguchi et al., 2008). Central tolerance is efficient but cannot clear all cells with autoreactivity yielding a considerable percentage of autoreactive lymphocytes to enter the periphery. Therefore, additional peripheral tolerance mechanisms have emerged to control tolerance of mature cells that have evaded central tolerance-triggered elimination and that emigrated from the primary lymphoid organs into peripheral organs. Peripheral tolerance is dominated by anergy and multiple other mechanisms such as the tolerance to antigens decorated with sialic acid–binding Ig-like lectins (SIGLECS), but these mechanisms do not involve receptor editing (Duong et al., 2010, Xing and Hogquist, 2012).

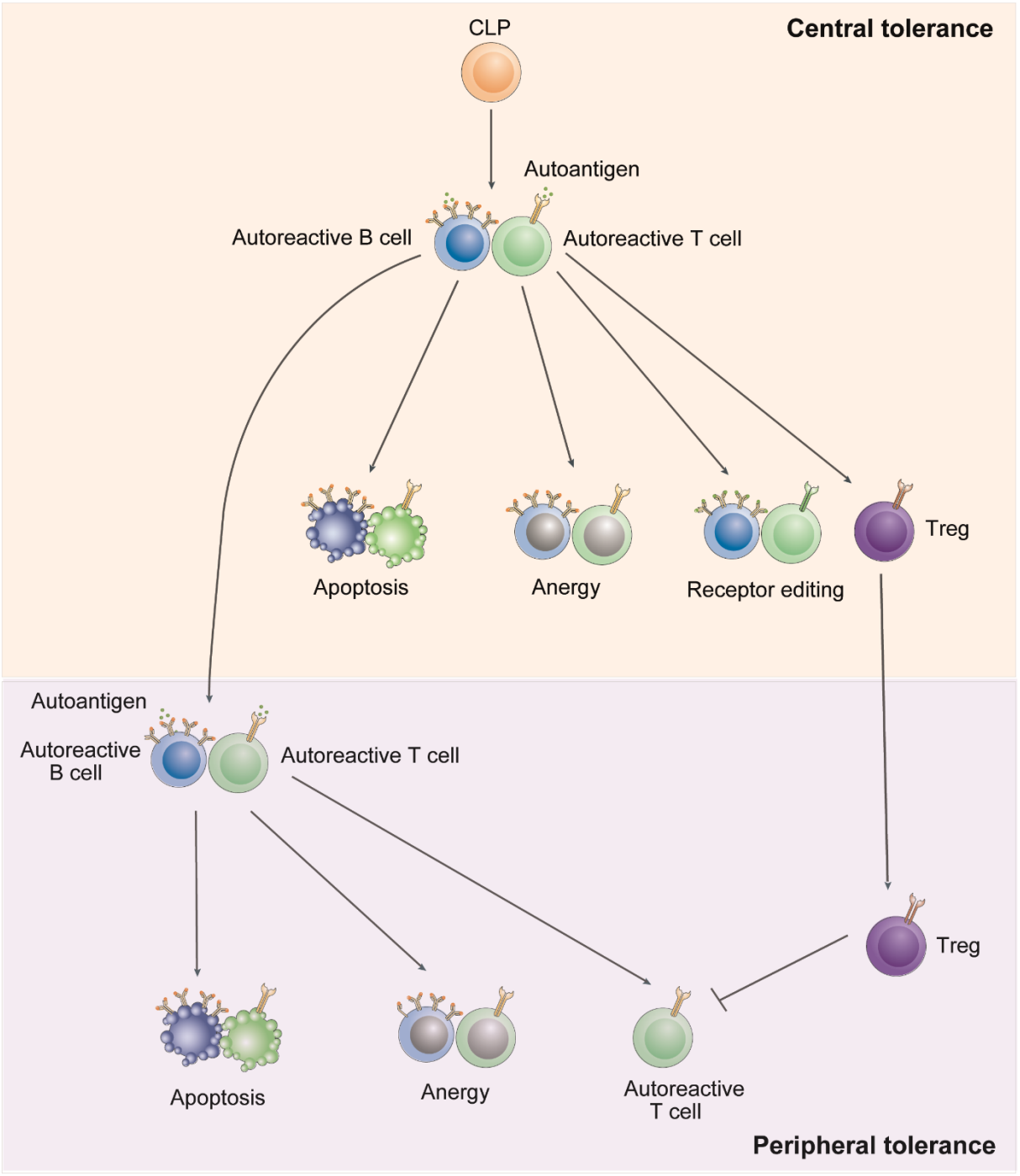

Figure 1.8 Schematic representation of immune tolerance
In central tolerance, recognition of autoantigens induces immature autoreactive B cells or T cells which undergo apoptosis, anergy or receptor editing. Additionally, autoreactive T cells can differentiate into T_{reg}. While mature lymphocytes leave primary lymphoid organs and encounter antigens in the periphery, autoreactive cells do not respond via apoptosis or anergy. Furthermore, T_{reg} cells generated during the central tolerance mechanisms can suppress autoreactive cells directly. CLP: Common lymphocyte progenitor.

1.3.2 Autoimmune disease

The breakdown of tolerance contributes to the failure of eliminating autoreactive cells, leading to recognition of self-antigens and consequently in some but not all instances causing self-destructive autoimmune disease (Miller et al., 2007). The reason responsible for tolerance breakdown is multifactorial, ranging from genetic defects to environmental factors. Gene mutations in the autoimmune regulator (AIRE) for example can break central tolerance and lead to autoimmune polyendocrinopathy syndrome type 1 (APS1), which is characterized by multiple endocrine gland dysfunctions (Akirav et al., 2011). By contrast, the autoimmune lymphoproliferative syndrome (ALPS) is characterized by impairment of peripheral tolerance (Rao and Oliveira, 2011). Failure to initial T_{reg} development by mutated forkhead box P3 (FOXP3) genes results in immune dysregulation, polyendocrinopathy and enteropathy, i.e. the X-linked syndrome (IPEX) (Gregersen and Behrens, 2006). Disorders resulting from failures to control self-tolerance are also attributed to environmental phenomena such as ischemic injury, gender, trauma, hormone dysregulation and chronic infection (Rosenblum et al., 2015). For instance, women suffer ten times higher prevalence of systemic lupus erythematosus (SLE) than men (Ngo et al., 2014).

1.4 Atherosclerosis

1.4.1 Atherosclerosis pathophysiology

Atherosclerosis is a Greek-originated term and refers to lipid accumulation and atheroma development in the innermost layer of medium to large-sized arteries, i.e. the lamina intima (Rafieian-Kopaei et al., 2014). The term is composed of two aspects: ‘atherosis’ which designates fat deposition and ‘sclerosis’ which designates excessive fibrosis (Rafieian-Kopaei et al., 2014). Atherosclerosis causes many types of cardiovascular diseases (CVDs) with organ manifestations including myocardial infarctions in the heart and ischaemic strokes in the brain, leading to globally high morbidity and mortality rates (Libby et al., 2019a). In 2021, more than 17 million people died due to CVDs, accounting for over 30% of deaths worldwide, and heart attack and stroke represented 85% of these deaths (WHO, 2021).

Despite international research efforts, the pathophysiology of atherosclerosis has not been clearly delineated. Based on a series of recent experimental data in mouse models of the disease and attempts to translate these data to human atherosclerosis, lipoproteins such as low-density lipoprotein (LDL) have been characterized to be involved in atherogenesis. While the artery receives insults from cardiovascular risk factors, blood leukocytes adhere to the intimal surface

with help of adhesion molecules expressed by endothelial cells and eventually migrate into the intima. Within the intima, monocytes differentiate into macrophages to take up lipid and yield foam cells, which is the hallmark of atherosclerosis initiation (Libby, 2021). Additionally, a set of smooth muscle cells (SMCs) undergo metaplasia and form foam cells that share markers with macrophages (Owsiany et al., 2019). Once plaques are established, the intima-resident and newly recruited SMCs undergo proliferation to thicken the intima by way of elaborating extracellular matrix macromolecules such as interstitial collagens and proteoglycans (Bennett et al., 2016). These macromolecules form the fibrous cap overlying the lipid-enriched necrotic core, which is composed of apoptotic SMCs and foam cells (Rafieian-Kopaei et al., 2014). Leukocytes secrete IFN-γ and matrix metalloproteinases (MMPs) to supress the collagen production and digest collagens, respectively, leading to weakening of the fibrous cap. The rupture of plaque occurs during the clinically important late stages of the disease thereby contributing to atherosclerotic complications (Libby et al., 2011). However, with the shift of dietary patterns and efficient lipid-lowing therapies, , an increasing number of coronary thrombosis events result from the desquamation of endothelial cells and superficial erosion which present in plaques with little or no lipid core (Libby et al., 2019b).

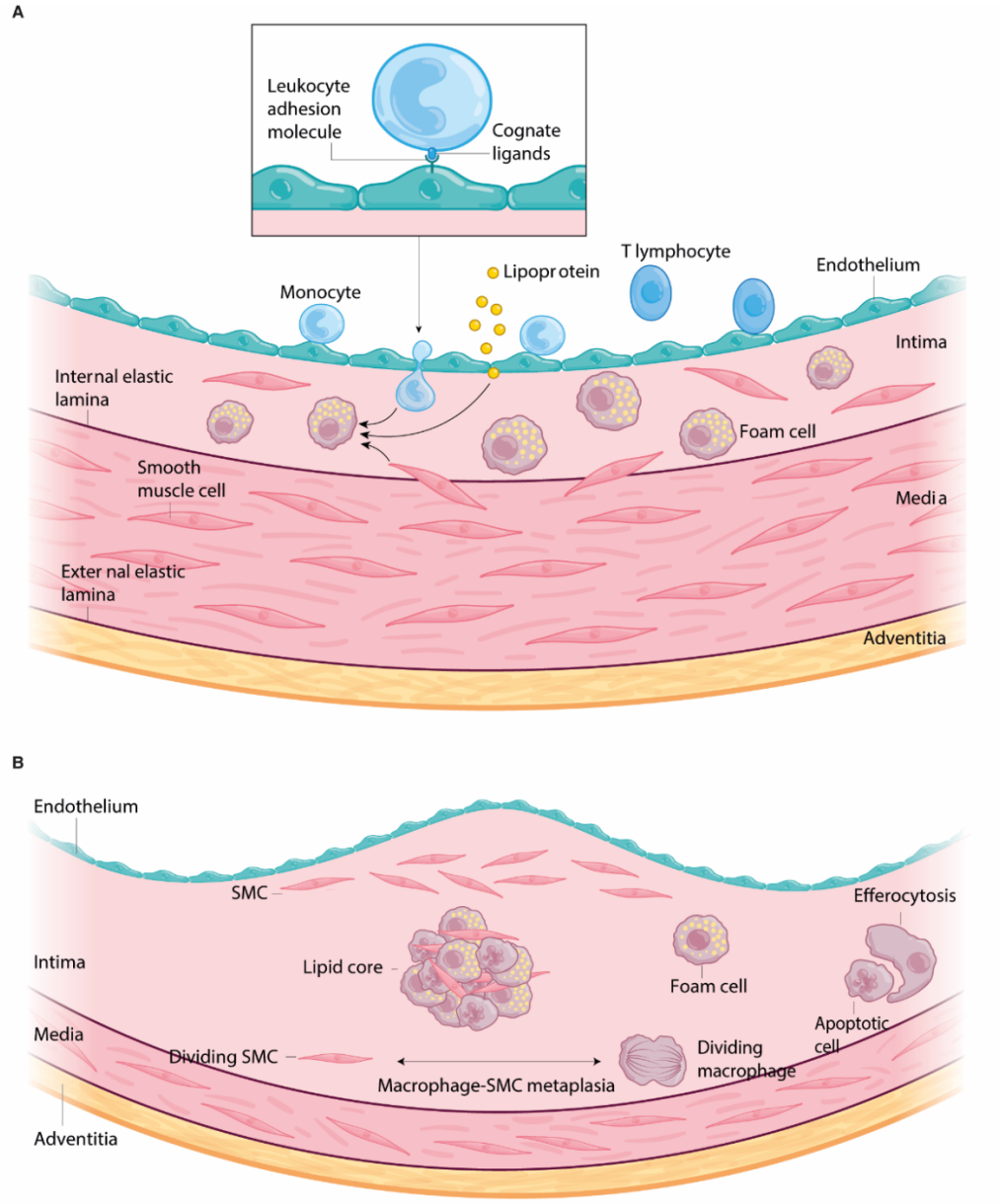

Figure 1.9 Pathophysiology of atherosclerosis
(A) Initiation of atherosclerosis. The normal artery has a three-layer structure: the adventitia, the media and the intima. Monocytes bind to adhesion molecules on the surface of endothelial cells and mature into macrophages after entering the intima, in where they uptake lipoprotein particles to form foam cells. T cells enter the intima and secrete cytokines. SMCs migrate to the intima in response to chemoattractant expressed during leukocyte infiltration. **(B)** Progression of atherosclerosis. The necrotic core is formed by accumulation of dead cells and debris remained due to inefficient efferocytosis. Fibrous caps overlying the necrotic core contain lymphocytes, SMCs and collagen-rich fibrous tissues. Thinning of the fibrous cap impairs the collagen by increasing collagen breakdown eventually leading to rupture and thrombosis (Modified from Libby et al., 2019a, Libby, 2021).

1.4.2 Atherosclerosis inflammation and artery tertiary lymphoid organs (ATLOs)

Evidence identifies atherosclerosis as a chronic inflammatory disease (Libby, 2021). The 'Canakinumab Anti-inflammatory Thrombosis Outcomes Study' (CANTOS) confirmed that neutralizing the IL-β with Canakinumab in patients which recovered from myocardial infarction would reduce the possibility of recurring CVDs (Ridker et al., 2017). Additionally, the anti-inflammatory agent colchicine is beneficial to reduce the recurrent CVD events in patients used to suffer from acute coronary syndromes (ACS) (Nidorf et al., 2020). During atherosclerosis progression, several types of immune cells are recruited to the plaque with the help of leukocyte adhesion molecules expressed by endothelial cells (Hansson and Libby, 2006). Monocyte-derived macrophages outnumber other immune cells in the plaque and mainly produce pro-inflammatory mediators (Gistera and Hansson, 2017). Uptake of modified lipoproteins mediated by scavenger receptors expressed on macrophages, contributes to proinflammatory events in the artery wall (Moore and Freeman, 2006). T cells are also abundant in the plaque. $CD4^+$ T cells may originate in the LNs and migrate into plaques (Angeli et al., 2004). They mainly produce pro-inflammatory cytokines such as IFN-γ and tumour necrosis factor (TNF) to activate other cells of the plaque and may trigger inflammation (Buono et al., 2003). However, regulatory $CD4^+$ T cells secrete anti-inflammatory cytokines and suppress pro-inflammatory T cells to exert a protective function of atherogenesis (Foks et al., 2015). $CD8^+$ T cells account for a substantial population in human and mouse plaque (Fernandez et al., 2019, Zernecke et al., 2020).They have also been reported to promote inflammation by secretion of TNFα (Kyaw et al., 2013). Whether significant numbers of B cells occur in plaques is controversial, while B cells in spleen and LN show both anti- and pro-atherogenic functions (Wolf and Ley, 2019). The innate B-1 cells are atheroprotective, whereas some adaptive B-2 cell subsets aggravate inflammation (Gillotte-Taylor et al., 2001, Kyaw et al., 2010).

The immune response of atherosclerosis is not restricted to plaque and draining LNs. Tertiary lymphoid structures were characterised as lymphoid aggregates adjacent to lesions in advanced atherosclerosis in mice and humans (Galkina et al., 2006, Grabner et al., 2009, Akhavanpoor et al., 2018). The normal adventitia contains a limited number of immune components, including few T cells, few conventional DCs (cDCs) and few macrophages. In response to inflammatory stress, however, both innate and adaptive immune cells are capable of infiltrating the adventitia, and the diseased adventitia promotes lymph vessel neogenesis and angiogenesis. ATLOs are located adjacent to lesions in abdominal adventitia of aged *Apoe*$^{-/-}$ mice and in coronary arteries in humans among other territories. It has been reported that there is a correlation between the

stage and size of ATLOs and the severity of atherosclerosis. *ATLO Stage I*: This stage forms parallel to the formation of plaques. The infiltration of B cells begins, but without separated T cell and B cell zones. *ATLO stage II*: Separated T and B areas are observed. This stage also involves the appearance of new lymph vessels, high endothelial venules (HEVs) and LN-like conduits. *ATLO stage III*: The advanced ATLOs contain separate T cell areas, B cell follicles harbouring FDCs in activated GC and niches of PCs (Mohanta et al., 2014, Yin et al., 2016). The formation of ATLOs indicates that they may be involved in the control of atherosclerosis progression. In mouse ATLOs, naïve $CD4^+$ T cells are recruited to generate $CD4^+$ and $CD8^+$ effector and memory T cells, as well as $CD4^+$ T_{reg} cells (Hu et al., 2015). Clement and colleagues suggested that under the assistance of T_{FH} cells, GC B cells are activated and differentiate in both secondary lymphoid organs (SLOs) and ATLOs. This T_{FH}-GC B cell axis is regulated by $CD8^+$ T_{reg} cells to limit the disease development (Clement et al., 2015).

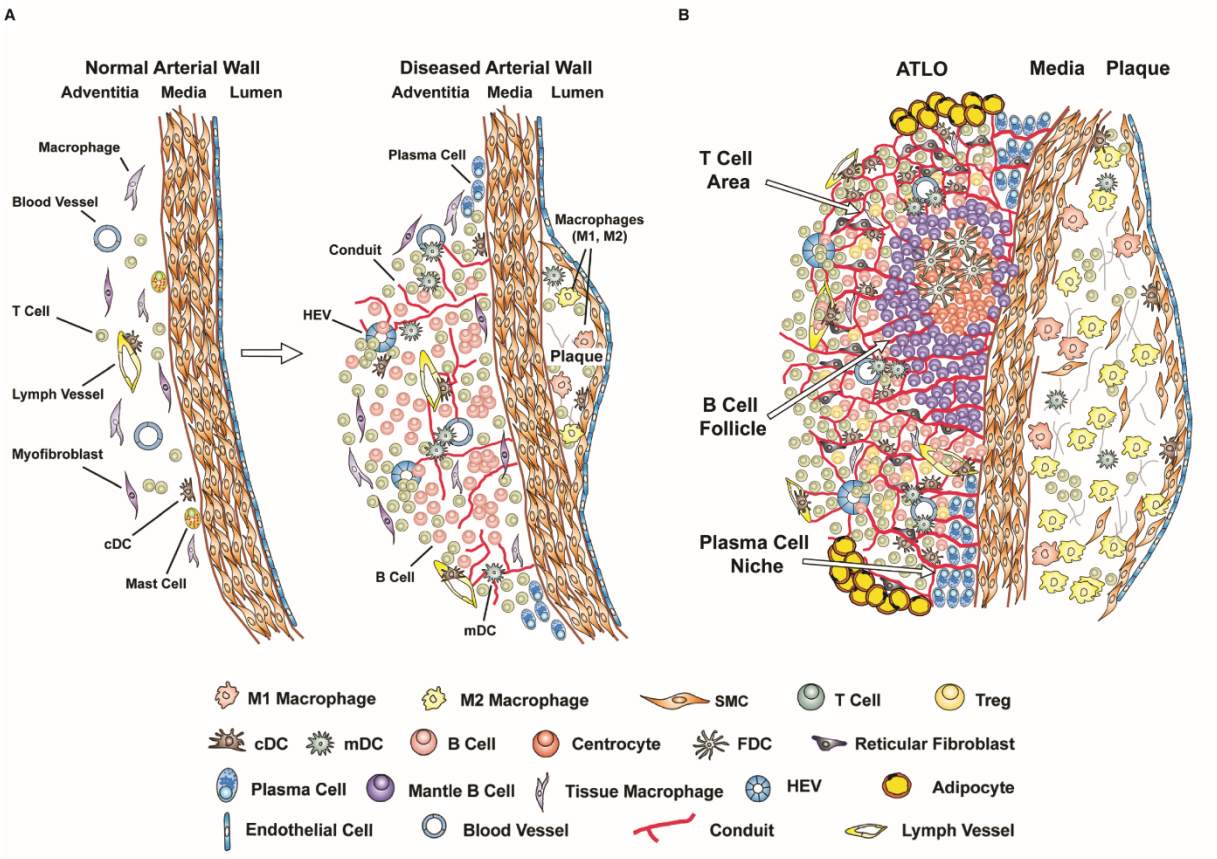

Figure 1.10 Structure of ATLOs in the abdominal aorta of aged apolipoprotein E-deficient (*Apoe*$^{-/-}$) mice
(A) The normal adventitia contains multiple immune cell subsets. During disease progression, the adventitia undergoes multiple types of restructuring including recruitment of various lymphocyte subsets and a variety of other leukocytes to generate a dense immune cell aggregate. ATLOs are exclusively observed adjacent to plaques. **(B)** ATLOs are organised into T cell areas,

B cell follicles and PC niches. ATLO neogenesis and its cellular constituents indicate both anti- and pro-inflammatory roles. mDC: monocyte-derived DC. (Taken from Mohanta et al., 2014).

1.4.3 The role of B cells in atherosclerosis

B cell subsets have been shown to have both atherogenic or atheroprotective roles depending on the subpopulations, pathways involved, stage of disease, experimental design and the mouse model used among multiple other factors. B-1 B cells developed from fetal liver and adult BM are involved in innate immune response. They can spontaneously secrete natural antibodies which have been suggested to be responsible for the neutralization of pro-inflammatory factors to limit pathogenesis (Baumgarth, 2011). Nearly 1/3 of natural IgM antibodies are capable of recognizing oxidation-specific epitopes (OSEs), which are considered as antigens to induce inflammation in atherosclerosis through activating endothelial cells and recruiting immune cells (Chou et al., 2009, Binder et al., 2016). Horkko and colleagues successfully cloned B-1-derived IgM antibodies from hypercholesterolemic mice, and these antibodies showed a protective effect on atherosclerosis by suppressing macrophages to take up oxidised LDLs (ox-LDLs) (Horkko et al., 1999). Contrarily, the conventional B-2 B cells are involved in adaptive immune response through T cell-dependent pathways that require affinity maturation. The role of B-2 cells in atherosclerosis is complicated. Some studies have reported that increased levels of IgG antibodies that bind to modified LDLs positively correlate with atherosclerosis in human (Ravandi et al., 2011, Prasad et al., 2017). Alternatively, Centa et al. reported reduced size of atherosclerotic plaques following transfer of $Pax5^{fl/-}$Aicda-Cre*Apoe*$^{-/-}$ BM into *Apoe*$^{fl/-}$ $ROSA26^{CreERt2/+}$ mice to specifically delete GC B cells. This study suggested that restraining GC reactions could attenuate murine atherosclerosis (Centa et al., 2018). Recent studies also pointed out that self-reactive antibodies that target precipitated aldehyde dehydrogenase 4 family member A1 (ALDH4A1) to trigger T cell-dependent responses retard the progression of atherosclerosis (Lorenzo et al., 2020). Besides the direct recognition and clearance of pathogens, B cells also influence atherogenesis by regulating the cellular immune responses and releasing cytokines. It has been reported that a complete deficiency of mature B-2 cells impeded the development of atherosclerosis due to the reduction of T cell responses (Ait-Oufella et al., 2010). Furthermore, proatherogenic roles have been identified on GM-CSF-producing B cells through the elevation of $CD4^+$ T cells (Hilgendorf et al., 2014). Regulatory B (B_{reg}) cells produce cytokines such as IL-10 and TNFβ to suppress immune responses. Gjurich et al. showed that decreasing aortic B_{reg} cells leads to decline of IL-10, which is associated with enhanced atherogenesis in mice (Gjurich et al., 2014). Storm and colleagues stated that the B_{reg} subset with $CD21^{hi}CD23^{hi}$CD24hi features is beneficial in *Apoe*$^{-/-}$ mice (Strom et al., 2015).

1.5 Objective

The underlying hypothesis of this thesis is that the presence of FDCs and proliferating B cells in GCs of ATLOs indicates that ATLO GC B-2 cells are involved in an autoimmune response directly against arterial wall-derived autoantigens. In fact, B-2 cells isolated from ATLO GCs using single-cell cloning technology by our colleagues have been identified to recognize autoantigen histone H2b and promote atherosclerosis in mice, supporting ATLOs organize autoimmune response in atherosclerosis (Zhang, 2022). However, due to the limitation of techniques, this is a biased investigation that could not systemically reveal the role of B cells in atherosclerosis. In order to approach the hypothesis and understand B cell autoimmune response in relation to atherosclerosis, aged *Apoe*$^{-/-}$ mice served as an experimental model and the bulk BCR repertoire, which shapes and reflects the immune landscape, was systematically analysed using NGS. Meanwhile, the combined single B cell transcriptome and the heavy-light chain paired BCR information was assessed by using single-cell RNA sequencing (scRNA-seq) technology. In particular, the following specific questions were addressed:

1. Is there a GC-dependent B-2 cell immune response in ATLOs?

2. Are immune tolerance checkpoints disrupted during early hyperlipidaemia or atherosclerosis in *Apoe*$^{-/-}$ mice?

3. Are immune tolerance checkpoints specifically breached in ATLOs?

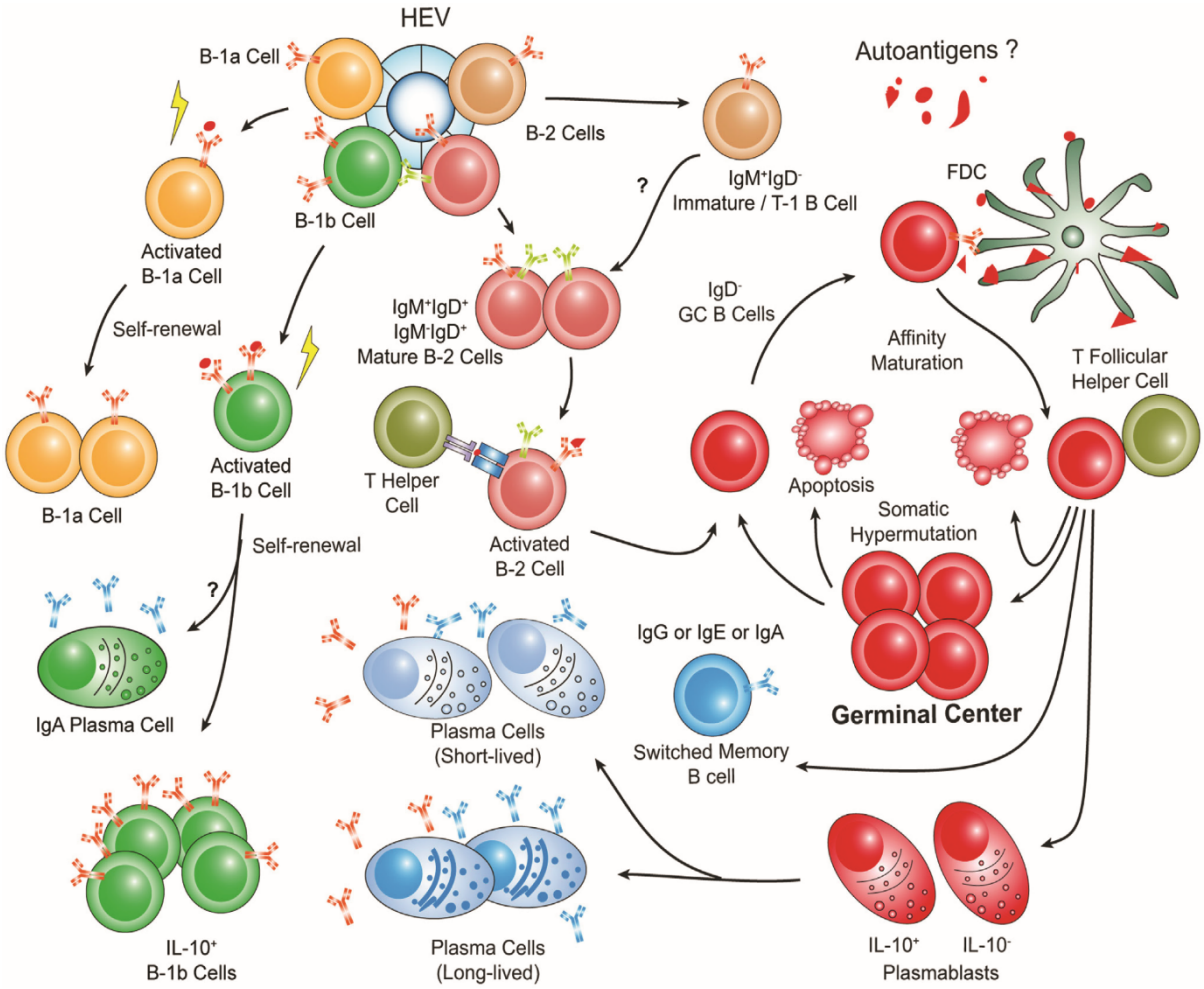

Figure 1.11 Hypothetical B cell response pathways in ATLOs
Circulating B-1 cells or mature naïve B-2 cells enter ATLOs through HEVs. B-1 cells activate and self-renew while encountering inflammatory to form B-1a and B-1b cells. B-2 cells undergo T-dependent GC response to generate memory B cells and PCs with high affinity BCRs. (Taken from Yin et al., 2016).

2 Materials and Methods

2.1 Materials

2.1.1 Mice

Wild type (WT) C57BL/6J and *Apoe*$^{-/-}$ mice on the C57BL/6J background were purchased from the Jackson Laboratories and maintained in the animal facility of Ludwig-Maximilians-Universität München (LMU) under specific pathogen-free conditions. All mice were fed with standard rodent chow and kept under a 12-hour light/dark cycle. Animal procedures were performed in strict adherence to guidelines of the local Animal Use and Care Committee and the National Animal Welfare Laws approved by the Regierung of Oberbayern.

2.1.2 Antibodies

Table 2-1: List of antibodies

Target antigen	Clone	Conjugation	Dilution	Company	Storage
Primary antibodies					
CD19	eBio1D3	APC	1:200	eBioscience	4 °C
CD24	30-F1	FITC	1:200	eBioscience	4 °C
CD43	eBioR2/60	PE	1:200	eBioscience	4 °C
CD45	30-F11	PerCP/Cy5.5	1:200	eBioscience	4 °C
GL7	GL-7	Biotin	1:200	eBioscience	4 °C
IgD	11-26c	V450	1:200	eBioscience	4 °C
IgM	II/41	PE-Cy7	1:200	eBioscience	4 °C
PNA	-	FITC	1:200	Vector	4 °C
Secondary antibodies					
Streptavidin	-	APC-eFluor™ 780	1:200	eBioscience	4 °C
Fluorescence dyes for dead cells					
Fixable viability dye (FVD)		APC-Cy7	1:1000	eBioscience	-80 °C
Isotype controls					
Invitrogen™ UltraComp eBeads™ compensation beads	-	-	1 drop	Thermo Fisher Scientific	4 °C

2.1.3 Reagents and kits

Table 2-2: List of reagents and kits

Name	Company	Storage	Application
CD138 microbeads, mouse	Miltenyi Biotec	4 °C	Cell purification
Chromium chip A single cell kit, 16 rxns	10x Genomics	Room temperature (RT)	10x library construction
Chromium i7 multiplex kit, 96 rxns	10x Genomics	-20 °C	10x library construction
Chromium single cell 5' library and gel bead kit, 4 rxns	10x Genomics	variable	10x library construction
Chromium single cell 5' library construction kit, 16 rxns	10x Genomics	-20 °C	10x library construction
Chromium single cell V(D)J enrichment kits, mouse	10x Genomics	-20 °C	10x library construction
DNF-910 dsDNA reagent kit	Advanced Analytical	variable	Library quality control
EB buffer	Qiagen	RT	Library construction
Encyclo plus PCR kit	Evrogen	-20 °C	Repertoire library construction
Fetal bovine serum (FBS)	Gibco	-20 °C	FACS
KAPA HiFi HotStart ReadyMix(2X)	Kapa Biosystems	-20 °C	Repertoire library construction
NEBNext Library Quant kit	New England BioLabs	-20 °C	Library quality control
Nextera® index kit	Illumina	-20 °C	Repertoire library construction
Qubit™ 1X dsDNA HS assay kit	Thermo Fisher Scientific	RT	Library quality control
RNaseZap™ RNase decontamination solution	Thermo Fisher Scientific	RT	RNA extraction

RNasin® plus ribonuclease inhibitors	Promega	-20 °C	Repertoire library construction
RNeasy mini Kit	Qiagen	RT	RNA extraction
SMARTScribe reverse transcriptase	TaKaRa	-20 °C	Repertoire library construction
SPRIselect	Beckman Coulter	RT	PCR product purification
TRIzol® reagent	Thermo Fisher Scientific	4 °C	RNA extraction
Uracil-DNA Glycosylase (UDG)	New England BioLabs	-20 °C	Repertoire library construction

2.1.4 Chemicals

Table 2-3: List of chemicals

Name	Company	Storage	Application
Acetic acid, glacial	SIGMA	RT	TAE buffer
Collagenase I (125 CDU/mg)	SIGMA	-20 °C	Enzyme cocktail
Collagenase XI (1200 CDU/mg)	SIGMA	-20 °C	Enzyme cocktail
DNAse I (2000 U/mg)	Carl Roth	-4 °C	Enzyme cocktail
Dulbecco's phosphate-buffered saline (DPBS)	GIBCO	RT	Enzyme cocktail, fluorescence-activated cell sorting (FACS)
EDTA	SIGMA	RT	EDTA
Ethanol absolute	VWR	RT	Library construction
Glycerol	MERCK	RT	10x library construction
HCI	Carl Roth	RT	pH adjustment
HEPES	SIGMA	RT	Enzyme cocktail
Hyaluronidase (400-1000 U/mg)	SIGMA	-20 °C	Enzyme cocktail
10% Ketamine	Medistar	RT	Mice anesthetization
$KHCO_3$	MERCK	RT	ammonium-chloride-potassium (ACK) buffer
$Na_2EDTA•2H_20$	SIGMA	RT	ACK buffer

NaOH	Carl Roth	RT	pH adjustment
NH_4Cl	SIGMA	RT	ACK buffer
Phenol/ chloroform/ isoamyl alcohol	Carl Roth	4 °C	RNA extraction
Sedaxylan	Ecuphar	RT	Mouse anesthetization
Tris	SIGMA	RT	TAE buffer
Tween 20	SIGMA	RT	10x library construction

2.1.5 Solutions and buffers

Table 2-4: List of solutions and buffers

Name	Chemical composition	Amount	Storage	Application
5X enzyme cocktail stock solution	Collagenase I	540 mg	-20 °C	Aorta digestion
	Collagenase XI	15.6 mg		
	Hyaluronidase	20.4 mg		
	DNAse I	4.5 mg		
	HEPES	714.6 mg		
	DPBS	30 ml		
0.5M EDTA (1L), pH = 8	EDTA	186.12g	RT	Tissue collection
	Distilled water	1 L		
	Adjust pH to 8			
FACS buffer	FBS	4 ml	4 °C	FACS
	DPBS	196 ml		
magnetic-activated cell sorting (MACS) buffer	FBS	2 ml	4 °C	Cell purification
	50 mM EDTA	4 ml		
	DPBS	94 ml		
1X ACK lysis buffer	NH_4Cl	8.92 g	RT	Erythrocyte lysis
	$KHCO_3$	1 g		
	$Na_2EDTA•2H_20$	0.354 g		
	Distilled water	1 L		
	Adjust pH to 7.2 - 7.4			
50X tris-acetat-EDTA (TAE) buffer	Tris	242 g	RT	Gel electrophoresis
	Acetic acid, glacial	57.1 ml		
	0.5 M EDTA, pH = 8	100 ml		
	Add distilled water to 1L			
10M NaOH	NaOH	40 g	RT	pH adjustment
	Distilled water	100 ml		
37% HCl	HCl	37 ml	RT	pH adjustment
	Distilled water	63 ml		
50% glycerol	Glycerol	5 ml	-20 °C	10X library construction
	RNase-free water	5 ml		
10% Tween 20	Tween 20	100 µl	-20 °C	10X library construction
	RNase-free water	900 µl		

2.1.6 Primers

Table 2-5: List of primers used for repertoire library construction

Primer	Application	Sequence	Concentration (nM)
First strand cDNA synthesis			
5'-adapter			
SmartNNN+G	Template switch adapter with unique molecular identifiers (UMIs), universal for all libraries	/5Biosg/AAGCAGUGGTAUCAACGCAG AGUNNNNUNNNNUNNNNUCTTrGrG+G	20
3'-primer			
cIgA-1	Primer for cDNA synthesis, mouse IgA heavy chain	TGGGAAGTTTACGGTG	20
cIgG-1	Primer for cDNA synthesis, mouse IgG heavy chain	AGAAGGTGTGCACACCG	20
cIgM-1	Primer for cDNA synthesis, mouse IgM heavy chain	GGGAAGGTTCTGATACC	20
First PCR amplification			
5'-primer			
Step-1	Step-out primer 1, universal for all libraries	CACTCTATCCGACAAGC AGTGGTATCAACGCAG	10
3'-primer			
MFA-3	Nested primer 1, mouse IgA heavy chain	GGTGGGAAGTTTACGGT GGTTATATCC	10
MFG-1	Nested primer 1, mouse IgG heavy chain	AGAAGGTGTGCACACCG CTGGAC	10
MFM-1	Nested primer 1, mouse IgM heavy chain	TGGGAAGGTTCTGATAC CCTGGATG	10
Second PCR amplification			
5'-primer			
TSO2	Step-out primer 2, universal for all libraries	TCGTCGGCAGCGTCAGA TGTGTATAAGAGA CAG(N)CAGTGGTATCAA CGCAGAG	10
3'-primer			
AS-2	Nested primer 2, mouse IgA heavy chain	GTCTCGTGGGCTCGGAG ATGTGTATAAGAGA CAG(N)TGTCAGTGGGTA GATGGTG	10
1/2GS-2	Nested primer 2, mouse IgG1 and IgG2 heavy chain	GTCTCGTGGGCTCGGAG ATGTGTATAAGAGA CAG(N)AGTGGATAGACM GATGG	10
3GS-1	Nested primer 2, mouse IgG3 heavy chain	GTCTCGTGGGCTCGGAG ATGTGTATAAGAGA	10

		CAG(N)AAGGGATAGACA GATG	
MS-2	Nested primer 2, mouse IgM heavy chain	GTCTCGTGGGCTCGGAG ATGTGTATAAGAGA CAG(N)GGGGGAAGACAT TTGG	10
Index ligation			
5' primer			
Index 2	Illumina P7 primer with index	CAAGCAGAAGACGGCAT ACGAGAT[i7]GTC TCGTGGGCTCGG	-
3' primer			
Index 1	Illumina P5 primer with index	AATGATACGGCGACCAC CGAGATCTACAC[i5]TCG TCGGCAGCGTC	-

2.1.7 Equipment

Table 2-6: List of equipment

Name	Company	Application
10x chip holder	10x Genomics	10x library construction
10x magnetic separator	10x Genomics	10x library construction
10x vortex adapter	10x Genomics	10x library construction
Applied Biosystems 7900HT fast real-time PCR system	Thermo Fisher Scientific	Library quality control
BD FACSAria III Cell Sorter	BD Biosciences	FACS
BP2100S analytical balance	Sartorius	Enzyme cocktail preparation
C1000 touch™ thermal cycler	BIO-RAD	10x library construction
Chromium controller	10x Genomics	10x library construction
DynaMag™ - 96 side skirted	Thermo Fisher Scientific	Repertoire library construction
Electrophoresis power supply	CONSORT	Gel electrophoresis
Eppendorf Research® plus single channel pipette, 0.1 - 2.5 µl	Eppendorf	Library construction
Eppendorf Research® plus single channel pipette, 0.5 - 10 µl	Eppendorf	Library construction
Eppendorf Research® plus single channel pipette, 10 - 100 µl	Eppendorf	Library construction
Eppendorf Research® plus single channel pipette, 100 - 1000 µl	Eppendorf	Library construction
Eppendorf Research® plus single channel pipette, 2 - 20 µl	Eppendorf	Library construction
Eppendorf Research® plus single channel pipette, 20 - 200 µl	Eppendorf	Library construction
Fragment analyzer	Advanced Analytical	Library quality control
Galaxy mini centrifuge	VWM	Repertoire library construction

Gel Doc EQ System	BIO-RAD	Gel electrophoresis
Heraeus Biofuge Fresco microcentrifuge	Thermo Fisher Scientific	RNA extraction
Heraeus megafuge 40R centrifuge	Thermo Fisher Scientific	FACS
HI 2211 pH/ORP meter	Hanna Instruments	pH adjustment
IKAMAG® RET maganetic stirrer	Janke & Kunkel (IKA)	pH adjustment
Innova 4230 refrigerated incubator shaker	New Brunswick Scientific	Aorta digestion
Leica DMil inverted microscope	Leica	FACS
Liebherr nofrost safe fridge	Liebherr	Storage
Liebherr premium fridge	Liebherr	Storage
Microwave oven	Fireline	Gel electrophoresis
NanoDrop 1000 spectrophotometer	Thermo Fisher Scientific	RNA extraction
New Brunswick ultra-low temperature	Eppendorf	Storage
Pipet-Lite™ XLS+ manual 8-channel pipette, 20-200 µl	Rainin	Library construction
Pipet-Lite™ XLS+ manual 8-channel pipette, 2-20 µl	Rainin	Library construction
Precision balacne S72	KERN	Gel electrophoresis
Qubit 3.0 fluorometer	Thermo Fisher Scientific	Library quality control
R160P analytical balance	Sartorius	Enzyme cocktail preparation
Scotsman flake ice machine AF 80	Scotsman Ice System	Library construction
Sub-Cell GT Cell	BIO-RAD	Gel electrophoresis
T100™ thermal cycler	BIO-RAD	Repertoire library construction
TC20™ automated cell counter	BIO-RAD	10x library construction
Thermomixer 5436	Eppendorf	Gel purification
Vortex shaker VF2	Janke & Kunkel	Library construction
VWR Signature™ ergonomic high performance multichannel pipettor, 20-200 µL	VWM	Library construction

2.1.8 Consumables

Table 2-7: List of consumables

Name	Company
Applied Biosystems™ MicroAmp® 8-cap strip	Thermo Fisher Scientific
Applied Biosystems™ MicroAmp® 8-tube strip (0.2 ml)	Thermo Fisher Scientific
Applied Biosystems™ MicroAmp® fast 96-well reaction plate (0.1ml)	Thermo Fisher Scientific
BD DISCARDIT II syringe, 10 ml	BD
BD DISCARDIT II syringe, 2 ml	BD
Cell counting slides for T210 ™ cell counter	BIO-RAD
Eppendorf PCR Tubes, 0.2 ml	Eppendorf

Eppendorf Safe-Lock Tubes, 0.5 ml	Eppendorf
Eppendorf Safe-Lock Tubes, 1.5 ml	Eppendorf
Eppendorf twin.tec® PCR plates 96, unskirted, clear	Eppendorf
Falcon® 5 ml round-bottom polystyrene tube	Corning
Falcon® 70 µm cell strainer	Corning
Haemacytometer cover glass	Thermo Fisher Scientific
MS columns	Miltenyi Biotec
Neubauer chamber	Merck
Omnifix® 100 solo syringe, 1 ml	B.Braun
Qubit™ assay tubes	Thermo Fisher Scientific
TipOne® filter tip (sterile), 10 µl	Star Lab
TipOne® filter tip (sterile), 1000 µl	Star Lab
TipOne® filter tip (sterile), 200 µl	Star Lab
TipOne® tip, refill, 10 µl	Star Lab
TipOne® tip, refill, 1000 µl	Star Lab
TipOne® tip, refill, 200 µl	Star Lab
Tips LTS 200UL filter RT-L200FLR	Rainin
Tips LTS 20UL filter RT-L10FLR	Rainin
Tube, 15 ml, 120x17 mm, PP	Sarstedt
Tube, 50 ml, 120x17 mm, PP	Sarstedt

2.2 Methods

2.2.1 Mouse dissection and tissue collection

Mice were anesthetized with 0.5 ml anaesthetics (containing 10% ketamine and 20mg sedaxylan, diluted with DPBS) through intraperitoneal injection. The genotype, sex, age and weight of mice were documented. For tissue collection, peritoneal cavities (PerC) were washed with 10 ml FACS buffer to collect lavage; blood was taken by heart puncture. The mice were perfused with 10 ml EDTA, 20 ml DPBS, followed by 20 ml FACS buffer. After perfusion, renal LNs (RLNs), spleens, aortas were isolated. BM was collected by flushing the femur and tibia with 10 ml FACS buffer. All tissues were kept on ice until further processing.

2.2.2 Single cell suspension preparation

The collected tissues were cut into pieces and crushed to pass 70 μm^2 strainers. Aorta samples were digested with 2.5 ml enzyme cocktail at 37 °C for 45 min before processing to filter. The filtered cell suspension was centrifuged under 300 x g for 5 min. After discarding the supernatant, 5 ml Ack lysis buffer was added to spleen, blood, and BM samples to lyse red blood cells. The lysis lasted for 5 min at RT, followed by twice washing to remove cell debris and residual lysis buffer. Cells were resuspended in 1 ml FACS buffer and filtered through 100 μm^2 filters before counting. The cell number was determined using Neubauer chamber under the microscope.

2.2.3 PC purification

PCs from spleen, RLNs, blood, BM and aorta were isolated by utilizing CD138 mouse microbeads. According to the protocol (Miltenyi Biotec, 2012), cells were centrifuged to pipette off the supernatant and resuspended in 40 µl ice-cold MACS buffer per 10^7 cells. 10 µl microbeads per 10^7 cells were added to incubate 20 min at 4° C. The incubation was terminated with 1-2 ml ice-cold MACS buffer per 10^7 cells and centrifuged to collect cells. Cells were then re-suspended with 500 µl MACS buffer. The cell suspension was applied onto the MACS MS columns and placed on the separator. The unlabelled cells were collected for subsequent B cell sorting. The magnetic-labelled PCs were flushed out using 1 ml MACS buffer when removing the columns from the separator.

2.2.4 Cell staining and sorting

The APC-Cy7-conjugated FVD was stained to label live cells which are FVD-negative. For BCR Rep-seq, the FACS was performed relying on CD45-PerCP/Cy5.5, CD19-APC, IgD-V450, IgM-PE/Cy7, CD24-FITC, CD43-PE, GL7-biotin and PNA-FITC. Total B cells were sorted as $CD45^+CD19^+$ cells. The immature naïve B cells were determined as $CD45^+CD19^+IgM^+IgD^-CD24^+CD43^-$ cells, and the mature naïve B cells were isolated as $CD45^+CD19^+IgM^+IgD^+CD24^-CD43^-$ cells. The GC B cells from spleen was sorted as $CD45^+CD19^+IgD^-GL7^+PNA^+$. All cells were sorted into 2 ml FBS, and the sorted samples were centrifuged to discard the supernatant and stored in 1 ml Trizol at -80 °C until RNA extraction. For scRNA-seq, $CD45^+$ cells were sorted into a cold tube pre-rinsed with FACS buffer. Cell number and viability were determined by using of TC20™ automated cell counter. The cells were maintained on ice until loaded to the Chromium controller.

2.2.5 RNA isolation

To construct the library for Rep-seq, mRNA was isolated according to a modified protocol using the RNeasy mini kit (Yin et al., 2015). Briefly, 200 µl choroform per sample was added to samples which stored in Trizol. After sharp shaking and centrifuging, the supernatant was transferred to a new column. 280 µl ethanol was added to the supernatant, followed by rinsing with 500 µl RW1 buffer, 500 µl RPE buffer and 500 µl 80% ethanol. Finally, RNA was eluted with 10 µl RNase-free water and their quality were checked by NanoDrop ND-1000 spectrophotometer. The RNA concentration was adjusted to 10 - 100 ng/µl before library construction.

2.2.6 Library construction

2.2.6.1 BCR heavy chain Rep-seq library construction and sequencing

The whole library construction protocol was modified from the paper published by Mamedov et al. (Mamedov et al., 2013). The reverse transcription of cDNA was performed in 10 µl reaction system: 2 µl RNA templates were combined with 1.5 µl IgA/ IgG/IgM mixed heavy chain reverse primer and incubated for 2 min at 72° C. The mixture was immediately cooled on ice and a second mixture comprising 2 µl first-strand buffer (5X), 1 µl DTT (20 mM), 1 µl dNTP, 1.5 µl UMI-contained template switch adapter, 1 µl SMARTScribe™ reverse transcriptase (10X) and 0.25 µl RNase inhibitor (40U/µl) was added to the mixture. The new reaction mixture was incubated at 42 °C for 60 min and followed by 10 min at 70 °C. 10 µl

uracil DNA glycosylase which consisted with 6 µl RNase-free water, 2 µl 10X UDG reaction buffer and 2 µl UDG was applied to the cDNA synthesis products with 1-hour incubation at 37 °C to hydrolyse the residual template switch adaptors.

Two rounds of nested PCR cycles were performed to amplify cDNA products. In each round, 5 µl template was mixed with 20 µl reaction mixture (14.5 µl sterile PCR water, 2.5 µl 10X Encyclo buffer, 0.5 µl 50X dNTP, 0.5 µl 50X Encyclo polymerase mix, 1 µl universal 5' primer and 1 µl 3' reverse primer mix). The condition of thermal cycling was set as 94 °C/2 min; 95 °C/20 s, 65 °C/20 s, 72 °C/50 s (repeated 20 cycles for the 1st round PCR and 18 cycles for the 2nd round PCR); 72 °C/5 min and followed by 10 s at 12 °C. The PCR products in each round were purified using SPRIselect reagent following the standard protocol (Picelli et al., 2014).

Since part of Illumina index sequences had been introduced to the amplified cDNA products through the 2nd round PCR, the distinct combination of Illumina indices was ligated by an additional round of PCR. 25 µl reaction mixture (1 µl template containing 1 ng purified PCR products, 6.5 µl sterile PCR water, 12.5 µl 2X KAPA HiFi ready mix, 2.5 µl Nextera XT index primer 1, 2.5 µl Nextera XT index primer 2 and 1 µl Nextera XT index primer 1) was carried out at the thermal cycling condition: 72 °C/3 min; 95 °C/3 min; 95 ° C/30 s, 55 °C/30 s, 72 °C/30 s (repeated 8 cycles); 72 °C/5 min; 12 °C/10 s. The index-ligated products were cleaned with SPRIselect reagent and pooled together equivalently for sequencing. Before loading to the sequencer, the concentration of pooled libraries was measured by Qubit and NEBNext library quant kit. The size of libraries was also checked using the Agilent bioanalyzer. Only libraries of high quality were loaded onto Illumina MiSeq platform and subjected to 2 x 300 bp paired-end sequencing, with 1% of PHiX spike-in as control library.

2.2.6.2 scRNA-seq 5' gene expression and immune profile library construction

The single-cell transcriptome library and B cell V(D)J library were prepared using Chromium single cell V(D)J reagent kits following the standard guidance. The single-cell suspension was loaded onto the Chromium chip with gel bead-in-emulsions (GEM) and reverse transcription mixture, targeting recovering 3000 single cells for each sample. The reverse transcription and following library construction were performed using C1000 Touch thermal cycler. Totally 14 cycles were set for cDNA amplification. 5' gene expression libraries or BCR libraries were pooled together with the same quality for sequencing. The size range of final libraries was

checked on a fragment analyser, and the concentration was determined using both Qubit and NEBNext library quant kit. Pooled libraries were sequenced by Illumina NextSeq 500 sequencer with 26 + 91 bp paired-end sequencing for the 5' gene expression library and 2 x 150 bp paired-end sequencing for the B cell V(D)J enriched library (Wang et al., 2022).

2.2.7 Raw data quality control and pre-processing

The sequences of each sample were split based on their unique index combination. The quality of FASTQ files contained raw sequence data was controlled with FastQC (version 0.11.5) software (Andrews, 2010). Sequences in the repertoire libraries were trimmed from 3' end using the PRINSEQ (version 0.20.4) tool to remove bases which had a Phred-like score lower than 20. And the sequences whose length were shorter than 250 bp were also discarded (Schmieder and Edwards, 2011).

2.2.8 Data processing

2.2.8.1 Rep-seq data processing

The UMIs are 8-22 random nucleotides added via template-switch oligos during cDNA reverse transcription. Constructing UMI-based libraries allows reduction of PCR amplification biases and correction of sequencing errors as well as ambiguities in combination with advanced algorithms and software (Kivioja et al., 2011, Kinde et al., 2011, Shugay et al., 2014). With the help of the MIGEC (version 1.2.7) software, the pre-processed high-quality sequences were de-multiplexed, and the UMIs were extracted as well as documented (Shugay et al., 2014). 'CAGTGgtatcaacgcagagtNNNNtNNNNtNNNNtctt' was used as a master barcode sequence to extract UMIs. Reads with the same sequences of UMI were collapsed and aligned to generate one consensus sequence. Only UMIs containing more than one read were retained, and the single-mismatched erroneous UMIs were dropped. De-multiplexed paired-end reads were mapped into built-in database to assign V/D/J segment and assembled into unique BCR sequences using MiXCR (version 3.0.5) software (Dmitriy et al., 2015). The 5' end and the 3' end of the library was respectively specified as 'v-primers' and 'c-primers'. The presence of the adapters in the library were also stated. Only VDJ region of BCR heavy chains were analysed for each library. The orientation of paired-end reads was set to 'collinear'. Sequences with the same VDJ region but different C genes were not merged during assemble. The average quality score across all reads was used to aggregate all sequences and the probability of single nucleotide mutation involved by PCR or sequencing error was set to '1E-5'. Sequences

containing at least one low-quality nucleotide were completely dropped. Only productive BCR sequences were filtered for downstream analyses which were performed based on VDJtools (version 1.2.1) software and R (version 3.6.0) software (Shugay et al., 2015, R Core Team, 2019).

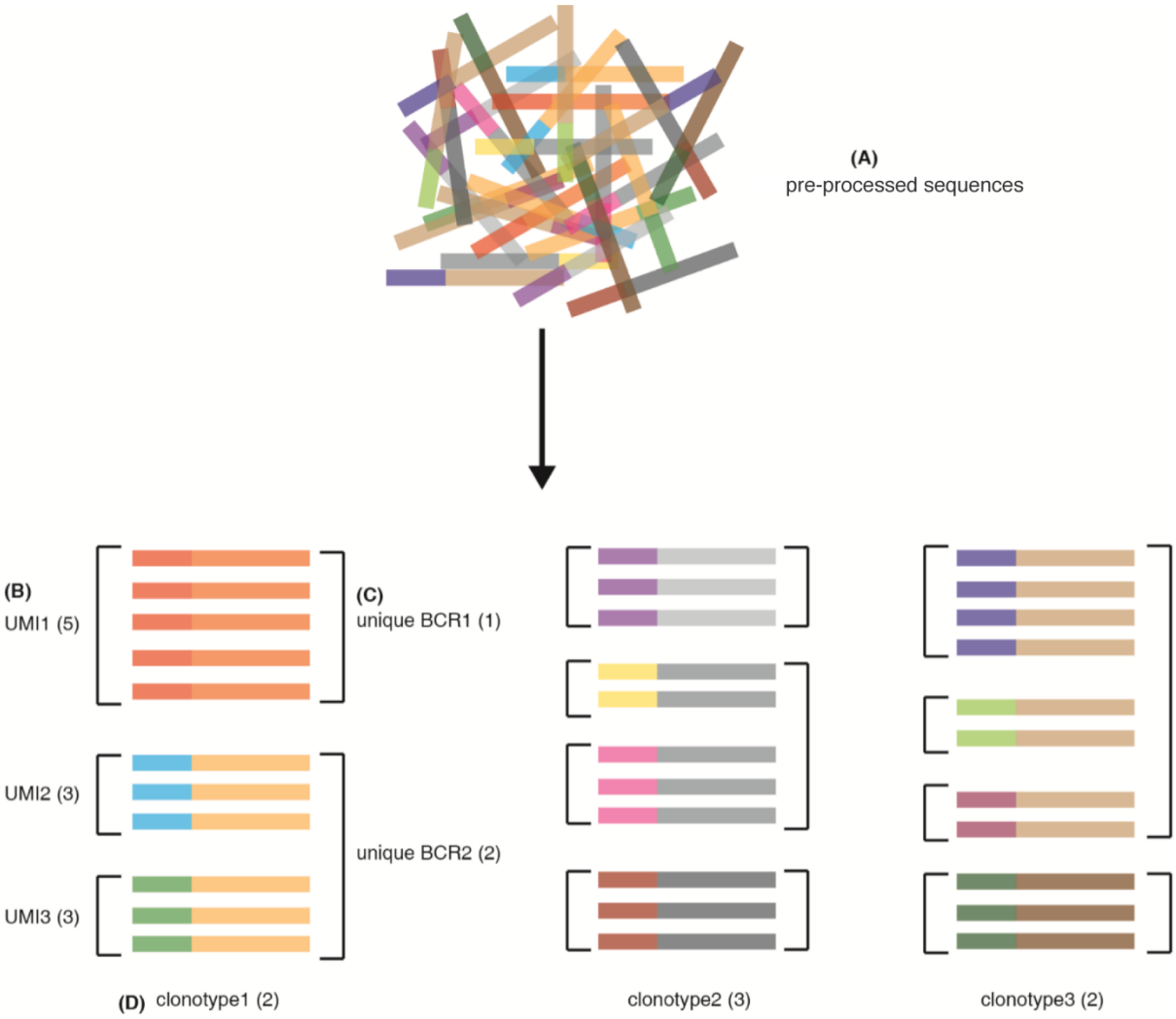

Figure 2.1 Data processing pipeline of BCR repertoire sequencing
(A) The raw data sequenced by Illumina were passed through PRINSEQ for quality filtering (data pre-processing). **(B)** The multiple read copies of UMIs (e.g., UMI1 contained 5 copies) were introduced by PCR amplification. Sequences with the same UMI were grouped, and the unique UMIs were extracted by MIGEC (UMI de-multiplex). **(C)** The unique BCRs were referred to the identical BCR sequences carrying diverse UMIs, reflecting the levels of mRNA expression (e.g., unique BCR2 was expressed twice). The unique BCRs were determined by MIXCR (VDJ assign and unique BCR assemble). **(D)** Unique BCRs shared identical CDR3 amino acid region, IGHV family and IGHJ family, but differed by mutation or isotype were defined as one clonotype as they were derived from a common progenitor.

2.2.8.2 scRNA-seq data processing

The sequencing data were de-multiplexed based on Illumina index using 10x Genomics Cell Range mkfastq pipeline (version 3.0.0). The gene expression matrix was generated by aligning the data to mm10 genome reference downloaded from the website of 10x Genomics, and the BCR sequences were assembled and annotated referring to GRCm38 reference. For B cell V(D)J enriched library, the assembled sequences of both functional heavy chains and light chains were subjected to the IMGT/HighV-QUEST database to assign germline segments and determine mutations. Repertoire information of productive sequences was analysed by R software (version 4.2.1). For 5' gene expression data, the count matrix of each sample was aggregated with the Cell ranger aggr function, and the combined data was read into R using the *Seurat* (version 3.4.0) package (Satija et al., 2015). For quality control, cells contained fewer than 200 genes, higher than 4,000 detected genes or > 8% of mitochondrial genes were filtered out as suspected doublets or debris (Zhang et al., 2022). Data from different tissues were log-normalized, and 2,000 highly variable features were calculated to integrate data. After integration, principal component analysis (PCA) was performed for following dimensional reduction and clustering. 20 dims were included to reduce the dimension and assign clusters. The clustering result was visualized using uniform manifold approximation and projection (UMAP) dimensionality reduction methods built in *Seurat* (McInnes and Healy, 2018). In order to focus on B subsets, clusters highly expressed CD19 or CD138 (Sdc1) genes were extracted and re-clustered for the following analyses. B cell clusters were re-named based on common-accepted cell markers and highly expressed genes observed by the FindAllMarkers function implemented in the *Seurat* package. GC B cells were extracted and integrated with published data [Gene Expression Omnibus (GEO): GSE154634] following the integration pipelines provided by the *Seurat* package (Chen et al., 2021). 0.2 resolution was introduced to nonsupervisory cluster all integrated GC B cells. The phase of cell cycle was annotated by calculating the expression of cell cycle-related markers provided by Tirosh et al. using the cell cycle scoring pipelines in the *Seurat* package (Kowalczyk et al., 2015). The cluster of GC B cells were named based on cell cycle and markers identified by Chen and colleagues (Chen et al., 2021). PCs were extracted to be re-clustered to 3 clusters base on 0.6 resolution. Cell cycle-, activation-, survival- and MHC II-related genes was introduced to classify PC subsets.

2.2.8.3 BCR network construction

The BCR network was constructed proposed by Bashford-Rogers et al. (Bashford-Rogers et al., 2013). Since the sequence number can influence the density and connection of networks, the

BCR sequences were downsampled into 5000 sequences per sample. The newly acquired sequences were re-grouped if they were the same. Each vertex represents one unique BCR sequence, and the size of a vertexes corresponds to the number of copies identical to that BCR. Unique BCRs shared common IGHV family, IGHJ family as well as identical CDR3 amino acid (CDR3aa) region were considered belonging to the same clonotype. BCRs sharing the same clonotype were clustered and connected as they were differed by nucleotide mutations. The immunoglobulin isotypes were coloured separately. Networks were illustrated with the *igraph* (version 1.2.4.2) package developed for R (Csardi G, 2006).

2.2.8.4 Clonal expansion index and clonal diversification index determination

The clonal expansion index is defined as the unevenness of the sequence numbers per unique BCR, whereas the clonal diversification index measures the unevenness of the unique BCR numbers per clone (Bashford-Rogers et al., 2019, Soto et al., 2019). To determine the clonal expansion index, the sequences of samples were subsampled regarding to 95% of the minimum sequence within each type of tissue. The subsampling was repeated 1,000 times, and the mean of expansion indices was calculated. The clonal diversification index was determined similarly as the unique BCRs in each sample was subsampled 1,000 times representing 95% of the minimum number of unique BCRs, and the mean was calculated. In each repeat, the index was determined by the *edgeR* (version 3.23.8) package in R software (Handcock, 2016).

2.2.8.5 CSR event analyses

The isotype of each BCR sequence was annotated by MIXCR. The CSR event was determined by quantifying the proportion of unique VDJ sequences that is shared by two isotypes. Each sample was randomly subsampled 1,000 times based on their minimum sample depth within the tissue type. The mean of the CSR proportion, as well as the mean of the isotype proportion were calculated for the following network visualization. The networks to present CSR event analyses were drawn by using of *igraph* package.

2.2.8.6 SHM analyses

In order to obtain mutation information, sequences of each unique BCR were re-aligned with the IMGT/HighV-QUEST database to search and summarize the number of mutations in V region (Alamyar et al., 2012, Hofman et al., 2013). The proportion of mutation-contained sequences and the average mutations per sequence in individuals were calculated and displayed using the *ggplot2* (version 3.2.1) R package (Hadley, 2016).

2.2.8.7 Gene segment assessment

The IGHV families and detailed segments, as well as the IGHJ segments were annotated by MIXCR, and the average percentage in each group were summarised. The proportion of VJ combinations was determined as the average percentage of a certain type of combination within the group. The selection of IGHV family was visualized with boxplots or bar plots. The mean fraction of IGHV, IGHJ segments in each group, as well as the fraction of V-J combination, were visualized using chord plot built in package *circlize* (version 0.4.10) (Gu et al., 2014). For comparisons between *Apoe*$^{-/-}$ mice and WT mice, the heatmaps showed the significant changes of selected combinations. For comparisons between individual tissues in *Apoe*$^{-/-}$ mice, the heatmaps showed the scaled proportion value of selected combinations.

2.2.8.8 Phylogenetic analyses

The germline sequences of each clone were parsed referring to IgBLAST database configured in Change-O (version 1.0.0) (Ye et al., 2013, Gupta et al., 2015). The output tab-delimited files were loaded to R for further analysis. The lineage tree of each clone was constructed by running of PHYLIP implemented in the *alakazam* package, and the final trees were visualized by using of the *igraph* package (Felsenstein, 1989, Stern et al., 2014). Only clones contained more than one unique BCRs were displayed.

2.2.8.9 Clonotype tracking

To determine the common clonotypes across different cell types or tissues, the overlap of clonotypes between two samples was evaluated using the *VennDiagram* package (Chen and Boutros, 2011). The fraction of overlapping clonotypes were calculated based on the obtained table and visualized with the *circlize* package. For the group comparison, the fraction was imported to the GraphPad software to visualize the tendency between two subpopulations.

2.2.8.10 Differentially expressed genes (DEGs) and pathway enrichment analyses

In scRNA-seq analysis, DEGs for each tissue or each B cell subset were determined with the following criteria: $|\text{Log(fold change, FC)}| > 0.25$ and adjusted p-value < 0.05. The normalized expression of DEGs in each cell was visualized with DoHeatmap function built in the *Seurat* package. DEGs originating in each tissue were subjected to the STRING database for Gene Ontology (GO) biological process enrichment analysis and Kyoto Encyclopedia of Genes and Genomes (KEGG) pathway enrichment analysis (Szklarczyk et al., 2019). DEGs obtained from

each B cell subset were parsed to the *clusterProfiler* package for functional enrichment and multiple comparisons (Yu et al., 2012). Terms showing a false discovery rate (FDR) less than 0.05 were considered as significant. Selected enriched terms were illustrated by *ggplot2*. The results of gene set enrichment analysis (GSEA) were also obtained using the *clusterProfiler* package and the GSEA plot for selective GO term was visualized by the *enrichplot* package.

2.2.8.11 Single-cell BCR clonality analyses

Expanded B cells were determined as cells containing paired heavy and light (H-L) chains, and shared identical V family, J family and CDR3aa region in heavy chains. The nonexpanded B cells were determined as cells containing paired H-L chains but without common V, J and CDR3aa features in heavy chains. Cells which missed BCR information in at least one chain were referred to as undetectable B cells. The BCR sequences of heavy chain in each cell were re-annotated with IMGT/HighV-QUEST database to determine mutations, and the mutations were analysed followed two parameters: the fraction of mutation-contained sequences and the average mutations per sequence.

2.2.8.12 Statistical analyses

The bar plots were presented as mean ± standard error of mean (SEM). For the statistical analysis, the Wilcoxon-Signed-Rank Test was employed for two-group comparison, and the Kruskal-Wallis one-way analysis of variance was performed for multiple-group comparison (Kruskal and Wallis, 1952, Rey and Neuhäuser, 2011). Furthermore, the p-value was adjusted by Benjamini-Hochberg correction for pairwise multiple-group comparison (Hochberg and Benjamini, 1990). Chi-square test with Benjamini-Hochberg correction was conducted to compare the cellular component, expansion and CSR in scRNA-seq data (McHugh, 2013). $p<0.05$ was considered statistically significant. *: $p<0.05$; **: $p<0.01$; ***: $p<0.001$; ****: $p<0.0001$; ns: not significant.

3 Results

3.1 GC-dependent B-2 cell immune response in ATLOs

To examine the possibility that hyperlipidemia/atherosclerosis is associated with alterations of the B-2 cell immune response and to determine where this response may occur, $CD19^+$ B cells were sorted from blood, SLOs including spleen and RLNs of both aged (78-85 weeks) WT and *Apoe*$^{-/-}$ mice, as well as from ATLOs of *Apoe*$^{-/-}$ mice. It has been reported that B-1 cells occupy around 5% and 20% of total $CD19^+$ B cells in SLOs and ATLOs, respectively (Srikakulapu et al., 2016). Therefore, the sorted $CD19^+$ B cells contained both B-1 and B-2 cells. PerC $CD19^+$ B cells were collected from the peritoneal cavity of the same mice as additional controls. They are mainly B-1 cells (>80%) in adult mice (Baumgarth, 2016). With the help of high-throughput sequencing (HTS), libraries of 58 samples were successfully constructed and sequenced, resulting in sequence information of approximately 1 million functional BCR sequences **(Supplemental Table 1)**. To understand B cell immunity in WT vs *Apoe*$^{-/-}$ mice, the BCR repertoire in each sample was assessed for the following parameters: 1.) clonal expansion – this parameter identifies a group of B cells sharing highly similar BCR sequences resulting from activation and proliferation in response to antigens; 2.) clonal diversification that estimates the heterogeneity of BCR sequences within clones that generates through SHMs; 3.) SHM and CSR which reflect the GC-dependent B-2 cell immune response to increase the antibody affinity to antigens and 5.) V-J recombination that contributes to construction of antigen-specific BCRs.

3.1.1 Higher levels of B cell clonal expansion in SLOs and ATLOs of aged *Apoe*$^{-/-}$ mice

Naïve B cells encountering invaders are activated to proliferate and divide, generating a group of B cells that share similar BCR sequences and target the same or similar antigens. This mechanism is termed clonal expansion. In order to estimate clonal expansion of B cells in WT and *Apoe*$^{-/-}$ mice, BCRs with the same sequences were grouped together in each sample, and a network was created to show all groups based on the copy number of BCR sequences appearing in that group **(Figure 3.1A)** (Bashford-Rogers et al., 2013, Bashford-Rogers et al., 2019). Networks of five samples from SLOs and ATLOs were presented as representatives (**Figure 3.1B and C)**. Each sample was normalized to the same number of BCR sequences by randomly selecting 5,000 sequences. This normalization method ensures comparability across samples with varying numbers of total BCR sequences. The levels of clonal expansion in each sample were determined by evaluating the abundance of unique BCRs present in the sample. In WT

SLOs, only a few dots representing unique BCR sequences were observed with large numbers of B cells **(Figure 3.1B)**, suggesting limited B cell proliferation and indicating a small number of expanded B cells in WT SLOs. However, in *Apoe*$^{-/-}$ SLO and ATLO B cells, over 10 dots displayed larger numbers in the network **(Figure 3.1C)**, suggesting an increase in the number of expanded B cells. These data indicate greater clonal expansion of B cells in *Apoe*$^{-/-}$ mice compared to WT mice. The network used in the analysis involves random selection of BCR sequences based on the lowest depth of sequencing (total number of BCR sequences one sample contains) present within a comparison group. As a result, this method may not be appropriate for analysing data sets containing only a small number of BCR sequences in a sample. To ensure the validity and accuracy of the network analysis, the clonal expansion index was determined from the network as an analysis that quantifies the unevenness of the number of copies for each unique BCR in the network (Bashford-Rogers et al., 2019). In WT spleen and RLN B cells, the indices were 0.1, but in *Apoe*$^{-/-}$ SLO B cells the value increased to 0.3 **(Figure 3.1D)**. These findings suggest *Apoe*$^{-/-}$ SLO B cells exhibit higher unevenness within the number of unique BCRs. This indicates a larger number of B cells share identical BCR sequences in *Apoe*$^{-/-}$ SLO B cells, pointing towards a higher degree of clonal expansion in these samples relative to their WT counterparts. The clonal expansion index of ATLO B cells was found to be comparable to that of *Apoe*$^{-/-}$ SLO B cells. This suggests that *Apoe*$^{-/-}$ SLOs and ATLOs exhibit similar levels of unevenness in the distribution of expanded B cells, indicating potential clonal expansion of CD19^{+} B cells (containing both B-1 and B-2 cells) in *Apoe*$^{-/-}$ SLOs and ATLOs. Interestingly, both WT and *Apoe*$^{-/-}$ blood B cells showed similar and low levels of clonal expansion index (expansion index: WT: ~0.05, *Apoe*$^{-/-}$: ~0.1), ruling out the possibility that the lack of *Apoe* leads to B cell clonal expansion systemically. Rather, this data supports the notion that the higher B cell clonal expansion in *Apoe*$^{-/-}$ SLOs and ATLOs, most likely, occurs in response to hyperlipidemia/atherosclerosis in aged *Apoe*$^{-/-}$ mice. To further estimate clonal expansion, the total percentage of the top 20 clones (called "D20" measurement) was used to quantitatively evaluate the sizes of the large clones (Rosenfeld et al., 2018, Kuri-Cervantes et al., 2020). The clones were determined as unique BCRs which shared identical CDR3aa regions as well as IGHV family usage and IGHJ family usage. The clones were ranked by total BCR sequences in order to calculate the total percentage of top 20 clones. Spleen and RLN B cells in *Apoe*$^{-/-}$ mice showed significantly larger clone sizes in the D20 fraction when compared to their counterparts in WT mice, ranging from 20% to 65% in *Apoe*$^{-/-}$ SLOs and 5% - 25% in WT SLOs **(Figure 3.1E)**. The overall D20 fraction of ATLO B cells was similar to the fraction in *Apoe*$^{-/-}$ SLO B cells, but significantly higher than WT SLO B cells **(Figure 3.1E)**. These data

indicated for *Apoe*$^{-/-}$ SLOs and ATLOs that higher numbers of B cells show similar - but not the same - BCR sequences. Thus, these B cells are daughters from the same ancestor, further supporting the notion of clonal expansion in *Apoe*$^{-/-}$ SLO and ATLO B cells. However, there was no difference of the D20 value in circulating B cells between aged WT and *Apoe*$^{-/-}$ mice, consistent with comparable clonal expansion index in WT and *Apoe*$^{-/-}$ blood B cells. The increased clonal expansion in *Apoe*$^{-/-}$ SLOs and ATLOs raised the important possibility that in inflammatory environments of atherosclerotic mice, autoantigens may elicit abnormal B cell activation and proliferation.

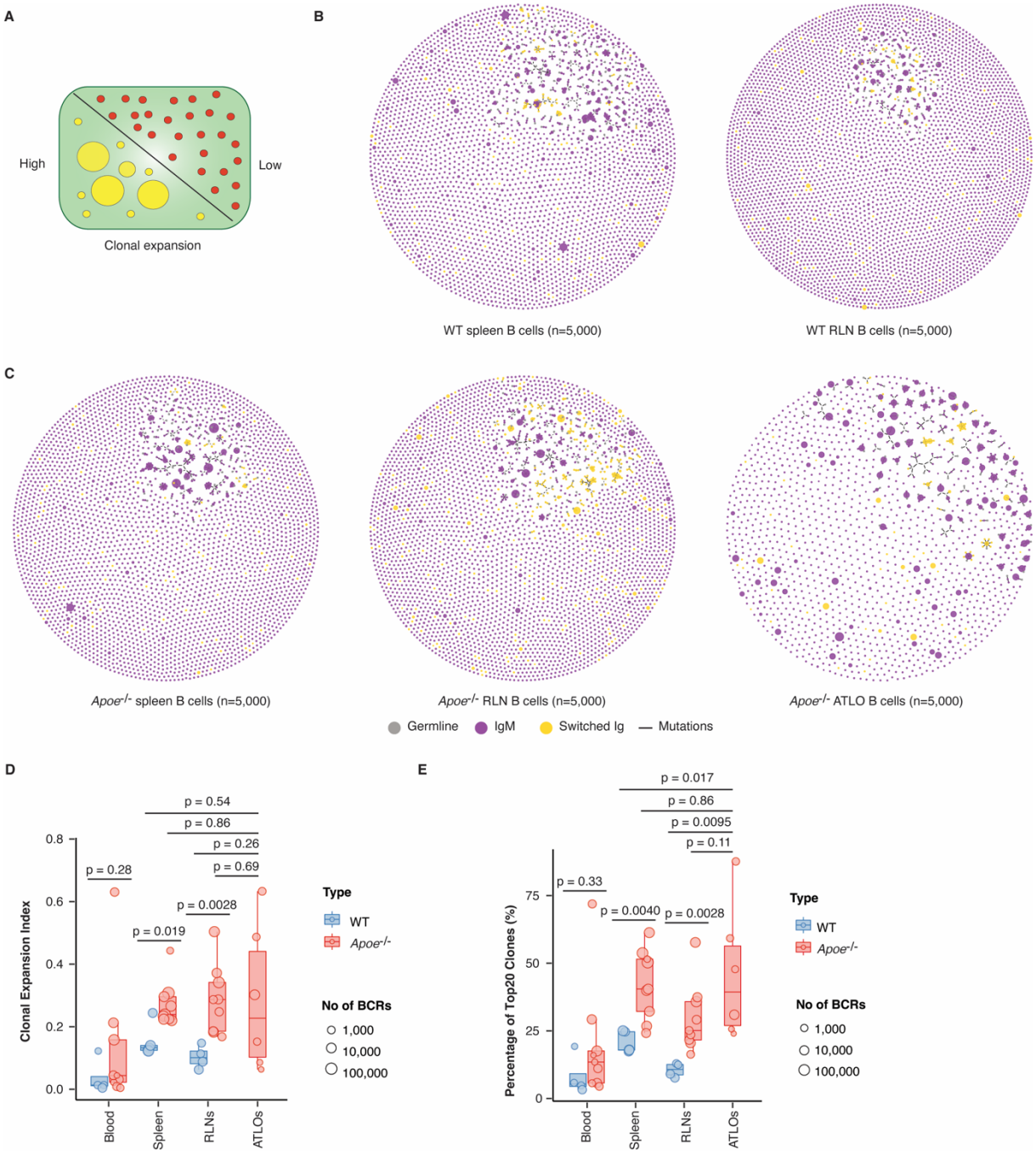

Figure 3.1 Higher levels of BCR clonal expansion in aged *Apoe*$^{-/-}$ SLO and ATLO B cells
(A) BCR clonal expansion is displayed by a network visualization approach. Each dot represents one unique BCR sequence. The size of the dot corresponds to the frequency of this BCR. **(B)** Representative graphic network of WT SLO B cells is shown. **(C)** Representative graphic network of *Apoe*$^{-/-}$ SLO and ATLO B cells. Each sample was downsampled to 5,000 sequences. Clones contained the same CDR3aa regions, IGHV family and IGHJ family were clustered and connected with short black lines based on the mutations. **(D)** The clonal expansion index in each sample is shown in the box plot. Each index was determined as the mean of 1,000 samplings as described in the method section. **(E)** The total percentage of top 20 clones contained most sequences in each sample is shown in the box plot. The ends of the boxes show the upper and lower quartiles; the central lines designate medians. The sizes of the dots represent the number of BCR sequences in each sample. In WT mice, blood n=4, spleen n=5, RLNs n=4; in *Apoe*$^{-/-}$ mice, blood n=9, spleen n=9, RLNs n=9, ATLOs n=6. The p-values for two-group comparisons were determined by Wilcoxon-Signed-Rank Test.

3.1.2 Higher levels of clonal diversification in SLOs and ATLOs of aged *Apoe*$^{-/-}$ mice

Clonal diversification refers to a clone of B cells that differed by SHM, which increasing the divergency of clones and results in a wider range of antigen specificity. In the network, the BCRs belong to the same clone but differed by single-nucleotide mutations were connected. Thus, the networks illustrated the diversification of these clones **(Figure 3.2A)**. Both WT and *Apoe*$^{-/-}$ B cells contained connected clusters, but more connections were noticed in *Apoe*$^{-/-}$ SLOs and ATLOs as compared to WT SLOs **(Figure 3.1B and C)**, indicating *Apoe*$^{-/-}$ SLOs and ATLO B cells have higher probability to undergo SHM. Moreover, most of the connected clusters contained large dots in both WT and *Apoe*$^{-/-}$ mice **(Figure 3.1B and C)**, suggesting that the expanded B cells have a higher SHM probability when compared to the non-expanded B cells. The clonal diversification index was determined to avoid the inaccuracy resulting from the varying number of BCR sequences in each sample. It describes the unevenness of the number of unique BCRs observed within each B cell clone. WT mice showed low values of clonal diversification in blood and SLO B cells (<0.05) **(Figure 3.2B)**, implicating less variability among the clones in WT mice. There was no significant difference in values of the clonal diversification index between WT and *Apoe*$^{-/-}$ blood B cells **(Figure 3.2B)**. Conversely, *Apoe*$^{-/-}$ SLO and ATLO B cells showed considerably higher index values when compared to WT SLOs, while the diversification indices in *Apoe*$^{-/-}$ SLO and ATLO B cells were comparable **(Figure 3.2B)**, indicating *Apoe*$^{-/-}$ SLO and ATLO clones harboured more diverse B cells that generated through mutations. This data is consistent with the results from network analysis to support the notion that *Apoe*$^{-/-}$ SLO and ATLO B cell clones have higher potential to undergo SHM than WT SLOs. Since the SHM occurs in GCs of B-2 cells, these data raised the

possibility that atherosclerosis/hyperlipidemia-related autoantigens trigger GC-dependent B-2 cell immune responses in *Apoe*$^{-/-}$ SLOs and ATLOs.

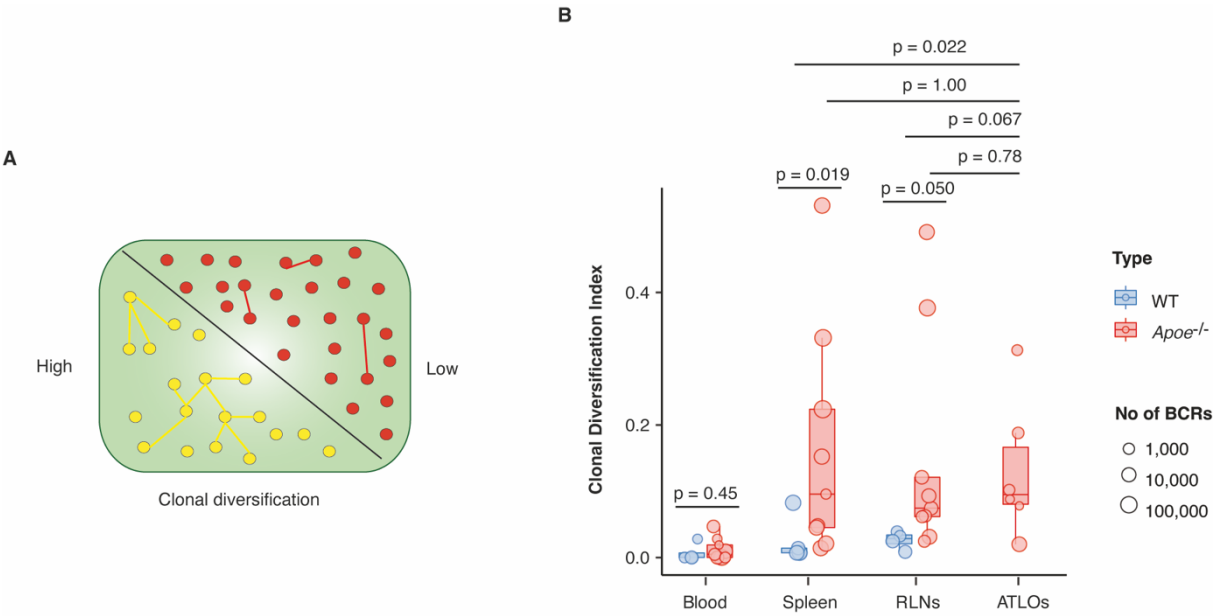

Figure 3.2 Higher levels of diversification in aged *Apoe*$^{-/-}$ SLO and ATLO B cell clones
(A) BCR clonal diversification is shown by network illustration. **(B)** The clonal diversification index in each sample is shown in the box plot. Each index was determined as the mean of 1,000 samplings as described in the method section. The upper and lower ends of the boxes show the upper and lower quartiles; the central lines represent medians. The sizes of the dots represent the number of BCR sequences in each sample. In WT mice, blood n=4, spleen n=5, RLNs n=4; in *Apoe*$^{-/-}$ mice, blood n=9, spleen n=9, RLNs n=9, ATLOs n=6. The p-values for two-group comparisons were determined by Wilcoxon-Signed-Rank Test.

3.1.3 PerC B-1 cells are characterized by high levels of clonal expansion but low levels of clonal diversification

To examine the clonal expansion and clonal diversification in B-1 cells, CD19^{+} B cells isolated from PerC (mainly B-1 cells) were analyzed **(Figure 3.3)**. In WT PerC, the clonal expansion index exceeded 0.4 and the percentage of top 20 BCR clones accounted for around 50% of the total PerC B-1 cells **(Figure 3.3A and B)**. This high level of clonal expansion indicates that WT PerC B-1 cells undergo renewal and therefore displays a high similarity in their BCR sequences. This data is as expected and is consistent with a previous study supporting limited B cell selection of B-1 cells during aging (Luo et al., 2022). Accordingly, WT PerC B-1 cells showed low levels of clonal diversification **(Figure 3.3C)**, suggesting few possibilities of SHM in WT PerC B-1 cells (Rodriguez-Zhurbenko et al., 2019). Surprisingly, however, when compared to WT PerC B-1 cells, *Apoe*$^{-/-}$ PerC B-1 cells presented significantly higher levels of

clonal expansion but comparable levels of clonal diversification **(Figure 3.3C)**. This data suggested the increased clonal expansion in *Apoe*$^{-/-}$ SLOs and ATLOs may result from expansion of B-1 and/or B-2, while the increased clonal diversification most likely resulted from B-2 cells, but not from B-1 cells. Therefore, this data further suggests an enhanced B-2 cell immune response in *Apoe*$^{-/-}$ mice when compared to WT mice.

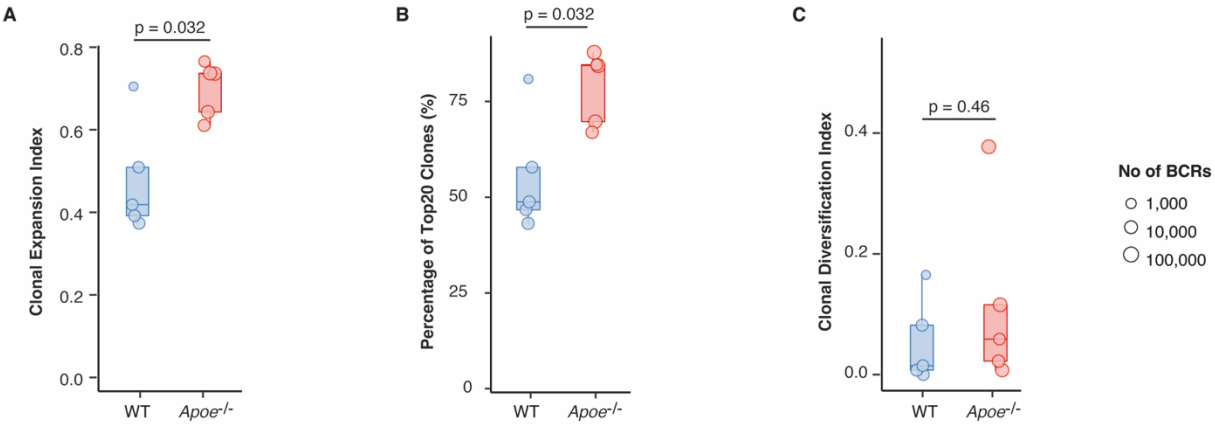

Figure 3.3 High levels of clonal expansion but low levels of clonal diversification in PerC B-1 cells
(A) The clonal expansion index, **(B)** the D20 value and **(C)** the clonal diversification index of both WT and *Apoe*$^{-/-}$ PerC B-1 cells. Each index was determined as the mean of 1,000 samplings as described in the method section. The ends of the boxes show the upper and lower quartiles; the central lines represent medians. The sizes of the dots represent the number of BCR sequences in each sample. Each group contained 5 replicates. The p-values for two-group comparisons were determined by Wilcoxon-Signed-Rank Test.

3.1.4 Higher levels of mutations in aged *Apoe*$^{-/-}$ SLO and ATLO B cells

The SHM of B cells contributes to bias shaping of antigen-prone repertoires containing affinity-matured BCRs. Therefore, examining SHM is critical to understand antigen-driven BCR selection. The levels of SHM were compared by quantifying the fraction of mutated sequences and average mutations per sequences in aged WT and *Apoe*$^{-/-}$ mice. Blood B cells only contained a small fraction of mutated BCRs, whereas a higher fraction of mutated BCRs was observed in SLOs and ATLOs in both aged WT and *Apoe*$^{-/-}$ mice **(Figure 3.4A)**, supporting an age-related accumulation of mutations (Zhang et al., 2019, Cagan et al., 2022). Importantly, the percentage of mutated BCRs in *Apoe*$^{-/-}$ SLOs and ATLOs sharply increased when compared to WT SLOs, accounting for 30% - 80% total of B cells, but the mutation-carrying B cells in *Apoe*$^{-/-}$ SLOs and ATLOs were comparable. The number of mean mutations per BCR was further examined. Blood B cells showed low levels of mean mutation when compared to B cells in SLOs and ATLOs, and there was no statistical difference between WT and *Apoe*$^{-/-}$ genotypes **(Figure**

3.4B). Increased numbers of mean mutations were noticed in both WT SLOs and *Apoe*$^{-/-}$ SLOs and ATLOs compared to blood. WT SLO B cells showed an average of 2 mutations in each sequence, but *Apoe*$^{-/-}$ SLO and ATLO B cells were higher with average mutations of ~4 compared to their WT counterparts **(Figure 3.4B)**. These findings imply increased levels of SHM in *Apoe*$^{-/-}$ SLOs and ATLOs when compared to WT SLOs. Therefore, the increased clonal expansion, clonal diversification and SHM together suggest enhanced GC reactions in *Apoe*$^{-/-}$ SLOs and ATLOs when compared to WT SLOs, indicating the existence of autoantigen-specific B cell immune response in *Apoe*$^{-/-}$ SLOs and ATLOs.

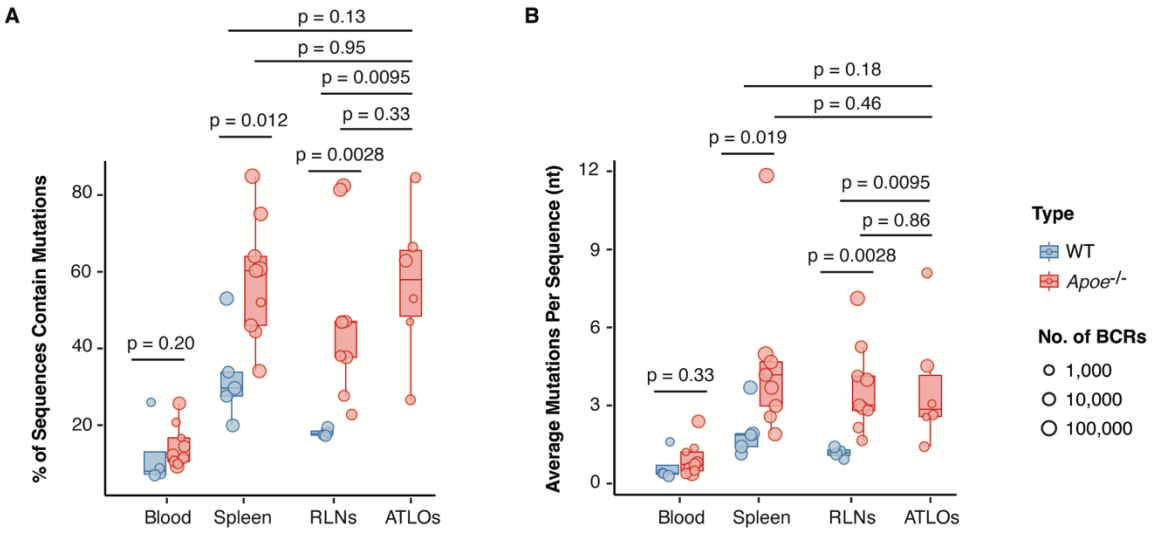

Figure 3.4 Higher levels of mutations in aged *Apoe*$^{-/-}$ SLOs and ATLO B cells
(A) The fraction of mutated sequences and **(B)** the average number of mutations per sequence in each sample is shown in the boxplot. The ends of the boxes show the upper and lower quartiles; the central lines represent medians. The sizes of the dots represent the number of BCR sequences in each sample. In WT mice, blood n=4, spleen n=5, RLNs n=4; in *Apoe*$^{-/-}$ mice, blood n=9, spleen n=9, RLNs n=9, ATLOs n=6. The p-values for two-group comparisons were determined by Wilcoxon-Signed-Rank Test.

3.1.5 Compromised CSR in ATLOs

To further study GC-dependent B-2 cell immune responses in aged *Apoe*$^{-/-}$ mice, the CSR was estimated by calculating the fraction of B cell isotypes in each sample. Blood B cells were dominated by unswitched IgM/IgD B cells with more than 90% in both WT and *Apoe*$^{-/-}$ mice, and there was no difference between two genotypes **(Figure 3.5A)**. In contrast, SLOs and ATLOs contained reduced numbers of unswitched B cells but a large fraction of class-switched B cells (IgA or IgG) when compared to blood. Furthermore, the fraction of class-switched B cells in *Apoe*$^{-/-}$ mice surpassed that in WT mice **(Figure 3.5A)**. Importantly, ATLOs showed

less class-switched B cells when compared to *Apoe*$^{-/-}$ SLOs, indicating aberrant CSR in ATLO GCs **(Figure 3.5A)**. The proportion of detailed isotypes were further analyzed. The WT blood B cells were mainly IgM as expected, but SLOs harboured a proportion of IgG1 and IgG3 B cells **(Figure 3.5B)**. Compared to WT, the fraction of IgG (especially IgG1, IgG2b and IgG2c) dramatically increased in *Apoe*$^{-/-}$ RLN B cells. While *Apoe*$^{-/-}$ RLNs contained around 20% IgG B cells, the percentage in the WT counterpart was less than 10%. This result is in agreement with the significant reduction of IgM in *Apoe*$^{-/-}$ RLNs. The isotype distribution in blood and spleen was comparable between *Apoe*$^{-/-}$ and WT mice **(Figure 3.5B)**. When taken together, the increased clonal expansion and the fraction of class-switched B cells in *Apoe*$^{-/-}$ SLOs when compared to WT SLOs further indicate enhanced GC responses in atherosclerosis. Since ATLO B cells showed similar clonal expansion, while it showed reduced switched isotypes when compared to *Apoe*$^{-/-}$ SLOs, these data raise the possibility that the CSR of ATLO GCs may be defective. Several mechanisms could account for the defect of CSR, such as down-expression of key enzyme activation-induced cytidine deaminase (AID), damage of DNA repair, dysregulation of subsequent recombination of C segments (Stavnezer et al., 2008). However, further studies are needed to identify the underlying mechanisms that result in CSR disruption in ATLOs.

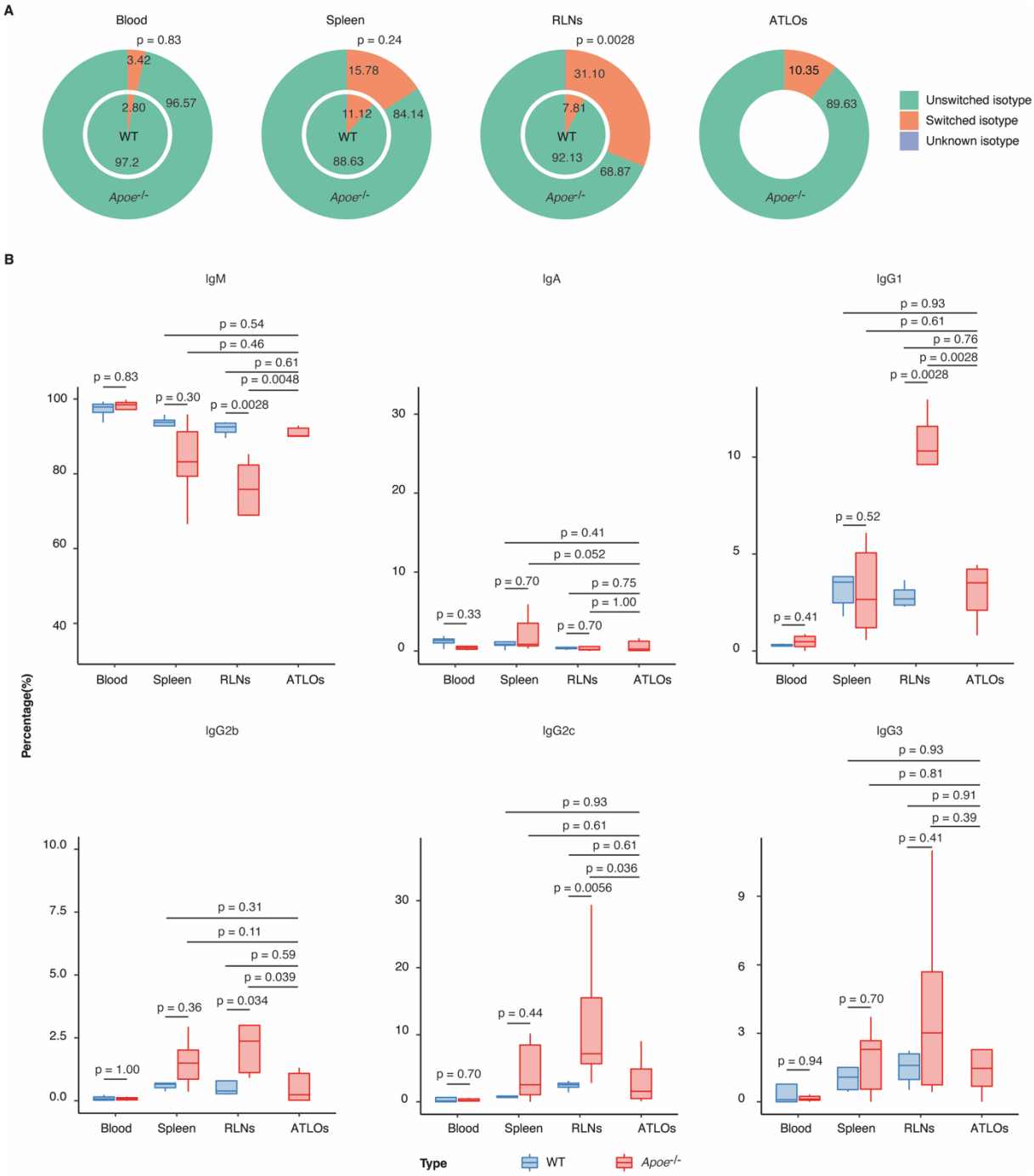

Figure 3.5 Increased numbers of class-switched isotypes in *Apoe*$^{-/-}$ SLOs but not in ATLO B cells

(A) The pie charts show the average percentages of unswitched and switched B cells in each tissue. The inner circles display WT results, and the outer circles display *Apoe*$^{-/-}$ results. **(B)** The boxplots show the isotype proportion in both *Apoe*$^{-/-}$ and WT B cells. The ends of the boxes show the upper and lower quartiles; the central lines represent medians. In WT mice, blood n=4, spleen n=5, RLNs n=4; in *Apoe*$^{-/-}$ mice, blood n=9, spleen n=9, RLNs n=9, ATLOs n=6. The p-values for two-group comparisons were determined by the Wilcoxon-Signed-Rank Test.

Upon antigen-triggered activation, DNA breaks and repair may occur to delete C segments and allow switching from upstream isotypes to downstream isotypes **(Figure 3.6A)**. Thus, the order of the C segment on the chromosome defines the possible switch direction from a given isotype **(Figure 3.6B)**. To further understand mechanisms of CSR in aged WT and *Apoe*$^{-/-}$ mice, CSR was determined between pairs of isotypes. Since IgD and IgE primers were not involved during library construction, only switching between IgM, IgA and IgG were detected **(Figure 3.6C)**. The CSR event was valued by quantifying the frequency of BCR sequences in the same clonotype but with different isotypes within a given sample **(Figure 3.6D)**. The CSR networks revealed the possibility that switch to different isotypes was unequal in both WT and *Apoe*$^{-/-}$ mice. IgM was more common to switch to IgG rather than IgA. IgG3 prefers to switch to IgG2 rather than IgG1 or IgA, although IgG2, IgG1 and IgA were all downstream segments of IgG3 **(Figure 3.6E-G)**. The percentage of isotypes and CSR patterns in *Apoe*$^{-/-}$ SLOs was compared to their WT counterparts. In *Apoe*$^{-/-}$ spleen, there was no systemically observed difference in the CSR frequency in B cells when compared to WT spleen, except for a significant drop of switching from IgM to IgG in *Apoe*$^{-/-}$ spleen B cells **(Figure 3.6E)**. In *Apoe*$^{-/-}$ RLNs, a considerable degree of IgG1 was switched into IgG2 versus WT RLNs which was associated with increased proportions of the IgG2 subset **(Figure 3.6F)**. ATLOs was compared to their corresponding isotypes and CSR events in *Apoe*$^{-/-}$ RLNs. Surprisingly, the majority of ATLO B cells remained as IgM without class-switching. The class-switching from IgG1 to IgG2 was decreased in ATLO B cells in comparison to *Apoe*$^{-/-}$ RLN B cells, which contribute to decrease of IgG2 isotypes in ATLOs **(Figure 3.6G)**. The networks systemically revealed detailed information of switching preference in WT and *Apoe*$^{-/-}$ mice. These data showed the upregulation of IgG1-IgG2 switching contributes to enhanced CSR in *Apoe*$^{-/-}$ SLOs, and the decrease of CSR in ATLO B cells may result from disruption of IgG1-IgG2 switching. Therefore, dysregulation of recombination between two C segments may be one factor to lead to defective CSR in ATLO GCs.

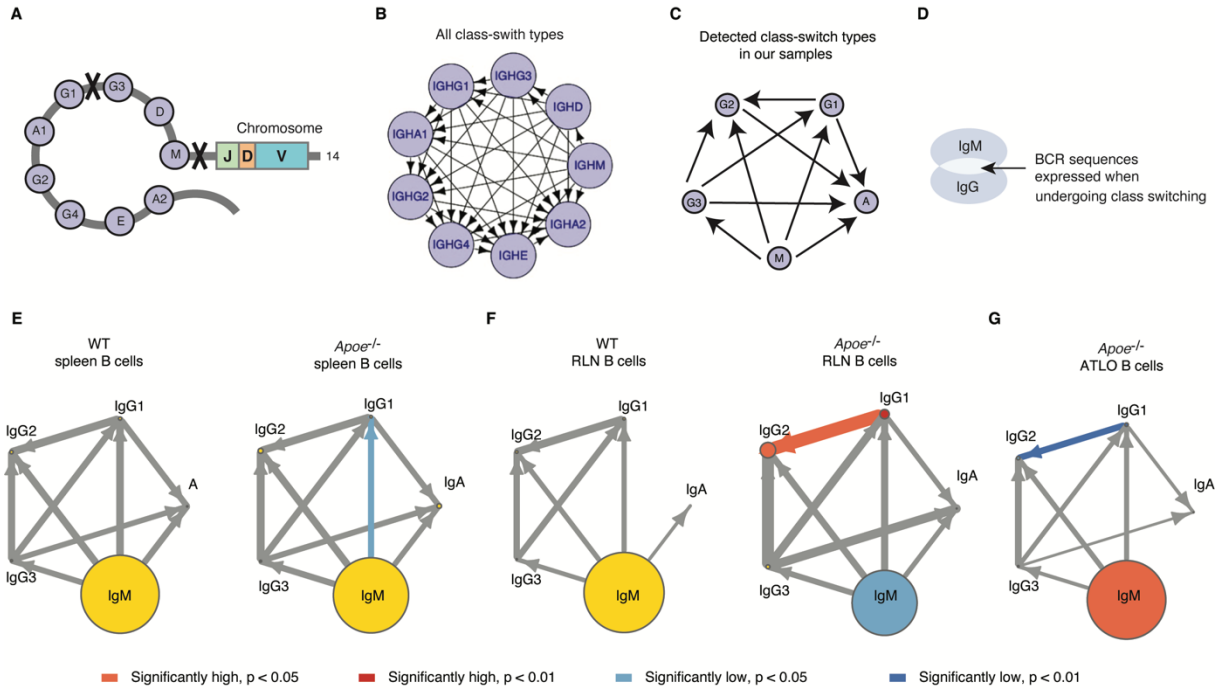

Figure 3.6 Different CSR preferences in aged WT and *Apoe*$^{-/-}$ mice
(A) Mechanism of deletional recombination. The circles represent isotypes. **(B)** All conceivable CSR possibilities. The circles represent isotypes, and the edges with arrows represent switch direction. **(C)** CSRs detected in our body of data. **(D)** The strategy to determine CSR frequency. CSR events were calculated as the percentage of BCR sequences that shared identical clonotypes but different C segments **(E-F)** The CSR events in SLO B cells of *Apoe*$^{-/-}$ and WT mice. The significance was calculated when comparing *Apoe*$^{-/-}$ mice to WT mice. **(G)** The CSR events in ATLO B cells. The significance was calculated when comparing ATLOs to *Apoe*$^{-/-}$ RLNs. Each circle represents one isotype, and the sizes of the circles is proportional to the percentage of unique BCR sequences in that isotype. The edges and arrows indicate class-switching direction between paired isotypes; the thickness of arrows is proportional to the relative frequency of CSR events. The p-values were determined by Wilcoxon-Signed-Rank Test. (Figure A, B and D were taken from Bashford-Rogers et al., 2019).

3.1.6 Variable usage of IGHV family in aged *Apoe*$^{-/-}$ B cells

Variation of IGHV family usages have been associated with specific diseases. For example, overrepresented IGHV5 family and underrepresented IGH1 family have been reported in splenic B cells isolated from SLE patients (Fraser et al., 2003). In addition, the frequencies of IGHV3 and IGHV4 was changed in membranous nephropathy (MN) when compared to healthy controls, demonstrating an altered immune status in those patients (Su et al., 2021). In order to examine whether there is a skewed IGHV family usage in relation to *Apoe*-deficiency or atherosclerosis, the frequency of each IGHV family in both WT and *Apoe*$^{-/-}$ mice was calculated. As shown in the boxplots, the blood samples which represented circulating B cells showed results similar to SLOs **(Figure 3.7)**. The IGHV1 family dominated the whole population in both WT and *Apoe*$^{-/-}$ mice, as more than half of blood, SLO and ATLO B cells recruited this

family **(Figure 3.7)**. Approximately 1% of WT B cells resembled IGHV4, IGHV11 or IGHV13 families. The underrepresentation of these families was apparent in all *Apoe*$^{-/-}$ B cell groups when compared to their WT counterparts, even though not all comparison pairs showed significance **(Figure 3.7)**. An increased use of IGHV7 family was also observed in *Apoe*$^{-/-}$ SLOs and ATLOs compared to WT SLOs. Only few WT B cells utilized the IGHV7 family, but this fraction sharply increased to 10% in *Apoe*$^{-/-}$ blood and spleen B cells **(Figure 3.7)**. This data implied that the variation of IGHV4, IGHV7, IGHV11 and IGHV13 was due to loss of *Apoe*. Despite the fact that ATLOs displayed similarity of IGHV family usage like WT and *Apoe*$^{-/-}$ SLOs, they were different. IGHV2 and IGHV9 were observed to be dramatically decreased in ATLOs when compared to SLOs **(Figure 3.7)**, suggesting further atherosclerosis-related bias of IGHV usage in ATLOs. These data imply that the variation of IGHV2 and IGHV9 may be biomarkers in relation to atherosclerosis-specific B cell immune response in ATLOs.

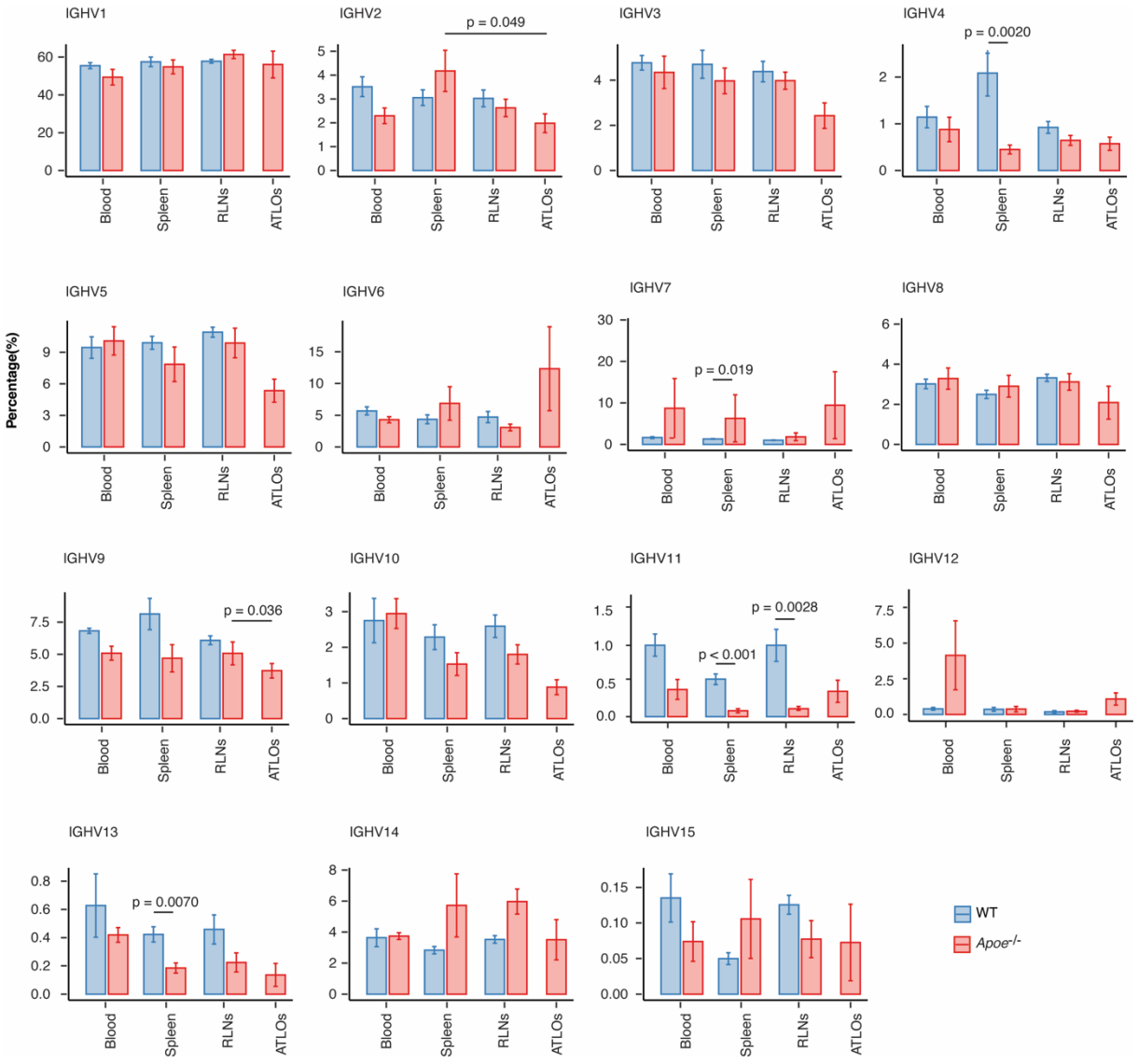

Figure 3.7 Distinct IGHV family usages in *Apoe*$^{-/-}$ B cells
The average frequency of B cell IGHV family usages in individuals is shown by barplots. The error bar indicates standard error of the mean. In WT mice, blood n=4, spleen n=5, RLNs n=4; in *Apoe*$^{-/-}$ mice, blood n=9, spleen n=9, RLNs n=9, ATLOs n=6. The p-values for two-group comparisons were determined by Wilcoxon-Signed-Rank Test. The significantly changed V families were labelled. *: $p<0.05$, **: $p<0.01$, ***: $p<0.001$.

3.1.7 Distinct V-J recombination in aged *Apoe*$^{-/-}$ B cells

V(D)J recombination determines the CDR3 region that plays a vital role in antigen recognition and responsiveness. Therefore, the frequencies of recombination have been associated to distinct stages of immune responses. For example, accumulation of particular V-J recombination has been detected in patients with an Influenza A infection (Hou et al., 2016). Since the D segments are much shorter and highly altered during recombination, only V and J were involved as more reliable parameters to assess the recombination (Yaari and Kleinstein, 2015). In order to systemically investigate the variation of V-J recombination between WT and *Apoe*$^{-/-}$ mice, chord plots were introduced to illustrate the proportion of V and J segment usage, as well as the proportion of their combination **(Figure 3.8A, C and E)**. Furthermore, the variation of several V segment and J segment recombinations [selected with criteria: 1). the fraction of V segments was higher than 1%; 2). the fraction of V segments which showed significant difference between two genotypes] was visualized by heatmaps **(Figure 3.8B, D and F)**. Some IGHV segments were commonly enriched in both WT and *Apoe*$^{-/-}$ B cells, including *IGHV1-64*, *IGHV3-6* and *IGHV9-3* **(Figure 3.8A, C and E)**. The most abundant V segments detected in circulating B cells in WT mice was *IGHV1-26*, and it was *IGHV7-3* in *Apoe*$^{-/-}$ mice. However, there was no significant difference of these two segments between WT and *Apoe*$^{-/-}$ blood **(Figure 3.8A)**. Instead, it is notable that the frequency of *IGHV1-5*, *IGHV6-6* and *IGHV14-2* dropped in *Apoe*$^{-/-}$ blood when compared to WT blood, with significant decreases of *V1-5:J2* and *V6-6:J3* recombination **(Figure 3.8A and B)**. The distribution of IGHV segments in spleen B cells was similar to that in circulating B cells that *IGHV9-3*, *IGHV1-26*, *IGHV1-64* and *IGHV3-6* ranked top 4 of IGHV segment usage in WT spleen B cells **(Figure 3.8C)**. They were also enriched in *Apoe*$^{-/-}$ spleen B cells as their frequencies only behind *IGHV7-3*, which were highly expressed in *Apoe*$^{-/-}$ spleen B cells when compared to WT spleen B cells **(Figure 3.8C)**. The markedly diminished selection of *IGHV1-18*, *IGHV1-81*, *IGHV4-1* and *IGHV5-17* was observed when comparing *Apoe*$^{-/-}$ mice to WT mice **(Figure 3.8C)**. In WT spleen B cells, *IGHV7-3* was approximately equal in recombination with different J segments, but in *Apoe*$^{-/-}$ spleen B cells, *IGHV7-3* mainly co-expressed with *IGHJ4*, leading to a notable reduction of *V7-3:J1* combination in *Apoe*$^{-/-}$ mice **(Figure 3.8D)**. The significant

reduction was also displayed in recombination such as *V5-17:J4* and *V1-18:J4*, resulting in diverse V-J recombination in different genotypes **(Figure 3.8D)**. The distribution of V segment usage in WT RLN B cells displayed similarities with WT spleen B cells, but the landscape of V segment in *Apoe*$^{-/-}$ RLN B cells was distinct from WT RLN B cells **(Figure 3.8E)**. *IGHV1-53* was the second-highest segment in *Apoe*$^{-/-}$ RLN B cells, following the expression of *IGHV1-26* **(Figure 3.8E)**. The significant underrepresentation of several segments like *IGHV1-72*, *IGHV1-81,* and *IGHV5-17* were also noticed in the frequency of certain V-J recombination in *Apoe*$^{-/-}$ RLN B cells **(Figure 3.8F)**. Integration of the findings obtained from three types of tissues, *IGHV1-5*, *IGHV1-81*, and *IGHV5-17* and their recombination to specific J segments showed a considerable drop of frequency across *Apoe*$^{-/-}$ tissues in contrast to WT tissues while the usage of *IGHV7-3* increased in *Apoe*$^{-/-}$ B cells **(Figure 3.8A, C and E)**. These data imply that the variation of these segments and V-J recombination may be associated with immune responses due to loss of *Apoe* or atherosclerosis.

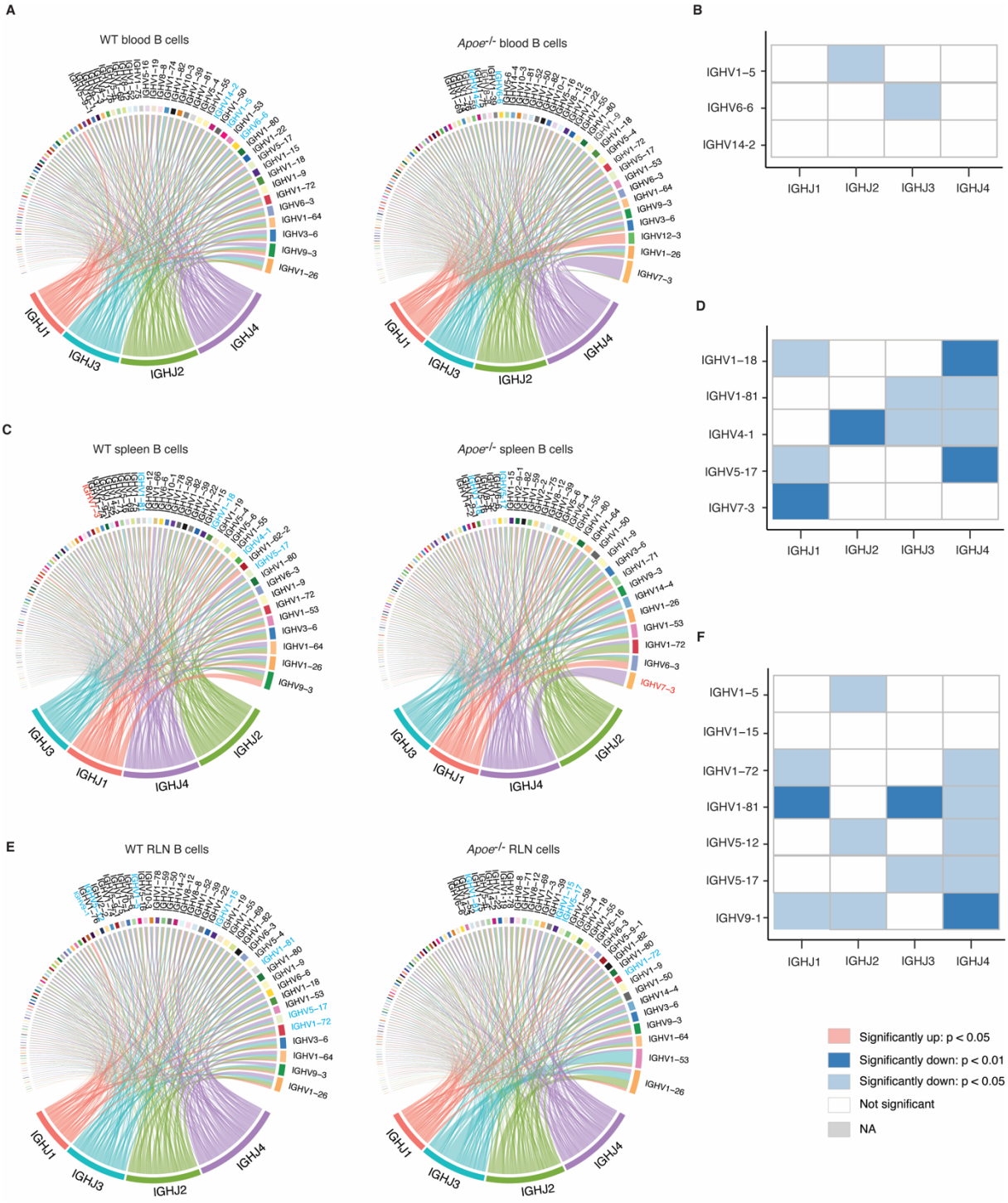

Figure 3.8 Distinct IGHV segment usage and V-J recombination in aged *Apoe*$^{-/-}$ B cells
The average frequency of IGHV segment, IGHJ segment and V-J recombination in **(A-B)** blood B cells, **(C-D)** spleen B cells and **(E-F)** RLN B cells were visualized in chord plots. **(A, C and E)** The segments were coloured and ordered by their frequency. The links represent recombination. The width of the rectangles and links are proportional to the frequency of the segments and combinations, respectively. For IGHV segments, only segments accounted for more than 1% of total segments were labelled. The red colour indicates significantly higher frequency, while the blue colour indicates significantly lower frequency in *Apoe*$^{-/-}$ mice when comparing *Apoe*$^{-/-}$ mice with WT mice. The black colour indicates no significance. **(B, D and F)** The significant changes of selected V-J recombination are shown in heatmaps. The results

of the comparison are displayed as *Apoe*$^{-/-}$ group versus WT mice. The p-values for two-group comparisons were determined by Wilcoxon-Signed-Rank Test.

3.1.8 Unique V-J recombination in ATLOs

To further examine whether there was variation of V-J recombination between *Apoe*$^{-/-}$ SLOs and ATLOs, the fraction of V and J segments as well as the fraction of V-J recombination pairs in ATLO was next estimated and visualized using chord plot. *IHGV7-3*, which was highly presented in *Apoe*$^{-/-}$ blood and spleen B cells and it was also observed to be highly expressed in ATLO B cells, ranking top 1 in V segment usage **(Figure 3.9A)**. *IGHV6-3*, which ranked second in *Apoe*$^{-/-}$ spleen B cells, also ranked top V segments in ATLO B cells **(Figure 3.9A)**. Enrichment of *IGHV6-6* was also observed in ATLO B cells **(Figure 3.9A)**. To further reveal the V segment usages across *Apoe*$^{-/-}$ tissues, the top 5 V segments of ATLO B cells were selected to compare their frequencies in different *Apoe*$^{-/-}$ tissues **(Figure 3.9B)**. There was no significant difference on the usage of these V segments in *Apoe*$^{-/-}$ blood, SLO and ATLO B cells **(Figure 3.9B)**, indicating that the overexpression of these V segments is more likely associated with systemic loss of *Apoe*. Interestingly, when investigating the V-J recombination across *Apoe*$^{-/-}$ tissues, a different situation was observed in ATLOs **(Figure 3.9C)**. The recombination to IGHJ was dominantly enriched in IGHJ2 and IGHJ4 in ATLO B cells, whereas blood and SLO B cells were involved with a high fraction of combined IGHJ1 and IGHJ3 occurred in some IGHV segments **(Figure 3.9C)**. Moreover, certain IGHV segments showed a unique preference to combine with IGHJ segments in different tissues. A large portion of *IGHV1-53* recombined with *IGHJ2* in ATLO B cells while the major recombination switched to *IGHJ3* in SLO B cells **(Figure 3.9C)**. Also, the majority recombination for *IGHV6-6* was *V6-6:J2* in ATLOs versus *V6-6:J1* in SLOs **(Figure 3.9C)**. Because the V-J recombination contributes to the coding of CDR3 regions to specifically target to antigens, the enrichment of *V1-53:J2* and *V6-6:J2* in ATLOs implies that these combination may generate auto-reactive B cells that could respond to unknown autoantigens in ATLOs.

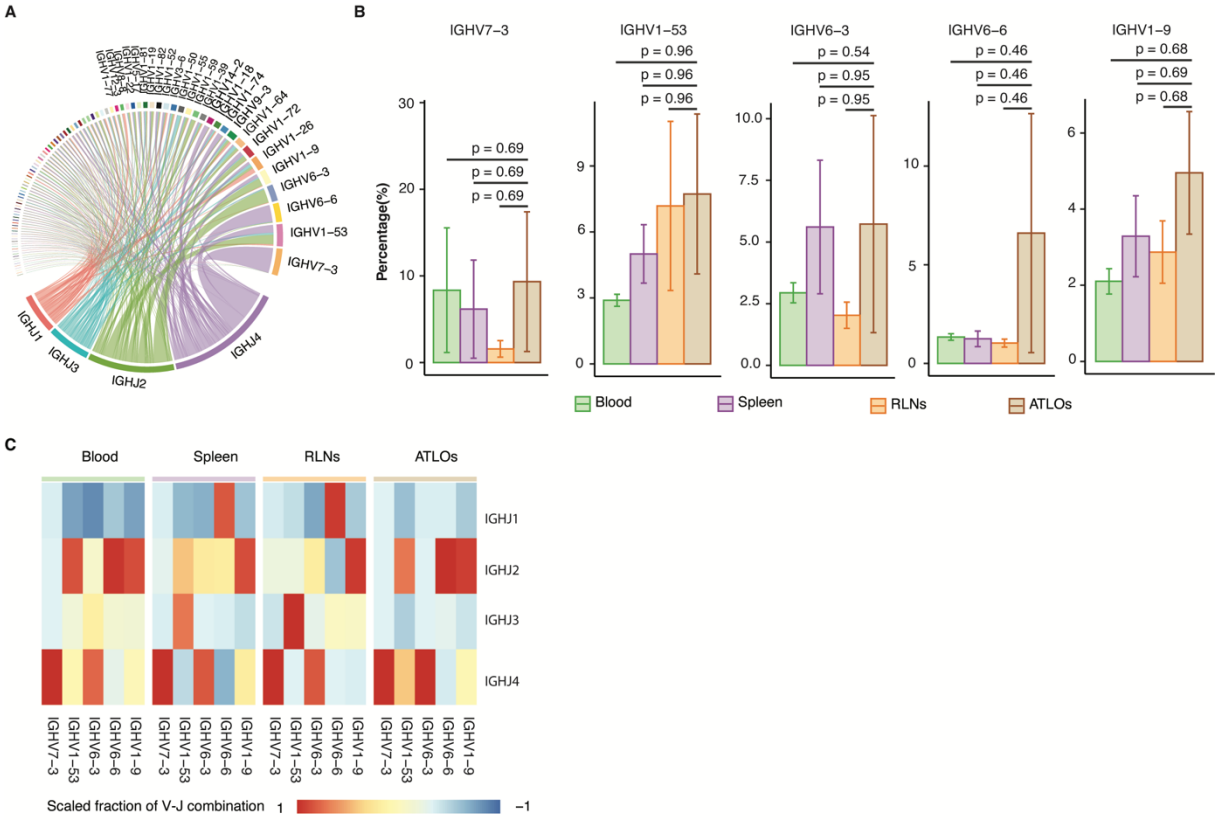

Figure 3.9 Unique V-J segment combinations in ATLOs
(A) The average frequency of IGHV segment, IGHJ segment and V-J combination in ATLO B cells is visualized in chord plots. The segments are coloured and ordered by their frequency. The links represent combinations. The width of the rectangles and links are proportional to the frequency of the segments and combinations, respectively. For IGHV segments, only segments which accounted for more than 1% were labelled. The top 5 IGHV segments in ATLO B cells were selected for further visualization. **(B)** The frequency of top 5 IGHV segments in different tissues in *Apoe*$^{-/-}$ B cells were displayed by the barplot. The error bar indicates standard error of the mean. Blood n=9, spleen n=9, RLNs n=9, ATLOs n=6. The multi-group p-values were determined by Wilcoxon-Signed-Rank Test and adjusted by Benjamini-Hochberg correction. The significantly changed V segments were labelled. **(C)** The average frequency of V-J combination for top 5 IGHV segments in *Apoe*$^{-/-}$ B cells were scaled by column and visualized using a heatmap.

3.1.9 Clonal expansion contributes to elevated IGHV segment usage in ATLOs

Two possibilities may be involved in the increased usage of specific IGHV segments in ATLOs: 1). the clonal expansion of several specific clones contributes to enrichment of some IGHV segments; 2). both expanded and non-expanded clones raise the selection of some IGHV segments during B cell development. To elucidate which factor contributes to the enriched frequency of top5 IGHV segments (*IGHV7-3*, *IGHV1-53*, *IGHV6-6*, *IGHV6-3* and *IGHV1-9*) in ATLO B cells, cells containing these segments were isolated in each sample to reconstruct the clonal lineage tree. BCRs in the same clone were aggregated into a tree, using germline

sequences as root and branching according to mutations. When visualized as a phylogenetic tree for selected clones who were using the top 5 IGHV segments, several remarkably expanded clones were noticed in ATLO B cells **(Figure 3.10)**. The biased expression of large clones was related to the increased frequency of specific IGHV segments. For example, the increasing of *IGHV6-6* may result from the expansion of *IGHV6-6*-containing clones **(Figure 3.10A)**. However, the expansion varied in individuals **(Figure 3.10)**. In the ATLO B cell sample obtained from the mouse no.1, *IGHV6-6*-containing BCRs dominated the expanded clones **(Figure 3.10A)**. However, in the ATLO B cell sample obtained from mouse no.2, clones expressed *IGHV6-3* and *IGHV1-53* showed higher expansion than clones expressed the other three IGHV segments **(Figure 3.10B)**. Furthermore, in the ATLOs obtained from mouse no.3, *IGHV1-53* and *IGHV1-9* comprised more expanded clones **(Figure 3.10C)**. The individual variation may imply the presence of diverse autoantibodies in response to a variety of autoantigens in ATLOs. These data support the notion that clonal expansion of selected clones contributed to higher IGHV segments in ATLOs.

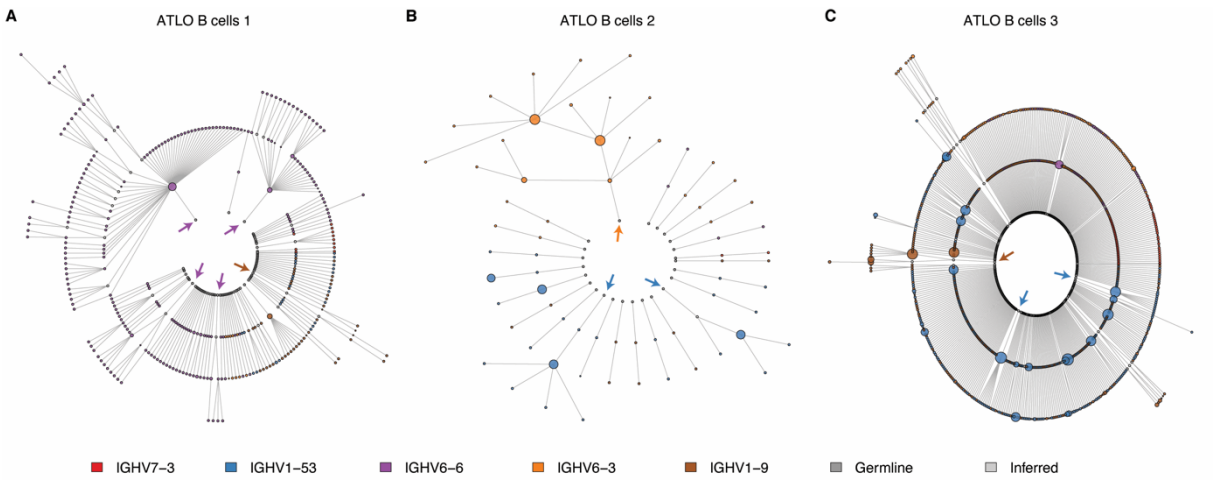

Figure 3.10 Clonal expansion contributes to elevated IGHV segment usage in ATLOs
The polygenetic tree of 3 individual samples of ATLO B cells is visualized. The sequences belonging to the same clone originated from one germline ancestor but diverged resulting from junctional insertion/deletions, SHM and CSR. Only BCR sequences that expressed *IGHV7-3*, *IGHV1-53*, *IGHV6-6, IGHV6-3* and *IGHV1-9* are included. The vertexes indicate unique BCR sequences, and the sizes of vertexes is proportional to the copy of the sequence. The edges represent the mutations. Sequences containing different IGHV segments were separated by colors. The dark and light grey colors indicate germline and inferred sequences, respectively. The arrows point to representatively expanded clones and their colour are the same to the colour of segment which they pointed at.

3.2 Compromised PC development in ATLOs

PCs express antibody mRNA at a higher rate than naïve B cells or memory B cells, i.e., 100-fold higher (Shi et al., 2015). In order to avoid the bias introduced by different capacities of BCR mRNA expression between B cells and PCs, $CD138^+$ PCs were separated from $CD19^+$ B cells for repertoire analyses. Apart from blood, SLOs and ATLOs, PCs were also isolated from BM to estimate the repertoire of homing PCs. A total of 57 samples were isolated to generate approximately 1.8 million BCR sequences **(Supplemental Table 2)**.

3.2.1 Expanded B cells preferentially differentiate into PCs in SLOs

PCs are generated from terminally differentiation of local B cells or they migrate from other tissues. To investigate the capability of B cells that would develop into PCs, chord plots were employed to estimate the BCR clones that could be observed in both B cells and PCs (namely shared BCRs) in each tissue within each mouse. One representative plot for each group was displayed in **Figure 3.11A-E**. In WT spleen, there was around 35% of shared BCRs in B cells, and these shared BCRs accounted for about 60% of the total PCs **(Figure 3.1A, F and G)**. WT RLNs showed similar results as WT spleen that the shared BCRs occupied 20% of total B cells, but the fraction raised to 40% in PCs **(Figure 3.11B, F and G)**. In *Apoe*$^{-/-}$ spleen, the mean frequency of B cells that contained shared BCR clones dramatically increased to about 60% when compared to WT spleen **(Figure 3.11C and F)**, indicating more *Apoe*$^{-/-}$ spleen B cells may differentiate into PCs when compared to WT spleen B cells. However, the percentage of these shared BCR clones showed no significant difference between WT and *Apoe*$^{-/-}$ spleen PCs **(Figure 3.11G)**. In *Apoe*$^{-/-}$ RLNs, the mean fraction of shared BCRs was approximately 40% and 50% in total B cells and PCs, respectively **(Figure 3.11D, F and G)**. There was no significant difference of shared BCRs in both *Apoe*$^{-/-}$ RLN B cells and PCs when compared to WT RLNs **(Figure 3.11F and G)**, suggesting that similar portions of WT and *Apoe*$^{-/-}$ RLN B cells could develop into PCs. The mean fraction of shared BCR clones in ATLO B cells showed major similarities when compared to *Apoe*$^{-/-}$ RLNs but significantly lower than *Apoe*$^{-/-}$ spleen **(Figure 3.11E, F and G)**. These data suggested similar fractions of B cells would develop into PCs when comparing ATLOs to *Apoe*$^{-/-}$ RLNs. In both WT and *Apoe*$^{-/-}$ SLOs, as well as *Apoe*$^{-/-}$ ATLOs, most of the shared BCRs enlarged their fraction when they enter the PC pools **(Figure 3.11A-E)**, leading to increase of total percentage of shared BCRs in PCs. These data may mean that clonally expanded B cell preferably differentiated into PCs. To explore this possibility, the clonally expanded index was calculated for B cells carrying the shared BCRs versus the remainder of B cells obtained from the same tissue **(Figure 3.11H)**. In WT spleen and RLNs,

B cells with shared BCRs showed a dramatically higher clonal expansion index when compared to their corresponding counterpart controls **(Figure 3.11H)**, indicating the expanded B cells enter the PC pool in these tissues. Similar results were observed in *Apoe*$^{-/-}$ SLOs, i.e., that the clonally expanded B cells prefer to enter the PC pools **(Figure 3.11H)**. The expanded B cells in SLOs have been characterized as GC-dependent B-2 cells in **Section 3.1**. Therefore, these observations support the notion that differentiation of PCs is limited to B cells which undergo GC reactions to undergo affinity maturation for antigens (Krautler et al., 2017). Furthermore, these data suggest that the B-PC differentiation in *Apoe*$^{-/-}$ SLOs is maintained without any apparent dysfunction. Interestingly, there was no significant difference in expanded index when comparing B cells with shared BCRs versus B cells without shared BCRs in ATLOs **(Figure 3.11H)**. These data suggested that both expanded and nonexpanded B cells have the ability to differentiate in ATLOs. There are two possibilities for this observation: 1). higher fraction of nonexpanded GC-independent B cells develop into PCs in ATLOs; 2). GCs are compromised in ATLOs, leading to unexpected differentiation of PCs from nonexpanded, low-affinity GC B cells.

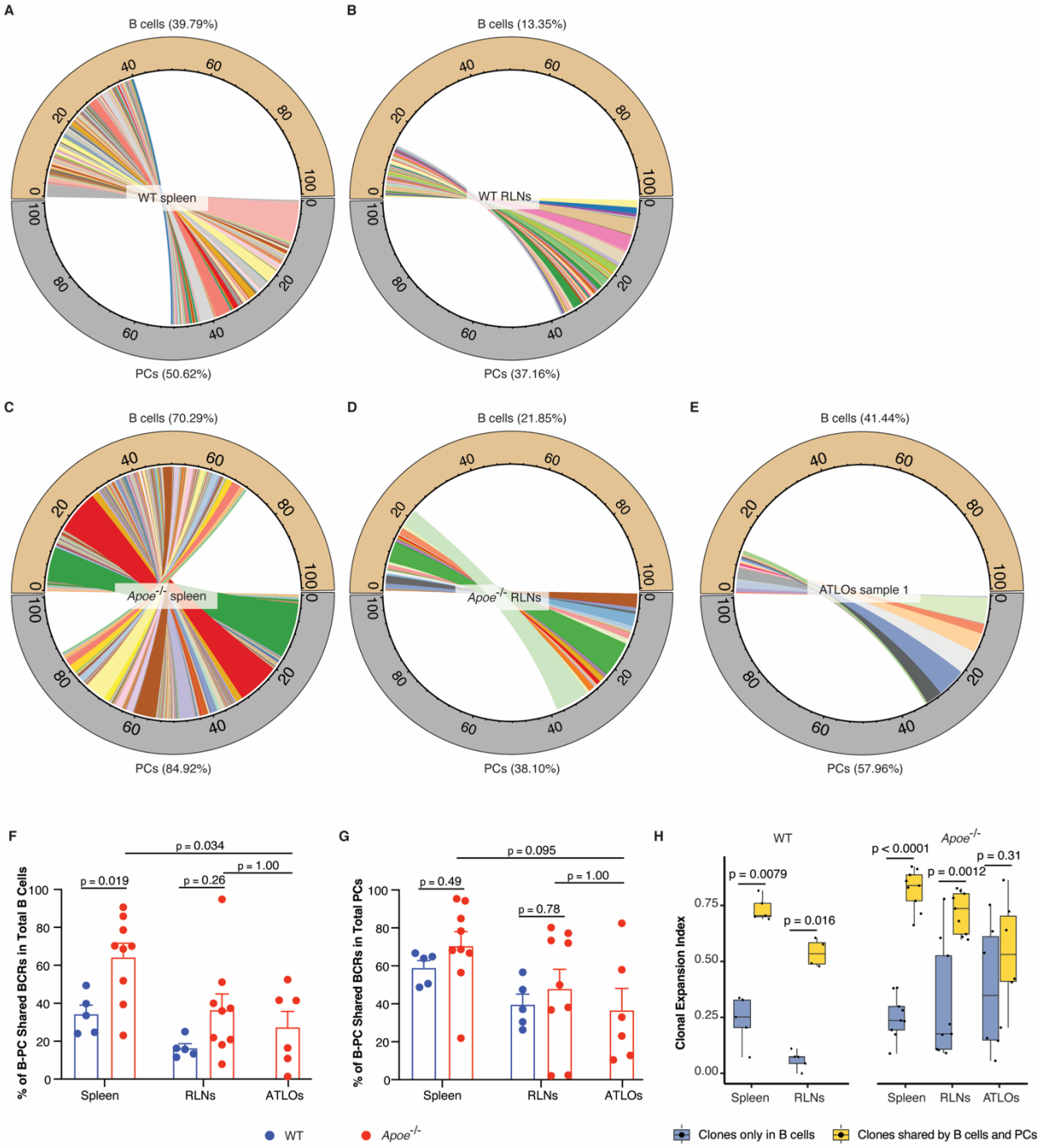

Figure 3.11 Expanded B cells show a higher probability to differentiate into PCs in SLOs (A-B) The representative chord plot displays shared BCR clones and the corresponding percentages between B cells and PCs in WT SLOs. **(C-D)** The representative chord plot displays shared BCR clones and the corresponding percentages between B cells and PCs in *Apoe*$^{-/-}$ SLOs. **(E)** The representative chord plot displays shared BCR clones and the corresponding percentages between B cells and PCs in *Apoe*$^{-/-}$ ATLOs. The semicircles represent B or PC subsets and the number inside indicate the fraction. The links represent clonotypes and their width are proportional to the portion of the BCR clones. The number outside the circles summarize the total fraction of shared BCR clones in the subset. **(F)** The total fraction of shared BCR clones in WT and *Apoe*$^{-/-}$ B cells. **(G)** The total fraction of shared BCR clones in WT and *Apoe*$^{-/-}$ PCs. **(H)** The clonal expansion index of shared or unshared BCR clones in B cells. The ends of the boxes show the upper and lower quartiles; the central lines

represent medians. Each dot represents one sample. In WT mice, n=5; in *Apoe*$^{-/-}$ mice, SLOs n=9 ATLOs n=6. The p-values were determined by Wilcoxon-Signed-Rank Test.

3.2.2 Decreased fraction of shared BCR clones between ATLOs/blood PCs and ATLOs/BM PCs

After terminally differentiation, PCs are capable to stay locally or home to the BM via the circulation, but they also can home into SLOs (Hargreaves et al., 2001). In order to define the tissue distribution of PCs, the percentage of PC BCRs which belong to the same clones across tissues were analyzed **(Figure 3.12)**. In WT SLOs, a large percentage of BCRs was also observed in blood and BM **(Figure 3.12A and C)**, supporting the notion that a large population of WT SLOs PCs home to the BM via the circulation. *Apoe*$^{-/-}$ SLOs showed major similarity to WT SLOs in that a high fraction of shared BCRs was observed between SLOs/blood and SLO/BM PCs **(Figure 3.12B and C)**. Shared BCRs were also found between ATLOs and other tissues in *Apoe*$^{-/-}$ mice **(Figure 3.12B)**, indicating ATLO PCs could migrate to SLOs and BM, or vice versa. However, the fraction of shared BCRs between ATLOs/blood and ATLOs/BM was significantly lower when compared to *Apoe*$^{-/-}$ spleen **(Figure 3.12C)**, suggesting that ATLO PCs preferably accumulate locally rather than emigrate to SLOs or BM.

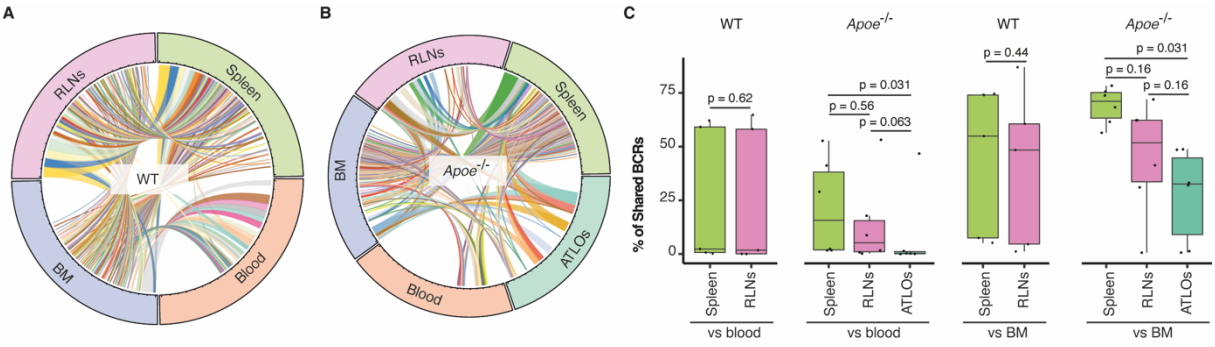

Figure 3.12 The fraction of shared BCRs between ATLOs/blood and ATLOs/BM is low
(A) The representative chord plot displays shared BCR clones in different tissues in WT mice. **(B)** The representative chord plot displays shared BCR clones in different tissues in *Apoe*$^{-/-}$ mice. **(C)** The fraction of shared BCR clones in SLOs or ATLOs when shared with blood or BM. The ends of the boxes show the upper and lower quartiles; the central lines represent median. Each dot represents one sample. In WT mice, n=5; in *Apoe*$^{-/-}$ mice, spleen n=6, RLNs n=5, ATLOs n=6. The p-values were determined by paired Wilcoxon-Signed-Rank Test.

3.2.3 Higher fraction of expansion-derived PCs in ATLOs

To further examine whether the higher clonal expansion of CD19^{+} B cells in *Apoe*$^{-/-}$ SLOs and ATLOs contribute to the presence of clonal populations in PCs, the clonality of PCs was

quantified by analysing the networks, the clonal expansion index and the D20 fraction **(Figure 3.13)**. Illustrated by networks, it was observed that both WT and *Apoe*$^{-/-}$ PCs, obtaining from different tissues, exhibited a significant abundance of large-sized dots (**3.13A and B)**. In addition, the number of large-sized dots in PCs was higher than that observed in B cells. In WT mice, the clonal expansion index in B cells was predominantly below 0.2. However, for WT PCs collected from the same tissue, the clonal expansion index increased to 0.5 **(Figure 3.1D and 3.13C)**. These results provide additional support for higher levels of BCR mRNA expression in PCs than in B cells. Since WT and *Apoe*$^{-/-}$ BM and blood PCs also showed higher index values than B cells **(Figure 3.1D and 3.13C)**, these data also suggest that expansion-derived PCs are capable for circulating in blood or homing to BM. Since 1.) the clonal expanded CD19^{+} B cells have a higher probability to develop into PCs than non-expanded B cells in both WT and *Apoe*$^{-/-}$ SLOs; 2.) the ability of PCs homing to BM via the circulation are comparable between WT and *Apoe*$^{-/-}$ SLOs, it is not surprisingly that the clonal expansion index of *Apoe*$^{-/-}$ BM, blood and SLO PCs showed no significant difference when compared to their WT counterparts **(Figure 3.13C)**. However, ATLO PCs showed a significantly higher clonal expansion index when compared to *Apoe*$^{-/-}$ SLO PCs **(Figure 3.13C)**. In line with this observation, the portion of top 20 clones in PCs were higher when compared to their counterpart B cell samples in blood, SLOs and ATLOs **(Figure 3.13D)**. There was no noticeable D20 difference in BM, blood, and RLNs between WT and *Apoe*$^{-/-}$ PCs, except for the higher D20 in *Apoe*$^{-/-}$ spleen when compared to WT spleen **(Figure 3.13D)**, implying further increased clonal expansion of top clones in *Apoe*$^{-/-}$ spleens. Of note, the D20 portion of ATLO PCs dramatically exceeded that in *Apoe*$^{-/-}$ SLOs PCs **(Figure 3.13D)**. In summary, ATLO PCs show significantly higher clonal expansion indices and a greater portion of top clones when compared to SLOs, indicating higher number of expanded PCs in ATLOs. There are two possibilities may contribute to these observations: 1). the highly expanded ATLO B cells develop into expanded PCs, and these PCs accumulate in ATLOs due to less emigration from there and thus less homing to blood and BM; 2). the ATLO B cells have distinct development to differentiate into more expanded PCs when compared to SLOs. Further evidence is required to understand the underlying mechanisms.

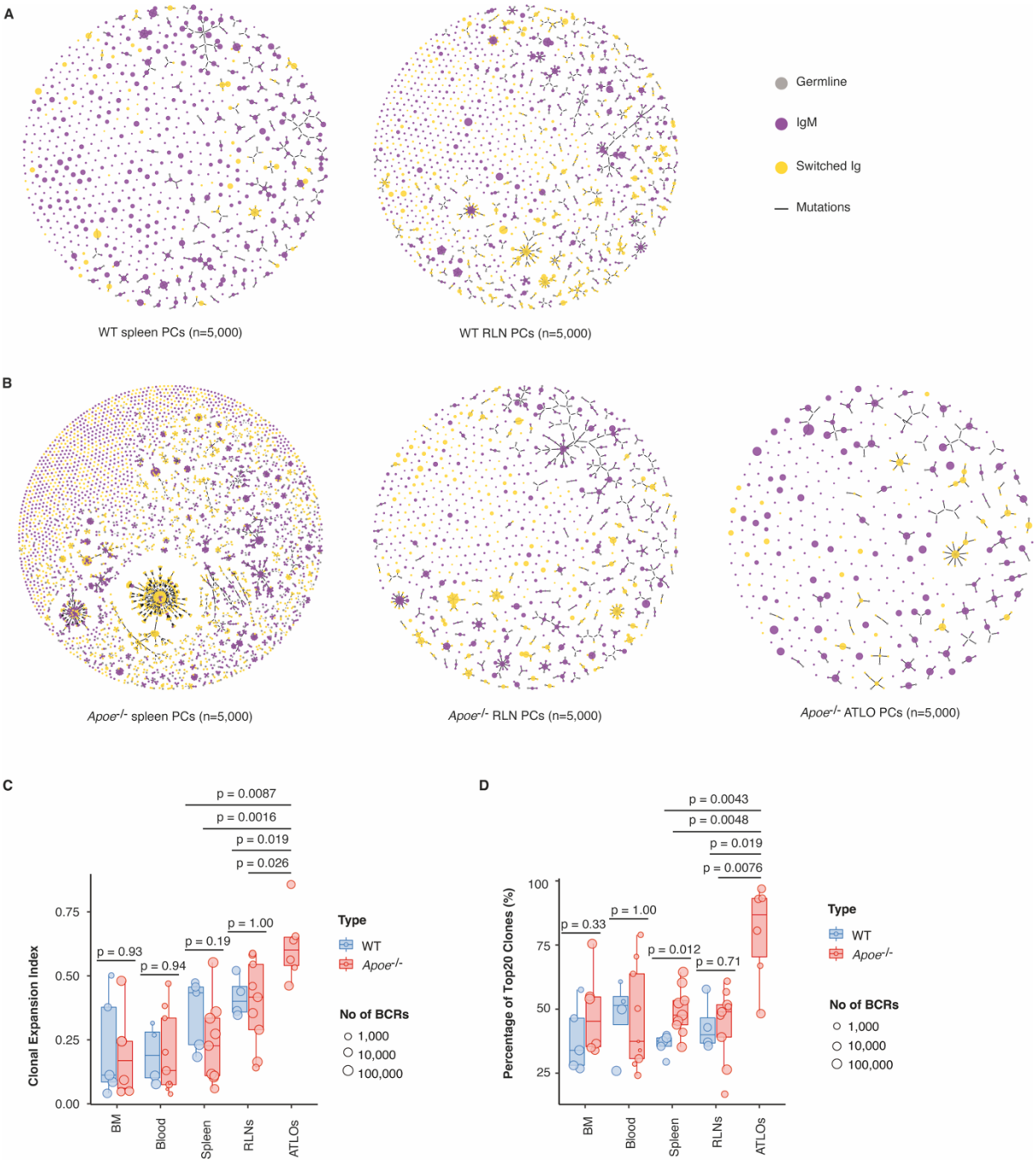

Figure 3.13 Higher fraction of expansion-derived PCs in ATLOs
(A) Representative graphic network of WT PCs. **(B)** Representative graphic network of *Apoe*$^{-/-}$ SLO and ATLO PCs. Each sample was downsampled to 5,000 sequences. Each dot represents one unique BCR sequence. The sizes of the dots correspond to the frequency of this BCR. Clones containing identical CDR3aa regions, IGHV family and IGHJ family were clustered and connected with short black lines based on the mutations. **(C)** The clonal expansion index in each sample is shown in the box plot. Each index was determined as the mean of 1,000 samplings as described in the method section. **(D)** The total percentages of top 20 clones containing most sequences in each sample was shown in the box plot. The ends of the boxes show the upper and lower quartiles; the central lines represent medians. The sizes of the dots represent the number of BCR sequences in each sample. In WT mice, BM n=5, blood n=4, spleen n=5, RLNs n=4; in *Apoe*$^{-/-}$ mice, BM n=6, blood n=9, spleen n=9, RLNs n=9, ATLOs n=6. The p-values for two-group comparisons were determined by Wilcoxon-Signed-Rank Test.

3.2.4 Lower levels of diversification in ATLO PC clones

Next, the diversification within PC clones was estimated by both graphic network and clonal diversification index analyses **(Figure 3.13A and B, 3.14)**. PCs overall showed more connections than B cells, supporting the concept that terminally differentiated PCs were more diversified than B cells, as expected (Phan et al., 2006) **(Figure 3.1B and C, 3.13A and B)**. A large number of connected clusters were observed in both WT spleen and RLN PCs **(Figure 3.13A)**. When comparing WT and *Apoe*$^{-/-}$ SLOs, *Apoe*$^{-/-}$ spleen PCs owned more diverse clusters in comparison to WT spleen PCs, indicating diversified B cells have higher probability to develop into PCs in *Apoe*$^{-/-}$ spleens **(Figure 3.13A and B)**. However, the diversified clusters in *Apoe*$^{-/-}$ RLN PCs were comparable to WT RLN PCs, suggesting the development of diversified PCs may vary among different *Apoe*-deficient tissues. ATLO PCs displayed comparable diverse clusters in comparison to *Apoe*$^{-/-}$ RLNs **(Figure 3.13A and B)**, indicating similar levels of diversified PCs between ATLOs and *Apoe*$^{-/-}$ RLNs. The value of clonal diversification index in WT SLOs was significantly higher when compared to WT blood and BM **(Figure 3.14)**, suggesting that other sources of PCs with low diversification, i.e., B-1 cell derived PCs, also contribute to the PC pool in BM via the circulation. *Apoe*$^{-/-}$ RLNs and blood PCs showed comparable diversification indices versus their WT counterparts; however, *Apoe*$^{-/-}$ spleens and BM showed markedly higher value of PC diversification index versus WT samples **(Figure 3.14)**. Since both spleen and RLN PCs have a comparable ability to home to the BM, the increase of diversified PCs in *Apoe*$^{-/-}$ BM may result from higher diversified PCs in *Apoe*$^{-/-}$ spleen versus their WT counterparts. The index in ATLO PCs was comparable to *Apoe*$^{-/-}$ RLNs but considerably lower than *Apoe*$^{-/-}$ spleen PCs **(Figure 3.14)**. Because there was no significant difference on clonal diversification of ATLO and *Apoe*$^{-/-}$ spleen B cells **(Figure 3.2)**, the lower clonal diversification of ATLO PCs when compared to *Apoe*$^{-/-}$ spleen PCs may suggest that lower levels of diversified B cells differentiate into PCs in ATLOs. Another possibility is that the lower levels of diversified PCs are preferably maintained locally rather than home to BM than the higher diversified PCs in ATLOs.

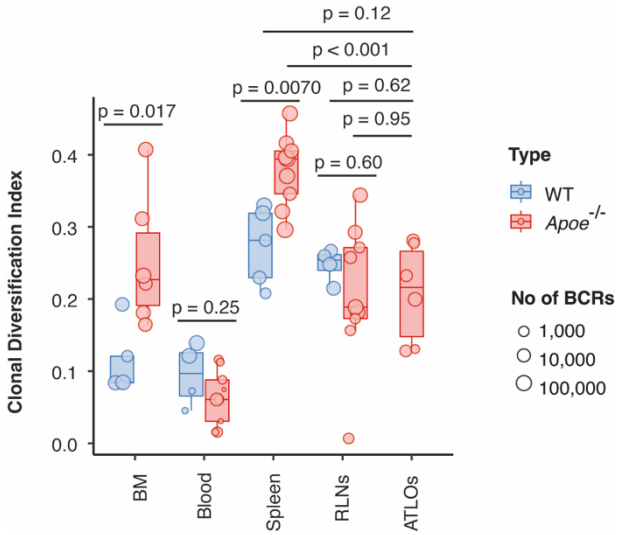

Figure 3.14 Lower levels of diversification in *Apoe*$^{-/-}$ RLN and ATLO PC clones
The clonal diversification index in each sample is shown in the box plot. Each index was determined as the mean of 1,000 samplings as described in the method section. The ends of the boxes show the upper and lower quartiles; the central lines represent medians. The sizes of the dots represent the number of BCR sequences in each sample. In WT mice, BM n=5, blood n=4, spleen n=5, RLNs n=4; in *Apoe*$^{-/-}$ mice, BM n=6, blood n=9, spleen n=9, RLNs n=9, ATLOs n=6. The p-values for two-group comparisons were determined by Wilcoxon-Signed-Rank Test.

3.2.5 Similar levels of mutation in *Apoe*$^{-/-}$ SLOs and ATLO PCs

To study the mutations in PCs, both percentage of mutated PCs and mean mutations per PCs were determined **(Figure 3.15)**. Both WT spleen and RLNs showed a high fraction of mutation-carrying PCs, further supporting the age-related accumulation of mutations **(Figure 3.15A)**. Blood and BM also contained high percentages of mutation-carrying PCs, indicating homing of mutated PCs from SLOs to BM **(Figure 3.15A)**. Interestingly, the composition of mutated BCRs in *Apoe*$^{-/-}$ spleen PCs was strongly increased when compared to WT spleen PCs (WT spleen: ~50%; *Apoe*$^{-/-}$ spleen: ~75%) **(Figure 3.15A)**, indicating the mutated B cells have higher probability to enter the PC pool in *Apoe*$^{-/-}$ spleen versus WT spleen. However, the percentages of mutated PCs showed no significant difference between WT and *Apoe*$^{-/-}$ RLN PCs, and the fraction in homed and circulating PCs were comparable in WT and *Apoe*$^{-/-}$ mice **(Figure 3.15A)**. The percentage of mutation-carrying PCs in ATLOs was similar to that in corresponding *Apoe*$^{-/-}$ SLOs, accounting for approximate 60% of total ATLO PCs **(Figure 3.15A)**. This data indicated the varied development of mutation-carrying B cells into PCs. When calculating the average mutation numbers in each BCR, the results were similar to the results of mutation fractions. (1). Similar numbers of mean mutations were found in WT SLOs, blood and BM **(Figure 3.15B)**; (2). Spleen PCs demonstrated higher numbers of average mutations per

sequence in *Apoe*$^{-/-}$ mice than those in WT mice **(Figure 3.15B)**; (3) No significant difference was observed when compared to the mean mutations in *Apoe*$^{-/-}$ RLN, blood and BM versus their WT counterparts **(Figure 3.15B)**; (4). ATLO PCs showed similar levels of mean mutations when compared to *Apoe*$^{-/-}$ SLO PCs **(Figure 3.15B)**. These results suggest increased diversification in *Apoe*$^{-/-}$ spleen PC clones may result from increased mutations. This data also implies the similar mechanisms of development of mutated B cells to PCs in *Apoe*$^{-/-}$ SLOs and ATLOs.

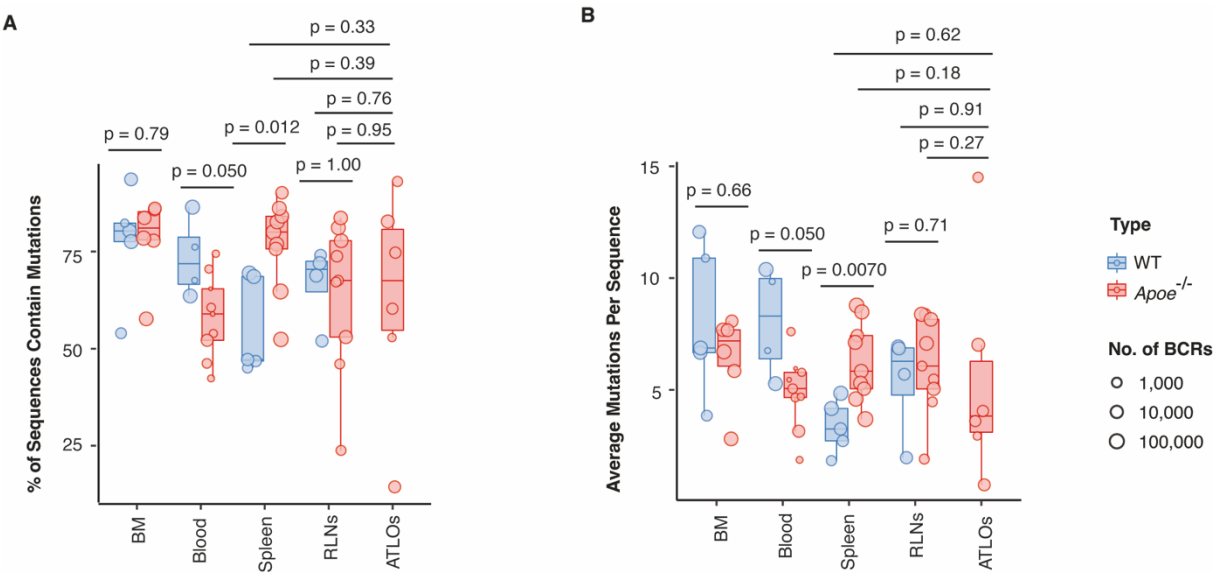

Figure 3.15 Similar levels of mutations in *Apoe*$^{-/-}$ SLOs and ATLOs
(A) The fraction of mutated sequences and **(B)** the average number of mutations per sequence in each sample is shown in the boxplot. The ends of the boxes showed the upper and lower quartiles; the central lines represent medians. The sizes of the dots represent the number of BCR sequences in each sample. In WT mice, BM n=5, blood n=4, spleen n=5, RLNs n=4; in *Apoe*$^{-/-}$ mice, BM n=6, blood n=9, spleen n=9, RLNs n=9, ATLOs n=6. The p-values for two-group comparisons were determined by Wilcoxon-Signed-Rank Test.

3.2.6 Decreased fraction of class-switched PCs in ATLOs

To examine the CSR in B-PC development, the percentages of switched PCs were analyzed in WT and *Apoe*$^{-/-}$ mice. In WT SLOs, only 1/4 to 1/3 of PCs were class-switched, and the most abundant switched isotype was IgG2c **(Figure 3.16A and B)**. There was also high fraction of IgG1 and IgG3 in WT SLO switched PCs **(Figure 3.16A and B)**. Around 50% of homed BM PCs and circulating blood PCs in WT mice had undergone class-switching, and IgA dominated the switched PCs **(Figure 3.16A and B)**. These data also indicate other origins of PCs that home to BM via the circulation. *Apoe*$^{-/-}$ blood showed less switched PCs, with a significantly

decreased fraction of IgA in *Apoe*$^{-/-}$ blood in comparison to WT blood **(Figure 3.16A and B)**. There was no significant difference when comparing the fraction of switched PCs in WT and *Apoe*$^{-/-}$ SLO PCs **(Figure 3.16A and B)**, though the percentage of switched B cells in *Apoe*$^{-/-}$ RLN surpassed WT RLN. These data implicate similar portion of switched B cells develop into PCs in both WT and *Apoe*$^{-/-}$ SLOs. Compared to *Apoe*$^{-/-}$ SLOs, there were less class-switched PCs in ATLOs, and the fraction of IgG dramatically dropped in ATLO PCs in comparison to *Apoe*$^{-/-}$ SLOs **(Figure 3.16A and B)**. These results suggest that a lower portion of switched B cell develop into PCs in ATLOs. To further delineate how the switching preference would influence PC development, the networks were introduced to estimate the switching between two isotypes **(Figure 3.16C-E)**. There was no systemic difference on CSR frequency between WT SLOs and *Apoe*$^{-/-}$ SLOs. The most common switching was IgG3 to IgG2 and IgG1 to IgG2, and these switches were seen in WT and *Apoe*$^{-/-}$ RLNs **(Figure 3.16C and D)**. However, when compared to *Apoe*$^{-/-}$ RLNs, ATLO PCs showed less switching from IgG1 to IgG2, accompanied by a lower frequency of IgG2 **(Figure 3.16E)**. This observation is consistent with the results in ATLO B cells, suggesting the decrease of IgG2 in ATLO PCs is associated with the reduced fraction of ATLO IgG2 B cells. Because ATLO showed less class-switched cells in both B cells and PCs, and the variation of switched preference were maintained from B cells to PCs. This data indicates the CSR is dysfunctional in ATLO B cells, but there was no further compromised CSR during B-PC development.

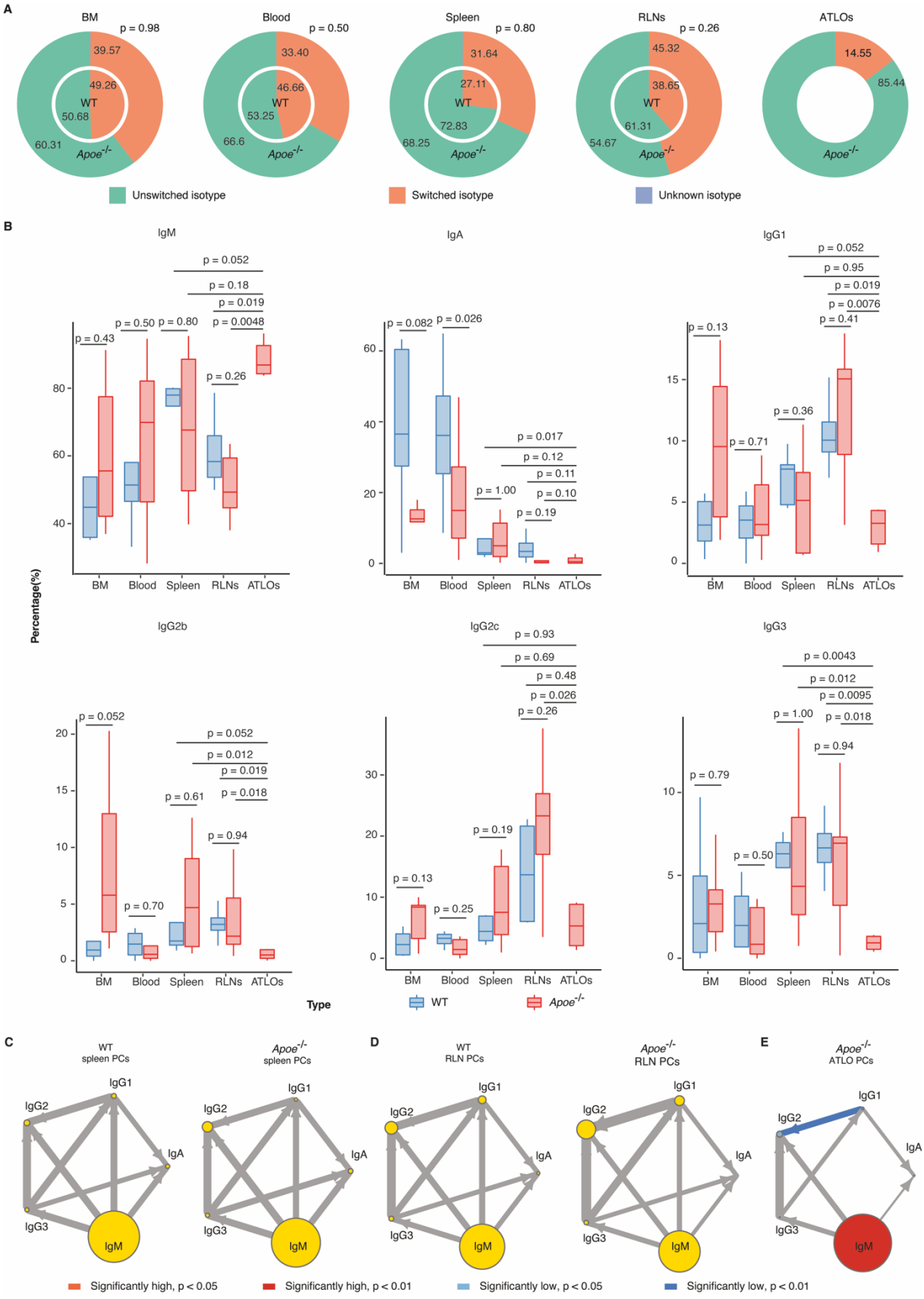

Figure 3.16 Decreased fraction of class-switched isotypes in ATLO PCs
(A) The piecharts show average percentages of unswitched and switched PCs in each tissue. The inner circles display WT results, and the outer circles display *Apoe*$^{-/-}$ results. **(B)** The boxplot shows the isotype proportion in both WT and *Apoe*$^{-/-}$ PCs. The ends of the boxes show

the upper and lower quartiles; the central lines represent medians. **(C-D)** The CSR events in SLO PCs of WT and *Apoe*$^{-/-}$ mice. The significance was calculated comparing *Apoe*$^{-/-}$ mice to WT mice. **(E)** The CSR events in ATLO PCs. The significance was calculated comparing ATLOs to RLNs. Each circle represents one isotype, and the size of the circles is proportional to the percentage of unique BCR sequences in that isotype. The edges and arrows indicate class-switching direction between paired isotypes; the thickness of arrows is proportional to the relative frequency of CSR events In WT mice, BM n=5, blood n=4, spleen n=5, RLNs n=4; in *Apoe*$^{-/-}$ mice, BM n=6, blood n=9, spleen n=9, RLNs n=9, ATLOs n=6. The p-values for two-group comparisons were determined by Wilcoxon-Signed-Rank Test.

3.2.7 Varied IGHV family selection in *Apoe*$^{-/-}$ PCs

To examine preference of IGHV family usage in PCs, the percentage of each IGHV family in PCs was analyzed. The IGHV1 family occupied a high fraction comprising both WT and *Apoe*$^{-/-}$ PCs, accounting for more than 50% of the total PC populations in each group **(Figure 3.17)**. The decreased fraction of IGHV4 and IGHV11 was noticed in *Apoe*$^{-/-}$ PCs in comparison to WT PCs **(Figure 3.17)**, consistent with their reduction in *Apoe*$^{-/-}$ B cells. While IGHV4 occupied around 4% of PCs in WT mice, the fraction sharply dropped to around 1% in *Apoe*$^{-/-}$ mice, and IGHV11 showed a significant decline from ~2.5% to ~0.5% between WT and *Apoe*$^{-/-}$ SLOs **(Figure 3.17)**. The tendency of increased IGHV7 was noticed in most of *Apoe*$^{-/-}$ tissues, and ATLO PCs had a very high potential to select IGHV7 family **(Figure 3.17)**. Besides, the IGHV14 family was considerably overrepresented in *Apoe*$^{-/-}$ PCs when compared to WT PCs **(Figure 3.17)**. These results are also consistent with the findings comparing *Apoe*$^{-/-}$ B cells to WT B cells, indicating the usage of IGHV families is maintained during B-PC development in mice lacking *Apoe*. The expression of IGHV family in ATLO PCs showed similarities with *Apoe*$^{-/-}$ SLO PCs, but the occupation of IGHV2 was significantly lower in ATLO PCs when compared to *Apoe*$^{-/-}$ SLO PCs **(Figure 3.17)**. ATLO also showed less IGHV9 PCs in comparison to *Apoe*$^{-/-}$ SLO PCs **(Figure 3.17)**. The significant decrease of IGHV3, IGHV4, IGHV5 and IGHV13 as well as the increase of IGHV12 was noticed when comparing ATLO PCs to *Apoe*$^{-/-}$ SLO PCs **(Figure 3.17)**. A similar tendency was observed in ATLO B cells although there was no significant difference. In summary, the variation of IGHV usage which we observed in ATLO B cells also presented in ATLO PCs when compared to *Apoe*$^{-/-}$ SLOs, indicating a preference of IGHV family usage is not disrupted in ATLOs during B-PC development.

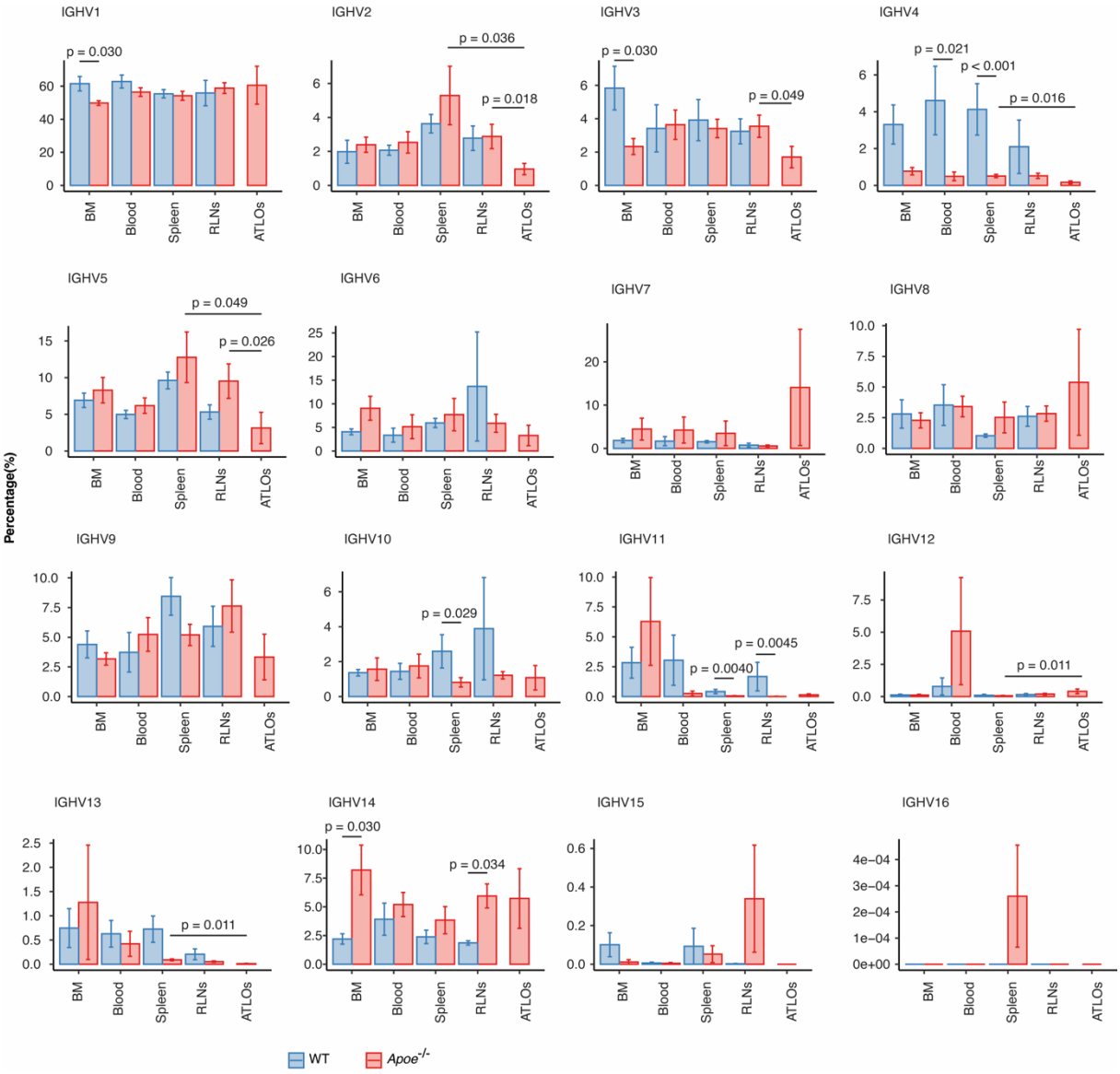

Figure 3.17 Specific IGHV family usage in *Apoe*$^{-/-}$ PCs
The average frequency of PC IGHV family usage in individual mice is shown by barplots. The error bar indicates standard error of the mean. In WT mice, BM n=5, blood n=4, spleen n=5, RLNs n=4; in *Apoe*$^{-/-}$ mice, BM n=6, blood n=9, spleen n=9, RLNs n=9, ATLOs n=6. The p-values for two-group comparisons were determined by Wilcoxon-Signed-Rank Test. The significantly changed V families were labelled. *: p<0.05, **: p<0.01, ***: p<0.001.

3.3 Breakdown of B cell immune tolerance in *Apoe*$^{-/-}$ mice

To estimate whether the *Apoe*$^{-/-}$-associated early hyperlipidaemia or late atherosclerosis affect B cell immune tolerance mechanisms, immature naïve B cells and mature naïve B cells were recruited at two checkpoints to examine if autoreactive B cells are detectable and whether this may be due to immune tolerance breakdown (Melchers, 2015). Using flow cytometry, immature naïve B cells ($CD19^+CD43^-CD24^+IgM^+IgD^-$) were isolated from the BM and mature naïve B

cells ($CD19^+CD43^-CD24^-IgM^+IgD^+$) were isolated from the spleen. Both young (8-10 weeks) and aged (78-85 weeks) mice were used for sorting and comparison. In total, 59 samples were sequenced to obtain more than 250,000 unique BCRs **(Supplemental table 3)**. Spleen GC B cells ($CD45^+CD19^+IgD^-GL7^+PNA^+$) and PCs, as well as BM PCs were also isolated from young mice to investigate the B cell development in young age. About 600,000 unique BCRs were obtained from a total of 30 samples **(supplemental table 4)**.

3.3.1 Increased clonality of B cells during B cell development in young *Apoe*$^{-/-}$ mice

Long-lived PCs either reside in SLOs or home to BM **(Figure 3.18A)**. In young mice (8-10 weeks), naïve B cells, GC B cells and PCs were sorted to estimate the development of B cells before and after exposure to antigen(s) by determining the clonal expansion index and clonal diversification index **(Figure 3.18B and C)**. WT BM immature naïve B cells and spleen mature naïve B cells showed low clonal expansion index **(Figure 3.18B)**, indicating less expanded cells in this population. This data, as expected, is consistent with the concept that major autoreactive B cells are removed during B cell development (Wardemann et al., 2003b). Of note, WT spleen GC B cells showed a low clonal expansion index, while WT spleen PCs and BM PCs showed high levels of clonal expansion indices (**Figure 3.18B**). However, a significantly higher clonal expansion index was found in both *Apoe*$^{-/-}$ immature naïve B cells and mature naïve B cells when compared to WT mice, suggesting increased expanded naïve B cells in young *Apoe*$^{-/-}$ mice **(Figure 3.18B)**. These data imply the autoreactive B cells are not properly removed at tolerance checkpoints early in life and trigger clonal expansion in *Apoe*$^{-/-}$ naïve B cells. Therefore, the mechanism of B cell central tolerance may break down in young *Apoe*$^{-/-}$ mice. Clonal expansion also increased in *Apoe*$^{-/-}$ spleen GC B cells when compared to WT GC B cells **(Figure 3.18B)**, supporting the concept that autoreactive B cells which escaped tolerance checkpoints may initiate GC responses, as reported (Degn et al., 2017). There was no significant difference between WT and *Apoe*$^{-/-}$ spleen PCs, indicating clonal expanded $CD19^+$ B cells have a higher probability to develop into PCs than non-expanded B cells in both young WT and *Apoe*$^{-/-}$ mice **(Figure 3.18B)**. In contrast, while comparing the BM PCs, the clonal expansion index in young *Apoe*$^{-/-}$ mice were lower than that in young WT mice **(Figure 3.18B)**, raising the possibility that 1). expansion-derived PCs are retained locally rather than homing to the BM in young *Apoe*$^{-/-}$ mice; 2). young *Apoe*$^{-/-}$ BM contains more non-expanded PCs that had migrated from other tissues. There were low values of clonal diversification indices in WT BM immature naïve B cells and spleen naïve B cells, and the indices were comparable between WT and *Apoe*$^{-/-}$ mice **(Figure 3.18C)**. This data indicates there are low mutations within clones in

both young WT and *Apoe*$^{-/-}$ naïve B in the absence of GC reactions, consistent with the concept that GC-dependent SHM is the major source for B cell mutations. In contrast, *Apoe*$^{-/-}$ GC B cells showed slightly higher values of clonal diversification index than WT GC B cells, and significantly elevated clonal diversification index in young *Apoe*$^{-/-}$ spleen PCs and BM PCs when compared to their WT counterparts **(Figure 3.18C)**. This data implies the important possibility aberrant GC reactions triggered by unknown autoantigens in young *Apoe*$^{-/-}$ mice.

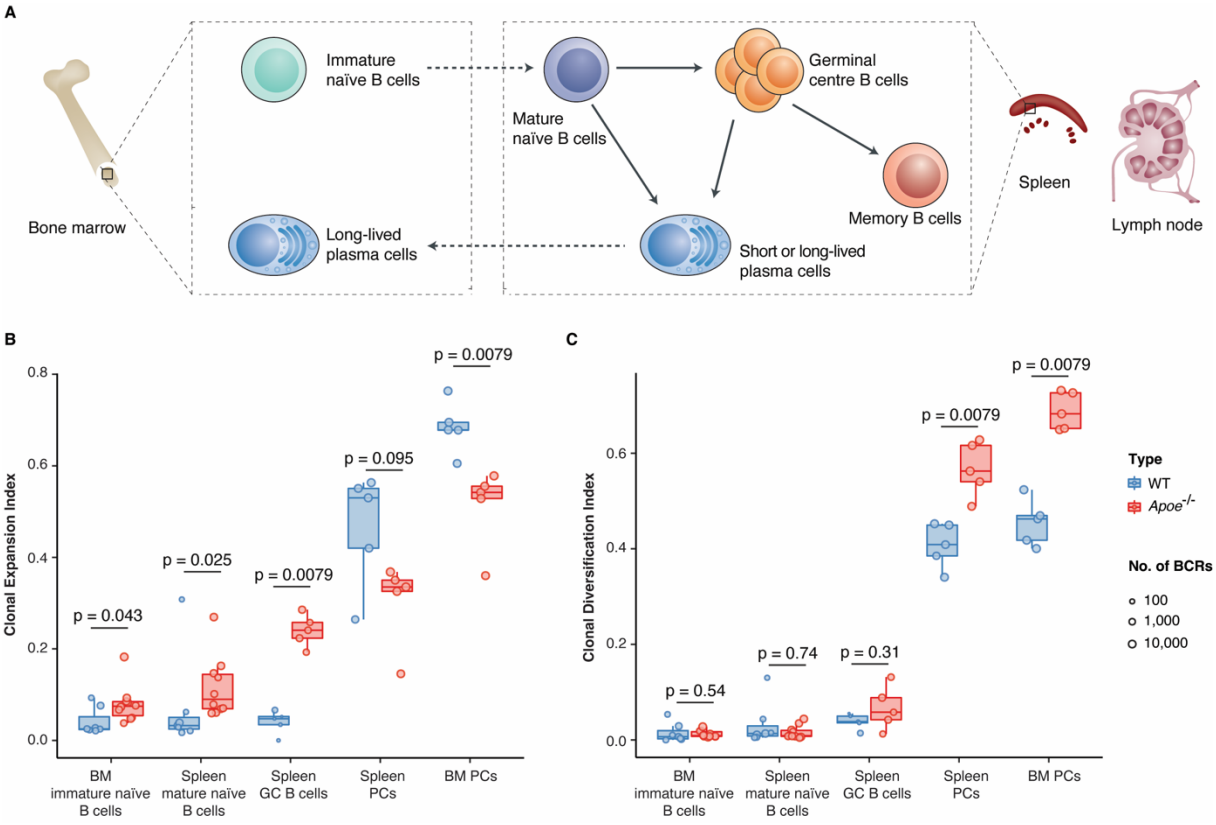

Figure 3.18 Increased clonal expansion and diversification in young *Apoe*$^{-/-}$ mice
(A) Schematic view shows the development paths of B cells. BM immature naïve B cells migrate to spleen or LNs for further maturation. After activation, antigen-experienced B cells enter GCs for affinity maturation, and consequently generate memory B cells or PCs. Activated B cells are also capable to bypass GCs to directly develop into PCs. Long-lived PCs reside in SLOs or home back to the BM. **(B)** The clonal expansion index and **(C)** clonal diversification index in young *Apoe*$^{-/-}$ and WT mice. The ends of the boxes show the upper and lower quartiles; the central lines represent medians. The sizes of the dots represent the relative number of sequences in each sample. BM immature naïve B cells: WT n=7, *Apoe*$^{-/-}$ n=10; spleen mature naïve B cells: WT n=7, *Apoe*$^{-/-}$ n=10; spleen GC B cells: WT n=5, *Apoe*$^{-/-}$ n=5; spleen PCs: WT n=5, *Apoe*$^{-/-}$ n=5; BM PCs: WT n=5, *Apoe*$^{-/-}$ n=5. The p-values for two-group comparisons were determined by Wilcoxon-Signed-Rank Test. *: $p<0.05$; **: $p<0.01$.

To conclude, the increased clonal expansion and diversification indicate the lack of *Apoe* gene or hyperlipidemia may disrupt B cell tolerance during B cell development in young *Apoe*$^{-/-}$ mice.

3.3.2 Similar clonality in aged WT and *Apoe*$^{-/-}$ naïve B cells

To investigate immune tolerance during aging, clonal expansion index, D20 value and clonal diversification index of naïve B cells isolated from aged mice (78-85 weeks) were also calculated **(Figure 3.19A-C)**. Both aged WT and *Apoe*$^{-/-}$ showed higher clonal expansion indices in naïve cells when compared to young mice **(Figure 3.18B and 3.19A)**, indicating more expanded B cells in aged mice, thus supporting the age-related skew of the BCR repertoire which has been described previously (Gibson et al., 2009). Of note, there was no significant difference on clonal expansion index when compared aged *Apoe*$^{-/-}$ naïve B cells to WT naïve B cells **(Figure 3.19A)**, suggesting similar levels of expanded naïve B cells in aged WT and *Apoe*$^{-/-}$ mice. Similar results were also obtained in the total fraction of top 20 clones as the D20 values was comparable between aged WT and *Apoe*$^{-/-}$ naïve B cells **(Figure 3.19B)**, further indicating similar levels of autoreactive immune responses in aged WT and *Apoe*$^{-/-}$ naïve B cells. The clonal diversification index in both aged WT and *Apoe*$^{-/-}$ naïve B cells was low and with no significant difference **(Figure 3.19C)**, supporting low mutations in aged naïve B cells.

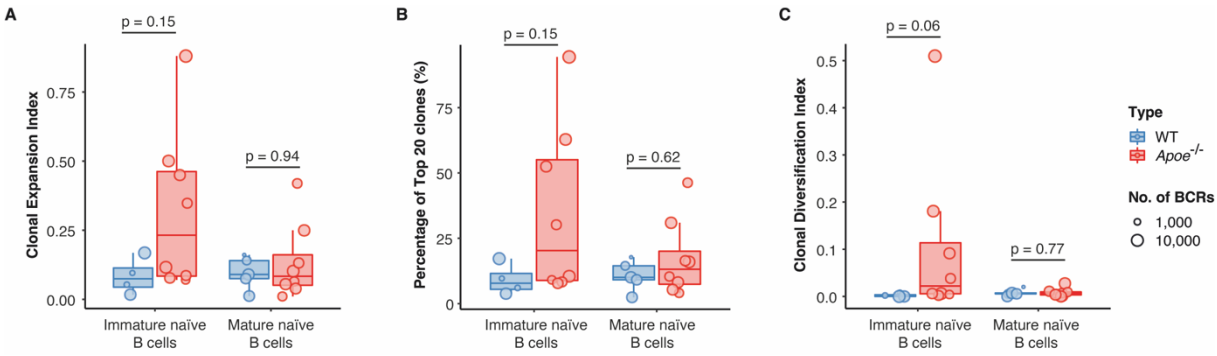

Figure 3.19 Similar clonality of naïve B cells in aged *Apoe*$^{-/-}$ mice
(A) The clonal expansion index **(B)** the D20 fraction and **(C)** the clonal diversification index of naïve B cells in both young and aged mice. The ends of the boxes show the upper and lower quartiles; the central lines represent medians. The sizes of the dots represent the number of sequences in each sample. BM immature naïve B cells: WT n=4, *Apoe*$^{-/-}$ n=8; spleen mature naïve B cells: WT n=5, *Apoe*$^{-/-}$ n=8. The p-values for two-group comparisons were determined by Wilcoxon-Signed-Rank Test.

Above, we reported increased clonal expansion in young *Apoe*$^{-/-}$ naïve B cells when compared to young WT mice, suggesting breakdown of tolerance to lead to autoreactive B cell response in young *Apoe*$^{-/-}$ mice. Since aging is one factor to shrink the BCR repertoire, it is not surprising to detect more clonal expanded naïve B cells in aged mice. The expansion was comparable between aged WT and *Apoe*$^{-/-}$ naïve B cells, implying aging plays a more important role in

naïve B cell clonal expansion than lack of *Apoe*. Although there was no significant difference, aged *Apoe*$^{-/-}$ naïve B cells displayed a tendency to increase their expansion versus WT naïve B cells, suggesting tolerance breakdown of aged *Apoe*$^{-/-}$ mice.

3.3.3 Atherosclerosis-specific overexpression of IGHV families in aged *Apoe*$^{-/-}$ mice

The results obtained from aged mice have uncovered the underrepresentation of IGHV4, IGHV11 and IGHV13 families, as well as overexpression of IGHV7 and IGHV14 families in aged *Apoe*$^{-/-}$ mice **(Section 3.1.6 and 3.2.7)**. However, whether the bias of IGHV gene expression is attributable to *Apoe* deficiency in young mice or late atherogenesis has not been investigated. To answer this question, the usage of IGHV family in naïve B cells from both young and aged mice were assessed **(Figure 3.20)**. The frequency of IGHV4 and IGHV11 families between young WT and *Apoe*$^{-/-}$ mice was comparable in both immature naïve B cells and mature naïve B cells **(Figure 3.20A and B)**. Low usage of IGHV7 and IGHV14 families, as well as increasing of IGHV13 family were found in young *Apoe*$^{-/-}$ mice when compared to young WT mice, which was opposite to the results obtained from aged B cells and PCs **(Figure 3.20A and B)**. This data indicates that the decreased selection of IGHV4, IGHV11 and IGHV13, as well as increased selection of IGHV7 and IGHV14 occur in aged *Apoe*$^{-/-}$ mice and may be in relation to atherosclerosis rather than *Apoe* deficiency. When comparing the IGHV family usage in aged WT and *Apoe*$^{-/-}$ naïve B cells, there was no significant difference in the frequencies of IGHV4, IGHV11, IGHV13 and IGHV14 between two genotypes, but IGHV7 showed tendency to increase in aged *Apoe*$^{-/-}$ naïve B cells **(Figure 3.20C and D)**. Therefore, in aged *Apoe*$^{-/-}$ mice, the lower usage of IGHV4, IGHV11 and IGHV13 families, as well the higher usage of IGHV14 family initiate in activated B cells, whereas the increasing of IGHV7 usage tends to initiate in naïve B cells **(Figure 3.20C and D)**. In addition, the significant changes of the fraction in IGHV1, IGHV2, IGHV3 and IGHV10 families in young mice were to some extent similar to variations in IGHV usage frequency in aged SLOs **(Figure 3.7, 3.17 and 3.20)**, and thus those changes may be associated with loss of *Apoe*. However, the young mice used here had an age of 8-10 weeks and were maintained under normal mouse chow. *Apoe*$^{-/-}$ mice are born hyperlipidemic with a very high level of total cholesterol. Although at 8-10 weeks of age there is no macroscopic visible atherosclerosis, evidence indicates that these mice have a series of morphological changes including macrophage/foam cell accumulation in the intima of the aortic arch. We therefore believe that it is too early to say whether the B cell immune response in young *Apoe*$^{-/-}$ mice is due to the absence of *Apoe* or due to changes that are related to hyperlipidemia and/or early stages of atherosclerosis.

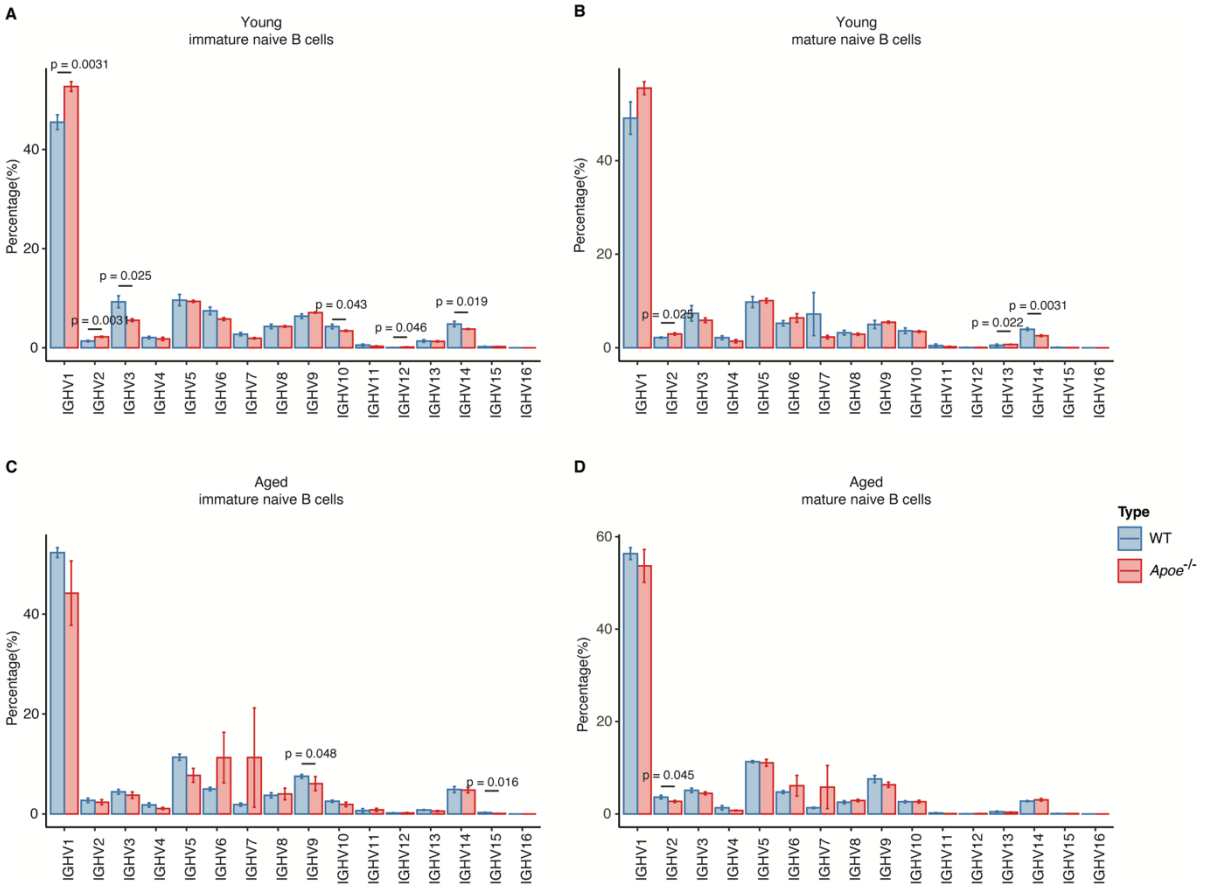

Figure 3.20 Frequency of IGHV family usage of naïve B cells in young WT and *Apoe*$^{-/-}$ mice

The average frequency of IGHV family usage in **(A)** young immature naïve B cells, **(B)** young mature naïve B cells, **(C)** aged immature naïve B cells and **(D)** aged mature naïve B cells were shown in barplots. The error bar indicates standard error of the mean. In WT mice, young immature naïve n=7, young mature naïve n=7, aged immature naïve n=4, aged mature naïve n=5; in *Apoe*$^{-/-}$ mice, young immature naïve n=10, young mature naïve n=10, aged immature naïve n=8, aged mature naïve n=8. The p-values for two-group comparisons were determined by Wilcoxon-Signed-Rank Test. *: p<0.05; **: p<0.01; ***: p<0.001.

3.4 Disruption of immune tolerance in ATLO GCs

To investigate the gene expression in relation to B cell functions and subtypes, scRNA-seq was applied to aged WT RLNs, *Apoe*$^{-/-}$ RLNs and ATLOs to determine the gene expression profile in each B cell. Importantly, the sequences of BCR heavy and light chain in each B cell were paired to the expression profile, giving us the opportunity to relate mRNA profiles to the respective BCR trees. After ruling out cells with low quality, a total of 12,854 B cells were obtained from three tissues (WT RLNs: 5,336; *Apoe*$^{-/-}$ RLNs: 5,102; ATLOs: 2,416).

3.4.1 Distinct gene expression profiles in ATLO B cells

First, the totality of DEGs in different tissues was determined. A total of 247 significantly up-regulated genes was obtained for three tissues. The WT RLNs and *Apoe*$^{-/-}$ RLNs showed major similarity in terms of total B cell gene expression **(Figure 3.21A)**. Only 4 significantly up-regulated genes were found in WT RLN B cells when compared to *Apoe*$^{-/-}$ RLNs and ATLOs **(Figure 3.21A)**. These genes cannot be enriched to any functional pathways when annotated in KEGG database, suggesting the identified genes do not display significant associations with any specific biological processes or molecular functions. *Apoe*$^{-/-}$ RLN B cells showed no significantly up-regulated genes when compared to the other two groups **(Figure 3.21A)**. The majority of DEGs were observed between ATLO B cells versus RLN B cells, i.e., 243 genes were significantly over-expressed, and 4 genes were down-regulated in ATLO B cells. Both ATLO up-regulated and down-regulated DEGs were used for further functional enrichment analysis. It was determined that the DEGs showed a significant enrichment in pathways associated with immune response. Specifically, the DEGs were found to be enriched in TNF signalling pathways, the chemokine signaling pathway and importantly B cell receptor signalling pathways **(Figure 3.21B)**. This suggests that the DEGs in ATLOs B cells have functional roles in regulating immune responses, potentially influencing processes such as inflammation, cell migration and autoantibody production. Therefore, the overall comparison on B cells between ATLOs and SLOs indicates distinct immune responses in ATLOs, providing evidence that ATLOs may be the unique site for atherosclerosis B cell immune response.

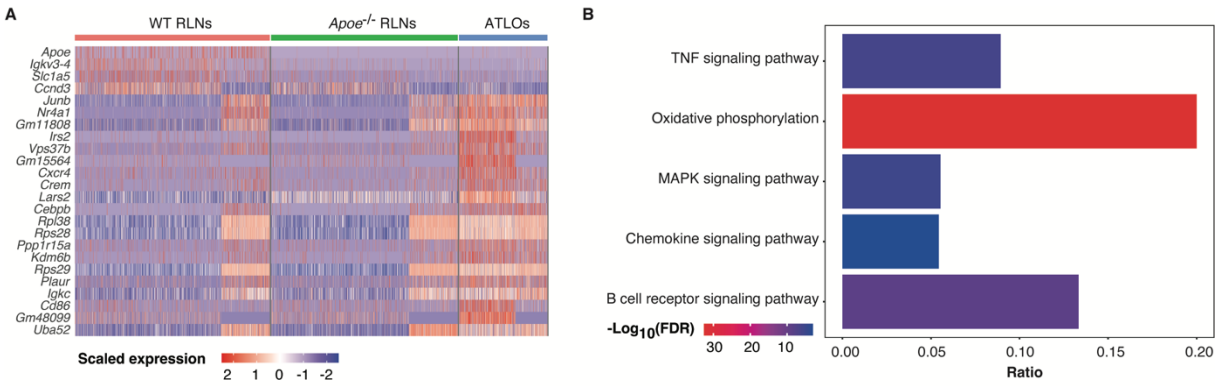

Figure 3.21 Distinct gene expression profiles in ATLO B cells versus SLO B cells
(A) The heatmap shows the expression of top 20 significantly up-regulated genes in each tissue. The expression was visualized as a scaled value after normalization. DEGs: log(FC)>0.25 and p<0.05. **(B)** Representative KEGG pathways enriched in ATLO DEGs. Ratio = observed genes / background genes. The significance of enrichment was determined as FDR < 0.05.

3.4.2 scRNA-seq identifies 7 B subsets from total B cells

To dissect B subsets, the top 2,000 highly variable genes in total B cells were used to construct the UMAP plot. UMAP is a method to reduce the dimensionality of scRNA-seq data and visualize the relationships of cells based on expression of thousands of genes. In our data, the total B cells obtained from three tissues were assigned to 10 clusters **(Figure 3.22A)**. Based on canonical markers and signature genes provided by Mathew and colleagues, the clusters were combined and identified as 7 B subsets, including a PC subset, a Mem/B-1 subset and 5 B-2 subsets (Mathew et al., 2021) **(Figure 3.22B-D)**. Cluster 7 (C7) was identified as the PC population by high expression of *Ighm* gene as well as marker genes including *Xbp1*, *Sdc1(Cd138)*, *Prdm1*, *Jchain* and *Slpi* (Shi et al., 2015) **(Figure 3.22C and D)**. C4 comprised B-1 B cells which were marked as *Cd19* and *Spn (Cd43)* double-positive cells (Cunningham et al., 2014). This cluster also expressed *Zeb2* and *Vim*, which are markers of memory B cells (Laidlaw et al., 2020, Riedel et al., 2020) **(Figure 3.22C and D)**. Therefore, this cluster was named as Mem/B-1 subset. The other 7 clusters were characterized as B-2 cells by high expression of *Cd19* but low expression of *Spn (Cd43)* (Muri et al., 2019) **(Figure 3.22C)**. C0-C3 accounted for the majority of B-2 cells. They were named as B-2 subsets since they were *Cd19*-positive and *Cd43*-negative but lacking other specific markers for further identification **(Figure 3.22C and D)**. C9 showed increased expression of interferon regulatory factor 7 (*Irf7*) and several interferon-inducible genes (e.g., *Ifi203* and *Ifit3*) **(Figure 3.22C and D)**. *Cd83, Fcer2a, Junb, Nr4a1 and CD69* were over-expressed in C5, indicating that this cluster comprised newly activated B cells (Nac B) (Mathew et al., 2021) **(Figure 3.22D)**. C6 showed higher expression of *Myc, Npm1*, *Eif5a*, *Ran*, *Mif* and *Eif4a1*, which were suggested to be expressed in early GC B cells (Mathew et al., 2021) **(Figure 3.22D)**. C8 was defined as late GC B cells by highly expressing *Aicda*, which plays a critical role in SHM and CSR (Victora and Nussenzweig, 2012) **(Figure 3.22C)**. This cluster also showed high expression of *Mki67*, which encodes Ki-67 protein associated with cell proliferation (Sobecki et al., 2016) **(Figure 3.22D)**.

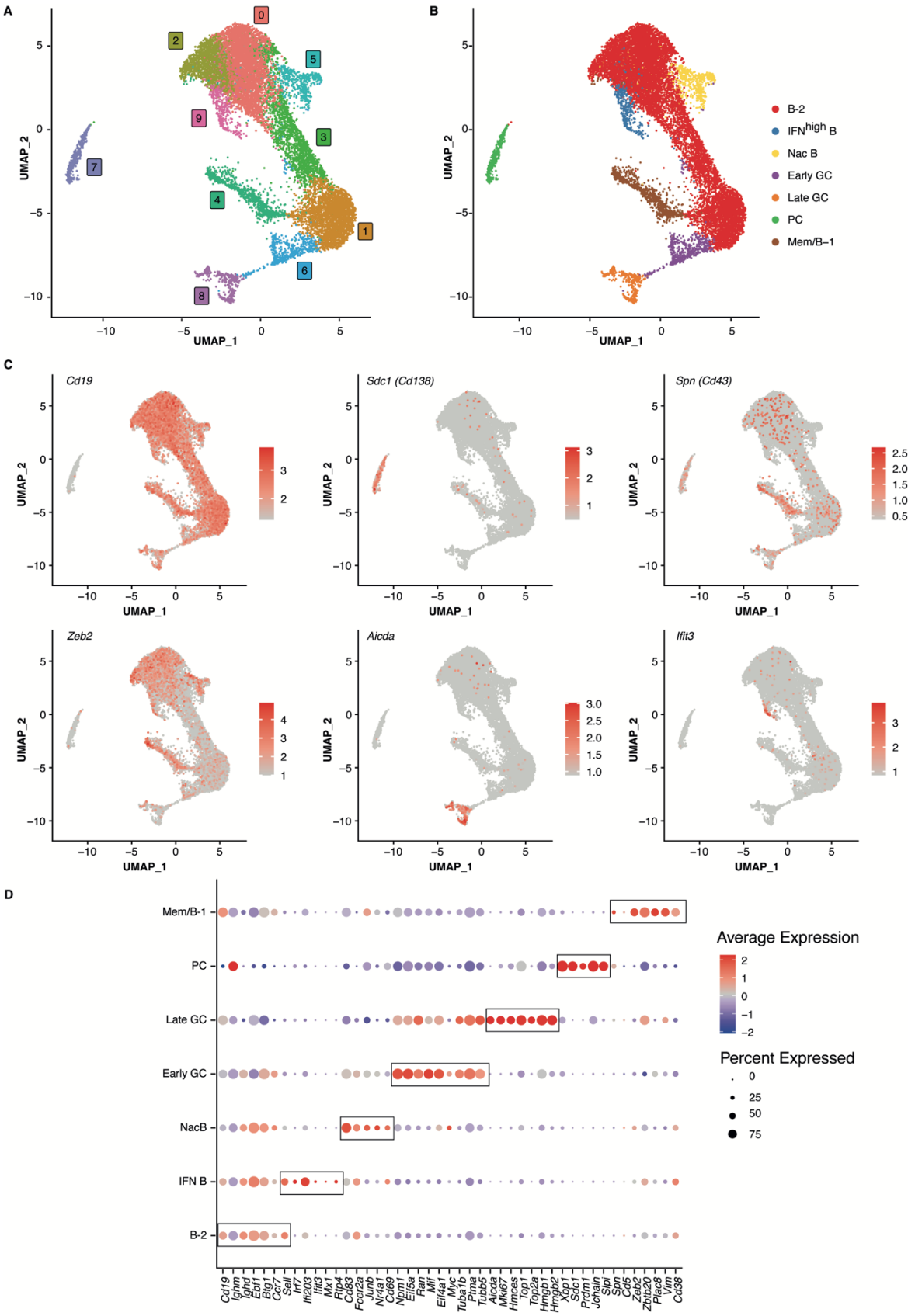

Figure 3.22 7 B subsets were identified from total B cells
(A) The UMAP algorithm used a total of 12,854 B cells which were separated into 10 clusters. **(B)** All clusters were classified into 7 B subsets based on gene expression profiles. The UMAP plot shows the name and the location of each population in the UMAP map. **(C)** Normalized

expression of B cell markers in UMAP plot. **(D)** Scaled expression of genes selected to define B subsets. The dot sizes are corresponding to the proportion of cells expressed that gene and the colors indicate the levels of average expression in each subpopulation.

Expression of top10 highly expressed genes in each B cell subset was next visualized **(Figure 3.23A)**. B-2 subset showed higher expression of *Cd55*, *Ccr2*, *Sell* and *Bank1*, indicating involvement of B cell immune responses **(Figure 3.23A)**. In addition to *Ifi203*, IFN^{high} B subset also showed high expression of *Stat1*, *Trim30a*, *Parp14*, *Rnf213*, *Irgm1*, which are involved in type-1 Interferon signalling pathways (D'Souza et al., 2021) **(Figure 3.23A)**. The expression of *Myc*, *Nfkb1*, *Rel*, *Egr1* and *Egr3* transcripts was detected in the Nac B subset to regulate cell survival, proliferation and death **(Figure 3.23A)**. The early GC and late GC subsets were separated by expression of cell cycle-related genes *Ranbp1*, *Eif5a*, *Nme2*, *Mki67*, *Hmgb2*, *Stmn1* and *Top2a* **(Figure 3.23A)**. The PC subset was identical by highly expressing BCR-related genes like *Jchain*, *Iglv1* and *Igkc* **(Figure 3.23A)**. The Mem/B-1 subset showed increased expression of memory-related genes *Fcrl5*, *Zeb2* and B-1-related genes *Plac8* (Kim et al., 2019, Luo et al., 2022) **(Figure 3.23A)**. The specifically highly-expressed genes in each subset were referred to the KEGG database for functional enrichment analysis. B-2 subsets were significantly enriched on B cell receptor signalling pathway and chemokine signalling pathway **(Figure 3.23B)**. The IFN^{high} B subset showed higher enrichment on several infection-related terms as expected (Honda et al., 2005, Ivashkiv and Donlin, 2014) **(Figure 3.23B)**. The ribosome biogenesis pathway was observed in the Nac B subset and Mem/B-1 subset, which was known to play a role in protein synthesis, cell proliferation and apoptosis (Jiao et al., 2023) **(Figure 3.23B)**. Oxidative phosphorylation (OXPHOS), which has been reported to be enhanced in activated B cells, was markedly enriched in early GC, late GC, PC and Mem/B-1 subsets (Price et al., 2018) **(Figure 3.23B)**. Early GC and late GC B cells also exhibiting enriched function pathways related to proteasome, spliceosome and protein processing in the endoplasmic reticulum **(Figure 3.23B)**. These pathways are crucial in regulating protein

homeostasis, antibody production and generation of high-affinity antibodies during immune response. PCs were noticed to be involved in protein export as expected, as this function is essential for the secretion of antibodies **(Figure 3.23B)**.

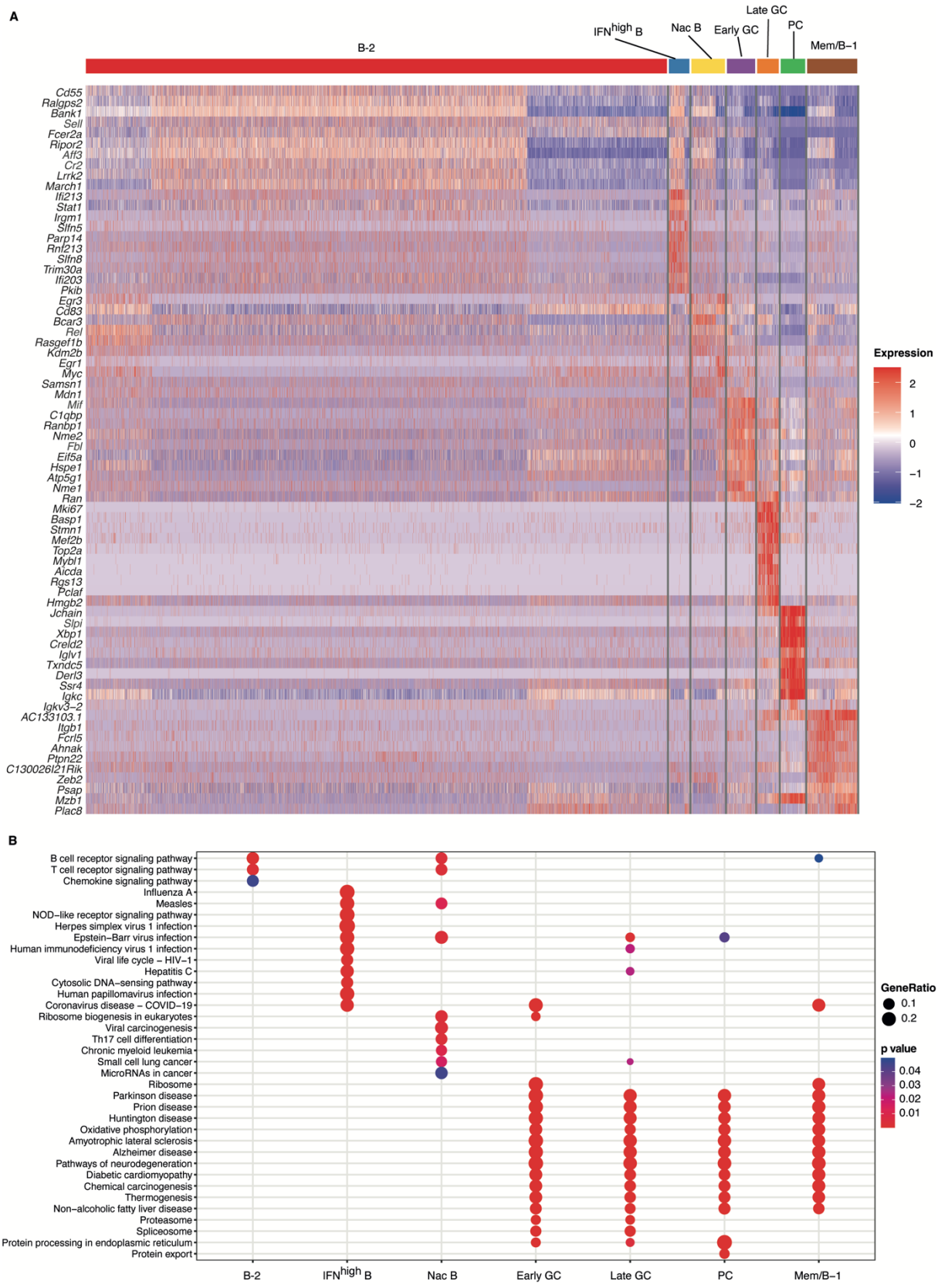

Figure 3.23 The transcriptome and functional prediction in different B cell subsets
(A) The heatmap shows the expression of top10 highly expressed genes in each B cell population. The expression was visualized as a scaled value after normalization. **(B)** Top10 KEGG terms enriched in each B cell subset. The ratio was calculated as the observed genes /

the background genes. The colors indicate adjusted p-values, and the sizes of dots are proportional to the ratio. The significance of enrichment was determined as $p<0.05$.

In conclusion, the different B cell subsets were distinguished by specific gene expression and functional enrichment, supporting distinct roles of each subset in the immune response.

3.4.3 Distinct B-cell compositions in ATLOs

To determine the differences of B cell compositions in WT RLNs, *Apoe*$^{-/-}$ RLNs and ATLOs, the proportion of B cell subsets in each tissue was compared **(Figure 3.24)**. All B cell subsets were presented in all tissues including in ATLOs **(Figure 3.24A)**, supporting the notion that the required spectrum of B cell adaptive immune responses can be organized not only in SLOs but also in ATLOs. WT and *Apoe*$^{-/-}$ RLNs showed major similarities in cellular composition and there was no significant difference on the percentages of most of B cell subsets **(Figure 3.24B and C)**. They both composed an overwhelming population of B-2 subsets, accounting for more than half of the total B cells (WT: 78.19%; *Apoe*$^{-/-}$: 79.67%) **(Figure 3.24B)**. RLNs also contained a significant percentage of Nac B cells (WT: 5.36%; *Apoe*$^{-/-}$: 4.39 %) and Mem/B-1 cells (WT: 5.23%; *Apoe*$^{-/-}$: 5.31%) **(Figure 3.24B)**. IFN^{high} B cells, early GC B cells, late GC B cells and PC subsets only occupied a small fraction in both WT and *Apoe*$^{-/-}$ RLN B cells **(Figure 3.24B)**. Compared to WT and *Apoe*$^{-/-}$ RLNs, ATLOs exhibited reduced number of B-2, IFN^{high} B and Nac B subsets **(Figure 3.24B)**. And the proportion of late GC B cells in ATLOs was decreased comparing to WT RLNs ($p=0.0058$) and *Apoe*$^{-/-}$ RLNs ($p=0.052$) **(Figure 3.24B)**. Additionally, the fraction of PCs in ATLOs markedly increased to 4-fold when compared to *Apoe*$^{-/-}$ RLNs **(Figure 3.24B)**. Furthermore, ATLOs harbor a higher proportion of early GC and Mem/B-1 cells **(Figure 3.24B)**. These observations were consistent with the data obtained by flow cytometry analysis based on protein expression published by our group (Srikakulapu et al., 2016).

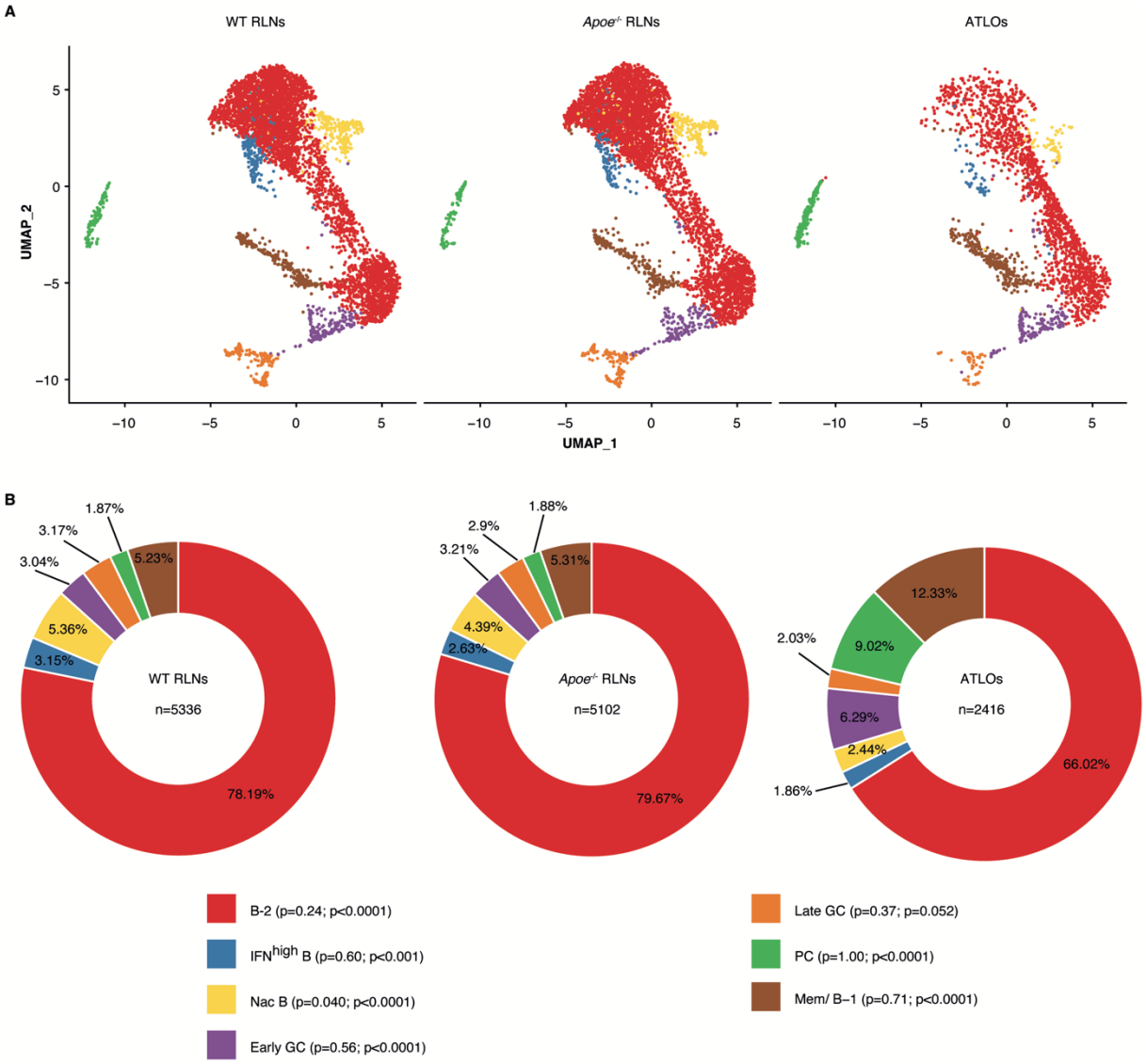

Figure 3.24 Distinct B cell compositions in ATLOs
(A) The UMAP plot shows the distribution of B cell subsets in each tissue. Each dot represents one cell. **(B)** The proportion of different B cell subsets in each tissue. The p-value was determined by the Chi-square test and adjusted by Benjamini-Hochberg correction. The first p-value in the brackets was determined by comparing *Apoe*$^{-/-}$ RLNs versus WT RLNs, while the second p-value was determined by comparing ATLO versus *Apoe*$^{-/-}$ RLNs.

In summary, these data indicate distinct differences in cellular composition between RLNs and ATLOs. ATLOs exhibit a modified distribution of B cell subsets, suggesting the potential for unique B cell immune responses in ATLOs. Further study is necessary to elucidate the functional differences and their implication in B cell immune response within these tissues. However, the data suggests the important possibility that ATLOs harbor dysfunctional GC dynamics and function.

3.4.4 Distinct gene expression profiles in ATLO B cell subsets

To further investigate the potential functional differences to conduct B cell immune responses in ATLOs versus SLOs, DEGs of each tissue (logFC>0.25, p<0.05) were determined in each B cell subset. Only a few genes were specifically dysregulated in WT and *Apoe*$^{-/-}$ RLNs, while ATLOs showed a pronounced number of DEGs in each B cell subset **(Figure 3.25A)**. ATLO early GC, late GC and Mem/B-1 subsets showed an increased number of dysregulated genes when compared to their corresponding RLN subsets. Around 100 DEGs are shown in each group **(Figure 3.25A)**. In ATLOs B-2, IFN^{high} and Nac B subsets, more than 200 genes were markedly dysregulated in comparison to their RLN counterparts **(Figure 3.25A)**. In order to investigate whether these DEGs are cell-specific or are expressed across B cell subtypes, the DEGs obtained from different ATLO B subsets were further analyzed. A total of 750 DEGs across B cell subsets were found to be dysregulated in ATLOs **(Figure 3.25B)**. There were a large number of DEGs observed across multiple ATLO B cell subsets. The overexpression of *Junb*, *Gm15564*, *lars2* and *Cebpb* were detected in all ATLO B cell subsets when compared to corresponding RLN B cell subset. And there were 8 DEGs across 6 B cell subset, 16 DEGs across 5 B cell subset, 39 DEGs across 4 B cell subsets **(Figure 3.25B)**. Most of DEGs were observed in less than 4 cell types **(Figure 3.25B)**, indicating their regulation are B cell subset-specific. Next, a total of 750 DEGs were referred to databases for functional projection, and the functional-related DEGs were clustered. The ATLO-specific genes were specifically enriched to regulate OXPHOS, ribosome assembly, cell activation and proliferation **(Figure 3.25C-F)**. This suggests that these dysregulated genes in ATLO B cells may play a role in regulating mitochondrial energy production, protein synthesis and immune response activation and proliferation.

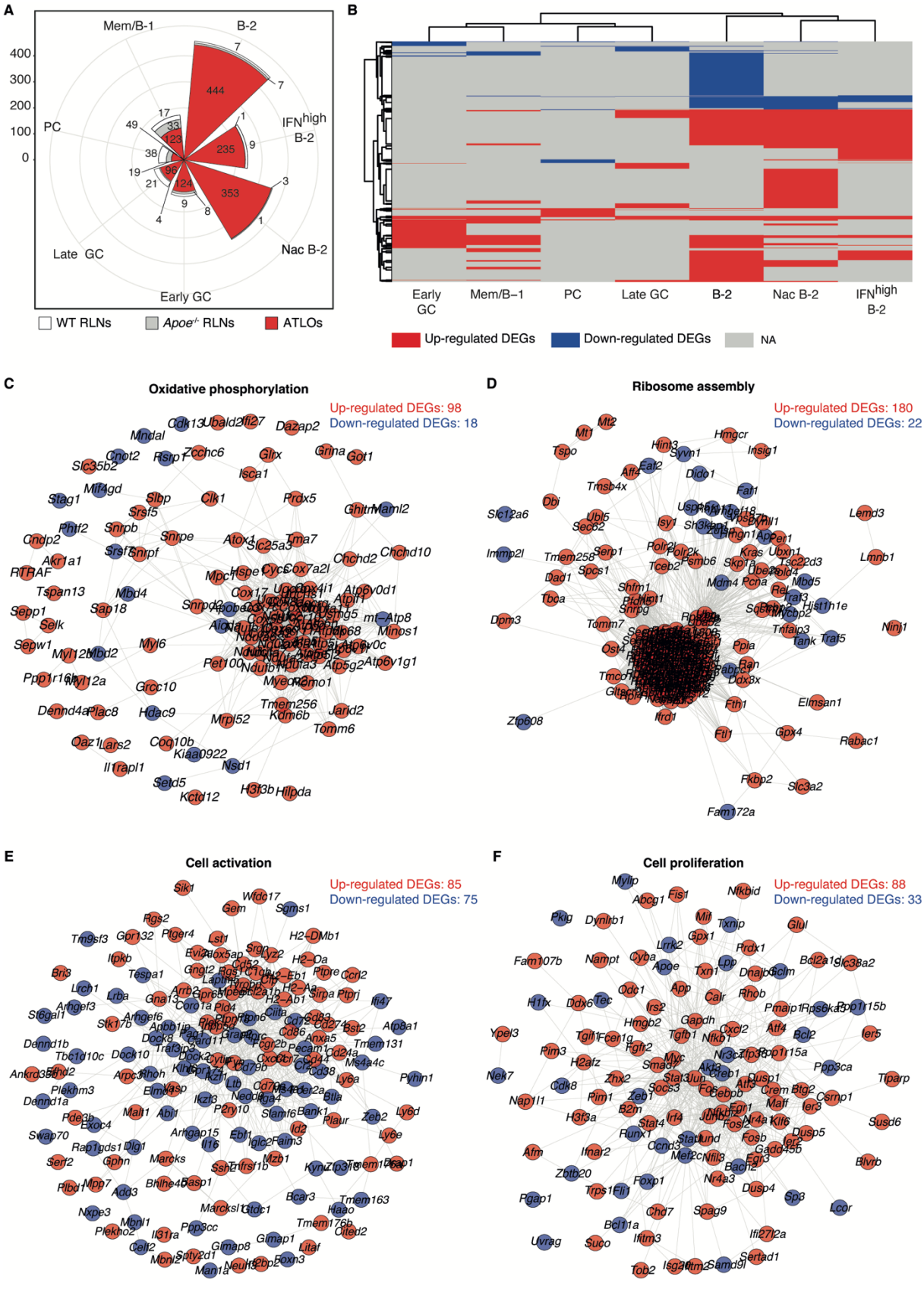

Figure 3.25 Potential functional implications of dysregulated gene expression profiles in ATLO B cell subsets

(A) The rose diagram shows the number of DEGs in each tissue within different B cell subsets. **(B)** Heatmap illustrates the distribution of ATLO DEGs across different B cell subsets. The

number of DEGs across tissues are shown at right in the table. **(C-F)** Clusters of functional-related DEGs in ATLO B cell subsets. The nodes indicate genes, and the edges indicate gene associations. The colors represent up-regulated DEGs and down-regulated DEGs, respectively.

Overall, these findings highlight the distinct gene expression profiles and functional differences in between ATLO and SLO B cell subsets. The dysregulated genes in ATLOs may contribute to the unique immune response of the specific B cell subsets in this TLO during atherosclerosis. The observation of both common and subset-specific DEGs in ATLOs suggests the presence of dysregulated functions shared by multiple ATLO B cell subsets, as well as subset-specific dysregulation of functionality.

3.4.5 Distinct B cell clonality in ATLOs

Apart from the transcriptome of single B cells, the BCRs of each single B cell was also sequenced using the pairing approach. This provided the important opportunity to pair individual B cell clonalities and their single cell gene expression profiles. Around 61% (3,248/5,336) WT RLN B cells, 68% (3,457/5,102) *Apoe*$^{-/-}$ RLN B cells and 81% (1,946/2,416) ATLO B cells were successfully paired with their BCR sequences, indicating a high quality of our data. Because the information of BCR heavy chain is sufficient to determine B cell clones, BCR clones were determined as cells containing identical V, J family and CDR3aa regions in heavy chains (Zhou and Kleinstein, 2019, Bashford-Rogers et al., 2019). All clonally expanded B cells were highlighted in the UMAP plot **(Figure 3.26A)**. Illustrated by the UMAP plot, the expanded B cells were mainly limited to three B cell subsets: (1) late GC subset; (2) PC subset and (4) Mem/B-1 subset **(Figure 3.26A)**. To quantify this observation, the fraction of expanded cells in each B cell subset was calculated. Late GC, PC and Mem/B-1 B cell subsets showed more than 20% of expanded cells, while expanded cells only accounted for a small fraction in B-2 cells, IFN^{high} B cells, Nac B cells and early GC B cells **(Figure 3.26B)**. These data were consistent with the concept that activated GC B cells undergo clonal expansion and terminally differentiated into PCs or memory B cells in GCs. To compare the tissue difference of expansion in late GC, PC and Mem/B-1 B cell subsets, the expansion of these 3 subsets in RLNs and ATLOs was analyzed. In WT and *Apoe*$^{-/-}$ RLNs, PCs showed the highest percentage of expanded cells, while the fraction in late GC and Mem/B-1 subsets was similar **(Figure 3.26C)**. However, the fraction of expanded cells in ATLO PCs decreased to levels similar to those in ATLO late GCs **(Figure 3.26C)**, suggesting dysfunctional ATLO GCs. Next, the mutation in heavy chain in each B cell was calculated **(Figure 3.26D and E)**. Only a few mutations were observed in B-2, IFN^{high}, Nac and early GC B cell subsets, while the mean mutations surged to

around 5 in Mem/B-1 and exceeded 7 in PCs **(Figure 3.26D)**. GCs showed the highest mean mutations, i.e. each cell on average contained more than 10 mutations **(Figure 3.26D)**. When compared the mutations in different tissues, WT RLNs and *Apoe*$^{-/-}$ RLNs were similar. Late GC B cells displayed significantly higher mutations than PCs and Mem/B-1 cells, supporting rapid SHM in WT and *Apoe*$^{-/-}$ RLN GCs **(Figure 3.26E)**. The mean mutations in ATLO late GC subsets decreased, however, with significantly increasing of mean mutations in PCs when compared to ATLO late GC and Mem/B-1 B cells **(Figure 3.26E)**. This data indicated that SHM in ATLO GCs may be compromised. The class-switched cells were also abundant in late GC, PC and Mem/B-1 B cell subsets **(Figure 3.26F)**. In WT and *Apoe*$^{-/-}$ RLNs, a large number of late GC and PCs were class-switched, and the fraction of switched cells in Mem/B-1 subsets was dramatically lower than that in late GC and PC subsets **(Figure 3.26G)**. However, ATLO late GC, PC and Mem/B-1 B cell subsets contained comparable percentages of class-switched cells **(Figure 3.26G)**. These findings implicate the mechanism of CSR in ATLO GCs may be disrupted.

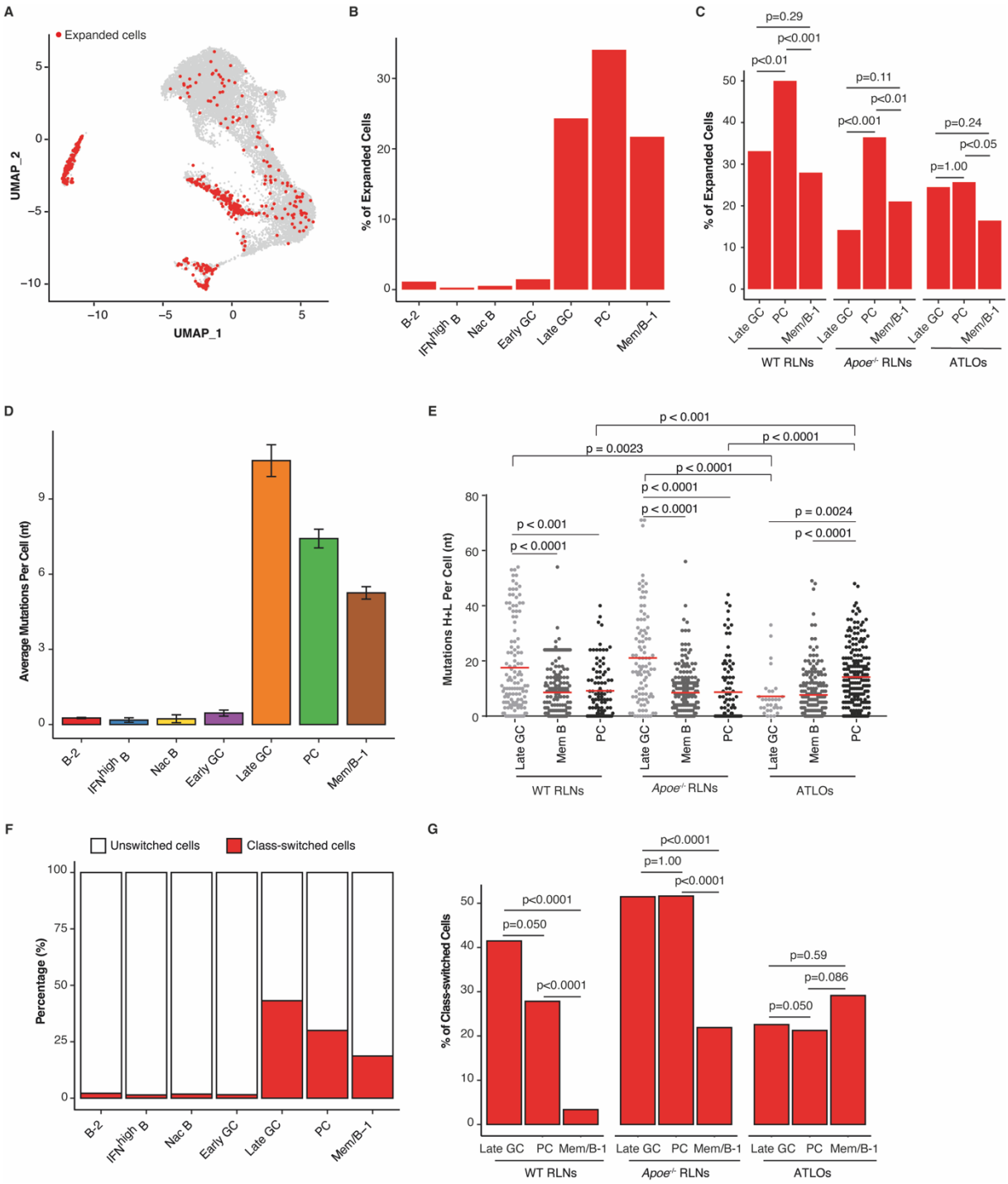

Figure 3.26 B cell subset clonality in ATLOs

(A) The UMAP plot highlights clonally expanded B cells. The expanded cells were coloured as red; the light grey indicates nonexpanded B cells, B cells without paired heavy and light chains, or B cells that BCR sequences remained undetected. **(B)** The fraction of expanded B cells in different B cell subsets. **(C)** The fraction of expanded cells in late GC, PC and Mem/B-1 B cell subsets in each tissue. **(D)** The mean mutations on heavy chain in different B cell subsets. The error bar indicates standard error of the mean. **(E)** Total mutations per cell on BCR heavy chain and light chain within different GC states in each tissue. Each dot represents one cell, and the red short lines indicate mean mutations in the group. **(F)** The fraction of unswitched and class-switched B cells in different B cell subsets. **(G)** The fraction of unswitched and class-switched B cells in late GC, PC and Mem/B-1 cell subsets in different

tissues. The p-value in **C** and **G** was determined by Chi-square test and adjusted by Benjamini-Hochberg correction. The p-value in **E** was calculated using Wilcoxon-Signed-Rank Test with Benjamini-Hochberg correction.

In summary, clonal expansion, mutation and fraction of class-switched cells are primarily observed in GC and post-GC B cells (PCs and memory B cells) in both RLNs and ATLOs. This observation is in line with concepts that activated GC B cells undergo clonal expansion and differentiate into PCs or memory B cells. ATLO displayed less expanded PCs, as well as decreased levels of mutation-carrying and class-switched late GC B cells when compared to RLNs, suggesting lower levels of SHM and CSR in ATLO GCs. These data indicated compromised GC-dependent immune response in ATLOs, raising the possibility that ATLO B cells may undergo tolerance checkpoint breakdown in GCs.

3.4.6 Identification of 3 GC B cell subsets in total GC B cells

Regrettably, the number of GC B cells in our data was insufficient for further delineation. Still, in order to determine the heterogeneity of GC B cells in SLOs and ATLOs, early GC and late GC B cell subsets were integrated with a published scRNA-seq data of GCs (GSE154634) (Chen et al., 2021). The published GC B cells data were obtained from mice immunized with either single antigen (4-hydroxy-3-nitrophenylacetyl conjugated with keyhole limpet hemocyanin, NP) or complex antigen (ovalbumin, OVA) based on cell surface markers $B220^{+}Fas^{hi}GL\text{-}7^{hi}NP^{+}$ and $B220^{+}Fas^{hi}GL\text{-}7^{hi}OVA^{+}$. After normalization and integration, no batch effect was observed between published data and our data **(Figure 3.27A)**. The UMAP strategy nonsupervisory assigned all integrated GC B cells into 7 clusters **(Figure 3.27B)**. A set of gene markers in relation to GC dark zone (DZ), light zone (LZ) and resting stage were introduced to identify the GC B cell subsets (Chen et al., 2021) **(Figure 3.27E and F)**. Expression of cell cycle-associated genes, i.e., genes prototypically expressed during the G2/M and S phases was evaluated to categorize cells based on their specific cell cycle phases. Cells exhibiting limited expression of both G2/M- and S-related genes were designated as non-cycling cells in the G0 or cells during their transition from G0 to S, i.e. the G1 phase (Tirosh et al., 2016) **(Figure 3.27C)**. The enriched expression of *Cd83* and *Myc* in C0, C4 and C6 indicated that they are mainly LZ GC B cells (Holmes et al., 2020) **(Figure 3.27E and F)**. They also highly expressed *H2-Eb1*, *Cd74*, *Cd79b* and *Syk*, implying they are involved in antigen presenting and BCR signalling pathways (Chen et al., 2021) **(Figure 3.27E)**. C0, C4 and C6 also showed enrichment of *Zbtb20*, which contributes to PC maintenance (Zhu et al., 2018) **(Figure 3.27E)**. Cells in the C0, C4 and C6 primarily undergo G0/G1 phase of the cell cycle

(Figure 3.27C), supporting they are non-cycling cells. The DZ markers such as *Mcm3*, *Pcna*, *Tubb5*, *Cenpa, Mki67*, *Cxcr4* and *Aicda* were markedly expressed in C1, C2 and C3, implying elevated cell proliferation and SHM in these clusters **(Figure 3.27E and F)** (Holmes et al., 2020, Chen et al., 2021). The cell cycle analysis also supported the conclusion that these cells were in phases of S-G2-M for mitosis and/or DNA synthesis **(Figure 3.27C)**. C5 showed low expression of activation- and proliferation-related genes, but exhibited highest expression on resting markers like *Ighd*, *Cd38* and *Ly6d* **(Figure 3.27E)** (Chen et al., 2021). Cells in C5 also indicated that they are in the G0/G1 phase **(Figure 3.27C)**. Additionally, the expression of *Rasgrp2* and *Ccr6* in C5 indicated the presence of precursors of memory B cells, suggesting resting GC B cells of C5 **(Figure 3.27E and F)** (Holmes et al., 2020).

In summary, integrating the in-house GC data with published GC data showed heterogeneity of GCs and identified three major GC subsets in total GC B cells, including LZ GC B cells (C0, C4 and C6), DZ GC B cells (C1, C2 and C3) and resting GC B cells (C5) **(Figure 3.27D)**.

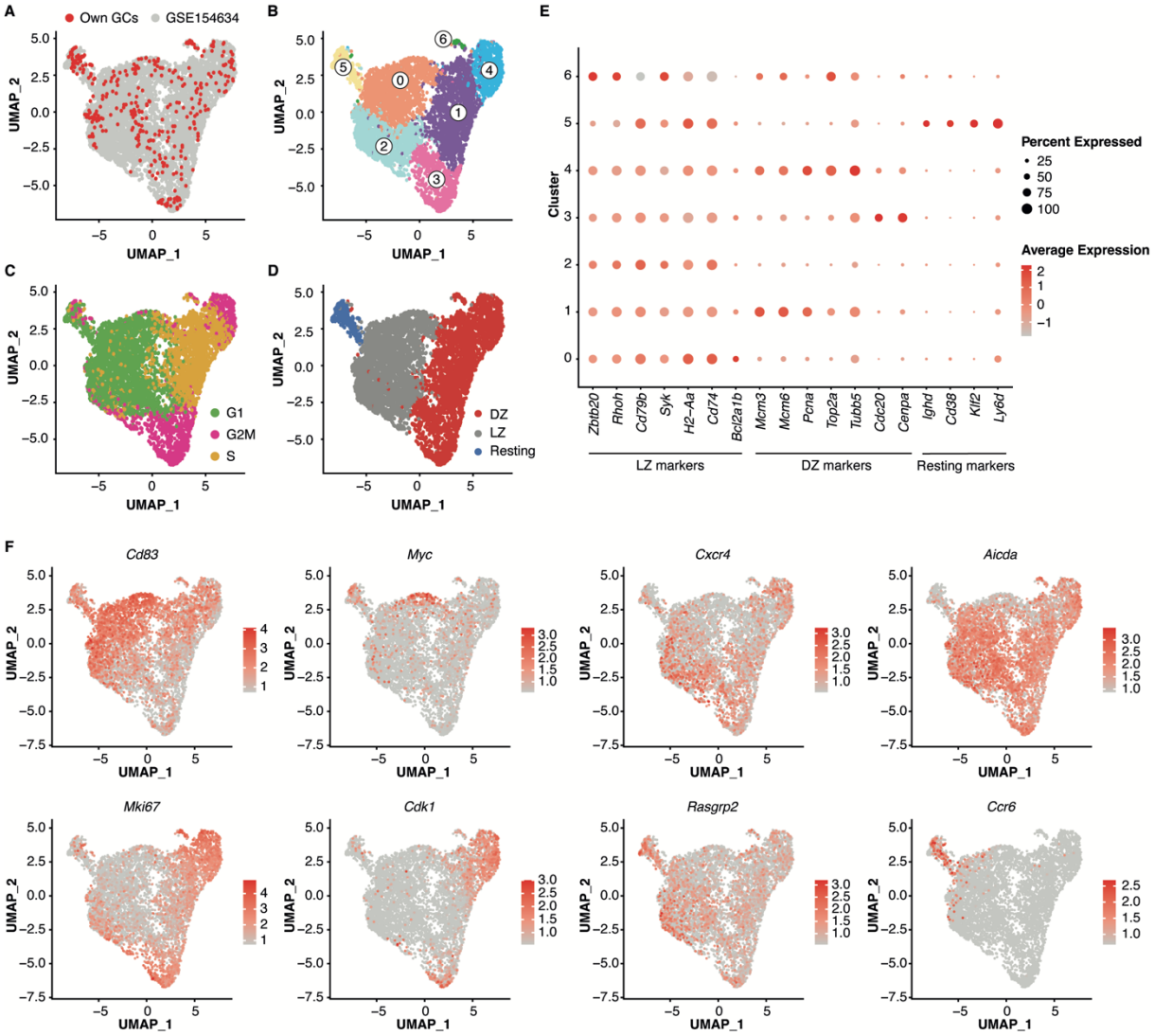

Figure 3.27 Identification of 3 GC B cell subsets in SLOs and ATLOs
(A) The UMAP plot shows overlap of two datasets after normalization and integration. **(B)** The UMAP algorithm constructed dimensionally reduced plots and nonsupervisory projected GC B cells into 7 clusters. **(C)** The UMAP plots show the projection of cell cycle stages in each GC B cell. **(D)** The cluster of DZ, LZ and resting GC B cells. **(E)** The scaled expression of markers involved in LZ, DZ and the resting state. The dot sizes correspond to the proportion of cells that expressed that gene, and the colors indicate the levels of average expression in each cluster. **(F)** The UMAP plot shows expression of a set of genes which are related to GC dynamics. Each dot represents one cell.

3.4.7 Disrupted GC dynamics in ATLOs

GC B cells shuttle between DZ and LZ compartments to undergo cycles of SHM and selection. This dynamic leads to accumulation of high-affinity B cells to antigens (Mesin et al., 2016). To investigate the GC dynamics in RLNs and ATLOs, the fraction of GC B cell from different compartments in WT RLNs, *Apoe*$^{-/-}$ RLNs and ATLOs were analyzed **(Figure 3.28)**. The

presence of all GC B subsets was observed in all tissues **(Figure 3.28A)**, indicating there was no tissue-specific GC B subsets and supporting the notion that ATLOs experience GC dynamics similar to RLN GCs. Comparative analyses between WT and *Apoe*$^{-/-}$ RLN GCs revealed similarities in their cellular composition, as there was no notable difference in the proportions of each GC B cell subsets **(Figure 3.28B)**. Both WT and *Apoe*$^{-/-}$ RLN GCs revealed substantial populations of DZ and LZ GC B cells, with only a minor fraction of resting GC B cells. Additionally, the relative abundance of DZ cells is lower compared to LZ cells in RLN GCs **(Figure 3.28B)**. Nevertheless, the cellular component of ATLO GCs were noticeably different from WT and *Apoe*$^{-/-}$ RLNs. The proportion of DZ GC B cells in ATLO GCs were significantly lower when compared to RLN GCs **(Figure 3.28B)**. Instead, there was a significant relative increase in the portion of LZ B cells in ATLO GCs **(Figure 3.28B)**.

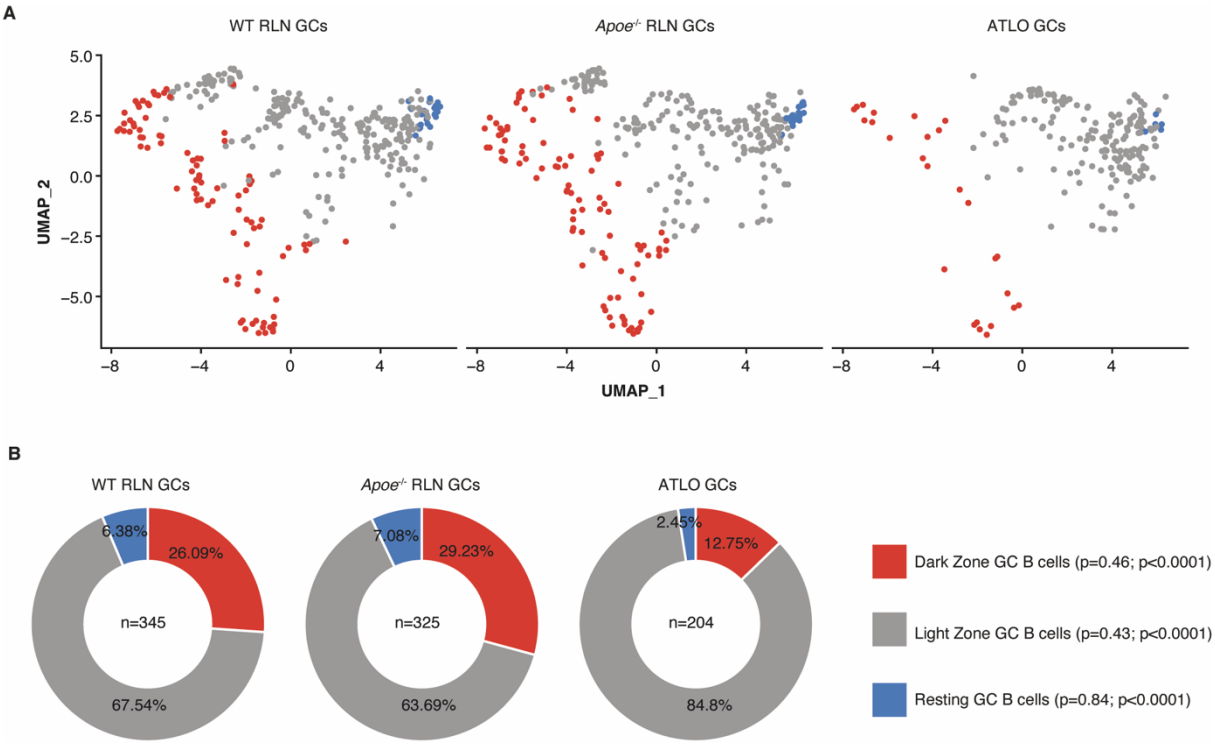

Figure 3.28 Distinct B cell compositions in ATLO GCs
(A) The UMAP plot shows the distribution of GC B cell subsets in each tissue. Each dot represents one cell. **(B)** The piecharts display proportion of DZ, LZ and resting GC B cells in each tissue. The p-value was determined by Chi-square test and adjusted by Benjamini-Hochberg correction. The first p-value was determined by comparing *Apoe*$^{-/-}$ RLN GC B subsets versus WT RLN GC B subsets, while the second p-value was determined by comparing ATLO versus *Apoe*$^{-/-}$ RLNs.

The difference in DZ and LZ cell distribution supports the concept of compromised GC dynamics in ATLOs, suggesting a distinct immune response and selection process in ATLOs compared to RLNs. The proliferation and SHM in ATLO DZ may decline, while the antigen presentation and T_{fh} cell interaction in LZ may be enhanced.

3.4.8 Compromised GC reactions in ATLOs

Taking the opportunity of pairing scRNA-seq profiling with single cell BCR sequencing (scBCR-seq) analysis, the BCR clonality between SLO GCs versus ATLO GCs were compared to evaluate GC reactions in different tissues. Both RLNs and ATLOs contained a large population of expanded B cells as identified previously **(Figure 3.26C)**. In WT RLNs, around 40% of DZ cells were clonally expanded **(Figure 3.29A)**, indicating that GC B cells undergo rapid proliferation in DZs. The percentage of expanded cells decreased to approximately 11% in WT LZ **(Figure 3.29A)**, supporting the notion that B cells experience positive selection to eliminate low-affinity cells in GC LZ. Resting GCs exhibited no expanded cells **(Figure 3.29A)**, raising the possibility that these cells newly enter GCs without proliferation and clonal expansion. Similar to WT RLN GCs, *Apoe*$^{-/-}$ RLN and ATLO DZ comprised more expanded cells than LZ cells, with no expanded cells in resting GCs **(Figure 3.29A)**. These findings indicate similar mechanisms of proliferation and affinity selection in *Apoe*$^{-/-}$ RLN and ATLO GCs. In both WT and *Apoe*$^{-/-}$ RLN GCs, DZ and LZ B cells displayed dramatically higher mutation levels compared to resting cells, with DZ cells showing significantly higher mutations than LZ B cells **(Figure 3.29B)**. These data indicate that extensive SHM occurs in RLN DZ. However, the mutation levels in ATLO DZ, LZ and resting GC B cells were comparable, with significantly decreased mutations in ATLO DZ **(Figure 3.29B)**. These observations indicate dysfunction of SHM in ATLO GCs. The class-switched B cells primarily accumulated in GC DZ in WT and *Apoe*$^{-/-}$ RLNs, showing a higher fraction of switched B cells in RLN DZ than LZ **(Figure 3.29C)**. Conversely, the class-switched BCRs in ATLO DZ were notably lower than RLN DZ, and no significance was observed between DZ, LZ and resting GC B cells **(Figure 3.29C)**. These results indicated disrupted CSR mechanism in ATLO GCs.

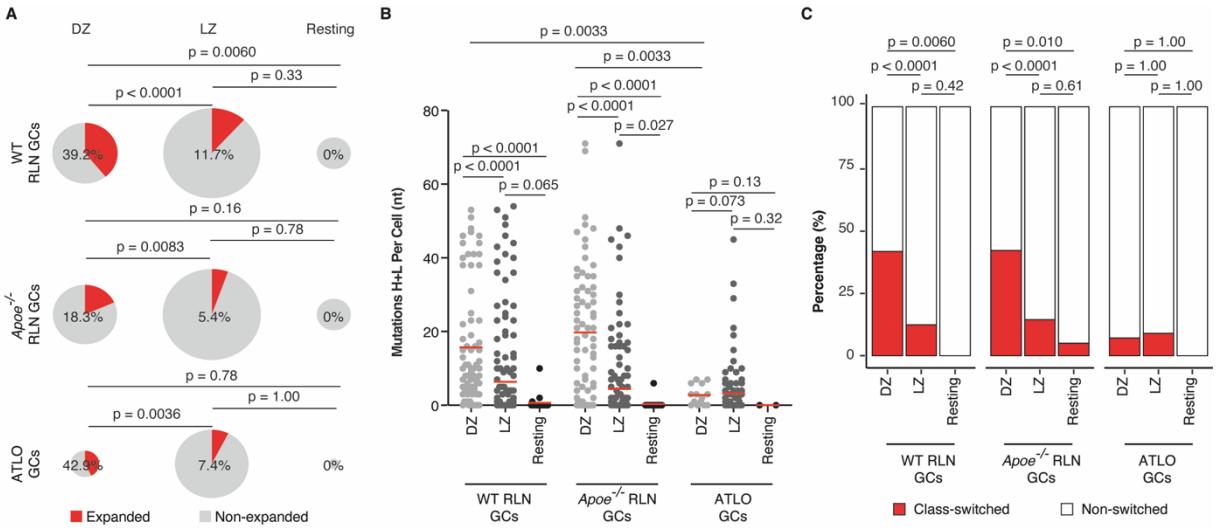

Figure 3.29 Compromised GC reactions in ATLOs
(A) The percentage of expanded B cells in each GC B subsets in each tissue. The size of the pie is proportional to the number of cells in the group. **(B)** Total mutations per cell on BCR heavy chain and light chain within different GC states in each tissue. Each dot represents one cell, and the red short lines indicate mean mutations in the group. **(C)** Proportion of class-switched cells within different GC states in each tissue. The p-value in **A** and **B** was determined by Chi-square test and adjusted by Benjamini-Hochberg correction. The p-value in **C** was calculated using Wilcoxon-Signed-Rank Test with Benjamini-Hochberg correction.

In conclusion, the findings indicate ATLO GCs exhibit aberrant mechanisms of SHM and CSR compared to RLN GCs, suggesting impaired GC dynamics in ATLOs. These data suggest GC reactions are compromised in ATLOs, which could be related to tolerance breakdown in ATLO GCs.

3.4.9 Functional enrichments in ATLO GC B cell subsets

To explore potential functional changes in RLN and ATLO GC B cell subsets, the gene expression profiles were compared between ATLO versus corresponding WT and *Apoe*$^{-/-}$ RLN GC subsets. The fold change values of gene expression were referred to the GO database to construct function projections using GSEA, allowing to identify potential pathways affected by these gene expression changes **(Figure 3.30)**. There was no significantly enriched GO term when compared ATLO resting GCs to SLO resting GCs, indicating functional similarities in SLO and ATLO resting GC B cells. Compared to RLN DZ GCs, ATLO DZ GCs significantly enriched in more than 150 GO terms, including regulation of leukocyte proliferation, positive regulation of apoptotic process and somatic diversification of immunoglobulins **(Figure 3.30A)**. The regulation of proliferation was observed in ATLO DZ GCs when compared to SLO DZ GCs, with overexpression of *Tyrobp*, *Cdkn1a*, *Ighm* and *Irs2* **(Figure 3.30A and B)**. *Tyrobp*

has been reported to limit B cell proliferation in humans, while *Cdkn1a* is involved in cell cycle arrest (Nakano-Yokomizo et al., 2011, Beguelin et al., 2017). Therefore, the proliferation in ATLO DZ GCs is under control of negatively and positively regulation. Apart from DZ, these genes were also up-regulated in LZ and resting GCs, indicating dysfunction of GCs in ATLOs **(Figure 3.30B)**. ATLO DZ GCs also showed up-regulation of the apoptotic process **(Figure 3.30A)**. Genes in relation to apoptosis were up regulated in DZ vs LZ and resting GCs **(Figure 3.30C)**. These data indicate increased apoptosis in ATLO DZ GCs, consistent with decreased numbers of DZ GC B cells in ATLOs. This data suggests that dysregulated apoptosis may contribute to the altered dynamics in ATLO GCs. The negative enrichment of somatic diversification of immunoglobulins, as well as the decreased expression of isotype switching-related genes like *Atad5*, *Bcl6*, *Rif1* and *Aicda* in ATLO DZ GCs is consistent with lower isotype-switching in ATLO GCs **(Figure 3.30A and D)**. These observations indicate disruption of antibody maturation and diversification in ATLO GCs. ATLO LZ GC B cells demonstrated enrichment in GO terms including BCR signaling, negative regulation of apoptotic process and tolerance induction when compared to RLN LZ GC B cells **(Figure 3.30E)**. The BCR signaling pathway was observed to be negatively regulated in ATLO LZ GCs **(Figure 3.30E)**. Importantly, CD22, which has been reported as a key inhibitory checkpoint to restrain B cell activation to self-antigens, was down-regulated in ATLO LZ GCs (Rubin et al., 2019) **(Figure 3.30F)**. This dysregulation may contribute to the pathogenesis of autoimmune diseases, which are often associated with the breakdown of tolerance mechanisms. Apoptosis in ATLO LZ GC B cells was down-regulated, and up-regulation of *Myc* and *Nfkb1* was detected to regulate cell survival **(Figure 3.30E and G)**. These data are consistent with higher portion of LZ GC B cells in ATLOs, suggesting the enrichment of this pathway may lead to accumulation of B cells potentially involved in autoimmune responses in ATLOs. Furthermore, ATLO LZ GCs showed enrichment in tolerance induction term **(Figure 3.30E)**. The expression of CD86 has also been positively associated with autoimmune disease, while CD274 has been reported to limit autoimmune responses (O'Neill et al., 2007, Mi et al., 2021). These findings further indicate dysregulation of tolerance in ATLO LZ GCs.

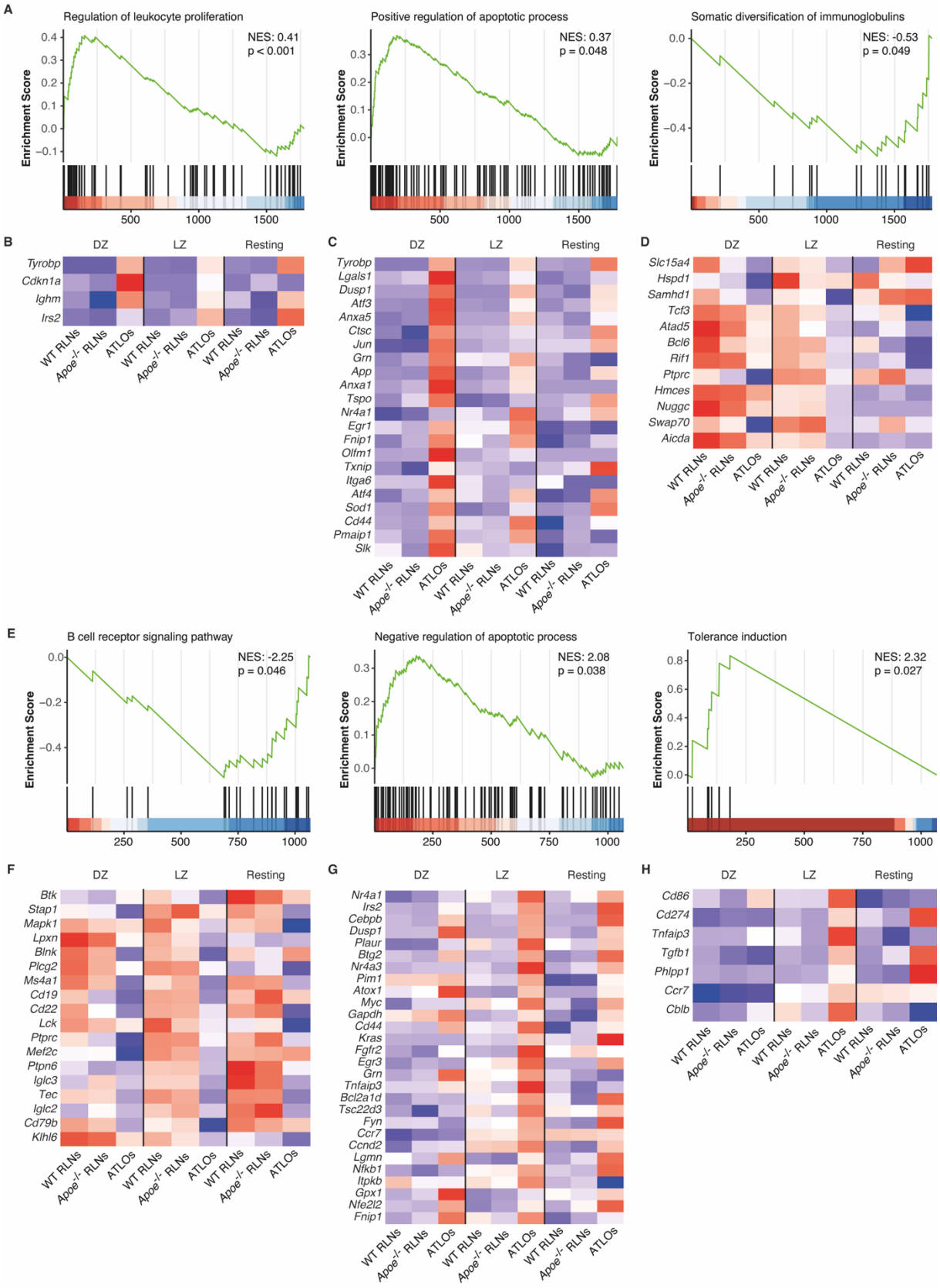

Figure 3.30 GSEA shows potential functional enrichments in ATLO DZ and LZ GCs
(A) The GSEA plot of selected GO terms enriched in ATLO DZ GC B cells. The x-axis shows genes (vertical black lines) represented in the GO terms; the color indicated positive (red) or negative (blue) correlations. The green line connected gene and enrichment score to show the

enrichment of the GO term. **(B-D)** The expression of selected GO term-related genes within GC subsets. **(E)** The GSEA plot of selected GO terms enriched in ATLO LZ GC B cells. **(F-H)** The expression of selected GO-term-related genes within each GC subset. NES: normalized enrichment score.

Overall, these data provide potential functional evidence of dysregulated immune processes in ATLO GC B cells, supporting that ATLOs may mount atherosclerosis-specific B cell autoimmune response.

3.4.10 Overexpression of survival factors in ATLO PCs

To study the characteristics of PCs in SLOs and ATLOs, PCs were analyzed and re-clustered into 3 subsets, each exhibiting different gene expression profiles **(Figure 3.31A and B)**. The expression of cell cycle-related genes *Tubb5*, *Actb*, *Mki67* and *Top2a* by *PC3* is in line with proliferation of plasmablasts or early PCs (Khodadadi et al., 2019) **(Figure 3.31B)**. Long-lived PCs lose expression of MHC II molecules, which has been observed in PC1 (Wilkinson et al., 2012). This subset also expressed *Rgcc*, *Fos* and *Nfkbia*, which in critical for PC differentiation and long-term survival (Gerondakis and Siebenlist, 2010) **(Figure 3.31B)**. PC2 was observed to be in an intermedia stage with lower expression of MHC II genes but higher expression of *Ms4a1*, *Pdia4* and *Hexb* **(Figure 3.31B)**. There were no tissue-specific PC subsets as the 3 subsets in either SLOs or ATLOs **(Figure 3.31C)**. In WT RLNs, most of PCs belong to the PC1 or PC2 subsets, while only a few PCs were identified in the PC3 subset. This trend was also observed in *Apoe*$^{-/-}$ RLN and ATLO PCs **(Figure 3.31C)**. However, compared to *Apoe*$^{-/-}$ RLNs, the proportion of PC2 subsets was higher in ATLOs, while the proportion of PC3 subsets was slightly lower, supporting a higher possibility of long-lived PCs in ATLOs **(Figure 3.31C)**. This data indicates distinct cellular component in ATLO PCs in comparison to RLNs. Next, survival factors were estimated in different tissues. The expression of *Tnfrsf17* (receptor of BAFF), *Cxcr4* (receptor of CXCL12) and *Tnfrsf1a* (receptor of TNF) was low in both WT and Apoe$^{-/-}$ RLNs, but significantly enhanced in ATLOs **(Figure 3.31D)**. *Tnfrsf13c* was expressed in both SLOs and ATLOs, and the expression was increased in ATLO PCs **(Figure 3.31D)**. The data suggest that BAFF, CXCL12 and TNF signaling pathways contribute to the enhanced survival of ATLO PCs (Lightman et al., 2019). Furthermore, upregulation of Cxcr4 was observed predominantly in the PC2 subset when comparing ATLO to RLN PCs. *Tnfrsf17* showed high expression levels in both PC1 and PC2 subsets within ATLOs, whereas the expression of *Tnfrsf13c* was increased in ATLO PC1. ATLO PC3 was found to be the primary

subset expressing *Tnfrsf1a* **(Figure 3.31E)**. These data implicate each PC subset relies on distinct survival factors to maintain their survival in ATLOs.

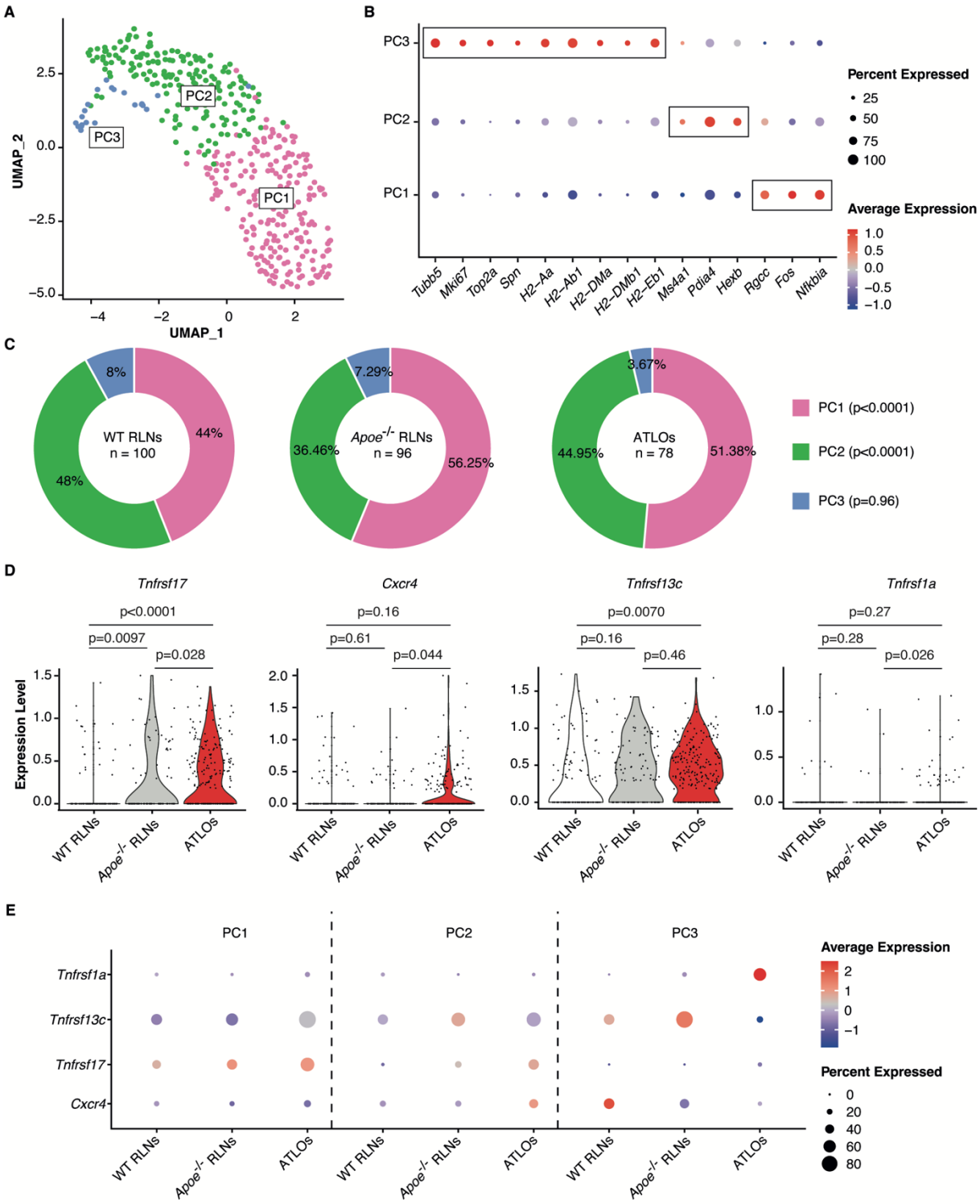

Figure 3.31 ATLO PCs up-regulate survival-related genes
(A) PCs were nonsupervisory separated into 3 subsets in the UMAP plot. **(B)** Dot plot shows expression of marker genes in 3 PC subsets. **(C)** The fraction of each PC subset in different tissues. The p-value was determined by Chi-square test. **(D)** Violin plots show expression of

survival-related genes in different tissues. Each dot represents one cell. The p-value was determined by Wilcoxon-Signed-Rank Test. **(E)** Dotplot shows expression of survival-related genes in 3 PC subsets in different tissues.

In conclusion, this result suggests the presence of different PC subsets with unique survival requirements in ATLOs. The enrichment of long-lived PCs in ATLOs, along with the upregulation of survival factors, supports the notion that ATLOs provide a suitable niche for the persistence of PCs in response to pathogenesis.

4 Discussion

Atherosclerosis and its complications incur enormous burdens on the health system worldwide. Although B cells have been reported to be involved in both atheroprotective and atherogenic mechanisms, the role of B cells in atherosclerosis remain poorly understood (Sage et al., 2019). Here, we employed NGS approach in both young and aged mice to get insight into the pathophysiology of atherosclerosis. For this purpose, we used a cross-tissue and cross genotype approach using bulk Rep-seq and scRNA-seq paired with scBCR-seq to map B cell immune responses in WT versus *Apoe*$^{-/-}$ mice. The following major conclusions are supported by this work: (1) ATLOs are capable to mount GC-dependent B-2 cell immune responses with evidence of clonal expansion, SHM, CSR and specific overexpression of several V-J recombinations; (2) The PC differentiation and migration pathways are compromised in ATLOs; (3) The breakdown of B cell tolerance occurs as early as in young (8-10 weeks) *Apoe*$^{-/-}$ mice in mice without visible macroscopic atherosclerosis; (4) Several checkpoints of peripheral B cell tolerance control are disrupted in ATLOs. When taken together, this work supports the conclusion that ATLOs may be involved in the generation of autoimmune B cell responses, opening the door to characterize atherosclerosis as a *bona fide* humoral B cell autoimmune disease.

4.1 Mapping of B cells indicates B cell differentiation occurs in SLOs and ATLOs of *Apoe*$^{-/-}$ mice

4.1.1 Increased clonal expansion and diversification in *Apoe*$^{-/-}$ mice

Several lines of evidence including highly significant up-regulation of clonal expansion and diversification of B-2 cells in aged *Apoe*$^{-/-}$ mice versus their WT control mice implicate the existence of atherosclerosis-specific autoantigens in SLOs and ATLOs. In contrast, as expected, B-1 cells in PerC showed high clonal expansion but lower clonal diversification in both WT and *Apoe*$^{-/-}$ mice. This result was in agreement with data discussed by Wong et al. that the repertoire of B-1 cells was biased in order to protect against microbial antigens (Wong et al., 2019). In addition, our data are consistent with those of Yang and colleagues who reported the repertoire of B-1a cells was more restricted than that of B-2 cells (Yang et al., 2015). Similar data on B-1a versus B-1b cells confirmed previous data of our group using FACS (Srikakulapu et al., 2016). Bashford-Rogers et al. characterized the disease-prone repertoires in six immune-

related diseases including Crohn's disease, SLE and IgA vasculitis, revealing that B cell repertoire mapping in different diseases and tissues is powerful approach towards understanding both mechanisms and locations where autoimmune B cell responses occur and - by the same token - autoimmune diseases may be initiated (Bashford-Rogers et al., 2019). Therefore, the clonal expansion and diversification of B-2 cell in aged *Apoe*$^{-/-}$ SLOs may be a result of the chronic inflammatory state associated with the *Apoe* deficiency and strongly suggests the existence of atherosclerosis-specific autoantigens and autoimmune B cells generated in GCs. Chronic inflammation can lead to the activation and proliferation of B cells, which would contribute to the expansion of certain B cell clones in the repertoire (Cain et al., 2009). This hypothesis is supported by previous studies that have shown increased clonal expansion in response to chronic inflammatory diseases. For example, the expanded B cells was observed in cerebrospinal fluid and central nervous system of patients suffering from multiple sclerosis (Obermeier et al., 2011). Itoh and colleagues recognized B cell clonal expansion as common and characteristic features in patients suffered rheumatic disease (Itoh et al., 2000). The increased diversification of clones in the aged *Apoe*$^{-/-}$ mice is a more complex phenomenon, however. One possibility is that the increased inflammation in the *Apoe*$^{-/-}$ mice could lead to the recruitment and activation of clonally related B cells. Another possibility is that the loss of *Apoe* could impact the affinity selection of specific B cell clones during development, leading to a more diverse repertoire. A third possibility is that both central tolerance as well as peripheral tolerance checkpoints are compromised in *Apoe*$^{-/-}$ mice. The dramatic differences in clonal expansion in the *Apoe*$^{-/-}$ SLOs and ATLOs versus their WT RLN and spleen counterparts, however, speak in favor of a major breakdown of B cell tolerance in SLOs and ATLOs.

4.1.2 Increased SHM and CSR in *Apoe*$^{-/-}$ mice

SHM and CSR occur within GCs to generate high-affinity antibodies in response to specific antigens (Klein and Dalla-Favera, 2008). Compared to germline mutations, this somatic mutation shows extremely higher frequency (10^6 fold) and predominately results from single-base substitutions in hypervariable regions of BCRs (Martin et al., 2015) . Therefore, the high frequency point mutations reported in our Rep-seq data explain the levels of SHM in the B cells. In this study, we observed higher levels of mutations in aged *Apoe*$^{-/-}$ mice when compared to WT mice, suggesting increased SHM in *Apoe*$^{-/-}$ mice. To increase the affinity to antigens, the activated B cells undergo high rates of somatic mutations. Many studies have shown extensive SHM in vaccination models and chronic inflammation diseases (Li et al., 2013, Beltran et al.,

2014). Therefore, the enhanced SHM in aged *Apoe*$^{-/-}$ mice results from the chronic inflammation afforded by atherosclerosis. B cells in GCs undergo CSR to generate different isotypes to deal with specific antigens. In our data, the larger proportion of isotype-switched B cells in *Apoe*$^{-/-}$ mice was also observed in comparison to WT mice. Our data is the first study to elucidate the specific features of B cell isotypes in atherosclerosis from not only percentage, but also the switching preference between individual isotypes. For example, we pointed out the enhanced class switching from IgG1 to IgG2 in aged *Apoe*$^{-/-}$ RLNs, which results in elevated IgG2. Since the SHM and CSR of B cells occurs in GCs with help of T_{FH} cells, the enhanced SHM and CSR in our data indicate enhanced antigen-triggered T cell-dependent response in *Apoe*$^{-/-}$ mice, implying the existence of atherosclerosis-specific antigens.

4.1.3 Differential V-J recombination in *Apoe*$^{-/-}$ mice

Some individual families have been associated with specific diseases. For example, overrepresented IGHV5 family and underrepresented IGH1 family have been reported in splenic B cells isolated from SLE patients (Fraser et al., 2003). In our data, the aged *Apoe*$^{-/-}$ B-2 cell were distinct from WT mice by underexpression of IGHV4, IGHV11 and IGHV13 families as well as overexpression of IGHV7 and IGHV14 families. Of note, the decrease of *IGHV1-5*, *IGHV1-81* and *IGHV5-17* gene segments as well as the increase of *IGHV7-3* gene segment were significant in at least two *Apoe*$^{-/-}$ tissues when compared to their corresponding WT tissues. This raise the possibility that atherosclerotic mice harbour a unique set of B cells in response to the inflammatory environment, which may predominately express IGHV7 and IGHV14 families, as the IGHV7 family was poorly expressed in WT mice but extremely high in *Apoe*$^{-/-}$ mice. In *Apoe*$^{-/-}$ mice, *IGHV7-3* mainly recombined with *IGHJ4* segment, therefore this combination may specifically occur in response to atherosclerosis.

4.2 ATLOs regulate atherosclerosis-specific B cell autoimmune responses

4.2.1 Why choosing ATLOs as sites for studying atherosclerosis-specific autoimmune responses?

Till now, the presence of B cells within atherosclerotic lesions is still controversial. Only a few B cells were positioned in human coronary plaques based on studies, but most researchers did not find any B cells in mouse plaques except for rare cases of mice that develop ATLO-like immune cell aggregates (Moos et al., 2005, Grabner et al., 2009, Canducci et al., 2012, Zhang et al., 2021, our unpublished data). Instead, Grabner et al. believed that ATLOs are the major

locations for infiltrated B cells in the diseased arterial wall emerging adjacent to plaques in the adventitia in advanced atherosclerosis (Grabner et al., 2009). Apart from ATLOs in atherosclerosis, the neogenesis of other TLOs have also been characterized in four major types of human diseases: autoimmune and autoimmune-related diseases, microbe infections, allograft rejection and some type of cancers (Mohanta et al., 2014). Climbing evidence has stated TLOs are at least partially maintained as sites to generate autoreactive B cells and sustain local autoimmune response (Lehmann-Horn et al., 2016, Corsiero et al., 2019). Regarding our current data we conclude that atherosclerosis triggers autoimmune B cells particularly in ATLOs as the evidence is weak that *Apoe*-deficiency is associated with an enhanced generation of expanded and clonally expanded B-2 cell that react to exogenous antigens.

4.2.2 Dysregulation of immune tolerance in mice lacking *Apoe*

Multiple central and peripheral tolerance mechanisms are developed to prevent autoreactive B cells become disease promoting B cells. We studied both young and aged mice to examine tolerance checkpoints. Surprisingly, increased clonal expansion was firstly noticed in young *Apoe*$^{-/-}$ naïve B cells, raising the possibility that B cell central tolerance compromises in young (8 weeks) hyperlipidemic mice, while more work is needed to confirm this possibility. The BCR clonal expansion is also observed in GC B cells of young *Apoe*$^{-/-}$ mice when compared to young WT mice, which raises another possibility that after few clonal expanded autoreactive B cells who escaped central tolerance deletion in the BM, they enter peripheral to initiate GC responses before macroscopically visible atherosclerosis occurs. We then analysed the clonal expansion in aged naïve B subsets. Similar to young mice, the clonal expansion is increased in *Apoe*$^{-/-}$ immature naïve B cells when comparing to WT immature naïve B cells in aged mice. While there was no statistical difference between *Apoe*$^{-/-}$ and WT mature naïve B cells. This may attribute to the age-induced shrink of repertoire in both aged WT and *Apoe*$^{-/-}$ mice. IGHV7 and IGHV14, which showed no significance in young mice, but were overrepresented in aged naïve and/or antigen-experienced B cells. It raised the possibility that the unbalanced immune tolerance may contribute to the accumulation of these families. Consequently, the breakdown of immune tolerance is likely inferred in both young hyperlipidemic mice and advanced atherosclerotic mice.

4.2.3 Existence of GC-dependent B-2 cell immune response in ATLOs

The structure of ATLOs is similar to SLOs as they are organized in separated B cell follicles, T cell zones and PC niches (Yin et al., 2016). B cells seed in ATLOs could be tissue-resident

B cells or circulating B cells that come from other tissues. Our data indicated that the BCR repertoire in ATLOs can be distinguished from its counterparts in the circulation and SLOs. The levels of clonal expansion, diversification and SHM in ATLO B cells is comparable to *Apoe*$^{-/-}$ SLO B cells, indicating presence of GC-dependent B-2 cell immune response in ATLOs. However, the landscape of B cell BCR repertoire in ATLOs is distinct in that CSR in ATLOs as more unswitched IgM sequences were observed in ATLOs in comparison with RLNs. Two possibilities may contribute to the high IgM in ATLOs: 1). ATLOs contain more B-1 B cells, which have been identified previously by FACS (Srikakulapu et al., 2016). Thus, the increased IgM isotype in ATLO may result from the increased B-1 B cells which mainly produce IgM. 2). The dysregulation of CSR-related genes may contribute to the defect of CSR and therefore more B-2 B cells are unswitched in ATLOs.

4.2.4 Disruption of immune tolerance in ATLO GCs

The dissimilarity between ATLOs and SLOs have been confirmed previously by microarray data (Hu et al., 2015). Our data extended this conclusion by providing B cell transcriptomes at single cell resolution in these three tissues. ATLO B cells differ from RLN B cells by upregulation of immune response-related transcripts, implying the enhanced B cell functions, i.e., antigen presentation, TNF signalling pathways, and B cell receptor signalling pathways. Relying on scRNA-seq, we identified distinct B cell subtype compositions and phenotypes in ATLOs when compared to WT RLNs and *Apoe*$^{-/-}$ RLNs. Therefore, our current studies are the first to describe B cell subtype and B cell phenotype atlas in ATLOs, allowing the possibility to dissect the mechanism of specific B subsets in atherosclerosis, i.e., to identify autoimmune B cells, clone their BCRs, express them in vitro and determine their disease-related functions, and define the cognate autoantigen(s) they respond to. Spontaneous GCs have been reported in both autoimmune and non-autoimmune conditions, but GCs in autoimmune diseases displayed higher frequencies of antibody-producing B cells (Domeier et al., 2017). In our data, the newly activated B cells - which may have encountered autoantigens - accounted for around 5% of total B cells in WT and *Apoe*$^{-/-}$ RLNs. This fraction significantly decreased, with considerable increasing of PCs and memory B cells in ATLOs. Therefore, these data also indicate that GCs in ATLOs may generate atherosclerosis-specific autoimmunity. By integrating with published GC data, we further analyzed GC B cells in WT and *Apoe*$^{-/-}$ RLNs, as well as ATLOs. This further indicated dysregulated GC reaction in ATLOs. By analyzing DEGs and their functional enrichment, we observed overexpression of proliferation-inhibitory genes, upregulation of apoptosis-related genes, as well as downregulation of CSR-related genes in ATLO DZs. These

data may provide the hints to understand the decreased fraction of DZ GC B cells and decreased CSR in ATLO GCs. CD22 has been reported to be required to maintain B cell tolerance by inhibiting BCR signaling (Muller and Nitschke, 2014). Deficiency of CD22 leads to spontaneous high affinity autoantibody generation (O'Keefe et al., 1999). Crosses of CD22-deficient mice with autoimmune-prone mice promoted autoimmune disorder, and mutations of CD22 has been detected in lupus-prone strains (Dorner et al., 2012). CD86 is upregulated in activated B cells to facilitate autoimmune response by co-stimulation of T cells, as previously reported (Wong et al., 2005). The overexpression of CD86 has been observed in autoimmune diseases like rheumatoid arthritis and autoimmune thyroid disease (Catalan et al., 2010, Watanabe et al., 2020). The down-regulation of CD22 and up-regulation of CD86 in ATLO LZ GCs encourage us to propose that immune tolerance breakdown in ATLO GCs occurs via dysregulation of CD22 and CD86.

4.2.5 Compromised PC machinery in ATLOs

PCs are capable for homing to BM or re-distribute to other lymphoid organs after terminal differentiation (Hargreaves et al., 2001). In our data, ATLO PCs shared BCR clones with blood, BM and SLO PCs, indicating that ATLO PCs could also migrate there. However, compared to SLOs, the fraction of ATLO/blood and ATLO/BM BCR clones significantly decreases, suggesting the persistence of PCs in ATLOs. This PC retention may contribute to the increased fraction of PCs in ATLOs when compared to SLOs. PCs are classified into two groups based on their lifespan. First, there are short-lived PCs or plasmablasts, which are actively proliferating cells with a lifespan of around 3 to 5 days. Second, there are long-lived PCs, which are non-proliferating and can survive for several months up to an individual's lifetime (Khodadadi et al., 2019). The long-lived PCs are the major source of PCs to home to the BM. Previous studies of our group have confirmed the existence of both short-lived and long-lived PCs in ATLOs (Srikakulapu et al., 2016). Our data suggests that ATLOs may have different portion of short-lived and long-lived PCs, which may contribute to the distinct BCR repertoire in ATLO PCs, WT RLN PCs, and *Apoe*$^{-/-}$ RLN PCs. Shrikakulpu and colleagues reported expression of PC survival factors such as CXCR12 and BAFF in ATLOs (Srikakulapu et al., 2016). BAFF, APRIL, CXCR12 and TNF are critical for PC survival (Roth et al., 2014, Tsiantoulas et al., 2021). By scRNA-seq data, we observed up-regulation of BCAM (receptor for BAFF and APRIL), CXCR4 (receptor for CXCR12) and TNFR (receptor for TNF) in ATLO PCs, which may also be a contributor of increasing PCs in ATLOs. Several other factors, such as adhesion molecule, NF-κB pathway activation and anti-apoptotic factors could also regulate

PC survival, however, though we did not observe ATLO-specific overexpression of these genes in our data (Khodadadi et al., 2019).

To conclude, this project, utilizing NGS, provides the first evidence suggesting atherosclerosis may be a *bona fide* autoimmune disease orchestrated within ATLOs. Our findings reveal multiple layers of tolerance breakdown and GC-dependent B cell immune responses in ATLOs. Corroborating our results, our colleagues have successfully isolated atherosclerosis-specific B-2 cells from ATLO GCs using single-cell cloning technology. These B cells demonstrate high affinity to plaque components, and notably, the administration of autoantigens or cognate autoantibodies accelerates disease progression in atherosclerotic mouse models (Zhang, 2022). These wet-lab experiments further substantiate the role of ATLOs in organizing atherosclerosis-specific B cell autoimmune responses, reinforcing our sequencing-based findings with functional evidence.

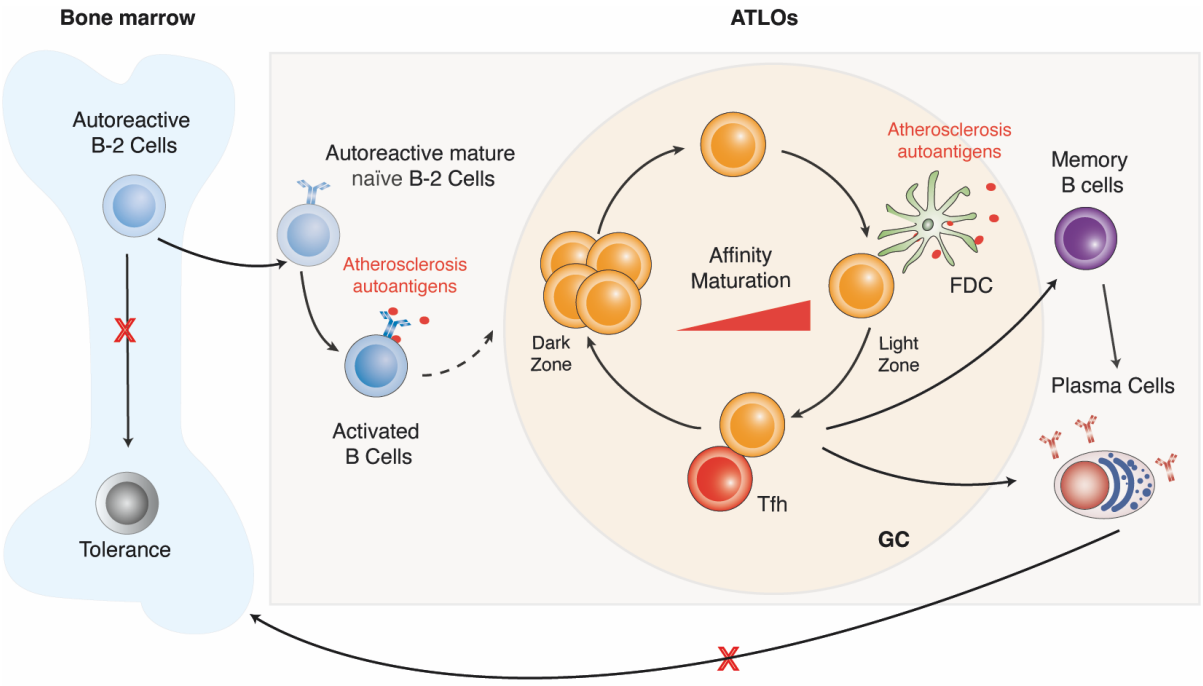

Figure 4.1 ATLOs organize atherosclerosis-specific B cell autoimmune responses
Due to the breach of central tolerance, autoreactive B cells in *Apoe*$^{-/-}$ mice escape sufficient deletion and potentially migrate into ATLOs. Within these structures, these autoreactive B cells encounter atherosclerosis-associated autoantigens, triggering GC reactions. This process culminates in the generation of high-affinity autoreactive memory B cells and plasma cells specifically tailored to respond to atherosclerosis.

4.3 Limitations and outlook

In our studies, we have characterized ATLOs as distinctive sites of the atherosclerosis B cell immune landscape and transcriptome profiling point of view. In particular, the current data provide a series of results that ATLOs are sites of generating autoimmune B cells. To our knowledge, this is the first systemic assessment of BCR repertoire in atherosclerosis, and particularly the first study to characterize the B cell landscape in ATLOs by Rep-seq and scRNA-seq. Nonetheless, there are still limitations in our studies. The limited number of B cells in ATLOs restricted a more detailed investigation of paired H-L BCR repertoire in drop-based scRNA-seq; thus, we focused more on the BCR repertoire of heavy chains obtained from bulk Rep-seq. By this way, unfortunately, the H-L paired information which is also important to delineate B cell specificity was not possible. For example, we lost the chance to investigate the underling relationship between specific gene expression and largely expanded clones. Therefore, it is not possible to produce specific autoantibodies only based on the results of Rep-seq to examine their affinity and screen potential autoantigens. Moreover, epitope spreading in inflammatory and autoimmune diseases allows B cells to target previously unrecognized antigenic components (Vanderlugt and Miller, 2002). And different ATLOs were identified to harbour large clones with unique features. These factors rise the complexity to isolate common atherosclerosis-specific autoantibodies and autoantigens. Besides, in our Rep-seq experiments, some samples, particularly small-sized ATLOs or RLNs, yielded insufficient BCR sequences for robust analysis. Consequently, samples containing only a limited number of sequences were excluded from further analysis after pre-processing. This necessary quality control resulted in unbalanced comparisons in the project. Modified scRNA-seq for low number B cell populations, optimized Rep-seq to reduce confounder and other advanced technologies need to be integrated in the future for a more precise evaluation of underlying B cell machinery in ATLOs and atherosclerosis.

Interruption of TLO formation has been reported as a clinically therapeutic strategy targeting autoimmune disease (Pitzalis et al., 2014, Bombardieri et al., 2017). Increasing evidence indicates that B cells could be considered as target for the intervention of atherosclerosis. For instance, depletion of B cells with rituximab, which is an anti-CD20 agent, led to a reduction role in atherosclerotic progression (Porsch and Binder, 2019). Hence with further investigation on ATLO B cell immune response, regulation of B cells in ATLOs and subsequent modification of ATLOs would be a promising prospect for clinical prevention and therapy of atherosclerosis.

References

AIT-OUFELLA, H., HERBIN, O., BOUAZIZ, J. D., BINDER, C. J., UYTTENHOVE, C., LAURANS, L., TALEB, S., VAN VRE, E., ESPOSITO, B., VILAR, J., SIRVENT, J., VAN SNICK, J., TEDGUI, A., TEDDER, T. F. & MALLAT, Z. 2010. B cell depletion reduces the development of atherosclerosis in mice. *J Exp Med,* 207**,** 1579-87.

AKHAVANPOOR, M., GLEISSNER, C. A., AKHAVANPOOR, H., LASITSCHKA, F., DOESCH, A. O., KATUS, H. A. & ERBEL, C. 2018. Adventitial tertiary lymphoid organ classification in human atherosclerosis. *Cardiovasc Pathol,* 32**,** 8-14.

AKIRAV, E. M., RUDDLE, N. H. & HEROLD, K. C. 2011. The role of AIRE in human autoimmune disease. *Nat Rev Endocrinol,* 7**,** 25-33.

ALAMYAR, E., GIUDICELLI, V., LI, S., DUROUX, P. & LEFRANC, M. 2012. IMGT/HighV-QUEST: the IMGT web portal for immunoglobulin (Ig) or antibody and T cell receptor (TR) analysis from NGS high throughput and deep sequencing. *Immunome Research*.

ANDREWS, S. 2010. *FASTQC: A quality control tool for high throughput sequence data* [Online]. Available: http://www.bioinformatics.babraham.ac.uk/projects/fastqc/ [Accessed].

ANGELI, V., LLODRA, J., RONG, J. X., SATOH, K., ISHII, S., SHIMIZU, T., FISHER, E. A. & RANDOLPH, G. J. 2004. Dyslipidemia associated with atherosclerotic disease systemically alters dendritic cell mobilization. *Immunity,* 21**,** 561-74.

BASHFORD-ROGERS, R. J., PALSER, A. L., HUNTLY, B. J., RANCE, R., VASSILIOU, G. S., FOLLOWS, G. A. & KELLAM, P. 2013. Network properties derived from deep sequencing of human B-cell receptor repertoires delineate B-cell populations. *Genome Res,* 23**,** 1874-84.

BASHFORD-ROGERS, R. J. M., BERGAMASCHI, L., MCKINNEY, E. F., POMBAL, D. C., MESCIA, F., LEE, J. C., THOMAS, D. C., FLINT, S. M., KELLAM, P., JAYNE, D. R. W., LYONS, P. A. & SMITH, K. G. C. 2019. Analysis of the B cell receptor repertoire in six immune-mediated diseases. *Nature,* 574**,** 122-126.

BATISTA, F. D. & HARWOOD, N. E. 2009. The who, how and where of antigen presentation to B cells. *Nat Rev Immunol,* 9**,** 15-27.

BAUMGARTH, N. 2011. The double life of a B-1 cell: self-reactivity selects for protective effector functions. *Nat Rev Immunol,* 11**,** 34-46.

BAUMGARTH, N. 2016. B-1 Cell Heterogeneity and the Regulation of Natural and Antigen-Induced IgM Production. *Front Immunol,* 7**,** 324.

BEGUELIN, W., RIVAS, M. A., CALVO FERNANDEZ, M. T., TEATER, M., PURWADA, A., REDMOND, D., SHEN, H., CHALLMAN, M. F., ELEMENTO, O., SINGH, A. & MELNICK, A. M. 2017. EZH2 enables germinal centre formation through epigenetic silencing of CDKN1A and an Rb-E2F1 feedback loop. *Nat Commun,* 8**,** 877.

BELTRAN, E., OBERMEIER, B., MOSER, M., CORET, F., SIMO-CASTELLO, M., BOSCA, I., PEREZ-MIRALLES, F., VILLAR, L. M., SENEL, M., TUMANI, H., HOHLFELD, R., CASANOVA, B. & DORNMAIR, K. 2014. Intrathecal somatic hypermutation of IgM in multiple sclerosis and neuroinflammation. *Brain,* 137**,** 2703-14.

BENNETT, M. R., SINHA, S. & OWENS, G. K. 2016. Vascular Smooth Muscle Cells in Atherosclerosis. *Circ Res,* 118**,** 692-702.

BERGMAN, Y. & CEDAR, H. 2004. A stepwise epigenetic process controls immunoglobulin allelic exclusion. *Nat Rev Immunol,* 4**,** 753-61.

BINDER, C. J., PAPAC-MILICEVIC, N. & WITZTUM, J. L. 2016. Innate sensing of oxidation-specific epitopes in health and disease. *Nat Rev Immunol,* 16**,** 485-97.

BIOTEC, M. 2012. *Protocol: CD138 MicroBeads, mouse* [Online]. Available: https://www.miltenyibiotec.com/upload/assets/IM0005947.PDF [Accessed].

BLACKMAN, M. A. & WOODLAND, D. L. 2011. The narrowing of the CD8 T cell repertoire in old age. *Curr Opin Immunol,* 23**,** 537-42.

BOMBARDIERI, M., LEWIS, M. & PITZALIS, C. 2017. Ectopic lymphoid neogenesis in rheumatic autoimmune diseases. *Nat Rev Rheumatol,* 13**,** 141-154.

BUONO, C., COME, C. E., STAVRAKIS, G., MAGUIRE, G. F., CONNELLY, P. W. & LICHTMAN, A. H. 2003. Influence of interferon-gamma on the extent and phenotype of diet-induced atherosclerosis in the LDLR-deficient mouse. *Arterioscler Thromb Vasc Biol,* 23**,** 454-60.

CAGAN, A., BAEZ-ORTEGA, A., BRZOZOWSKA, N., ABASCAL, F., COORENS, T. H. H., SANDERS, M. A., LAWSON, A. R. J., HARVEY, L. M. R., BHOSLE, S., JONES, D., ALCANTARA, R. E., BUTLER, T. M., HOOKS, Y., ROBERTS, K., ANDERSON, E., LUNN, S., FLACH, E., SPIRO, S., JANUSZCZAK, I., WRIGGLESWORTH, E., JENKINS, H., DALLAS, T., MASTERS, N., PERKINS, M. W., DEAVILLE, R., DRUCE, M., BOGESKA, R., MILSOM, M. D., NEUMANN, B., GORMAN, F., CONSTANTINO-CASAS, F., PEACHEY, L., BOCHYNSKA, D., SMITH, E. S. J., GERSTUNG, M., CAMPBELL, P. J., MURCHISON, E. P., STRATTON, M. R. & MARTINCORENA, I. 2022. Somatic mutation rates scale with lifespan across mammals. *Nature,* 604**,** 517-524.

CAIN, D., KONDO, M., CHEN, H. & KELSOE, G. 2009. Effects of acute and chronic inflammation on B-cell development and differentiation. *J Invest Dermatol,* 129**,** 266-77.

CALIS, J. J. & ROSENBERG, B. R. 2014. Characterizing immune repertoires by high throughput sequencing: strategies and applications. *Trends Immunol,* 35**,** 581-590.

CANDUCCI, F., SAITA, D., FOGLIENI, C., PISCOPIELLO, M. R., CHIESA, R., COLOMBO, A., CIANFLONE, D., MASERI, A., CLEMENTI, M. & BURIONI, R. 2012. Cross-reacting antibacterial auto-antibodies are produced within coronary atherosclerotic plaques of acute coronary syndrome patients. *PLoS One,* 7**,** e42283.

CATALAN, D., ARAVENA, O., SABUGO, F., WURMANN, P., SOTO, L., KALERGIS, A. M., CUCHACOVICH, M., AGUILLON, J. C., MILLENIUM NUCLEUS ON, I. & IMMUNOTHERAPY, P. F. 2010. B cells from rheumatoid arthritis patients show important alterations in the expression of CD86 and FcgammaRIIb, which are modulated by anti-tumor necrosis factor therapy. *Arthritis Res Ther,* 12**,** R68.

CENTA, M., PROKOPEC, K. E., GARIMELLA, M. G., HABIR, K., HOFSTE, L., STARK, J. M., DAHDAH, A., TIBBITT, C. A., POLYZOS, K. A., GISTERA, A., JOHANSSON, D. K., MAEDA, N. N., HANSSON, G. K., KETELHUTH, D. F. J., COQUET, J. M., BINDER, C. J., KARLSSON, M. C. I. & MALIN, S. 2018. Acute Loss of Apolipoprotein E Triggers an Autoimmune Response That Accelerates Atherosclerosis. *Arterioscler Thromb Vasc Biol,* 38**,** e145-e158.

CHAN, T. D. & BRINK, R. 2012. Affinity-based selection and the germinal center response. *Immunol Rev,* 247**,** 11-23.

CHAPLIN, D. D. 2003. 1. Overview of the immune response. *Journal of Allergy and Clinical Immunology,* 111**,** S442-S459.

CHAPLIN, D. D. 2010. Overview of the immune response. *J Allergy Clin Immunol,* 125**,** S3-23.

CHEN, D., WANG, Y., MANAKKAT VIJAY, G. K., FU, S., NASH, C. W., XU, D., HE, D., SALOMONIS, N., SINGH, H. & XU, H. 2021. Coupled analysis of transcriptome and BCR mutations reveals role of OXPHOS in affinity maturation. *Nat Immunol*.

CHEN, H. & BOUTROS, P. C. 2011. VennDiagram: a package for the generation of highly-customizable Venn and Euler diagrams in R. *BMC Bioinformatics,* 12**,** 35.

CHOU, M. Y., FOGELSTRAND, L., HARTVIGSEN, K., HANSEN, L. F., WOELKERS, D., SHAW, P. X., CHOI, J., PERKMANN, T., BACKHED, F., MILLER, Y. I., HORKKO,

S., CORR, M., WITZTUM, J. L. & BINDER, C. J. 2009. Oxidation-specific epitopes are dominant targets of innate natural antibodies in mice and humans. *J Clin Invest,* 119**,** 1335-49.

CLEMENT, M., GUEDJ, K., ANDREATA, F., MORVAN, M., BEY, L., KHALLOU-LASCHET, J., GASTON, A. T., DELBOSC, S., ALSAC, J. M., BRUNEVAL, P., DESCHILDRE, C., LE BORGNE, M., CASTIER, Y., KIM, H. J., CANTOR, H., MICHEL, J. B., CALIGIURI, G. & NICOLETTI, A. 2015. Control of the T follicular helper-germinal center B-cell axis by CD8(+) regulatory T cells limits atherosclerosis and tertiary lymphoid organ development. *Circulation,* 131**,** 560-70.

CORSIERO, E., DELVECCHIO, F. R., BOMBARDIERI, M. & PITZALIS, C. 2019. B cells in the formation of tertiary lymphoid organs in autoimmunity, transplantation and tumorigenesis. *Curr Opin Immunol,* 57**,** 46-52.

CSARDI G, N. T. 2006. *The igraph software package for complex network research* [Online]. Complex Systems. Available: http://igraph.org [Accessed].

CUNNINGHAM, A. F., FLORES-LANGARICA, A., BOBAT, S., DOMINGUEZ MEDINA, C. C., COOK, C. N., ROSS, E. A., LOPEZ-MACIAS, C. & HENDERSON, I. R. 2014. B1b cells recognize protective antigens after natural infection and vaccination. *Front Immunol,* 5**,** 535.

CZAJKOWSKY, D. M. & SHAO, Z. 2009. The human IgM pentamer is a mushroom-shaped molecule with a flexural bias. *Proc Natl Acad Sci U S A,* 106**,** 14960-5.

D'SOUZA, S. S., ZHANG, Y., BAILEY, J. T., FUNG, I. T. H., KUENTZEL, M. L., CHITTUR, S. V. & YANG, Q. 2021. Type I Interferon signaling controls the accumulation and transcriptomes of monocytes in the aged lung. *Aging Cell,* 20**,** e13470.

DE TAEYE, S. W., RISPENS, T. & VIDARSSON, G. 2019. The Ligands for Human IgG and Their Effector Functions. *Antibodies (Basel),* 8.

DEGN, S. E., VAN DER POEL, C. E., FIRL, D. J., AYOGLU, B., AL QURESHAH, F. A., BAJIC, G., MESIN, L., REYNAUD, C. A., WEILL, J. C., UTZ, P. J., VICTORA, G. D. & CARROLL, M. C. 2017. Clonal Evolution of Autoreactive Germinal Centers. *Cell,* 170**,** 913-926 e19.

DEMPSEY, P. W., VAIDYA, S. A. & CHENG, G. 2003. The art of war: Innate and adaptive immune responses. *Cell Mol Life Sci,* 60**,** 2604-21.

DESMET, C. J. & ISHII, K. J. 2012. Nucleic acid sensing at the interface between innate and adaptive immunity in vaccination. *Nat Rev Immunol,* 12**,** 479-91.

DMITRIY, B., STANISLAV, P., IGOR, M., MIKHAIL, S., ILGAR, M., EKATERINA, P. & DMITRIY, C. 2015. MiXCR software for comprehensive adaptive immunity profiling. *Nat Methods,* 12**,** 379-80.

DOMEIER, P. P., SCHELL, S. L. & RAHMAN, Z. S. 2017. Spontaneous germinal centers and autoimmunity. *Autoimmunity,* 50**,** 4-18.

DORNER, T., SHOCK, A. & SMITH, K. G. 2012. CD22 and autoimmune disease. *Int Rev Immunol,* 31**,** 363-78.

DRANOFF, G. 2004. Cytokines in cancer pathogenesis and cancer therapy. *Nat Rev Cancer,* 4**,** 11-22.

DUNN-WALTERS, D. K. 2016. The ageing human B cell repertoire: a failure of selection? *Clin Exp Immunol,* 183**,** 50-6.

DUONG, B. H., TIAN, H., OTA, T., COMPLETO, G., HAN, S., VELA, J. L., OTA, M., KUBITZ, M., BOVIN, N., PAULSON, J. C. & NEMAZEE, D. 2010. Decoration of T-independent antigen with ligands for CD22 and Siglec-G can suppress immunity and induce B cell tolerance in vivo. *J Exp Med,* 207**,** 173-87.

DUSTIN, M. L. 2014. The immunological synapse. *Cancer Immunol Res,* 2**,** 1023-33.

EDELMAN, G. M. 1991. Antibody structure and molecular immunology. *Scand J Immunol,* 34**,** 1-22.

FEARON, D. T. & LOCKSLEY, R. M. 1996. The instructive role of innate immunity in the acquired immune response. *Science,* 272**,** 50-3.

FELSENSTEIN, J. 1989. PHYLIP - Phylogeny Inference Package (Version 3.2). *Cladistics,* 5**,** 164-166.

FERNANDEZ, D. M., RAHMAN, A. H., FERNANDEZ, N. F., CHUDNOVSKIY, A., AMIR, E. D., AMADORI, L., KHAN, N. S., WONG, C. K., SHAMAILOVA, R., HILL, C. A., WANG, Z., REMARK, R., LI, J. R., PINA, C., FARIES, C., AWAD, A. J., MOSS, N., BJORKEGREN, J. L. M., KIM-SCHULZE, S., GNJATIC, S., MA'AYAN, A., MOCCO, J., FARIES, P., MERAD, M. & GIANNARELLI, C. 2019. Single-cell immune landscape of human atherosclerotic plaques. *Nat Med,* 25**,** 1576-1588.

FOKS, A. C., LICHTMAN, A. H. & KUIPER, J. 2015. Treating atherosclerosis with regulatory T cells. *Arterioscler Thromb Vasc Biol,* 35**,** 280-7.

FRASER, N. L., ROWLEY, G., FIELD, M. & STOTT, D. I. 2003. The VH gene repertoire of splenic B cells and somatic hypermutation in systemic lupus erythematosus. *Arthritis Res Ther,* 5**,** R114-21.

GALKINA, E., KADL, A., SANDERS, J., VARUGHESE, D., SAREMBOCK, I. J. & LEY, K. 2006. Lymphocyte recruitment into the aortic wall before and during development of atherosclerosis is partially L-selectin dependent. *J Exp Med,* 203**,** 1273-82.

GARCIA, K. C., DEGANO, M., SPEIR, J. A. & WILSON, I. A. 1999. Emerging principles for T cell receptor recognition of antigen in cellular immunity. *Rev Immunogenet,* 1**,** 75-90.

GAUDINO, S. J. & KUMAR, P. 2019. Cross-Talk Between Antigen Presenting Cells and T Cells Impacts Intestinal Homeostasis, Bacterial Infections, and Tumorigenesis. *Front Immunol,* 10**,** 360.

GEORGIOU, G., IPPOLITO, G. C., BEAUSANG, J., BUSSE, C. E., WARDEMANN, H. & QUAKE, S. R. 2014. The promise and challenge of high-throughput sequencing of the antibody repertoire. *Nat Biotechnol,* 32**,** 158-68.

GERMAIN, R. N. 1994. MHC-dependent antigen processing and peptide presentation: providing ligands for T lymphocyte activation. *Cell,* 76**,** 287-99.

GERONDAKIS, S. & SIEBENLIST, U. 2010. Roles of the NF-kappaB pathway in lymphocyte development and function. *Cold Spring Harb Perspect Biol,* 2**,** a000182.

GIBSON, K. L., WU, Y. C., BARNETT, Y., DUGGAN, O., VAUGHAN, R., KONDEATIS, E., NILSSON, B. O., WIKBY, A., KIPLING, D. & DUNN-WALTERS, D. K. 2009. B-cell diversity decreases in old age and is correlated with poor health status. *Aging Cell,* 8**,** 18-25.

GILLOTTE-TAYLOR, K., BOULLIER, A., WITZTUM, J. L., STEINBERG, D. & QUEHENBERGER, O. 2001. Scavenger receptor class B type I as a receptor for oxidized low density lipoprotein. *J Lipid Res,* 42**,** 1474-82.

GISTERA, A. & HANSSON, G. K. 2017. The immunology of atherosclerosis. *Nat Rev Nephrol,* 13**,** 368-380.

GJURICH, B. N., TAGHAVIE-MOGHADAM, P. L., LEY, K. & GALKINA, E. V. 2014. L-selectin deficiency decreases aortic B1a and Breg subsets and promotes atherosclerosis. *Thromb Haemost,* 112**,** 803-11.

GRABNER, R., LOTZER, K., DOPPING, S., HILDNER, M., RADKE, D., BEER, M., SPANBROEK, R., LIPPERT, B., REARDON, C. A., GETZ, G. S., FU, Y. X., HEHLGANS, T., MEBIUS, R. E., VAN DER WALL, M., KRUSPE, D., ENGLERT, C., LOVAS, A., HU, D., RANDOLPH, G. J., WEIH, F. & HABENICHT, A. J. 2009. Lymphotoxin beta receptor signaling promotes tertiary lymphoid organogenesis in the aorta adventitia of aged ApoE-/- mice. *J Exp Med,* 206**,** 233-48.

GREGERSEN, P. K. & BEHRENS, T. W. 2006. Genetics of autoimmune diseases--disorders of immune homeostasis. *Nat Rev Genet,* 7**,** 917-28.

GU, Z., GU, L., EILS, R., SCHLESNER, M. & BRORS, B. 2014. circlize Implements and enhances circular visualization in R. *Bioinformatics,* 30**,** 2811-2.

GUPTA, N. T., VANDER HEIDEN, J. A., UDUMAN, M., GADALA-MARIA, D., YAARI, G. & KLEINSTEIN, S. H. 2015. Change-O: a toolkit for analyzing large-scale B cell immunoglobulin repertoire sequencing data. *Bioinformatics,* 31**,** 3356-8.

HADLEY, W. 2016. *ggplot2: Elegant Graphics for Data Analysis* [Online]. Available: https://ggplot2-book.org/ [Accessed].

HAN, Y., LI, H., GUAN, Y. & HUANG, J. 2016. Immune repertoire: A potential biomarker and therapeutic for hepatocellular carcinoma. *Cancer Lett,* 379**,** 206-12.

HANDCOCK, M. S. 2016. *Relative Distribution Methods* [Online]. Available: https://CRAN.R-project.org/package=reldist [Accessed].

HANSEL, T. T., KROPSHOFER, H., SINGER, T., MITCHELL, J. A. & GEORGE, A. J. 2010. The safety and side effects of monoclonal antibodies. *Nat Rev Drug Discov,* 9**,** 325-38.

HANSSON, G. K. & LIBBY, P. 2006. The immune response in atherosclerosis: a double-edged sword. *Nat Rev Immunol,* 6**,** 508-19.

HARGREAVES, D. C., HYMAN, P. L., LU, T. T., NGO, V. N., BIDGOL, A., SUZUKI, G., ZOU, Y. R., LITTMAN, D. R. & CYSTER, J. G. 2001. A coordinated change in chemokine responsiveness guides plasma cell movements. *J Exp Med,* 194**,** 45-56.

HARWOOD, N. E. & BATISTA, F. D. 2010. Early events in B cell activation. *Annu Rev Immunol,* 28**,** 185-210.

HILGENDORF, I., THEURL, I., GERHARDT, L. M., ROBBINS, C. S., WEBER, G. F., GONEN, A., IWAMOTO, Y., DEGOUSEE, N., HOLDERRIED, T. A., WINTER, C., ZIRLIK, A., LIN, H. Y., SUKHOVA, G. K., BUTANY, J., RUBIN, B. B., WITZTUM, J. L., LIBBY, P., NAHRENDORF, M., WEISSLEDER, R. & SWIRSKI, F. K. 2014. Innate response activator B cells aggravate atherosclerosis by stimulating T helper-1 adaptive immunity. *Circulation,* 129**,** 1677-87.

HOCHBERG, Y. & BENJAMINI, Y. 1990. More Powerful Procedures for Multiple Significance Testing. *Statistics in Medicine,* 9**,** 811-818.

HOFFMANN, J. & AKIRA, S. 2013. Innate immunity. *Curr Opin Immunol,* 25**,** 1-3.

HOFMAN, A., DARWISH MURAD, S., VAN DUIJN, C. M., FRANCO, O. H., GOEDEGEBURE, A., IKRAM, M. A., KLAVER, C. C., NIJSTEN, T. E., PEETERS, R. P., STRICKER, B. H., TIEMEIER, H. W., UITTERLINDEN, A. G. & VERNOOIJ, M. W. 2013. The Rotterdam Study: 2014 objectives and design update. *Eur J Epidemiol,* 28**,** 889-926.

HOLMES, A. B., CORINALDESI, C., SHEN, Q., KUMAR, R., COMPAGNO, N., WANG, Z., NITZAN, M., GRUNSTEIN, E., PASQUALUCCI, L., DALLA-FAVERA, R. & BASSO, K. 2020. Single-cell analysis of germinal-center B cells informs on lymphoma cell of origin and outcome. *J Exp Med,* 217.

HONDA, K., YANAI, H., NEGISHI, H., ASAGIRI, M., SATO, M., MIZUTANI, T., SHIMADA, N., OHBA, Y., TAKAOKA, A., YOSHIDA, N. & TANIGUCHI, T. 2005. IRF-7 is the master regulator of type-I interferon-dependent immune responses. *Nature,* 434**,** 772-7.

HORKKO, S., BIRD, D. A., MILLER, E., ITABE, H., LEITINGER, N., SUBBANAGOUNDER, G., BERLINER, J. A., FRIEDMAN, P., DENNIS, E. A., CURTISS, L. K., PALINSKI, W. & WITZTUM, J. L. 1999. Monoclonal autoantibodies specific for oxidized phospholipids or oxidized phospholipid-protein adducts inhibit macrophage uptake of oxidized low-density lipoproteins. *J Clin Invest,* 103**,** 117-28.

HOU, D., YING, T., WANG, L., CHEN, C., LU, S., WANG, Q., SEELEY, E., XU, J., XI, X., LI, T., LIU, J., TANG, X., ZHANG, Z., ZHOU, J., BAI, C., WANG, C., BYRNE-STEELE, M., QU, J., HAN, J. & SONG, Y. 2016. Immune Repertoire Diversity

Correlated with Mortality in Avian Influenza A (H7N9) Virus Infected Patients. *Sci Rep,* 6**,** 33843.

HU, D., MOHANTA, S. K., YIN, C., PENG, L., MA, Z., SRIKAKULAPU, P., GRASSIA, G., MACRITCHIE, N., DEVER, G., GORDON, P., BURTON, F. L., IALENTI, A., SABIR, S. R., MCINNES, I. B., BREWER, J. M., GARSIDE, P., WEBER, C., LEHMANN, T., TEUPSER, D., HABENICHT, L., BEER, M., GRABNER, R., MAFFIA, P., WEIH, F. & HABENICHT, A. J. 2015. Artery Tertiary Lymphoid Organs Control Aorta Immunity and Protect against Atherosclerosis via Vascular Smooth Muscle Cell Lymphotoxin beta Receptors. *Immunity,* 42**,** 1100-15.

ITOH, K., PATKI, V., FURIE, R. A., CHARTASH, E. K., JAIN, R. I., LANE, L., ASNIS, S. E. & CHIORAZZI, N. 2000. Clonal expansion is a characteristic feature of the B-cell repetoire of patients with rheumatoid arthritis. *Arthritis Res,* 2**,** 50-8.

IVASHKIV, L. B. & DONLIN, L. T. 2014. Regulation of type I interferon responses. *Nat Rev Immunol,* 14**,** 36-49.

JIANG, N., HE, J., WEINSTEIN, J. A., PENLAND, L., SASAKI, S., HE, X. S., DEKKER, C. L., ZHENG, N. Y., HUANG, M., SULLIVAN, M., WILSON, P. C., GREENBERG, H. B., DAVIS, M. M., FISHER, D. S. & QUAKE, S. R. 2013. Lineage structure of the human antibody repertoire in response to influenza vaccination. *Sci Transl Med,* 5**,** 171ra19.

JIAO, L., LIU, Y., YU, X. Y., PAN, X., ZHANG, Y., TU, J., SONG, Y. H. & LI, Y. 2023. Ribosome biogenesis in disease: new players and therapeutic targets. *Signal Transduct Target Ther,* 8**,** 15.

KHODADADI, L., CHENG, Q., RADBRUCH, A. & HIEPE, F. 2019. The Maintenance of Memory Plasma Cells. *Front Immunol,* 10**,** 721.

KIM, C. C., BACCARELLA, A. M., BAYAT, A., PEPPER, M. & FONTANA, M. F. 2019. FCRL5(+) Memory B Cells Exhibit Robust Recall Responses. *Cell Rep,* 27**,** 1446-1460 e4.

KIM, D. & PARK, D. 2019. Deep sequencing of B cell receptor repertoire. *BMB Rep,* 52**,** 540-547.

KINDE, I., WU, J., PAPADOPOULOS, N., KINZLER, K. W. & VOGELSTEIN, B. 2011. Detection and quantification of rare mutations with massively parallel sequencing. *Proc Natl Acad Sci U S A,* 108**,** 9530-5.

KIVIOJA, T., VAHARAUTIO, A., KARLSSON, K., BONKE, M., ENGE, M., LINNARSSON, S. & TAIPALE, J. 2011. Counting absolute numbers of molecules using unique molecular identifiers. *Nat Methods,* 9**,** 72-4.

KLEIN, U. & DALLA-FAVERA, R. 2008. Germinal centres: role in B-cell physiology and malignancy. *Nat Rev Immunol,* 8**,** 22-33.

KLINMAN, N. R. 1996. The "clonal selection hypothesis" and current concepts of B cell tolerance. *Immunity,* 5**,** 189-95.

KOWALCZYK, M. S., TIROSH, I., HECKL, D., RAO, T. N., DIXIT, A., HAAS, B. J., SCHNEIDER, R. K., WAGERS, A. J., EBERT, B. L. & REGEV, A. 2015. Single-cell RNA-seq reveals changes in cell cycle and differentiation programs upon aging of hematopoietic stem cells. *Genome Res,* 25**,** 1860-72.

KRAUTLER, N. J., SUAN, D., BUTT, D., BOURNE, K., HERMES, J. R., CHAN, T. D., SUNDLING, C., KAPLAN, W., SCHOFIELD, P., JACKSON, J., BASTEN, A., CHRIST, D. & BRINK, R. 2017. Differentiation of germinal center B cells into plasma cells is initiated by high-affinity antigen and completed by Tfh cells. *J Exp Med,* 214**,** 1259-1267.

KRUSKAL, W. H. & WALLIS, W. A. 1952. Use of Ranks in One-Criterion Variance Analysis. *Journal of the American Statistical Association,* 47**,** 583-621.

KUMAR, H., KAWAI, T. & AKIRA, S. 2011. Pathogen recognition by the innate immune system. *Int Rev Immunol,* 30**,** 16-34.

KURI-CERVANTES, L., PAMPENA, M. B., MENG, W., ROSENFELD, A. M., ITTNER, C. A. G., WEISMAN, A. R., AGYEKUM, R. S., MATHEW, D., BAXTER, A. E., VELLA, L. A., KUTHURU, O., APOSTOLIDIS, S. A., BERSHAW, L., DOUGHERTY, J., GREENPLATE, A. R., PATTEKAR, A., KIM, J., HAN, N., GOUMA, S., WEIRICK, M. E., AREVALO, C. P., BOLTON, M. J., GOODWIN, E. C., ANDERSON, E. M., HENSLEY, S. E., JONES, T. K., MANGALMURTI, N. S., LUNING PRAK, E. T., WHERRY, E. J., MEYER, N. J. & BETTS, M. R. 2020. Comprehensive mapping of immune perturbations associated with severe COVID-19. *Sci Immunol,* 5.

KUROSAKI, T., KOMETANI, K. & ISE, W. 2015. Memory B cells. *Nat Rev Immunol,* 15**,** 149-59.

KURTS, C., PANZER, U., ANDERS, H. J. & REES, A. J. 2013. The immune system and kidney disease: basic concepts and clinical implications. *Nat Rev Immunol,* 13**,** 738-53.

KYAW, T., TAY, C., KHAN, A., DUMOUCHEL, V., CAO, A., TO, K., KEHRY, M., DUNN, R., AGROTIS, A., TIPPING, P., BOBIK, A. & TOH, B. H. 2010. Conventional B2 B cell depletion ameliorates whereas its adoptive transfer aggravates atherosclerosis. *J Immunol,* 185**,** 4410-9.

KYAW, T., WINSHIP, A., TAY, C., KANELLAKIS, P., HOSSEINI, H., CAO, A., LI, P., TIPPING, P., BOBIK, A. & TOH, B. H. 2013. Cytotoxic and proinflammatory CD8+ T lymphocytes promote development of vulnerable atherosclerotic plaques in apoE-deficient mice. *Circulation,* 127**,** 1028-39.

LAIDLAW, B. J., DUAN, L., XU, Y., VAZQUEZ, S. E. & CYSTER, J. G. 2020. The transcription factor Hhex cooperates with the corepressor Tle3 to promote memory B cell development. *Nat Immunol,* 21**,** 1082-1093.

LEHMANN-HORN, K., WANG, S. Z., SAGAN, S. A., ZAMVIL, S. S. & VON BUDINGEN, H. C. 2016. B cell repertoire expansion occurs in meningeal ectopic lymphoid tissue. *JCI Insight,* 1**,** e87234.

LI, Y., MYERS, J. L., BOSTICK, D. L., SULLIVAN, C. B., MADARA, J., LINDERMAN, S. L., LIU, Q., CARTER, D. M., WRAMMERT, J., ESPOSITO, S., PRINCIPI, N., PLOTKIN, J. B., ROSS, T. M., AHMED, R., WILSON, P. C. & HENSLEY, S. E. 2013. Immune history shapes specificity of pandemic H1N1 influenza antibody responses. *J Exp Med,* 210**,** 1493-500.

LIBBY, P. 2021. The changing landscape of atherosclerosis. *Nature,* 592**,** 524-533.

LIBBY, P., BURING, J. E., BADIMON, L., HANSSON, G. K., DEANFIELD, J., BITTENCOURT, M. S., TOKGOZOGLU, L. & LEWIS, E. F. 2019a. Atherosclerosis. *Nat Rev Dis Primers,* 5**,** 56.

LIBBY, P., PASTERKAMP, G., CREA, F. & JANG, I. K. 2019b. Reassessing the Mechanisms of Acute Coronary Syndromes. *Circ Res,* 124**,** 150-160.

LIBBY, P., RIDKER, P. M. & HANSSON, G. K. 2011. Progress and challenges in translating the biology of atherosclerosis. *Nature,* 473**,** 317-25.

LIGHTMAN, S. M., UTLEY, A. & LEE, K. P. 2019. Survival of Long-Lived Plasma Cells (LLPC): Piecing Together the Puzzle. *Front Immunol,* 10**,** 965.

LORENZO, C., DELGADO, P., BUSSE, C. E., SANZ-BRAVO, A., MARTOS-FOLGADO, I., BONZON-KULICHENKO, E., FERRARINI, A., GONZALEZ-VALDES, I. B., MUR, S. M., ROLDAN-MONTERO, R., MARTINEZ-LOPEZ, D., MARTIN-VENTURA, J. L., VAZQUEZ, J., WARDEMANN, H. & RAMIRO, A. R. 2020. ALDH4A1 is an atherosclerosis auto-antigen targeted by protective antibodies. *Nature*.

LU, L. L., SUSCOVICH, T. J., FORTUNE, S. M. & ALTER, G. 2018. Beyond binding: antibody effector functions in infectious diseases. *Nat Rev Immunol,* 18**,** 46-61.

LUO, Y., WANG, J., LI, K., LI, M., XU, S., LIU, X., ZHANG, Z., XU, X., ZHANG, Y., PAN, J., LIU, P., GAO, S., MIAO, Z. & YU, Y. 2022. Single-cell genomics identifies distinct B1 cell developmental pathways and reveals aging-related changes in the B-cell receptor repertoire. *Cell Biosci,* 12**,** 57.

MACLENNAN, I. C., TOELLNER, K. M., CUNNINGHAM, A. F., SERRE, K., SZE, D. M., ZUNIGA, E., COOK, M. C. & VINUESA, C. G. 2003. Extrafollicular antibody responses. *Immunol Rev,* 194**,** 8-18.

MAMEDOV, I. Z., BRITANOVA, O. V., ZVYAGIN, I. V., TURCHANINOVA, M. A., BOLOTIN, D. A., PUTINTSEVA, E. V., LEBEDEV, Y. B. & CHUDAKOV, D. M. 2013. Preparing unbiased T-cell receptor and antibody cDNA libraries for the deep next generation sequencing profiling. *Front Immunol,* 4**,** 456.

MARKET, E. & PAPAVASILIOU, F. N. 2003. V(D)J recombination and the evolution of the adaptive immune system. *PLoS Biol,* 1**,** E16.

MARTIN, A., CHAHWAN, R., PARSA, J. Y. & SCHARFF, M. D. 2015. Chapter 20 - Somatic Hypermutation: The Molecular Mechanisms Underlying the Production of Effective High-Affinity Antibodies. *In:* ALT, F. W., HONJO, T., RADBRUCH, A. & RETH, M. (eds.) *Molecular Biology of B Cells (Second Edition).* London: Academic Press.

MATHEW, N. R., JAYANTHAN, J. K., SMIRNOV, I. V., ROBINSON, J. L., AXELSSON, H., NAKKA, S. S., EMMANOUILIDI, A., CZARNEWSKI, P., YEWDELL, W. T., SCHON, K., LEBRERO-FERNANDEZ, C., BERNASCONI, V., RODIN, W., HARANDI, A. M., LYCKE, N., BORCHERDING, N., YEWDELL, J. W., GREIFF, V., BEMARK, M. & ANGELETTI, D. 2021. Single-cell BCR and transcriptome analysis after influenza infection reveals spatiotemporal dynamics of antigen-specific B cells. *Cell Rep,* 35**,** 109286.

MCHUGH, M. L. 2013. The chi-square test of independence. *Biochem Med (Zagreb),* 23**,** 143-9.

MCINNES, L. & HEALY, J. 2018. UMAP: Uniform Manifold Approximation and Projection for Dimension Reduction. *ArXiv e-prints,* 1802.03426.

MEDZHITOV, R., SHEVACH, E. M., TRINCHIERI, G., MELLOR, A. L., MUNN, D. H., GORDON, S., LIBBY, P., HANSSON, G. K., SHORTMAN, K., DONG, C., GABRILOVICH, D., GABRYSOVA, L., HOWES, A. & O'GARRA, A. 2011. Highlights of 10 years of immunology in Nature Reviews Immunology. *Nat Rev Immunol,* 11**,** 693-702.

MELCHERS, F. 2015. Checkpoints that control B cell development. *J Clin Invest,* 125**,** 2203-10.

MESIN, L., ERSCHING, J. & VICTORA, G. D. 2016. Germinal Center B Cell Dynamics. *Immunity,* 45**,** 471-482.

MI, Y., HAN, J., ZHU, J. & JIN, T. 2021. Role of the PD-1/PD-L1 Signaling in Multiple Sclerosis and Experimental Autoimmune Encephalomyelitis: Recent Insights and Future Directions. *Mol Neurobiol,* 58**,** 6249-6271.

MILLER, S. D., TURLEY, D. M. & PODOJIL, J. R. 2007. Antigen-specific tolerance strategies for the prevention and treatment of autoimmune disease. *Nature Reviews Immunology,* 7**,** 665-677.

MOHANTA, S. K., YIN, C., PENG, L., SRIKAKULAPU, P., BONTHA, V., HU, D., WEIH, F., WEBER, C., GERDES, N. & HABENICHT, A. J. 2014. Artery Tertiary Lymphoid Organs Contribute to Innate and Adaptive Immune Responses in Advanced Mouse Atherosclerosis. *Circ Res,* 114**,** 1772-1787.

MOORE, K. J. & FREEMAN, M. W. 2006. Scavenger receptors in atherosclerosis: beyond lipid uptake. *Arterioscler Thromb Vasc Biol,* 26**,** 1702-11.

MOOS, M. P., JOHN, N., GRABNER, R., NOSSMANN, S., GUNTHER, B., VOLLANDT, R., FUNK, C. D., KAISER, B. & HABENICHT, A. J. 2005. The lamina adventitia is

the major site of immune cell accumulation in standard chow-fed apolipoprotein E-deficient mice. *Arterioscler Thromb Vasc Biol,* 25**,** 2386-91.

MULLER, J. & NITSCHKE, L. 2014. The role of CD22 and Siglec-G in B-cell tolerance and autoimmune disease. *Nat Rev Rheumatol,* 10**,** 422-8.

MURI, J., THUT, H., BORNKAMM, G. W. & KOPF, M. 2019. B1 and Marginal Zone B Cells but Not Follicular B2 Cells Require Gpx4 to Prevent Lipid Peroxidation and Ferroptosis. *Cell Rep,* 29**,** 2731-2744 e4.

NAKANO-YOKOMIZO, T., TAHARA-HANAOKA, S., NAKAHASHI-ODA, C., NABEKURA, T., TCHAO, N. K., KADOSAKI, M., TOTSUKA, N., KURITA, N., NAKAMAGOE, K., TAMAOKA, A., TAKAI, T., YASUI, T., KIKUTANI, H., HONDA, S., SHIBUYA, K., LANIER, L. L. & SHIBUYA, A. 2011. The immunoreceptor adapter protein DAP12 suppresses B lymphocyte-driven adaptive immune responses. *J Exp Med,* 208**,** 1661-71.

NEEFJES, J., JONGSMA, M. L., PAUL, P. & BAKKE, O. 2011. Towards a systems understanding of MHC class I and MHC class II antigen presentation. *Nat Rev Immunol,* 11**,** 823-36.

NEMAZEE, D. 2006. Receptor editing in lymphocyte development and central tolerance. *Nat Rev Immunol,* 6**,** 728-40.

NEMAZEE, D. 2017. Mechanisms of central tolerance for B cells. *Nat Rev Immunol,* 17**,** 281-294.

NGO, S. T., STEYN, F. J. & MCCOMBE, P. A. 2014. Gender differences in autoimmune disease. *Front Neuroendocrinol,* 35**,** 347-69.

NIDORF, S. M., FIOLET, A. T. L., MOSTERD, A., EIKELBOOM, J. W., SCHUT, A., OPSTAL, T. S. J., THE, S. H. K., XU, X. F., IRELAND, M. A., LENDERINK, T., LATCHEM, D., HOOGSLAG, P., JERZEWSKI, A., NIEROP, P., WHELAN, A., HENDRIKS, R., SWART, H., SCHAAP, J., KUIJPER, A. F. M., VAN HESSEN, M. W. J., SAKLANI, P., TAN, I., THOMPSON, A. G., MORTON, A., JUDKINS, C., BAX, W. A., DIRKSEN, M., ALINGS, M., HANKEY, G. J., BUDGEON, C. A., TIJSSEN, J. G. P., CORNEL, J. H., THOMPSON, P. L. & LODOCO2 TRIAL, I. 2020. Colchicine in Patients with Chronic Coronary Disease. *N Engl J Med,* 383**,** 1838-1847.

O'KEEFE, T. L., WILLIAMS, G. T., BATISTA, F. D. & NEUBERGER, M. S. 1999. Deficiency in CD22, a B cell-specific inhibitory receptor, is sufficient to predispose to development of high affinity autoantibodies. *J Exp Med,* 189**,** 1307-13.

O'NEILL, S. K., CAO, Y., HAMEL, K. M., DOODES, P. D., HUTAS, G. & FINNEGAN, A. 2007. Expression of CD80/86 on B cells is essential for autoreactive T cell activation and the development of arthritis. *J Immunol,* 179**,** 5109-16.

OBERMEIER, B., LOVATO, L., MENTELE, R., BRUCK, W., FORNE, I., IMHOF, A., LOTTSPEICH, F., TURK, K. W., WILLIS, S. N., WEKERLE, H., HOHLFELD, R., HAFLER, D. A., O'CONNOR, K. C. & DORNMAIR, K. 2011. Related B cell clones that populate the CSF and CNS of patients with multiple sclerosis produce CSF immunoglobulin. *J Neuroimmunol,* 233**,** 245-8.

ODEGARD, V. H. & SCHATZ, D. G. 2006. Targeting of somatic hypermutation. *Nat Rev Immunol,* 6**,** 573-83.

OWSIANY, K. M., ALENCAR, G. F. & OWENS, G. K. 2019. Revealing the Origins of Foam Cells in Atherosclerotic Lesions. *Arterioscler Thromb Vasc Biol,* 39**,** 836-838.

PARKER, D. C. 1993. T cell-dependent B cell activation. *Annu Rev Immunol,* 11**,** 331-60.

PARKIN, J. & COHEN, B. 2001. An overview of the immune system. *Lancet,* 357**,** 1777-89.

PELANDA, R. & TORRES, R. M. 2012. Central B-cell tolerance: where selection begins. *Cold Spring Harb Perspect Biol,* 4**,** a007146.

PEPERZAK, V., VIKSTROM, I. B. & TARLINTON, D. M. 2012. Through a glass less darkly: apoptosis and the germinal center response to antigen. *Immunol Rev,* 247**,** 93-106.

PHAN, T. G., PAUS, D., CHAN, T. D., TURNER, M. L., NUTT, S. L., BASTEN, A. & BRINK, R. 2006. High affinity germinal center B cells are actively selected into the plasma cell compartment. *J Exp Med,* 203**,** 2419-24.

PICELLI, S., FARIDANI, O. R., BJORKLUND, A. K., WINBERG, G., SAGASSER, S. & SANDBERG, R. 2014. Full-length RNA-seq from single cells using Smart-seq2. *Nat Protoc,* 9**,** 171-81.

PITZALIS, C., JONES, G. W., BOMBARDIERI, M. & JONES, S. A. 2014. Ectopic lymphoid-like structures in infection, cancer and autoimmunity. *Nat Rev Immunol,* 14**,** 447-62.

PORSCH, F. & BINDER, C. J. 2019. Impact of B-Cell-Targeted Therapies on Cardiovascular Disease. *Arterioscler Thromb Vasc Biol,* 39**,** 1705-1714.

PRASAD, A., CLOPTON, P., AYERS, C., KHERA, A., DE LEMOS, J. A., WITZTUM, J. L. & TSIMIKAS, S. 2017. Relationship of Autoantibodies to MDA-LDL and ApoB-Immune Complexes to Sex, Ethnicity, Subclinical Atherosclerosis, and Cardiovascular Events. *Arterioscler Thromb Vasc Biol,* 37**,** 1213-1221.

PRICE, M. J., PATTERSON, D. G., SCHARER, C. D. & BOSS, J. M. 2018. Progressive Upregulation of Oxidative Metabolism Facilitates Plasmablast Differentiation to a T-Independent Antigen. *Cell Rep,* 23**,** 3152-3159.

RAFIEIAN-KOPAEI, M., SETORKI, M., DOUDI, M., BARADARAN, A. & NASRI, H. 2014. Atherosclerosis: process, indicators, risk factors and new hopes. *International journal of preventive medicine,* 5**,** 927-946.

RAO, V. K. & OLIVEIRA, J. B. 2011. How I treat autoimmune lymphoproliferative syndrome. *Blood,* 118**,** 5741-5751.

RAVANDI, A., BOEKHOLDT, S. M., MALLAT, Z., TALMUD, P. J., KASTELEIN, J. J., WAREHAM, N. J., MILLER, E. R., BENESSIANO, J., TEDGUI, A., WITZTUM, J. L., KHAW, K. T. & TSIMIKAS, S. 2011. Relationship of IgG and IgM autoantibodies and immune complexes to oxidized LDL with markers of oxidation and inflammation and cardiovascular events: results from the EPIC-Norfolk Study. *J Lipid Res,* 52**,** 1829-36.

REY, D. & NEUHÄUSER, M. 2011. Wilcoxon-Signed-Rank Test. *In:* LOVRIC, M. (ed.) *International Encyclopedia of Statistical Science.* Berlin, Heidelberg: Springer Berlin Heidelberg.

RIDKER, P. M., EVERETT, B. M., THUREN, T., MACFADYEN, J. G., CHANG, W. H., BALLANTYNE, C., FONSECA, F., NICOLAU, J., KOENIG, W., ANKER, S. D., KASTELEIN, J. J. P., CORNEL, J. H., PAIS, P., PELLA, D., GENEST, J., CIFKOVA, R., LORENZATTI, A., FORSTER, T., KOBALAVA, Z., VIDA-SIMITI, L., FLATHER, M., SHIMOKAWA, H., OGAWA, H., DELLBORG, M., ROSSI, P. R. F., TROQUAY, R. P. T., LIBBY, P., GLYNN, R. J. & GROUP, C. T. 2017. Antiinflammatory Therapy with Canakinumab for Atherosclerotic Disease. *N Engl J Med,* 377**,** 1119-1131.

RIEDEL, R., ADDO, R., FERREIRA-GOMES, M., HEINZ, G. A., HEINRICH, F., KUMMER, J., GREIFF, V., SCHULZ, D., KLAEDEN, C., CORNELIS, R., MENZEL, U., KROGER, S., STERVBO, U., KOHLER, R., HAFTMANN, C., KUHNEL, S., LEHMANN, K., MASCHMEYER, P., MCGRATH, M., NAUNDORF, S., HAHNE, S., SERCAN-ALP, O., SIRACUSA, F., STEFANOWSKI, J., WEBER, M., WESTENDORF, K., ZIMMERMANN, J., HAUSER, A. E., REDDY, S. T., DUREK, P., CHANG, H. D., MASHREGHI, M. F. & RADBRUCH, A. 2020. Discrete populations of isotype-switched memory B lymphocytes are maintained in murine spleen and bone marrow. *Nat Commun,* 11**,** 2570.

ROBINS, H. 2013. Immunosequencing: applications of immune repertoire deep sequencing. *Curr Opin Immunol,* 25**,** 646-52.

RODRIGUEZ-ZHURBENKO, N., QUACH, T. D., HOPKINS, T. J., ROTHSTEIN, T. L. & HERNANDEZ, A. M. 2019. Human B-1 Cells and B-1 Cell Antibodies Change With Advancing Age. *Front Immunol,* 10**,** 483.

ROMAGNANI, S. 2006. Immunological tolerance and autoimmunity. *Intern Emerg Med,* 1**,** 187-96.

ROSENBLUM, M. D., REMEDIOS, K. A. & ABBAS, A. K. 2015. Mechanisms of human autoimmunity. *Journal of Clinical Investigation,* 125**,** 2228-2233.

ROSENFELD, A. M., MENG, W., CHEN, D. Y., ZHANG, B., GRANOT, T., FARBER, D. L., HERSHBERG, U. & LUNING PRAK, E. T. 2018. Computational Evaluation of B-Cell Clone Sizes in Bulk Populations. *Front Immunol,* 9**,** 1472.

ROTH, K., OEHME, L., ZEHENTMEIER, S., ZHANG, Y., NIESNER, R. & HAUSER, A. E. 2014. Tracking plasma cell differentiation and survival. *Cytometry A,* 85**,** 15-24.

RUBIN, S. J. S., BLOOM, M. S. & ROBINSON, W. H. 2019. B cell checkpoints in autoimmune rheumatic diseases. *Nat Rev Rheumatol,* 15**,** 303-315.

SAGE, A. P., TSIANTOULAS, D., BINDER, C. J. & MALLAT, Z. 2019. The role of B cells in atherosclerosis. *Nat Rev Cardiol,* 16**,** 180-196.

SAKAGUCHI, S., YAMAGUCHI, T., NOMURA, T. & ONO, M. 2008. Regulatory T cells and immune tolerance. *Cell,* 133**,** 775-87.

SATIJA, R., FARRELL, J. A., GENNERT, D., SCHIER, A. F. & REGEV, A. 2015. Spatial reconstruction of single-cell gene expression data. *Nat Biotechnol,* 33**,** 495-502.

SCHATZ, D. G. & JI, Y. 2011. Recombination centres and the orchestration of V(D)J recombination. *Nat Rev Immunol,* 11**,** 251-63.

SCHMIEDER, R. & EDWARDS, R. 2011. Quality control and preprocessing of metagenomic datasets. *Bioinformatics,* 27**,** 863-4.

SCHROEDER, H. W., JR. & CAVACINI, L. 2010. Structure and function of immunoglobulins. *J Allergy Clin Immunol,* 125**,** S41-52.

SEDA, V. & MRAZ, M. 2015. B-cell receptor signalling and its crosstalk with other pathways in normal and malignant cells. *Eur J Haematol,* 94**,** 193-205.

SELA-CULANG, I., KUNIK, V. & OFRAN, Y. 2013. The structural basis of antibody-antigen recognition. *Front Immunol,* 4**,** 302.

SHI, W., LIAO, Y., WILLIS, S. N., TAUBENHEIM, N., INOUYE, M., TARLINTON, D. M., SMYTH, G. K., HODGKIN, P. D., NUTT, S. L. & CORCORAN, L. M. 2015. Transcriptional profiling of mouse B cell terminal differentiation defines a signature for antibody-secreting plasma cells. *Nat Immunol,* 16**,** 663-73.

SHIRAI, H., KIDERA, A. & NAKAMURA, H. 1999. H3-rules: identification of CDR-H3 structures in antibodies. *FEBS Lett,* 455**,** 188-97.

SHUGAY, M., BAGAEV, D. V., TURCHANINOVA, M. A., BOLOTIN, D. A., BRITANOVA, O. V., PUTINTSEVA, E. V., POGORELYY, M. V., NAZAROV, V. I., ZVYAGIN, I. V., KIRGIZOVA, V. I., KIRGIZOV, K. I., SKOROBOGATOVA, E. V. & CHUDAKOV, D. M. 2015. VDJtools: Unifying Post-analysis of T Cell Receptor Repertoires. *PLoS Comput Biol,* 11**,** e1004503.

SHUGAY, M., BRITANOVA, O. V., MERZLYAK, E. M., TURCHANINOVA, M. A., MAMEDOV, I. Z., TUGANBAEV, T. R., BOLOTIN, D. A., STAROVEROV, D. B., PUTINTSEVA, E. V., PLEVOVA, K., LINNEMANN, C., SHAGIN, D., POSPISILOVA, S., LUKYANOV, S., SCHUMACHER, T. N. & CHUDAKOV, D. M. 2014. Towards error-free profiling of immune repertoires. *Nat Methods,* 11**,** 653-5.

SIEBENLIST, U., BROWN, K. & CLAUDIO, E. 2005. Control of lymphocyte development by nuclear factor-kappaB. *Nat Rev Immunol,* 5**,** 435-45.

SIEGRIST, C. A. & ASPINALL, R. 2009. B-cell responses to vaccination at the extremes of age. *Nat Rev Immunol,* 9**,** 185-94.

SOBECKI, M., MROUJ, K., CAMASSES, A., PARISIS, N., NICOLAS, E., LLERES, D., GERBE, F., PRIETO, S., KRASINSKA, L., DAVID, A., EGUREN, M., BIRLING, M. C., URBACH, S., HEM, S., DEJARDIN, J., MALUMBRES, M., JAY, P., DULIC, V., LAFONTAINE, D., FEIL, R. & FISHER, D. 2016. The cell proliferation antigen Ki-67 organises heterochromatin. *Elife,* 5**,** e13722.

SOTO, C., BOMBARDI, R. G., BRANCHIZIO, A., KOSE, N., MATTA, P., SEVY, A. M., SINKOVITS, R. S., GILCHUK, P., FINN, J. A. & CROWE, J. E., JR. 2019. High frequency of shared clonotypes in human B cell receptor repertoires. *Nature,* 566**,** 398-402.

SPRENT, J. 1995. Antigen-presenting cells. Professionals and amateurs. *Curr Biol,* 5**,** 1095-7.

SRIKAKULAPU, P., HU, D., YIN, C., MOHANTA, S. K., BONTHA, S. V., PENG, L., BEER, M., WEBER, C., MCNAMARA, C. A., GRASSIA, G., MAFFIA, P., MANZ, R. A. & HABENICHT, A. J. 2016. Artery Tertiary Lymphoid Organs Control Multilayered Territorialized Atherosclerosis B-Cell Responses in Aged ApoE-/- Mice. *Arterioscler Thromb Vasc Biol,* 36**,** 1174-85.

STAVNEZER, J., GUIKEMA, J. E. & SCHRADER, C. E. 2008. Mechanism and regulation of class switch recombination. *Annu Rev Immunol,* 26**,** 261-92.

STERN, J. N., YAARI, G., VANDER HEIDEN, J. A., CHURCH, G., DONAHUE, W. F., HINTZEN, R. Q., HUTTNER, A. J., LAMAN, J. D., NAGRA, R. M., NYLANDER, A., PITT, D., RAMANAN, S., SIDDIQUI, B. A., VIGNEAULT, F., KLEINSTEIN, S. H., HAFLER, D. A. & O'CONNOR, K. C. 2014. B cells populating the multiple sclerosis brain mature in the draining cervical lymph nodes. *Sci Transl Med,* 6**,** 248ra107.

STROM, A. C., CROSS, A. J., COLE, J. E., BLAIR, P. A., LEIB, C., GODDARD, M. E., ROSSER, E. C., PARK, I., HULTGARDH NILSSON, A., NILSSON, J., MAURI, C. & MONACO, C. 2015. B regulatory cells are increased in hypercholesterolaemic mice and protect from lesion development via IL-10. *Thromb Haemost,* 114**,** 835-47.

SU, Z., JIN, Y., ZHANG, Y., GUAN, Z., LI, H., CHEN, X., XIE, C., ZHANG, C., LIU, X., LI, P., YE, P., ZHANG, L., KONG, Y. & LUO, W. 2021. The Diagnostic and Prognostic Potential of the B-Cell Repertoire in Membranous Nephropathy. *Front Immunol,* 12**,** 635326.

SZKLARCZYK, D., GABLE, A. L., LYON, D., JUNGE, A., WYDER, S., HUERTA-CEPAS, J., SIMONOVIC, M., DONCHEVA, N. T., MORRIS, J. H., BORK, P., JENSEN, L. J. & MERING, C. V. 2019. STRING v11: protein-protein association networks with increased coverage, supporting functional discovery in genome-wide experimental datasets. *Nucleic Acids Res,* 47**,** D607-D613.

TEAM, R. C. 2019. *R: A language and environment for statistical computing*. [Online]. R Foundation for Statistical Computing, Vienna, Austria. Available: https://www.R-project.org/ [Accessed].

TENG, G. & PAPAVASILIOU, F. N. 2007. Immunoglobulin somatic hypermutation. *Annu Rev Genet,* 41**,** 107-20.

TIROSH, I., IZAR, B., PRAKADAN, S. M., WADSWORTH, M. H., 2ND, TREACY, D., TROMBETTA, J. J., ROTEM, A., RODMAN, C., LIAN, C., MURPHY, G., FALLAHI-SICHANI, M., DUTTON-REGESTER, K., LIN, J. R., COHEN, O., SHAH, P., LU, D., GENSHAFT, A. S., HUGHES, T. K., ZIEGLER, C. G., KAZER, S. W., GAILLARD, A., KOLB, K. E., VILLANI, A. C., JOHANNESSEN, C. M., ANDREEV, A. Y., VAN ALLEN, E. M., BERTAGNOLLI, M., SORGER, P. K., SULLIVAN, R. J., FLAHERTY, K. T., FREDERICK, D. T., JANE-VALBUENA, J., YOON, C. H., ROZENBLATT-ROSEN, O., SHALEK, A. K., REGEV, A. & GARRAWAY, L. A. 2016. Dissecting the multicellular ecosystem of metastatic melanoma by single-cell RNA-seq. *Science,* 352**,** 189-96.

TSIANTOULAS, D., ESLAMI, M., OBERMAYER, G., CLEMENT, M., SMEETS, D., MAYER, F. J., KISS, M. G., ENDERS, L., WEISSER, J., GODERLE, L., LAMBERT, J., FROMMLET, F., MUELLER, A., HENDRIKX, T., OZSVAR-KOZMA, M., PORSCH, F., WILLEN, L., AFONYUSHKIN, T., MURPHY, J. E., FOGELSTRAND, P., DONZE, O., PASTERKAMP, G., HOKE, M., KUBICEK, S., JORGENSEN, H. F., DANCHIN, N., SIMON, T., SCHARNAGL, H., MARZ, W., BOREN, J., HESS, H., MALLAT, Z., SCHNEIDER, P. & BINDER, C. J. 2021. APRIL limits atherosclerosis by binding to heparan sulfate proteoglycans. *Nature,* 597**,** 92-96.

TSUBATA, T. 2017. B-cell tolerance and autoimmunity. *F1000Res,* 6**,** 391.

TURVEY, S. E. & BROIDE, D. H. 2010. Innate immunity. *J Allergy Clin Immunol,* 125**,** S24-32.

TWIGG, H. L., 3RD 2004. Macrophages in innate and acquired immunity. *Semin Respir Crit Care Med,* 25**,** 21-31.

VAN DRIEL, I. R. 2007. Tolerance and autoimmunity: entwined pathways lead to immunological tolerance. *Immunol Cell Biol,* 85**,** 267-8.

VAN ERP, E. A., LUYTJES, W., FERWERDA, G. & VAN KASTEREN, P. B. 2019. Fc-Mediated Antibody Effector Functions During Respiratory Syncytial Virus Infection and Disease. *Front Immunol,* 10**,** 548.

VANDERLUGT, C. L. & MILLER, S. D. 2002. Epitope spreading in immune-mediated diseases: implications for immunotherapy. *Nat Rev Immunol,* 2**,** 85-95.

VICTORA, G. D. & NUSSENZWEIG, M. C. 2012. Germinal centers. *Annu Rev Immunol,* 30**,** 429-57.

WANG, Z., ZHANG, X., ZHANG, C., LI, Y., LU, S., MOHANTA, S., WEBER, C., HABENICHT, A. & YIN, C. 2022. Combined Single-Cell RNA and Single-Cell alpha/beta T Cell Receptor Sequencing of the Arterial Wall in Atherosclerosis. *Methods Mol Biol,* 2419**,** 727-746.

WARDEMANN, H., YURASOV, S., SCHAEFER, A., YOUNG, J. W., MEFFRE, E. & NUSSENZWEIG, M. C. 2003a. Predominant autoantibody production by early human B cell precursors. *Science,* 301**,** 1374-7.

WARDEMANN, H., YURASOV, S., SCHAEFER, A., YOUNG, J. W., MEFFRE, E. & NUSSENZWEIG, M. C. 2003b. Predominant Autoantibody Production by Early Human B Cell Precursors. *Science,* 301.

WATANABE, A., INOUE, N., WATANABE, M., YAMAMOTO, M., OZAKI, H., HIDAKA, Y. & IWATANI, Y. 2020. Increases of CD80 and CD86 Expression on Peripheral Blood Cells and their Gene Polymorphisms in Autoimmune Thyroid Disease. *Immunol Invest,* 49**,** 191-203.

WEINSTEIN, J. A., JIANG, N., WHITE, R. A., 3RD, FISHER, D. S. & QUAKE, S. R. 2009. High-throughput sequencing of the zebrafish antibody repertoire. *Science,* 324**,** 807-10.

WHO. 2021. *World Health Organization : Cardiovascular diseases (CVDs)* [Online]. Available: https://www.who.int/news-room/fact-sheets/detail/cardiovascular-diseases-(cvds) [Accessed].

WILKINSON, S. T., VANPATTEN, K. A., FERNANDEZ, D. R., BRUNHOEBER, P., GARSHA, K. E., GLINSMANN-GIBSON, B. J., GROGAN, T. M., TERUYA-FELDSTEIN, J. & RIMSZA, L. M. 2012. Partial plasma cell differentiation as a mechanism of lost major histocompatibility complex class II expression in diffuse large B-cell lymphoma. *Blood,* 119**,** 1459-67.

WINGREN, C., MICHAELSEN, T. E., MAGNUSSON, C. G. & HANSSON, U. B. 1996. Comparison of surface properties of human IgA, IgE, IgG and IgM antibodies with identical and different specificities. *Scand J Immunol,* 44**,** 430-6.

WOLF, D. & LEY, K. 2019. Immunity and Inflammation in Atherosclerosis. *Circ Res,* 124**,** 315-327.

WONG, C. K., LIT, L. C., TAM, L. S., LI, E. K. & LAM, C. W. 2005. Aberrant production of soluble costimulatory molecules CTLA-4, CD28, CD80 and CD86 in patients with systemic lupus erythematosus. *Rheumatology (Oxford),* 44**,** 989-94.

WONG, J. B., HEWITT, S. L., HELTEMES-HARRIS, L. M., MANDAL, M., JOHNSON, K., RAJEWSKY, K., KORALOV, S. B., CLARK, M. R., FARRAR, M. A. & SKOK, J. A. 2019. B-1a cells acquire their unique characteristics by bypassing the pre-BCR selection stage. *Nat Commun,* 10**,** 4768.

WOOF, J. M. & BURTON, D. R. 2004. Human antibody-Fc receptor interactions illuminated by crystal structures. *Nat Rev Immunol,* 4**,** 89-99.

XING, Y. & HOGQUIST, K. A. 2012. T-cell tolerance: central and peripheral. *Cold Spring Harb Perspect Biol,* 4.

YAARI, G. & KLEINSTEIN, S. H. 2015. Practical guidelines for B-cell receptor repertoire sequencing analysis. *Genome Med,* 7**,** 121.

YANG, Y., WANG, C., YANG, Q., KANTOR, A. B., CHU, H., GHOSN, E. E., QIN, G., MAZMANIAN, S. K., HAN, J. & HERZENBERG, L. A. 2015. Distinct mechanisms define murine B cell lineage immunoglobulin heavy chain (IgH) repertoires. *Elife,* 4**,** e09083.

YE, J., MA, N., MADDEN, T. L. & OSTELL, J. M. 2013. IgBLAST: an immunoglobulin variable domain sequence analysis tool. *Nucleic Acids Res,* 41**,** W34-40.

YIN, C., MOHANTA, S., MA, Z., WEBER, C., HU, D., WEIH, F. & HABENICHT, A. 2015. Generation of Aorta Transcript Atlases of Wild-Type and Apolipoprotein E-null Mice by Laser Capture Microdissection-Based mRNA Expression Microarrays. *Methods Mol Biol,* 1339**,** 297-308.

YIN, C., MOHANTA, S. K., SRIKAKULAPU, P., WEBER, C. & HABENICHT, A. J. 2016. Artery Tertiary Lymphoid Organs: Powerhouses of Atherosclerosis Immunity. *Front Immunol,* 7**,** 387.

YU, G., WANG, L. G., HAN, Y. & HE, Q. Y. 2012. clusterProfiler: an R package for comparing biological themes among gene clusters. *OMICS,* 16**,** 284-7.

ZERNECKE, A., WINKELS, H., COCHAIN, C., WILLIAMS, J. W., WOLF, D., SOEHNLEIN, O., ROBBINS, C. S., MONACO, C., PARK, I., MCNAMARA, C. A., BINDER, C. J., CYBULSKY, M. I., SCIPIONE, C. A., HEDRICK, C. C., GALKINA, E. V., KYAW, T., GHOSHEH, Y., DINH, H. Q. & LEY, K. 2020. Meta-Analysis of Leukocyte Diversity in Atherosclerotic Mouse Aortas. *Circ Res,* 127**,** 402-426.

ZHANG, C. 2022. *Searching for Autoimmune B Cells in Atherosclerosis.* Doctoral dissertation, University of Munich.

ZHANG, L., DONG, X., LEE, M., MASLOV, A. Y., WANG, T. & VIJG, J. 2019. Single-cell whole-genome sequencing reveals the functional landscape of somatic mutations in B lymphocytes across the human lifespan. *Proc Natl Acad Sci U S A,* 116**,** 9014-9019.

ZHANG, S., ZHANG, S., LIN, Z., ZHANG, X., DOU, X., ZHOU, X., WANG, X., WANG, Z. & ZHANG, Q. 2021. Deep sequencing reveals the skewed B-cell receptor repertoire in plaques and the association between pathogens and atherosclerosis. *Cell Immunol,* 360**,** 104256.

ZHANG, X., WANG, Z., ZHANG, C., LI, Y., LU, S., STEFFENS, S., MOHANTA, S., WEBER, C., HABENICHT, A. & YIN, C. 2022. Laser Capture Microdissection-Based mRNA Expression Microarrays and Single-Cell RNA Sequencing in Atherosclerosis Research. *Methods Mol Biol,* 2419**,** 715-726.

ZHOU, J. Q. & KLEINSTEIN, S. H. 2019. Cutting Edge: Ig H Chains Are Sufficient to Determine Most B Cell Clonal Relationships. *J Immunol,* 203**,** 1687-1692.

ZHU, C., CHEN, G., ZHAO, Y., GAO, X. M. & WANG, J. 2018. Regulation of the Development and Function of B Cells by ZBTB Transcription Factors. *Front Immunol,* 9**,** 580.

References

Supplemental Tables

Supplemental table 1: Basic information of B cells in aged mice

ID	Mouse	Genotype	Tissue	BCRs	Clones	D20	Expansion index	Diversification index
1	1625	WT	Blood	431	367	0.19	0.12	0.03
2	1629	WT	Blood	951	924	0.05	0.01	0.00
3	33	WT	Blood	792	765	0.06	0.01	0.00
4	1627	WT	Blood	3,897	3,481	0.03	0.00	0.00
5	1625	WT	RLNs	1,616	1,334	0.13	0.15	0.04
6	1629	WT	RLNs	1,243	1,096	0.12	0.11	0.03
7	33	WT	RLNs	5,181	4,529	0.08	0.06	0.02
8	1627	WT	RLNs	4,127	3,492	0.09	0.09	0.01
9	1625	WT	PerC	3,370	1,598	0.47	0.42	0.00
10	1629	WT	PerC	4,487	2,348	0.43	0.37	0.01
11	33	WT	PerC	502	140	0.81	0.70	0.17
12	1627	WT	PerC	3,968	1,932	0.49	0.39	0.08
13	1801	WT	PerC	3,167	1,307	0.58	0.51	0.01
14	1625	WT	Spleen	7,716	4,745	0.17	0.13	0.01
15	1629	WT	Spleen	27,622	15,131	0.18	0.12	0.01
16	33	WT	Spleen	5,092	3,099	0.25	0.24	0.01
17	1627	WT	Spleen	33,588	21,257	0.25	0.12	0.08
18	1801	WT	Spleen	16,043	8,603	0.18	0.14	0.01
19	6375	*Apoe*$^{-/-}$	ATLOs	806	610	0.48	0.15	0.31
20	6423	*Apoe*$^{-/-}$	ATLOs	991	459	0.59	0.49	0.10
21	9013	*Apoe*$^{-/-}$	ATLOs	225	207	0.24	0.06	0.08
22	9017	*Apoe*$^{-/-}$	ATLOs	304	271	0.26	0.09	0.09
23	7751	*Apoe*$^{-/-}$	ATLOs	1,341	226	0.88	0.63	0.19
24	7785	*Apoe*$^{-/-}$	ATLOs	17,434	4,323	0.31	0.30	0.02
25	5	*Apoe*$^{-/-}$	Blood	10,326	9,479	0.06	0.03	0.00
26	7	*Apoe*$^{-/-}$	Blood	44,631	34,557	0.18	0.16	0.00
27	9	*Apoe*$^{-/-}$	Blood	13,475	8,281	0.29	0.21	0.01
28	6375	*Apoe*$^{-/-}$	Blood	394	372	0.13	0.02	0.03
29	6423	*Apoe*$^{-/-}$	Blood	2,906	821	0.72	0.63	0.05
30	7751	*Apoe*$^{-/-}$	Blood	4,069	3,461	0.11	0.04	0.00
31	9017	*Apoe*$^{-/-}$	Blood	1,855	1,756	0.04	0.01	0.00
32	9013	*Apoe*$^{-/-}$	Blood	231	220	0.16	0.04	0.02
33	7785	*Apoe*$^{-/-}$	Blood	834	808	0.06	0.00	0.00
34	5	*Apoe*$^{-/-}$	RLNs	18,392	12,201	0.21	0.18	0.03
35	7	*Apoe*$^{-/-}$	RLNs	6,172	3,987	0.22	0.19	0.12
36	9	*Apoe*$^{-/-}$	RLNs	82,082	14,409	0.36	0.34	0.38
37	6375	*Apoe*$^{-/-}$	RLNs	5,598	3,131	0.29	0.29	0.07
38	6423	*Apoe*$^{-/-}$	RLNs	10,144	4,296	0.37	0.37	0.09
39	7751	*Apoe*$^{-/-}$	RLNs	25,818	5,388	0.58	0.50	0.49
40	9017	*Apoe*$^{-/-}$	RLNs	2,495	1,777	0.24	0.25	0.06

41	9013	*Apoe*$^{-/-}$	RLNs	1,913	1,268	0.25	0.29	0.06
42	7785	*Apoe*$^{-/-}$	RLNs	1,789	1,442	0.16	0.17	0.02
43	6375	*Apoe*$^{-/-}$	PerC	24,847	2,783	0.84	0.74	0.12
44	6423	*Apoe*$^{-/-}$	PerC	26,865	4,750	0.88	0.74	0.38
45	7751	*Apoe*$^{-/-}$	PerC	3,103	535	0.85	0.77	0.06
46	9013	*Apoe*$^{-/-}$	PerC	15,213	3,823	0.70	0.64	0.01
47	7785	*Apoe*$^{-/-}$	PerC	6,160	1,994	0.67	0.61	0.02
48	5	*Apoe*$^{-/-}$	Spleen	30,038	18,951	0.27	0.22	0.01
49	7	*Apoe*$^{-/-}$	Spleen	278,876	122,751	0.50	0.31	0.22
50	9	*Apoe*$^{-/-}$	Spleen	131,345	43,846	0.54	0.24	0.33
51	6375	*Apoe*$^{-/-}$	Spleen	34,695	11,585	0.40	0.27	0.02
52	6423	*Apoe*$^{-/-}$	Spleen	39,249	20,867	0.61	0.23	0.53
53	7751	*Apoe*$^{-/-}$	Spleen	559	295	0.52	0.44	0.10
54	9017	*Apoe*$^{-/-}$	Spleen	8,940	4,325	0.24	0.22	0.05
55	9013	*Apoe*$^{-/-}$	Spleen	29,343	10,663	0.40	0.22	0.15
56	7785	*Apoe*$^{-/-}$	Spleen	25,314	7,495	0.32	0.30	0.05

Supplemental table 2: Basic information of PCs in aged mice

ID	Mouse	Genotype	Tissue	BCRs	Clones	D20	Expansion index	Diversification index
1	1625	WT	Blood	61,065	18,945	0.50	0.11	0.12
2	1629	WT	Blood	151	98	0.53	0.27	0.07
3	33	WT	Blood	145	80	0.61	0.32	0.05
4	1627	WT	Blood	75,949	43,916	0.26	0.08	0.14
5	1625	WT	BM	2,316	504	0.46	0.38	0.12
6	1629	WT	BM	17,521	12,475	0.27	0.04	0.19
7	33	WT	BM	34,965	21,060	0.28	0.09	0.08
8	1627	WT	BM	351	108	0.58	0.50	0.08
9	1801	WT	BM	59,140	31,019	0.34	0.11	0.08
10	1625	WT	RLNs	8,744	1,071	0.58	0.52	0.27
11	1629	WT	RLNs	5,340	934	0.43	0.44	0.26
12	33	WT	RLNs	22,319	3,586	0.37	0.36	0.21
13	1627	WT	RLNs	20,651	3,798	0.36	0.35	0.25
14	1625	WT	Spleen	1,317	531	0.29	0.43	0.21
15	1629	WT	Spleen	3,826	777	0.40	0.47	0.28
16	33	WT	Spleen	87,590	43,112	0.37	0.23	0.33
17	1627	WT	Spleen	9,681	1,292	0.35	0.46	0.23
18	1801	WT	Spleen	64,864	37,144	0.39	0.18	0.32
19	6375	*Apoe*$^{-/-}$	ATLOs	6,445	255	0.97	0.86	0.28
20	6423	*Apoe*$^{-/-}$	ATLOs	3,065	345	0.81	0.56	0.13
21	9013	*Apoe*$^{-/-}$	ATLOs	384	173	0.67	0.53	0.13
22	9017	*Apoe*$^{-/-}$	ATLOs	3,438	255	0.93	0.64	0.23
23	7751	*Apoe*$^{-/-}$	ATLOs	1,354	146	0.93	0.65	0.28
24	7785	*Apoe*$^{-/-}$	ATLOs	18,502	1,301	0.48	0.46	0.20
25	5	*Apoe*$^{-/-}$	Blood	870	575	0.24	0.08	0.02
26	7	*Apoe*$^{-/-}$	Blood	472	244	0.50	0.20	0.06
27	9	*Apoe*$^{-/-}$	Blood	345	165	0.64	0.38	0.09
28	6375	*Apoe*$^{-/-}$	Blood	112	101	0.34	0.08	0.03
29	6423	*Apoe*$^{-/-}$	Blood	390	67	0.79	0.47	0.12
30	7751	*Apoe*$^{-/-}$	Blood	7,828	4,228	0.31	0.13	0.06
31	9017	*Apoe*$^{-/-}$	Blood	196	178	0.29	0.04	0.02
32	9013	*Apoe*$^{-/-}$	Blood	107	101	0.37	0.06	0.07
33	7785	*Apoe*$^{-/-}$	Blood	227	95	0.70	0.33	0.11
34	6375	*Apoe*$^{-/-}$	BM	46,431	14,689	0.75	0.48	0.41
35	6423	*Apoe*$^{-/-}$	BM	24,423	10,179	0.55	0.24	0.31
36	7751	*Apoe*$^{-/-}$	BM	8,916	7,337	0.34	0.05	0.22
37	9017	*Apoe*$^{-/-}$	BM	31,051	20,842	0.37	0.09	0.18
38	9013	*Apoe*$^{-/-}$	BM	96,434	42,530	0.54	0.24	0.23
39	7785	*Apoe*$^{-/-}$	BM	15,747	12,715	0.35	0.05	0.16
40	5	*Apoe*$^{-/-}$	RLNs	46,525	5,351	0.39	0.35	0.18
41	7	*Apoe*$^{-/-}$	RLNs	4,190	968	0.47	0.46	0.26
42	9	*Apoe*$^{-/-}$	RLNs	75,224	37,184	0.26	0.16	0.19

43	6375	*Apoe*$^{-/-}$	RLNs	38,616	15,471	0.52	0.29	0.34
44	6423	*Apoe*$^{-/-}$	RLNs	1,143	965	0.17	0.14	0.01
45	7751	*Apoe*$^{-/-}$	RLNs	1,535	313	0.57	0.58	0.27
46	9017	*Apoe*$^{-/-}$	RLNs	1,012	368	0.61	0.59	0.17
47	9013	*Apoe*$^{-/-}$	RLNs	1,029	391	0.51	0.54	0.16
48	7785	*Apoe*$^{-/-}$	RLNs	24,614	2,637	0.49	0.42	0.29
49	5	*Apoe*$^{-/-}$	Spleen	260,855	81,915	0.48	0.36	0.30
50	7	*Apoe*$^{-/-}$	Spleen	119,105	20,123	0.64	0.55	0.37
51	9	*Apoe*$^{-/-}$	Spleen	161,694	45,364	0.52	0.33	0.39
52	6375	*Apoe*$^{-/-}$	Spleen	85,435	39,037	0.60	0.27	0.46
53	6423	*Apoe*$^{-/-}$	Spleen	40,919	25,294	0.53	0.23	0.42
54	7751	*Apoe*$^{-/-}$	Spleen	10,970	9,455	0.41	0.06	0.35
55	9017	*Apoe*$^{-/-}$	Spleen	58,033	37,253	0.35	0.10	0.32
56	9013	*Apoe*$^{-/-}$	Spleen	65,125	46,165	0.45	0.12	0.40
57	7785	*Apoe*$^{-/-}$	Spleen	30,558	21,971	0.44	0.11	0.41

Supplemental table 3: Basic information of naïve B cell samples

ID	Mouse	Genotype	Tissue	Cell	Age	BCRs	Clones	D20	Expansion index	Diversification index
1	1625	WT	BM	IN*	Aged	778	698	0.10	0.10	0.01
2	1629	WT	BM	IN	Aged	831	782	0.06	0.05	0.00
3	33	WT	BM	IN	Aged	6,764	6,038	0.04	0.02	0.00
4	1801	WT	BM	IN	Aged	10,903	6,477	0.17	0.17	0.00
5	1625	WT	Spleen	MN*	Aged	681	570	0.18	0.16	0.02
6	1629	WT	Spleen	MN	Aged	1,997	1,648	0.14	0.14	0.01
7	33	WT	Spleen	MN	Aged	5,156	4,922	0.02	0.01	0.00
8	1627	WT	Spleen	MN	Aged	6,935	5,748	0.10	0.09	0.01
9	1801	WT	Spleen	MN	Aged	4,414	3,809	0.09	0.08	0.01
10	679	WT	BM	IN	Young	1,898	1,745	0.04	0.02	0.00
11	685	WT	BM	IN	Young	235	211	0.20	0.09	0.05
12	1827	WT	BM	IN	Young	921	895	0.04	0.00	0.00
13	1829	WT	BM	IN	Young	359	350	0.08	0.03	0.00
14	1831	WT	BM	IN	Young	740	724	0.05	0.02	0.00
15	1837	WT	BM	IN	Young	303	296	0.10	0.01	0.00
16	1839	WT	BM	IN	Young	659	642	0.06	0.00	0.00
17	679	WT	Spleen	MN	Young	6,612	6,392	0.01	0.00	0.00
18	685	WT	Spleen	MN	Young	6,309	6,058	0.01	0.00	0.00
19	1827	WT	Spleen	MN	Young	374	366	0.08	0.00	0.00
20	1829	WT	Spleen	MN	Young	140	131	0.22	0.04	0.01
21	1831	WT	Spleen	MN	Young	118	81	0.58	0.32	0.13
22	1837	WT	Spleen	MN	Young	407	400	0.07	0.00	0.00
23	1839	WT	Spleen	MN	Young	273	265	0.15	0.03	0.00
24	6375	*Apoe*$^{-/-}$	BM	IN	Aged	8,550	2,150	0.63	0.50	0.18
25	6423	*Apoe*$^{-/-}$	BM	IN	Aged	14,545	514	0.94	0.88	0.51
26	7751	*Apoe*$^{-/-}$	BM	IN	Aged	9,194	6,557	0.10	0.12	0.01
27	9017	*Apoe*$^{-/-}$	BM	IN	Aged	3,372	1,683	0.30	0.35	0.04
28	9013	*Apoe*$^{-/-}$	BM	IN	Aged	6,022	1,948	0.52	0.45	0.09
29	7785	*Apoe*$^{-/-}$	BM	IN	Aged	1,847	1,611	0.09	0.07	0.00
30	3397	*Apoe*$^{-/-}$	BM	IN	Aged	3,428	2,787	0.08	0.09	0.00
31	3405	*Apoe*$^{-/-}$	BM	IN	Aged	4,415	3,714	0.08	0.08	0.01
32	6375	*Apoe*$^{-/-}$	Spleen	MN	Aged	8,700	6,987	0.16	0.10	0.00
33	6423	*Apoe*$^{-/-}$	Spleen	MN	Aged	2,861	1,488	0.46	0.42	0.01
34	7751	*Apoe*$^{-/-}$	Spleen	MN	Aged	2,332	2,214	0.04	0.01	0.01
35	9017	*Apoe*$^{-/-}$	Spleen	MN	Aged	3,813	2,950	0.16	0.13	0.01
36	9013	*Apoe*$^{-/-}$	Spleen	MN	Aged	7,151	4,490	0.31	0.25	0.03
37	7785	*Apoe*$^{-/-}$	Spleen	MN	Aged	2,516	2,216	0.10	0.07	0.01
38	3397	*Apoe*$^{-/-}$	Spleen	MN	Aged	6,425	5,651	0.08	0.06	0.00
39	3405	*Apoe*$^{-/-}$	Spleen	MN	Aged	5,574	4,968	0.05	0.04	0.00
40	8295	*Apoe*$^{-/-}$	BM	IN	Young	2,251	2,071	0.04	0.01	0.00
41	8297	*Apoe*$^{-/-}$	BM	IN	Young	7,371	6,793	0.01	0.00	0.00
42	8299	*Apoe*$^{-/-}$	BM	IN	Young	1,119	1,061	0.05	0.03	0.00

43	8301	*Apoe*$^{-/-}$	BM	IN	Young	1,427	1,371	0.03	0.00	0.00
44	8309	*Apoe*$^{-/-}$	BM	IN	Young	6,904	6,559	0.01	0.00	0.00
45	233	*Apoe*$^{-/-}$	BM	IN	Young	18,838	14,842	0.03	0.00	0.00
46	237	*Apoe*$^{-/-}$	BM	IN	Young	3,318	3,087	0.03	0.00	0.00
47	249	*Apoe*$^{-/-}$	BM	IN	Young	5,655	5,154	0.02	0.00	0.00
48	251	*Apoe*$^{-/-}$	BM	IN	Young	4,785	4,352	0.03	0.01	0.00
49	253	*Apoe*$^{-/-}$	BM	IN	Young	8,134	7,320	0.02	0.00	0.00
50	8295	*Apoe*$^{-/-}$	Spleen	MN	Young	4,982	4,224	0.07	0.03	0.00
51	8297	*Apoe*$^{-/-}$	Spleen	MN	Young	8,429	6,080	0.10	0.04	0.00
52	8299	*Apoe*$^{-/-}$	Spleen	MN	Young	7,592	6,316	0.05	0.01	0.00
53	8301	*Apoe*$^{-/-}$	Spleen	MN	Young	1,247	1,068	0.11	0.03	0.00
54	8309	*Apoe*$^{-/-}$	Spleen	MN	Young	2,282	2,044	0.07	0.01	0.00
55	233	*Apoe*$^{-/-}$	Spleen	MN	Young	3,401	3,161	0.04	0.01	0.00
56	237	*Apoe*$^{-/-}$	Spleen	MN	Young	4,864	4,556	0.02	0.00	0.00
57	249	*Apoe*$^{-/-}$	Spleen	MN	Young	5,661	5,313	0.03	0.00	0.00
58	251	*Apoe*$^{-/-}$	Spleen	MN	Young	2,696	2,504	0.06	0.00	0.00
59	253	*Apoe*$^{-/-}$	Spleen	MN	Young	3,809	3,501	0.05	0.00	0.00

*: IN: immature naïve B cells; MN: mature naïve B cells

Supplemental table 4: Basic information of GC B cells and PC samples in young mice

ID	Mouse	Genotype	Tissue	Cell	BCRs	Clones	D20	Expansion index	Diversification index
1	1827	WT	BM	PC	32,788	8,257	0.25	0.59	0.43
2	1829	WT	BM	PC	31,365	5,547	0.27	0.61	0.35
3	1831	WT	BM	PC	14,590	4,646	0.31	0.6	0.44
4	1837	WT	BM	PC	28,262	4,189	0.41	0.7	0.4
5	1839	WT	BM	PC	18,892	3,878	0.27	0.64	0.46
6	1827	WT	Spleen	GC	20	19	-	-	-
7	1829	WT	Spleen	GC	299	279	0.15	0.06	0.01
8	1831	WT	Spleen	GC	25	25	-	-	-
9	1837	WT	Spleen	GC	28	27	-	-	-
10	1839	WT	Spleen	GC	18	17	-	-	-
11	1827	WT	Spleen	PC	27,310	10,825	0.24	0.39	0.32
12	1829	WT	Spleen	PC	29,347	12,404	0.17	0.32	0.3
13	1831	WT	Spleen	PC	12,103	6,504	0.18	0.32	0.34
14	1837	WT	Spleen	PC	5,051	3,644	0.19	0.26	0.38
15	1839	WT	Spleen	PC	17,851	6,879	0.2	0.4	0.26
16	233	*Apoe*$^{-/-}$	BM	PC	46,956	20,942	0.38	0.47	0.58
17	237	*Apoe*$^{-/-}$	BM	PC	42,215	17,027	0.34	0.5	0.5
18	249	*Apoe*$^{-/-}$	BM	PC	18,206	11,407	0.27	0.34	0.53
19	251	*Apoe*$^{-/-}$	BM	PC	43,078	18,463	0.28	0.48	0.52
20	253	*Apoe*$^{-/-}$	BM	PC	51,165	23,057	0.25	0.42	0.55
21	233	*Apoe*$^{-/-}$	Spleen	GC	717	568	0.19	0.13	0.03
22	237	*Apoe*$^{-/-}$	Spleen	GC	2,546	1,842	0.07	0.02	0.01
23	249	*Apoe*$^{-/-}$	Spleen	GC	575	396	0.19	0.18	0.01
24	251	*Apoe*$^{-/-}$	Spleen	GC	4,271	2,751	0.11	0.08	0.01
25	253	*Apoe*$^{-/-}$	Spleen	GC	1,163	848	0.17	0.11	0.06
26	233	*Apoe*$^{-/-}$	Spleen	PC	53,148	34,857	0.3	0.2	0.42
27	237	*Apoe*$^{-/-}$	Spleen	PC	50,921	31,458	0.17	0.19	0.33
28	249	*Apoe*$^{-/-}$	Spleen	PC	20,042	12,782	0.23	0.25	0.34
29	251	*Apoe*$^{-/-}$	Spleen	PC	10,784	9,192	0.3	0.11	0.45
30	253	*Apoe*$^{-/-}$	Spleen	PC	33,055	21,801	0.21	0.18	0.42

Acknowledgements

Time flies. When I finally type ‘acknowledgements’ here, it is mixed feelings with a myriad of thoughts and ideas. Joy and sorrow to the past, expectation and fear to the future. But I’ve never regretted with my choice to come to Munich. Now while the thesis is going to be completed, I would like to give my appreciate to all the person who have supported, helped, and encouraged me during my study.

First of all, the profound acknowledgement is given to my respectful supervisors: Professor Sabine Steffens and Professor Andreas Habenicht, who have kept supporting me in both life and work. Only with their invaluable supervision and constructive criticism, I can successfully understand the proposal, finish the project, write the thesis, and polish the text. Thanks for their patience and time.

Also, my heartiest thanks flow to Prof. Changjun Yin for his training, guidance, and suggestions. Each time of discussion with him counts as it always offered me new and excellent ideas to advance the project.

Special thanks to Dr. Zhihua Wang, who helped me to analyze the scRNA-seq data. And thank Dr. med Michael Hristov for his help on cell sorting.

I would also like to express my sincere gratitude to Dr. Sarajo Kumar Mohanta, Dr. Chuankai Zhang, Dr. Ting Sun, Dr. Shu Lu, Yutao Li and other members in our group. Thank you for your critical advice and help in the past years. I have spent a very nice moment with all of you in Munich.

Particular thanks to all my collaborators: Dr. Klaus Donmair, Dr. Eduardo Beltran, Prof. Racheal Bashford-Rogers et al. who shared me their protocols and scripts. Their help led me avoid the misunderstanding at the beginning of my project.

I also want to extend my deep gratefulness to my beloved families for their understanding and encouragement in these years. They create a harbor for my heart where I can take a rest and draw strength. Thanks to my lovely daughter: Tianyou Chu, you are the best gift in my life.

My life in Munich will end soon but my journey to be a researcher just start. Then thanks myself, for I never gave up my dream which ingrained in my heart when I was only a little girl: to be a scientist.

Affidavit

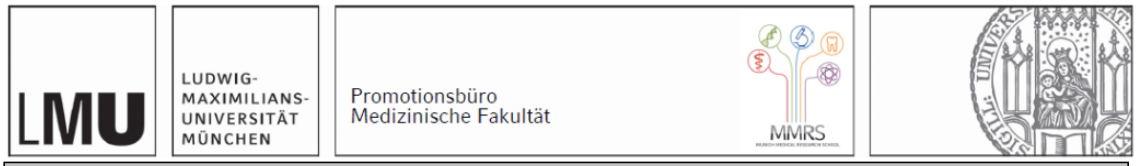

Affidavit

Zhang, Xi

Surname, first name

Pettenkoferstr. 9

Street

80336, Munich, Germany

Zip code, town, country

I hereby declare, that the submitted thesis entitled:

Elucidating atherosclerosis B cell immunity in hyperlipidemic mice by next-generation sequencing

is my own work. I have only used the sources indicated and have not made unauthorized use of services of a third party. Where the work of others has been quoted or reproduced, the source is always given.

I further declare that the submitted thesis or parts thereof have not been presented as part of an examination degree to any other university.

Munich 18.07.2024 — Xi Zhang

place, date — Signature

doctoral candidate